Quantitative Proteomics using Chemical Probes

Sibasish Dolai

Bachelor of Veterinary Medicine (O.U.A.T. India)

Master of Biotechnology and Business (Macquarie University)

Doctor of Philosophy

Department of Chemistry and Biomolecular Sciences

Macquarie University, Sydney, Australia

July 2011

Declaration

The work presented in this thesis titled, "Quantitative Proteomics using Chemical Probes" has not been submitted, in either whole or part, for the purpose of obtaining any other degree to another university or institution. Several aspects of this work have been performed in collaboration with others; these people have been acknowledged and their contributions recognised in the section in which their assistance was received. Unless otherwise acknowledged, the work presented in this thesis was carried out by the author. I consent to a copy of this thesis being available in the University library for consultation, loan and photocopying forthwith.

Sibasish Dolai
40634329

July 2011

Abstract

Chemical proteomics utilizes synthetic chemical probes to selectively capture and enrich particular classes of proteins from complex biological samples, enabling their characterization by proteomic techniques. The study focused on development of a robust chemical proteomics method to characterise and quantitate cellular protein targets in biological models using an in-house developed chemical probe that harbor's a potent protein kinase C inhibitor, bisindolylmaleimide (Bis) as the reactive group. The newly developed chemical proteomics method was applied to characterise the Bis-binding protein targets in basal breast cancer cell line (MDA-MB-231). Two protein kinases, serine/arginine-rich protein-specific kinase 1 (SRPK1) and interferon induced RNA-dependent protein kinase (PKR) were identified that were not previously known to bind to Bis. Further, a SILAC based quantitation strategy was used to examine changes in Bis-binding proteins following phorbol ester (PMA) stimulation. This provided novel evidence for PMA regulation of the enzymes glyceraldehyde-3-phosphate dehydrogenase (GAPDH), nucleolar RNA helicase 2 (DDX21) and heterogenous ribonucleoprotein M (HNRPM). This cell culture based cancer model provided the foundation to expand the chemical proteomics study to a tissue based system using Bis-probes. The study focused on Bis-binding metabolic enzymes from the liver of mice bearing a C26 adenocarcinoma with accompanying high IL-6 levels that induced cancer cachexia (cachectic). Bis-binding enzymes were compared with mice bearing a C26 adenocarcinoma with low IL-6 levels that failed to induced cancer cachexia (non-cachectic) and control mice with no tumour. Spectral counting was used to quantify the relative abundance of the Bis-captured enzymes. In the cachectic model overall carbohydrate metabolism, the branched chain amino acid degradation and lipid metabolism was significantly reduced, while the hepatic acute phase protein synthesis was induced. Further, the marked reduction in the cytochrome P450 enzymes is consistent with the impaired xenobiotic metabolism and the subsequent

chemotoxicity encountered in cancer cachexia patients. The Bis-probe was also applied in a human adipose derived stem cell (hADSC) model to characterise and quantitate the differential expression of Bis-binding proteins during chemical induction of neurogenic differentiation. Several key enzymes involved in the neuronal differentiation of stem cells were captured by the Bis-probe at different time points of chemical induction. In the final study, kinase active-site peptide enrichment analysis was carried out in phorbol ester stimulated and resting basal breast cancer cells using a newly commercialised desthiobiotin-ATP probe. This analysis showed more than two-thirds of the identified targets in both the PMA treated and the resting MDA-MB-231 cells as ATP binding proteins which included 23 protein kinases. Of the identified protein kinases 16 were common to both the treated and resting groups and 7 protein kinases each were unique to the PMA treated samples and the resting cells. In summary, this thesis demonstrates the versatile use of quantitative chemical proteomics for biomedical investigations.

Acknowledgements

First and foremost I would like to express my sincerest gratitude to Mark Molloy for giving me the opportunity to pursue PhD under his supervision and believing in me, when I went through some very tough times. Thanks would be an understated word to acknowledge his contributions, in making this thesis possible. Mark you were a fabulous advisor: sharp, positive, perceptive, and mindful of the things that truly matter. Your amazing mentorship enabled me to calmly work towards my final objective. I would also like to thank my associate supervisor Fei Liu, who introduced me to the world of 'Chemical Probes'.

I would like to thank Paul Haynes, who provided invaluable advice, training and patience while answering my long list of never ending questions about mass spectrometry. Thanks to Albert Lee, Rohit Saldanha, Matthew McKay and Joel Chick for sharing their expertise with me. Special thanks to Naveid Ali for your friendship, encouragement, support and expertise.

It is a pleasure to thank the present and past Macquarie University students and APAF staff including Pauliina, Karlie, Sri, Katherine, Garine, Mehdi, Michael M, Michael H, Sarah, Chi-Li, Arun, Dylan, Thiri and the biomarker lab crew who have given me the support and made me feel very comfortable right from the day I stepped into the lab. I would also like to thank the Bioinformatics team Brett, Dana and Tim for their help and advice in data analysis. Thanks to my friends, particularly to Rama, Kiran, Sudhir, Nandan and Chandrika for their continued support and useful scientific and non scientific discussions throughout. I would also like to thank Macquarie University for providing me International Macquarie University Research Scholarship (iMURS) for pursuing my research.

Above all I would like to acknowledge the tremendous sacrifices that my parents made to ensure that I had the best education. For this and much more, I am forever in their debt. It is to them that I dedicate this thesis. Thanks to my sisters, Julie and Dolly for their immense support and encouragement, despite the geographical distance. Guru and Maddy, huge thanks to you both for adopting all my responsibilities back home, so that I could focus on my studies. Finally, to my wife and best friend Pooja, not necessarily for coming along at the right time, but for the very special person that she is. I was able to complete this thesis because she has taught me, and demonstrates for me everyday-just what love is. Thankyou for all your support, encouragement and patience-all my love.

“In loving memory of my mum”

Publications

Sibasish Dolai, Fei Liu and Mark P. Molloy., Quantitative Chemical Proteomics in small scale culture of Phorbol ester stimulated Basal Breast Cancer Cells. *Proteomics* 2011, volume 11, issue 13, 2683–2692**.**

Presentations

Sibasish Dolai, Fei Liu and Mark P. Molloy (2010) Quantitative Chemical Proteomics Investigation of the Bisindolylmaleimide binding proteome**.**

Poster presentation, *15th Annual Proteomics Symposium*, Lorne Victoria, Australia

Sibasish Dolai, Fei Liu and Mark P. Molloy (2009) Quantitative Chemical Proteomics Investigation of the Bisindolylmaleimide binding proteome in a phorbol ester stimulated breast cancer cell line.

Poster presentation, *HuPO 8th Annual Congress*, Toronto, Canada

Sibasish Dolai, Fei Liu and Mark P. Molloy (2009) Chemical Proteomics to study the ATP binding sub-proteome in cancer cell models.

Poster presentation*, 14th Annual Proteomics Symposium*, Lorne Victoria, Australia

Sibasish Dolai, Fei Liu and Mark P. Molloy (2008) Chemical Proteomics for Characterisation of Protein Kinase C in Cancer.

Poster presentation, *13th Annual Proteomics Symposium*, Lorne Victoria, Australia

Awards

- International Macquarie University Research Scholarship (iMURS)
- Lorne Proteomics Conference 2010 Best Poster Award: Feb 2010
- Macquarie University Postgraduate Research Fund (PGRF): June 2009
- Macquarie University Vice Chancellors Commendation Travel Grant Award: June 2009
- Macquarie University International Research Travel Grant: June 2009
- Young Investigators Travel Award (HuPO): Sept 2009

Common Abbreviations

2BME β-mercaptoethanol

ACN Acetonitrile

BCA Bicinchoninic acid

Bis Bisindolylmaleimide

cAMP Cyclic adenosine monophosphate

C26 Colon 26 Adenocarcinoma

CYP Cytochrome p450

DMEM Dulbecco's Modified Eagle Media

DTT Dithiothreitol

ESI Electrospray ionisation

FDR False discovery rate

GO Gene Ontology

GPM Global Proteome Machine

hADSC Human Adipose Derived Stem Cell

IAA Iodoacetamide

IB Immunoblot

IDA Independent data acquisition

LC Liquid chromatography

LDS Lithium dodecyl sulphate

MAPK Mitogen activated protein kinase

MS Mass spectrometry

NSAF Normalised Spectral Abundance Factors

PKC Protein Kinase C

PMA Phorbol 12- myristate 13-acetate

RIPA Radio Immunoprecipitation Assay

SILAC Stable isotope labelling with amino acids in cell culture

TFA Trifluoroacetic acid

m/z Mass/charge

Table of Contents

Chapter 1: Introduction

1.1. Introduction: Opportunities and challenges for proteomics

The elucidation of complete genome sequences of prokaryotic and eukaryotic organisms has provided enormous new understanding of the molecular basis of life. However, most of the complex physiological and pathological processes cannot be explained alone on the basis of genome sequences because of the fundamental role played by the proteins and RNA molecules in the control and regulation of molecular events. Considering that proteins are by far the major mediators of most cellular biochemical events, investigation of protein expression on a global scale (i.e. proteomics) has become a primary focal point of post-genomic research [1-3]. Proteomics, in its most fundamental definition, aims to investigate the total protein complement of a biological sample. However, considering the biochemical complexity intrinsic to protein science and the large dynamic range of cellular protein expression, the identification, quantitation and global characterisation of all proteins within a given proteome remains elusive. Further, the restricted absolute detection limits of analytical technology and the extreme diversity and heterogeneity of the proteome compounds the challenge. Hence, the expanded goal of proteomics to comprehensively characterise the expression, modification state, interaction map and activity of all proteins in cell and tissues will only be achieved by complementary analytical strategies [4].

Conventional proteomic technologies involved two-dimensional gel electrophoresis (2DE) coupled with mass spectrometry (MS) for the separation, quantification, and eventually the identification of proteins. This has proved a robust approach that permitted the identification of proteins that are associated with discrete physiological and/or pathological states and has been extensively used for the comparative proteomic investigations to identify, for example, proteins that are differentially expressed in normal and disease tissues [5]. Although, the advent of fluorescent dyes for protein detection such as SYPRO Ruby [6] increased the sensitivity and dynamic range of 2DE, this method has well known

limitations. Some of these limitations include the separation of very acidic/basic proteins, very large >250kDa and small <10kDa proteins, hydrophobic proteins and the sample loading capacity. Consequently, the analysis of several important classes of proteins, including membrane-associated and low-abundance proteins become extremely challenging [7-9]. Perhaps one of the largest drawbacks of 2DE is the decoupling of protein quantitation (gels) from identification (MS). Further, it is well known that some gel spots can contain multiple proteins, thus quantitation accuracy can be compromised [10]. To address these limitations liquid chromatography (LC)-MS based "gel free" methods have emerged along with major advances in MS hardware, which has matured into an attractive technology for proteome analysis [11-13].

Despite the advances in proteomic technologies, the typical dynamic range offered by the 2-DE or LC-MS/MS separation techniques is approximately 10^2–10^4 [8, 14, 15]. This is less than the wide dynamic range of cellular protein expression, which is as great as six orders of magnitude between the most abundant and the least abundant protein [14] and even greater in circulating biofluids such as plasma (10^{12}) [16]. In 2-DE, such limitations are evident when protein loading is increased to facilitate the visualisation of less abundant proteins, which ultimately results in spot fusion and co-migration of the high abundant proteins, making them irresolvable [8]. In MS-based methods the dynamic range depends on the type of MS instrument, the peak capacity (the number of peaks that can be separated in one gradient run) of the LC separation [17] and the effectiveness of protein sample fractionation/preparation strategies prior to MS analysis. The factors that limit protein identification in the MS-methods include: co-eluting peptides during chromatographic separation [13]; peptide ion suppression [13, 17] and the limited duty cycle and resolving power of the MS. This means that the required rate to complete a precursor scan and fragmentation experiment for a single peptide may not be fast enough to allow all peptides

from a given sample to be analysed. Consequently, the number of ions selected for fragmentation is limited, which can decrease the chance of detecting low abundance peptides. These issues of sensitivity and the size and diversity of the proteome has particularly limited the study of low expression level proteins, which play pivotal roles in cellular regulation such as mediators of gene transcription or intracellular signalling and metabolic pathways [11]. To address these issues fractionation strategies have been developed which includes sub-proteomics, where proteins that reside in different cellular compartments and organelles are differentially extracted [18, 19], and affinity or function based protein profiling where subgroups of proteins are captured by bait proteins, small molecules or ions that interact with relevant proteins [20, 21]. More recently, the field of chemical proteomics is increasingly gaining attention as a useful strategy for the selective enrichment of functionally related proteins [22, 23].

1.2. Chemical Proteomics

Chemical proteomics is a multidisciplinary field that makes use of synthetic organic chemistry, cell biology, biochemistry and mass spectrometry to identify, quantitate and validate the interaction of target proteins with small molecule probes in a rapid, systematic and comprehensive manner [24, 25]. The central component of this field is the design, synthesis and application of synthetic small molecule probes that specifically interact with proteins (often enzymes) and enable their subsequent enrichment through affinity purification. As it is an enrichment technique it overcomes the limitations in dynamic range of traditional large-scale proteomics experiments [24]. The chemical probes designed for these studies are often based on pharmacological inhibitors of enzyme activity. Proteomic characterisation of chemical probe-enriched proteins provides some insight into studying enzyme classes and assessing the cellular binding affinity of these inhibitors [26, 27]. Often target proteins are masked by other more abundant proteins and

chemical probes offer avenues for their enrichment. Based on the design of the chemical probes, chemical proteomics is broadly divided into two different categories: (i) activity based protein profiling (ABPP), characterised by enzymatic *activity* of a particular protein family, and (ii) compound-centric chemical proteomics (CCCP), which focuses on characterizing the binding targets of small molecule or drug inhibitors [28]. Regardless of their mechanism of action chemical probes are finding increasing use in the field of proteomics to aid in target identification, target validation and enrichment of low abundant enzyme classes.

1.2.1. Activity Based Chemical Proteomics (ABPP)

Activity based chemical proteomics or as most commonly referred to as activity based protein profiling (ABPP) is a chemical proteomics strategy that makes use of active-site-directed, small molecule based covalent probes to report on the functional state of enzyme activities directly in native biological systems [29, 30]. ABPP detects members of a defined class of enzymes that are *active* under certain conditions (e.g. disease) and/or can lead to the identification of new proteins with the respective biochemical activity. To date, several ABPP probes have been successfully developed for the proteomic profiling of many enzyme classes that includes serine hydrolases [31-33], cysteine proteases [34, 35], aspartyl proteases [36], metalloproteases [37-39], kinases [40], glycosidases [41, 42], histone deacetylases [43] and oxidoreductases [44, 45]. These probes have been shown to selectively label active enzymes but not their inactive precursors (zymogen) or inhibitor-bound forms, thus allowing researchers to capture functional information that is beyond the scope of standard proteomic methods [31, 46]. For a recent review on ABPP see [47, 48].

1.2.2. Compound Centric Chemical Proteomics (CCCP)

Compound centric chemical proteomics, which is the focus of this thesis, is a chemical proteomics strategy that makes use of selective inhibitors or drugs to affinity purify their binding targets and subsequently characterise them using MS. Majority of publications in the area of CCCP have focused on protein kinase inhibitors (discussed in detail in Section 1.3.1.). In other studies endogenous signalling molecules such as ATP/ADP [49], phosphatidylinositols [50, 51] and cyclic nucleotides [52] have been used for the affinity enrichment of interacting proteins. The use of specific peptide sequences as baits has also been reported [53, 54].

1.2.3. Anatomy of a chemical probe

Chemical probes are typically engineered to contain three distinct molecular elements (**Figure 1.1**): (i) a reactive group (RG) for covalent or affinity attachment to intended target proteins; (ii) affinity/reporter groups (tags), like biotin or a fluorophore, for the rapid detection and isolation of probe labelled enzymes; and (iii) a linker, like alkyl or polyethylene glycol (PEG) that provide spatial separation in between the RG and tag [25].

1.2.3.1. Reactive Group

The reactive group (RG) defines the specificity of the chemical probe. The greatest challenge in the selection of RG lies in the fact that this functional group must be reactive towards a specific residue or an affinity moiety on a protein and at the same time is inert towards other reactive species within the cell extract (**Figure 1.1**).

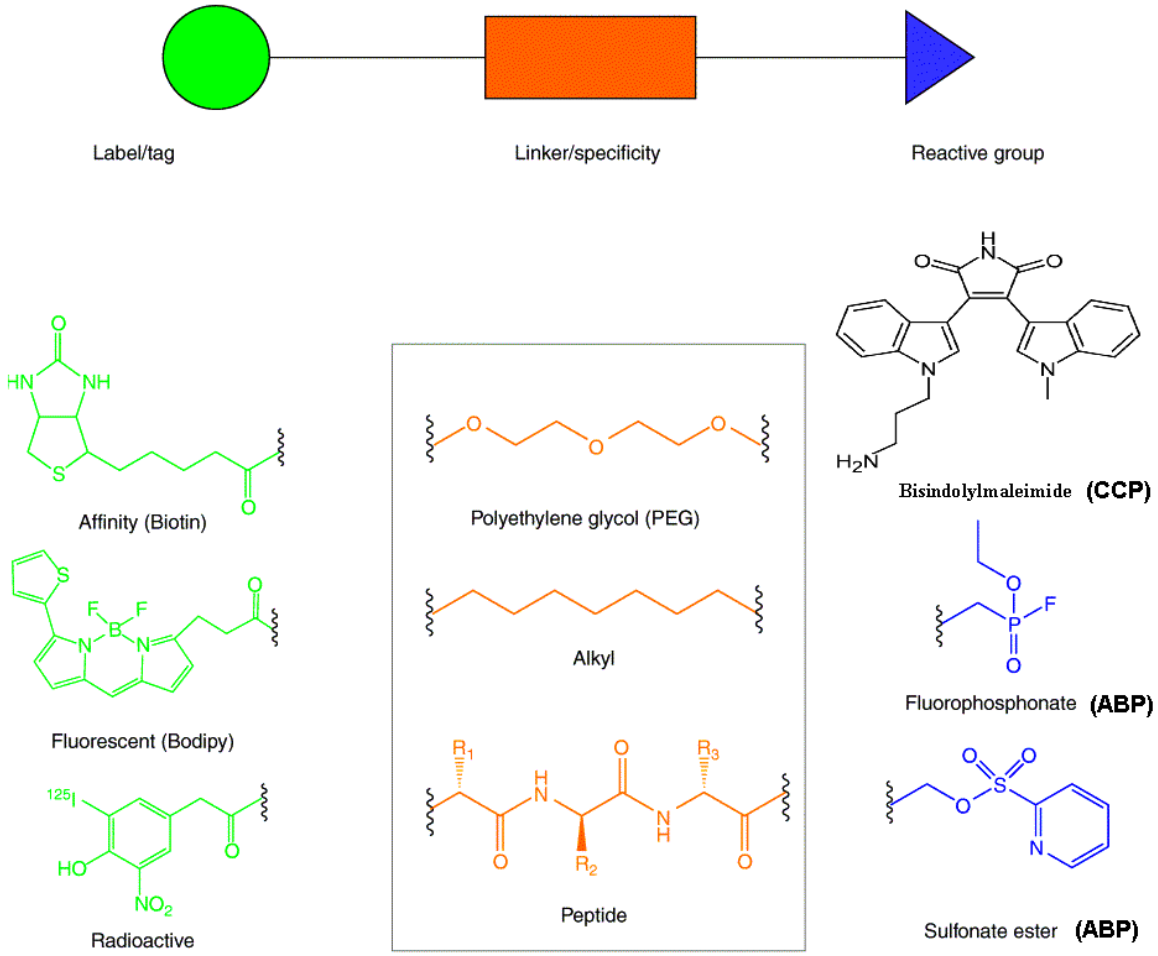

Figure 1.1: Structure of a chemical probe. A chemical probe has three basic components: a reactive group for covalent/affinity attachment to the enzyme of interest; a linker region to provide spacing and specificity; and a tag to allow for identification and/or purification. Examples of compound centric probe (CCP) (black) and Activity Based Probes (ABP) (blue) are shown [25].

1.2.3.1.1. Activity based probes RG's

The RG's of activity based probes (ABPs) are based on the chemistries of covalent, mechanism based inhibitors of various enzyme families and are designed to target a subset of the proteome based on shared principle of binding and/or reactivity (**Figure 1.1**). In ABPs the RG that mimics a substrate and has an electropositive carbon that could be used to covalently modify the active-site residue of an enzyme that uses a nucleophilic attack mechanism. For example, peptide acyloxymethyl ketones and epoxides have been shown to efficiently and selectively label cysteine proteases of the caspase and papain families, respectively [34, 55]. Similarly, ABPs have been designed that contains RG as a 'masked electrophile' that is uncovered after the probe functions as the substrate for the target

enzyme. The unmasked electrophile is then able to react with the nearby, non-catalytic, nucleophile residues in the active-site. For example, Difluoromethylphenyl bis (cyclohexylammonium) phosphate (DFPP) has been used to alkylate protein phosphatases [56, 57]. Similarly, successful design chemistries have been developed for serine and cysteine proteases, which utilize a catalytic amino acid nucleophile in the active-site, yet each has a different nucleophile residue and a distinct catalytic mechanism [32, 58].

1.2.3.1.2. Compound centric probes RG's

For compound centric studies several kinase inhibitors have been used as reactive groups for the affinity capture of cellular targets [59]. Design of inhibitors as RG's are usually based on structural data from co-crystallised enzyme–inhibitor complexes that permit the identification of positions in the enzyme inhibitor molecule, which are accessible from the outside solvent and thereby can be utilised as attachment points for covalent immobilisation to linker [26, 60]. The majority of the compound centric probes reported in literature have focused on protein kinase inhibitors (see Section 1.3.1). For example, Brehmer *et al.* used bisindolylmaleimide analogues for functional immobilization in combination with the specific purification for proteome wide identification of cellular binding proteins [27]. Similarly, Godl *et al.* applied the widely used p38 kinase inhibitor SB203580 for identifying cellular targets [61]. More recently, linkable versions of commercially available drugs such as imatinib (a chronic myeloid leukaemia drug), and two second-generation drugs, nilotinib and dasatinib, that were originally developed for the inhibition of the fusion oncoprotein BCR-ABL were analyzed for their target spectrum in affinity precipitation experiments [62]. Further, nucleotide groups (ATP/ADP) have also been used as RG's to target the ATP binding site of protein kinases (see Section 1.3.2) [40, 49]. As an alternative to ATP mimetics, kinase inhibitors have also been designed that can

bind to allosteric and cofactor binding sites and acts as effective RG's in the compound centric approach (see Section 1.3.3).

1.2.3.2. The linker

The linker domain of a chemical probe connects the RG to the tag used for identification and/or purification (**Figure 1.1**). The primary function of the linker in chemical probe design is to provide sufficient space between the RG and the tag to prevent steric hindrance that could block access of the reactive group or accessibility of the tag for affinity purification. Generally, long-chain alkyl groups or polyethelene oxide/glycol (PEO/PEG) groups are used as linkers. Alkyl linkers are primarily used to modulate the membrane permeability of a chemical probe in living cells and tissues, whereas PEG/PEO linkers are used to increase the bioavailability of probes by improving the solubility of more hydrophobic probes in aqueous solutions. Further, there are also studies which incorporated specificity elements such as peptide or peptide like structures to provide specific binding of the probes to desired enzymes or family of enzymes. In particular, these specificity elements have been used for ABPs that target proteases [63, 64].

1.2.3.3. The Affinity/Reporter Tag

The third element in probe design is the molecule 'tag' used for affinity purification or reporting of the probe labelled proteins (**Figure 1.1**). The most commonly used tags have either affinity, fluorescent or radioactive properties. Biotin remains the most commonly used tag for affinity purification because of its ability to bind to streptavidin with very high affinity (association constant $10^{15}M^{-1}$ [65]) enabling efficient purification of probe-bound proteins. Nonetheless, fluorescent and radioactive tags have the advantage of visualisation by direct scanning of gels with a fluorescent scanner or phosphorimager. The use of

fluorescent tags with non-overlapping excitation/emission spectra also enables multiplexing [33].

1.3. Compound Centric Chemical Proteomics

Compound centric chemical proteomics (CCCP) makes use of inhibitor-enzyme interaction binding [66-69] in combination with modern high-resolution mass spectrometry analysis to characterise and quantify cellular binding targets of inhibitors/drugs. CCCP offers the most feasible and versatile methods to profile the proteome against selected inhibitors by affinity chromatography of immobilised inhibitors. Once immobilised, the inhibitor must be further tested with appropriate biochemical or cell based assays to ensure the desired binding activity is retained (see Section 1.4). Subsequently, cell lysates or tissue extract are incubated with the affinity matrix and washed extensively [70]. The inhibitor bound proteins are then eluted under denaturing conditions and analysed. Unlike ABPP, which relies on specific RG to covalently bind to enzyme receptors, CCCP usually relies on non-covalent, inhibitor-enzyme active-site interactions. **Figure 1.2** shows the comparison of ABPP and CCCP. Interaction of proteins with the chemical bait in CCCP occurs *in vitro* and as a result chemical proteomics finds its application in characterising interaction partners in cell lysates, tissue and fluids. The compound centric approach lends itself to the characterisation of target profiles of a bioactive compound in an unbiased manner, along with the identification of protein targets of unexpected biochemical classes, including entirely novel targets [27, 62, 71]. For example, Brehmer *et al.* confirmed the protein kinases Ste20-related kinase and cyclin-dependent kinase 2 (CDK2) and the non-protein kinases adenosine kinase and quinone reductase type 2 as novel targets of protein kinase C inhibitor, bisindolylmaleimide in HeLa cells [27]. Similarly, Bach *et al.* used a selective cyclin-dependent kinase inhibitor, Roscovitine, and reported the binding of an unexpected, non-protein kinase target, pyridoxal kinase when screened in COS and HEK293 cells [71].

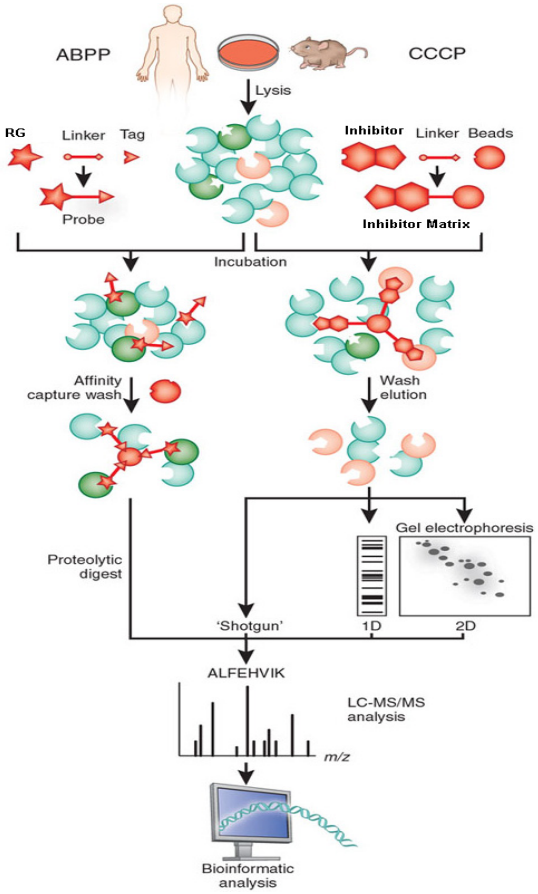

Figure 1.2: Comparison of Activity-based protein profiling and Compound centric chemical proteomics. Adapted from Ref [28].

Further Rix *et al.* observed oxidoreductase NQO2 to be bound and inhibited by imatinib and nilotinib at physiologically relevant drug concentrations, representing the first non kinase target of these drugs [62].

1.3.1. Kinase inhibitors for target identification by CCCP

Small molecule inhibitors of protein kinases are widely employed for therapeutic intervention in a variety of human disease. Protein kinases are well known drug targets in oncology and more recently their relevance is increasingly recognised in inflammation, autoimmune disease [72-74], metabolic disorders [75] and central nervous system disorders [76, 77]. It is estimated that the human genome encodes 518 protein kinases and more than 2000 other ATP- and purine-binding proteins [78, 79]. The ATP-binding pocket of kinases is formed by a conserved arrangement of secondary structure elements and is

readily accessible to small-molecule inhibitors, making them attractive sites for inhibitor design. In fact, most of the kinase inhibitors discovered to date are designed to target this highly conserved binding pocket and are based on the mechanism of ATP competition [80]. However, many other proteins also have ATP binding sites and offer equal opportunity to be targeted by these inhibitors. Several studies have reported the discovery of additional targets for kinase inhibitors that are presumed to be selective, revealing their often broadly promiscuous nature [27, 61, 70, 81, 82]. Nevertheless, the discovery of these novel "off-targets" of kinase inhibitors has contributed immensely in understanding the diverse molecular interactions of drugs in cellular environment and has allowed the characterisation of expressed 'interactome' of a drug/inhibitor directly from cell extracts.

The use of immobilised kinase inhibitors for affinity purification of protein kinases was reported for the first time almost two decades ago [83]. In their study, Hidaka and colleagues covalently coupled the isoquinoline H-9 via its primary amino group to a linker extending from resin material and demonstrated chromatographic enrichment of kinase activities attributed to protein kinase C, as well as the cyclic AMP- and cyclic GMP-dependent protein kinases. However, it was only after the structural aspects of inhibitor binding were revealed by the discovery of cyclic AMP-dependent protein kinase co-crystal structure [84] and more structure-activity relationship data became available that direct covalent attachment of kinase inhibitors to affinity matrices could be efficiently achieved. With the maturation of MS methods for proteomics a true chemical proteomic method could be developed to more efficiently conduct large-scale screens for the detection of binding targets of kinase inhibitors [26, 27, 61, 69, 70, 81, 82, 85]. **Table 1.1** summarises the use of different kinase inhibitors for affinity enrichment in chemical proteomic studies. For example, Godl *et al.* identified targets of the widely used p38 kinase inhibitor SB 203580 [26]. They also identified several protein kinases that were bound to the

immobilized SU6668 derivative including aurora kinase A (AurA) and TBK1 [61]. In follow-up experiments the authors could show that a cell cycle block induced by SU6668 was caused by the inhibition of AurA and that SU6668 potently suppressed antiviral and inflammatory responses by interfering with TBK1-mediated signal transmission, thereby indicating the relevance of their findings. Similarly, Brehmer *et al.* used bisindolylmaleimide analogues for functional immobilization in combination with the specific purification of cellular binding proteins by affinity chromatography, leading to the identification of several known and previously unknown enzyme targets. More recently, linkable version of imatinib (a chronic myeloid leukaemia drug), and two second-generation drugs nilotinib and dasatinib that were originally developed for the inhibition of the fusion oncoprotein BCR-ABL were analyzed for their target spectrum in affinity precipitation experiments [62]. Imatinib is known for its remarkable selectivity for ABL (IC_{50}=100 ηM), KIT (IC_{50}=50 ηM) and PDGFR (IC_{50}=100 ηM) [86, 87]. Apart from the several kinase targets known and unknown that were characterised, this study also reported, strong binding of immobilized imatinib to the quinone oxidoreductase NQO2. The novel non-kinase target of imatinib was recently confirmed by a crystal structure of the imatinib–NQO2 complex [88]. For the related analog, nilotinib, discoidin receptor tyrosine kinase (DDR1) and ARG tyrosine kinase were identified as additional target proteins. Further, dasatinib developed as a dual-specificity ABL- and SRC-family kinase inhibitor [89] was found to bind a total of 24 protein kinases in experiments done with K562 cells.

Table 1.1: Summary of different kinase inhibitors used for affinity enrichment in CCCP

Author	Year	Kinase Inhibitor	Notes
Cuatrecasas *et al.* [66]	1968	Isoquinoline H-9	► Enrichment of kinase activities of protein kinase C, cyclic AMP- and cyclic GMP-dependent protein kinases.
Inagaki *et al.* [83]	1985	N-(2-Aminoethyl)-5-isoquinolinesulfonamide (H-9)	► Purification of Ca2+-activated, phospholipid-dependent and other protein kinases.
Haystead *et al.* [90]	1993	Gamma-phosphate-linked ATP-sepharose	►Rapid purification of skeletal muscle mitogen-activated protein kinase kinase.
Davies *et al.* [91]	1994	Gamma-phosphate-linked ATP-sepharose	►Purification of the AMP-activated protein kinase and analysis of its subunit structure.
Wymann *et al.* [92]	1996	Wortmannin-specific inhibitor of phosphoinositide (PI) 3-kinase	► Identified specific site (Lys-802) of interaction of wortmannin on the catalytic subunit of PI 3-kinase.
Kim *et al.* [93]	1997	ATP-sepharose	► One step affinity purification of nucleoside diphosphate kinases (NDP kinases) isoforms.
Tong *et al.* [60]	1997	Pyridinyl-imidazole	► Demonstrated the inhibitor to be specific for p38 mitogen-activated protein (MAP) kinase by crystal structure determination.
Knockaert *et al.* [69]	2000	Cyclin-dependent kinase (CDK) inhibitors: purvalanol B and N6-methylated, CDK-inactive derivative	► Using two purine derivatives facilitated isolation of a small set of highly purified kinases including CDK1, Erk 1, Erk2, CK1, CaMKII, and RS6K.
Graves *et al.* [49]	2002	Quinoline compounds	► First chemical proteomics approach with quinoline compounds. ► Identified quinoline-binding proteins. ► Aldehyde dehydrogenase 1 (ALDH1) and quinone reductase 2 (QR2) were reported as selective targets of quinoline.
Godl *et al.* [26]	2003	SB 203580-p38 kinase inhibitor	► Chemical proteomics approach using immobilised drugs to identify cellular kinase targets. ► Dramatic enrichment and identification of several previously unknown protein kinase targets of SB 203580.
Lolli *et al.* [70]	2003	PHA-539136-CDK2 inhibitor-cyclopropylpyrazol	► PHA-539136 interaction with different potencies with a number of kinases including CDK2,CDK1,p42MAPK and with various other proteins propionyl-CoA carboxylase, acylCoA dehydrogenase,enolase, tubulin and the Hsps.
Brehmer *et al.* [27]	2004	Bisindolylmaleimides (Bis)	►Proteome-wide identification of cellular targets of Bis. ►Protein kinases Ste20-related kinase and cyclin-dependent kinase 2 (CDK2) and the non-protein kinases adenosine kinase and quinone reductase type 2 as novel targets of bisindolylmaleimide inhibitors.
Wissing *et al.* [85]	2004	pyrido[2,3-d]pyrimidine-protein tyrosine kinases inhibitors	► Established an efficient proteomics method ► 30 human protein kinases affected by this class of compounds. ► Demonstrated inhibition of both p38 and RICK kinase activities in intact cells.
Bach *et al.* [71]	2005	Roscovitine-selective cyclin-dependent kinase inhibitor	► Immobilised Roscovitine and found protein kinases and unexpected non-protein kinase target, pyridoxal kinases.
Brehmer *et al.* [81]	2005	AX14596-Gefitinib derivative-epidermal growth factor receptor kinase inhibitor	► In addition to known target EGFR, identified, putative gefitinib targets such as the protein tyrosine kinases BRK, Yes, CSK, and EphB4 and the serine/threonine kinases RICK (also known as RIPK2, RIP2, and CARDIAK), GAK, CaMKII, Aurora A, JNK2 and p38.
Godl *et al.* [61]	2005	SU6668-anticancer drug	► Identified previously unknown targets of SU6668 including Aurora kinases and TANK-binding kinase 1.
Scholten *et al.* [52]	2006	2AHA-cAMP, 8AEA-cAMP, 2-AH-cGMP and 8AET-cGMP-Immobilized cyclic nucleotides	► MS identification of cAMP or cGMP binding proteins by sequential elution with ADP, GDP, cGMP, and/or cAMP. ► Specific pull-down of known cAMP/cGMP binding proteins such as cAMP and cGMP dependent protein kinases PKA and PKG, several phosphodiesterases and 6 AKAPs.

Bantscheff *et al.* [94]	2007	"Kinobeads"-immobilized 7 non-selective kinase inhibitors: Bis-(III) indolyl-maleimide Purvalanol B Staurosporine CZC8004 PD173955 analogs Sunitinib Vandetanib	► Quantitative Chemical proteomics using iTRAQ. ► Identified 174 and 183 protein kinases, from HeLa and K562 cells in single pull-down experiment. ► 307 non redundant protein kinases were identified from 14 different human and mouse cell lines. ► Kinobeads for quantitative profiling of three inhibitors [imatinib (Gleevec), dasatinib (Sprycel) and bosutinib] of the tyrosine kinase ABL and confirmed known targets including ABL and SRC family kinases and identifies novel targets of imatinib; the receptor tyrosine kinase DDR1 and the oxidoreductase NQO2 as novel targets.
Gharbi *et al.* [51]	2007	PI828-Analogue of phosphatidylinositol 3-kinases(PI3K) inhibitors,LY294002	► Study revealed the inhibitor binds to class I PI3Ks and other PI3K-related kinases, but also to novel targets seemingly unrelated to the PI3K family.
Patricelli *et al.* [40]	2007	Nucleotide (ATP/ADP) acyl phosphates	► Active-site labelling of conserved lysine residues in the ATP binding pocket of kinases. ► 4000 MS runs in more than 100 human, mouse, rat, and dog proteomes - 394 protein kinases were identified.
Rix *et al.* [62]	2007	Imatinib, Nilotinib and Dasatinib-BCR-ABL tyrosine kinase inhibitor drugs-	► Dasatinib bound in excess of 30 Tyr and Ser/Thr kinases. ► Receptor tyrosine kinase DDR1 was identified and validated as an additional major target of Nilotinib. ► The oxidoreductase NQO2 was bound and inhibited by imatinib and nilotinib - representing the first non-kinase target of these drugs.
Scholten *et al.* [95]	2007	Immobilized cAMP	► Enriched, isolated, and detected (protein kinase A) PKA and its low abundant interaction partners, like (A-kinase anchoring proteins) AKAPs. ► Detected 11 different AKAPs. ► Detected distinguishable phosphorylation patterns.
Daub *et al.* [96]	2008	Bis X, AX14596, SU6668, purvalanol B and VI16832	► Kinase selective enrichment. ► Quantitative phosphoproteomics (SILAC). ► Quantified 219 protein kinases from S and M phase-arrested human cancer cells with 1000 phosphorylation sites.
Aye *et al.* [97]	2009	three different immobilized cAMP analogs	► Affinity chromatography and mass spectrometry-based quantitative proteomics (SILAC) to investigate specificity in PKA-AKAP interactions. ► All four isoforms of the regulatory subunits of PKA enriched and concomitantly identified more than 10 AKAPs. ► Selective enrichment of the PKA RI and RII isoforms.
Ong *et al.* [98]	2009	Ro-31-7549 and SB202190 (selective kinase inhibitors) , K252a (broad-specificity kinase inhibitor)	► SILAC based quantitative approach with kinase affinity enrichment strategies. ► Improved sensitivity and specificity of unbiased affinity purification-based target identification methods.
Sharma *et al.* [99]	2009	Gefitinib(clinical kinase inhibitor) , AX14596 (immobilised derivative of gefitinib) , VI16742 (broadly selective kinase inhibitor)	► SILAC-based quantitative chemical proteomic strategy. ► Identify and quantify cellular target protein interaction with externally introduced ligands (small molecule kinase inhibitors, tyrosine-phosphorylated peptide and antibodies).

1.3.1.1. Bisindolylmaleimide (Bis) - potent inhibitors of Protein Kinase C

The Bisindolylmaleimide (Bis) family of small molecule inhibitors of PKC are structurally related to the marine alkaloid, Staurosporine, the most potent known natural product inhibitor of PKC (IC_{50}=10 ηM) [100]. The mechanism of inhibition of these small molecule inhibitors of PKC is through competitive interaction at the ATP binding site. PKC contains two domains: a regulatory domain which interacts with calcium,

phosphatidylserine, and diacylglycerol, and, a catalytic domain with ATP and protein substrate-binding sites. Both the regulatory and catalytic moieties of PKC have been considered as pharmacological targets for the design of inhibitors. For example, the inhibitors calphostin C (IC_{50} = 0.05 pM) and sphingosine (IC_{50} = 10 pM) has been described to interact with the regulatory moiety [101, 102], where as sangivamycin (IC_{50} = 11 pM), the isoquinoline H7 (IC_{50} = 6 pM), and staurosporine (IC50 = 10 ηM) has been reported to interact with the ATP binding site [103-105]. However, most of the reported inhibitors display poor selectivity both in vitro and in vivo, including Staurosporine (8, 11-13). Although, Staurosporine has been widely used to investigate the role of PKC in cellular responses [106-108], it is poorly selective when assessed against many other protein kinases [109, 110]. The same is true for other reported analogues of Staurosporine such as K252a [110]. **Figure 1.3** shows the structure of Staurosporine and K252a.

In order to improve the selectivity and retain the PKC inhibitory activity of this natural compound, several structurally related aminoalkyl Bis molecules were synthesised by Toullec *et al.* with IC_{50} values ranging from 5 to 70 ηM. Among all the molecules synthesised, the Bis analogue GF 109203X was one of the more potent and selective inhibitors of PKC with IC_{50} values same as Staurosporine (IC_{50}= 10 ηM) (**Figure 1.3**) [100]. However, the IC_{50} values for phosphorylase kinase and cAMP-dependent protein kinase was 0.7 and 2 μM respectively, indicating much greater selective inhibition of PKC by GF 109203X compared to Staurosporine.

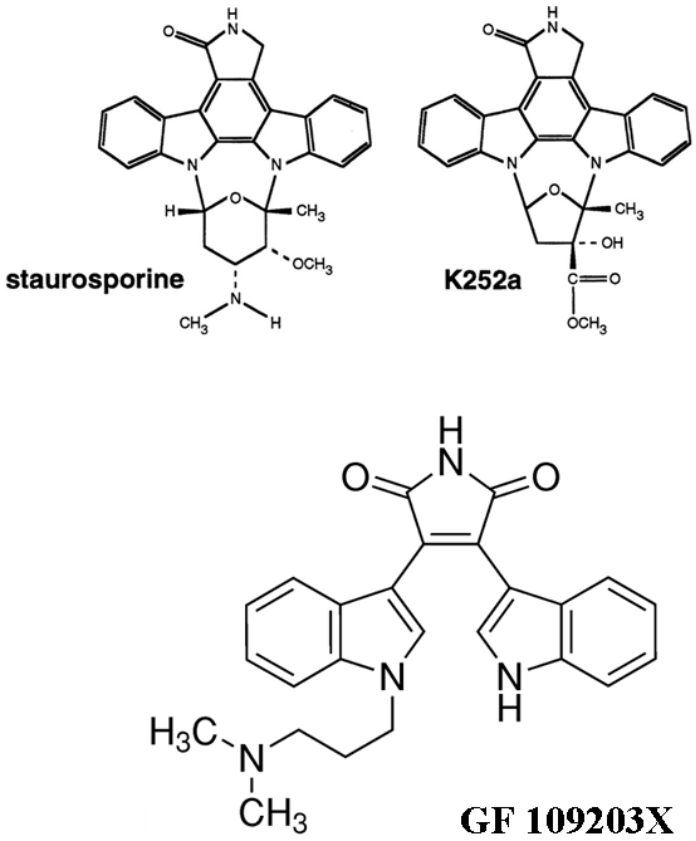

Figure 1.3: Structure of most potent Bis derivative GF 109203X [100], Staurosporine and its structural analogue K252a. Ref [111].

Several other studies have also reported the design and synthesis of series of novel Bis compounds based on the structural lead provided by Staurosporine and its related analogue K252a. For example, Davis *et al.* reported the improved potency of 2,3-Bisindolylmaleimides by a chloro substituent at the 5-position of one indole ring (IC_{50}= 0.11 μM) [112] and Bit *et al*. reported an introduction of cationic side chains (e.g. isothiourea) into these compounds for improved potency and selectivity [113].

More recently, studies have derivatised the widely used Bis inhibitors to obtain suitable compounds that could be used for immobilisation on chromatography beads, which would subsequently allow kinase affinity capture. One of the earliest studies used sepharose-linked Bis to purify RSK2 kinase from PC12 cell lysates by affinity chromatography [114]. Further, derivatised Bis has also been used for affinity purification and MS identification of kinase inhibitor selectivity on a proteome wide scale [27]. For example Brehmer *et al.*

incorporated minor chemical variations of the ligand and immobilised closely related analogues of GF 109203X (**Figure 1.4**) to identify cellular targets of Bis in HeLa cells.

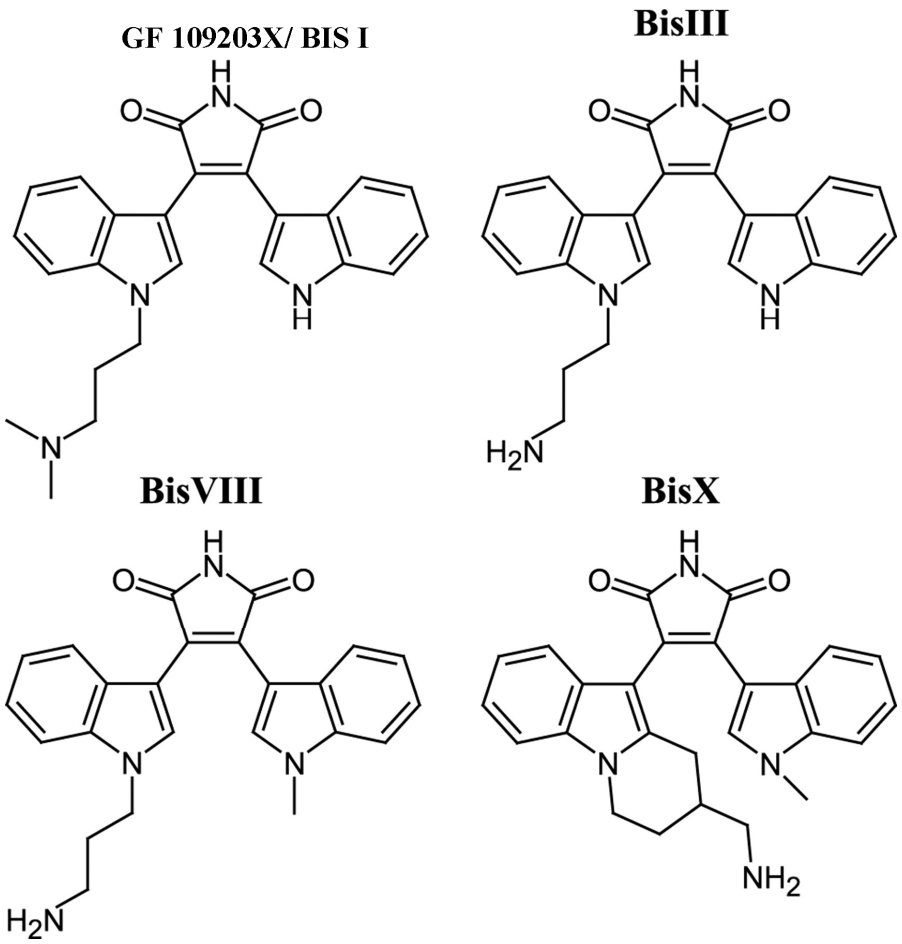

Figure 1.4: Chemical structure of Bis derivatives immobilised on sepharose beads for affinity purification. Bis I is identical to the widely used PKC inhibitor GF 109203X, Bis III, Bis VIII and Bis X are related derivatives. Ref [27].

Additionally, they demonstrated that small structural variations on the Bis scaffold of the immobilised ligand strongly affected the affinity matrices selectivity for cellular targets [27]. Similarly, another study coupled Bis to a peptide FLAG epitope for immunoprecipitation and mass spectrometry characterisation [115]. These studies showed that Bis inhibitors are rather promiscuous binders of protein kinases, and that this characteristic could be exploited to enrich these proteins from cell samples for proteomic analysis. With the increasing applications of suitable Bis derivatives in affinity purification

studies, these widely used PKC inhibitors can be used to design chemical probes and characterise Bis-targeted subproteomes in cell and tissue based models. The proteome wide MS characterisation of the Bis-enriched protein fractions would provide a comprehensive picture of the effects of this widely used class of signal transduction inhibitor.

1.3.2. Immobilised adenosine nucleotides for CCCP

The structure of a ternary complex of the catalytic subunit of cAMP-dependent protein kinase (cyclic A kinase), MgATP and a 20-residue inhibitor peptide reported by Sowadski enabled researchers to develop alternate strategies using ATP mimetics for affinity purification of kinases [116]. Haystead *et al.* were the first to report the covalent linkage of ATP to sepharose through its γ phosphate and demonstrated the effectiveness of adenosine-5′-(γ-4-aminophenyl) triphosphate–Sepharose as an affinity column for protein kinases, by affinity purification of rabbit skeletal muscle mitogen-activated protein kinase kinase [90]. Subsequently, several studies have demonstrated the rapid purification and characterisation of ATP binding protein targets including kinases using immobilised ATP sepharose [49, 91, 93]. Further, Graves *et al.* demonstrated a functional proteomics approach to characterise purine binding proteome captured with gamma-phosphate-linked ATP-Sepharose [49]. In their approach, they first used the ATP-affinity matrix to enrich ATP-binding proteins and then incubated the matrix with increasing amounts of the compound of interest to illustrate elution in a dose dependent manner. Furthermore, in a variation to this approach, Patricelli *et al.* used biotin derivatives of acyl-phosphate containing ATP/ADP to covalently modify ATP binding proteins and characterised hundreds of kinases and other ATP binding proteins [40].

1.3.3. Cyclic nucleotides as kinase inhibitors for CCCP

As an alternative to ATP mimetics, kinase inhibitors have also been designed for CCCP to bind to allosteric and cofactor binding sites. In a recent study, Scholten and co-workers investigated the specific interactome of four differently immobilized cyclic nucleotides (2AHA-cAMP, 8AEA-cAMP, 2-AH-cGMP and 8AET-cGMP) to assess cAMP-dependent protein kinase (PKA) targeting efficiency of the beads and evaluate cross-reactivity [95]. Their chemical proteomics approach allowed the efficient enrichment of the generally low abundant cAMP signalling proteins, and their interactors, directly from mouse ventricular tissue. More recently, Aye *et al.* employed a combination of affinity chromatography and mass spectrometry-based quantitative proteomics (SILAC) to investigate specificity in protein kinase A (PKA)-A kinase anchoring proteins (AKAP) interactions [97]. They used three different immobilized cAMP analogs to enrich PKA and its interacting proteins from several systems; HEK293 and RCC10 cells and rat lung and testis tissues. This approach allowed them to enrich all four isoforms of the regulatory subunits of PKA and concomitantly identify more than 10 AKAPs.

1.4. Characterisation of Chemical probes by radioactive binding assays

Radioactivity offers the most sensitive option to characterise newly synthesised chemical probes by measuring binding affinity and enzyme inhibitory activity. Initially, radioactive competitive experiments are performed to access the binding affinity of the probes for its receptor enzyme and the affinity is compared with the affinities of control probe (Linker and tag only) and commercially available inhibitors. The affinity of the receptor for the competing inhibitor is usually quantified as the equilibrium dissociation constant, K_i. Afterwards radioactive steady state assays are performed to measure the inhibition of enzyme activity by the probe. The inhibition of enzyme activity is quantified by measuring the IC_{50} values, which is the concentration at which 50% of enzyme binding sites are

competitively occupied by the inhibitor. Relative IC_{50} of the probes are determined with regards to free inhibitor in presence of appropriate concentrations of substrate.

1.4.1. Competitive binding assays

Competitive experiments are performed to test the affinity of the newly synthesised probes for its receptor enzyme and are compared with the affinity of the free inhibitor and control probe. As most of the ligands/inhibitors for the receptors are non-radioactive, there is no way to directly measure their affinity for the receptor. Hence, the affinity of the unlabelled ligand/inhibitor for the receptor is determined indirectly by measuring its ability to compete with a radio ligand. In a competitive experiment increasing concentrations of the unlabelled ligand/inhibitor are allowed to compete against a fixed concentration of radioligand. As the concentration of the unlabelled ligand/inhibitor increases the amount of radioligand bound to the receptor decreases as illustrated in **Figure 1.5A&B**. Various concentrations of the unlabelled ligand/inhibitor (chemical probe, control probe and free inhibitor) are allowed to compete with a fixed concentration of radiolabelled ligand (*e.g.* γ-P^{32}ATP) for its receptor (*e.g.* Protein Kinase Cα). Measuring the decreasing CPM counts with increasing inhibitor concentration can then be used to determine the affinity of the receptor for the competing inhibitor and the equilibrium dissociation constant, K_i can be determined.

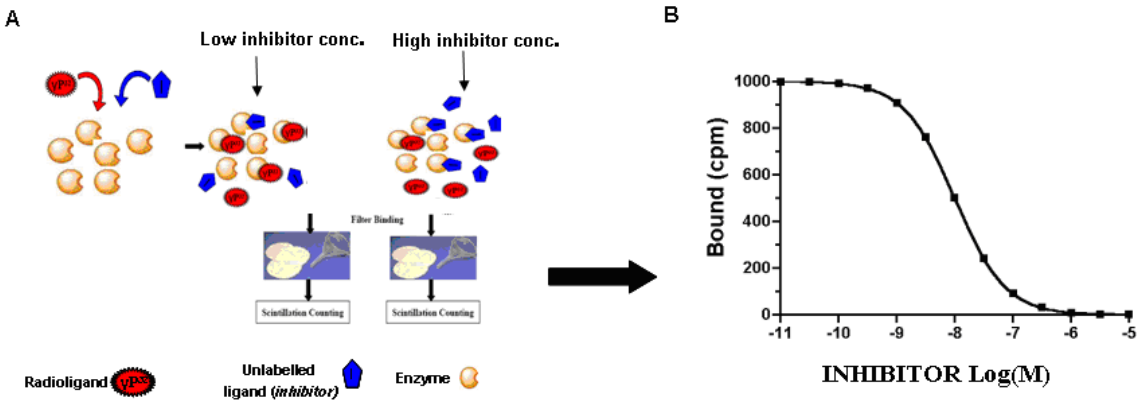

Figure 1.5: (A) Competitive binding experiments to determine the affinity of the receptor (enzyme) for the competing inhibitor (probe/free inhibitor) and measure the equilibrium dissociation constant, K_i. Fixed

concentration of radioligand and increasing concentration of probe/inhibitor (non-labelled) are used to determine the affinity of the probe/inhibitor. The CPM counts are determined by filter binding and scintillation counting. **(B)** Nonlinear regression analysis of CPM counts at a particular concentration of the inhibitor. The Y-axis represents the CPM counts at various log molar concentrations of the inhibitor (X-axis). No inhibitor, CPM count = 1000; 100% inhibition CPM count ~ 0.

1.4.2. Steady state kinase assays

Chemical probes, particularly probes bearing a kinase inhibitor as RG, can be characterised by a radioactive steady state kinase binding assay [117] designed to measure inhibition of protein kinase activity by the probe. In a steady state kinase assay increasing concentrations of the unlabelled ligand/inhibitor are allowed to compete against a fixed concentration of radioligand for the receptor kinase. The substrate phosphorylation is then measured to assess the inhibition of kinase activity by the inhibitor under steady state conditions. As the concentration of the unlabelled ligand/inhibitor increases, the amount of radioligand bound to the receptor decreases, which consequently deceases the substrate phosphorylation as illustrated in **Figure 1.6A&B**.

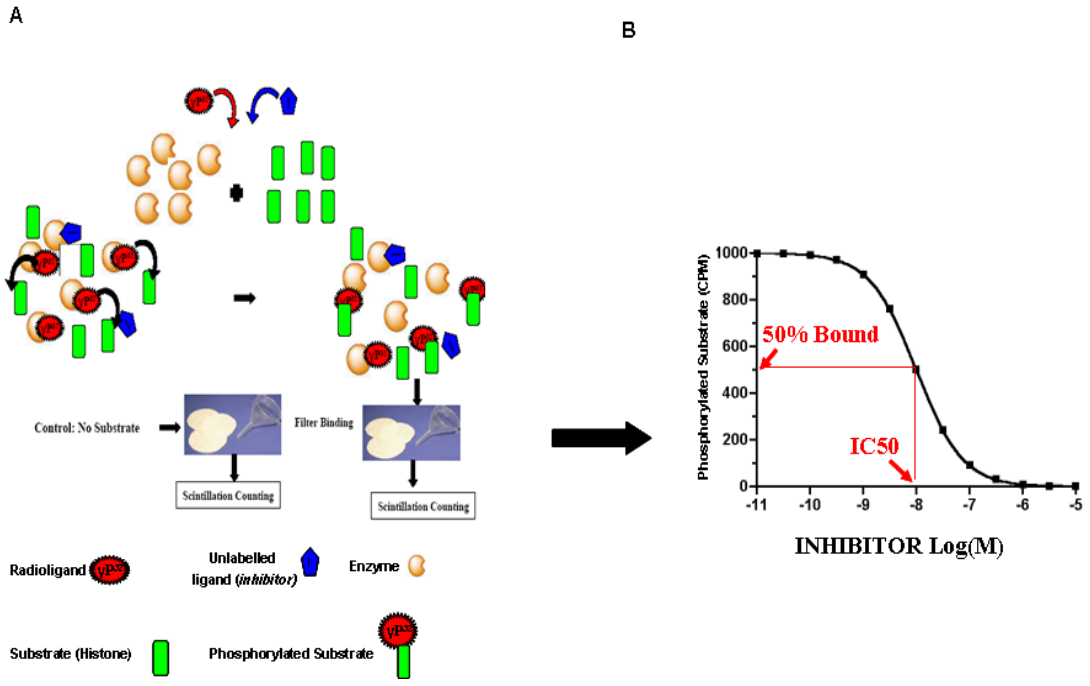

Figure 1.6: (A) Steady state kinase assay to measure enzyme inhibitory activity by chemical probe. Increasing concentration of the inhibitor would decrease the radioligand binding to the receptor enzyme, which would eventually decrease the transfer of the radioactive phosphate to the substrate. Measuring the CPM counts of the phosphorylated substrate at different concentration of the inhibitor in steady state condition would enable assessment of inhibitory enzyme activity of a drug/inhibitor. **(B)** Nonlinear regression analysis of CPM counts of the phosphorylated substrate at a particular concentration of the inhibitor. The Y-axis represents the CPM counts at various log molar concentrations of the inhibitor (X-axis).

No inhibitor, CPM count = 1000; 100% inhibition CPM count ~ 0. The concentration of the inhibitor where 50% inhibition is achieved is considered as the IC_{50}.

Measuring the CPM counts of the phosphorylated substrate at different concentration of the inhibitor in steady state condition enables assessment of inhibitory enzyme activity IC_{50} of a drug/inhibitor.

1.5. Quantitative Strategies in chemical proteomics

MS-based proteomic approaches using immobilised kinase inhibitors for protein enrichment and identification have been successfully used to identify the cellular targets of kinase inhibitors (Section 1.2.4.1). However, to rank and prioritize molecular interactions, quantitative information is important to identify the strongest molecular associations. Usually, the strongest molecular associations are likely to be the most relevant in physiological conditions and quantitative information allows discarding the non-specific interactors, which usually have very low inhibitor affinities. Further, quantitative approaches also enable the differential capture of specific protein targets in probe enriched proteomes in treated compared with control biological systems or in healthy compared with diseased biological specimens. Among the many MS-based methods applied for protein quantification, isobaric tagging for relative and absolute quantitation (iTRAQ) and stable isotope labelling in cell culture (SILAC) have become key approaches used in chemical proteomics. As an alternative the relatively simple approach of spectral counting [118, 119] has been reported.

1.5.1. Isobaric Tagging for Relative and Absolute Quantitation (iTRAQ)

Isobaric Tagging for Relative and Absolute Quantitation (iTRAQ) is a chemical derivatization based MS protein quantitation strategy that allows sample multiplexing and enables relative quantitation and identification of proteins within a single MS experiment. A typical iTRAQ workflow and quantitation output is shown in **Figure 1.7**. In the iTRAQ

method, peptides are derivatised with chemical isobaric tags that consist of a charged reporter group, a peptide reactive group and a neutral balance group to maintain and equal overall mass through the elegant use of chemical isotopes, which is useful for the determination of the precursor peptide [120]. The iTRAQ label employs *N*-hydroxysuccinimide (NHS) chemistry to label peptide free amines on the epsilon amino group of lysine residues [121]. When combined with tryptic digestion this approach ensures expansive peptide coverage for any given protein with either 2 iTRAQ labels (Lys terminating peptide) or 1 label (Arg terminating peptide). The structure of the reporter groups used in iTRAQ labels give rise to unique product ions in the mass regions 114-117 *m/z* (for a 4-plex iTRAQ assay) and 113-121 *m/z* (for an 8-plex iTRAQ assay). This low molecular mass range has been shown to have minimal contamination with low mass fragments produced from CID of peptides, with the exception of *m/z* 120 which is the immonium ion of phenylalanine [120, 122]. Following CID fragmentation, the iTRAQ reporter groups are detected in the low mass region as distinct peaks while all other sequence informative fragment ions remain isobaric. Quantitation of iTRAQ labelled peptides is performed by integration of iTRAQ reporter ion peak areas whose abundance is directly proportional to the relative concentration of the labelled peptide. The relative protein abundances can be deduced by calculating individual peptide abundances [120].

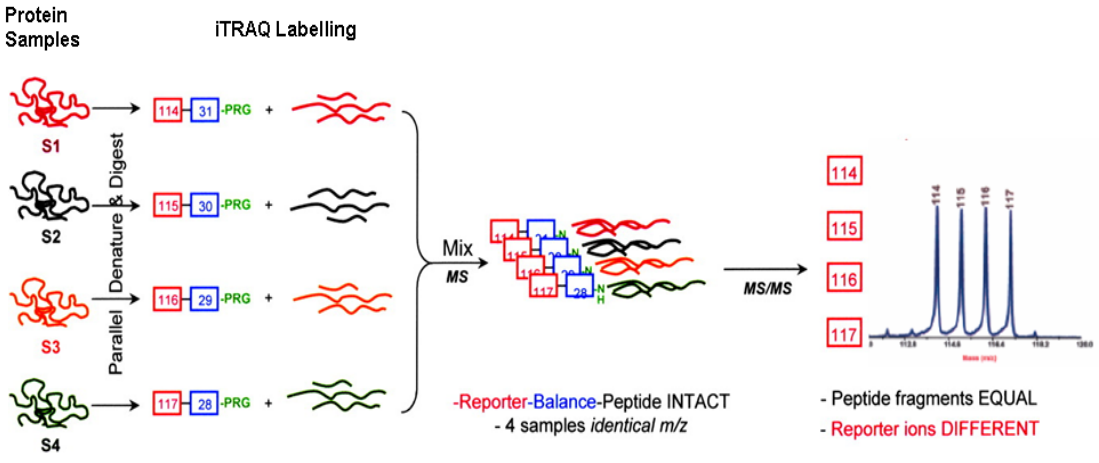

Figure 1.7: Schematic of a representative 4-plex iTRAQ workflow. Peptides from different experimental conditions are labelled separately with representative iTRAQ labels and mixed. Following LC-MS/MS, the

intensities of the reporter peaks from tandem MS spectra are directly correlated to relative abundance for a given peptide. Ref [122].

1.5.1.1. iTRAQ analysis in chemical proteomics

Quantitative analysis using the iTRAQ strategy is increasingly finding novel applications in chemical proteomics. A chemical proteomics strategy for the quantitative monitoring of dose-dependent inhibitor effects on target protein binding to a mixed broad specificity kinase inhibitor matrix ("Kinobeads"), using iTRAQ was reported by Bantscheff *et al.* [94]. In this approach "kinobeads"containing 7 non-selective kinase inhibitors: Bis-(III), Purvalanol B, Staurosporine, CZC8004, PD173955 analogs, Sunitinib, and Vandetanib were used to profile hundreds of endogenously expressed protein kinases and purine-binding proteins. 146 of the bound protein kinases were quantified in parallel by mass spectrometry using the iTRAQ approach. "Kinobeads" were also used for quantitative profiling of three drug inhibitors imatinib (Gleevec), dasatinib (Sprycel) and bosutinib. Dose-dependent inhibitor effects on the probe captured kinase targets were quantitatively monitored by increasing concentration of the free, unmodified kinase inhibitors. Consequently, the reduced binding of the cellular targets to kinobeads resulted in decreased iTRAQ ion intensity for peptides derived from the target protein as shown in **Figure 1.8**.

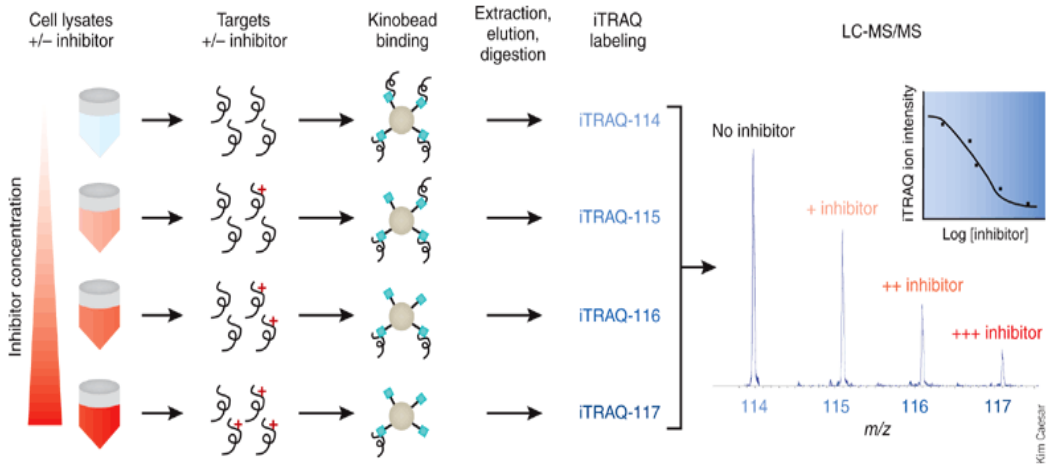

Figure 1.8: Increasing concentration of a free, unmodified kinase inhibitor is associated with reduced binding of its cellular targets to "kinobeads". Consequently, there is decreased iTRAQ ion intensity for

peptides derived from the target protein. IC_{50} values for proteins retained on the "kinobeads" are calculated by quantification of iTRAQ-marker ion intensities for multiple inhibitor concentrations by LC-MS/MS. Adopted from Ref [94].

Further, IC_{50} values for proteins retained on the kinobeads were also calculated by quantification of iTRAQ-marker ion intensities for multiple inhibitor concentrations by LC-MS/MS (**Figure 1.8**).

1.5.2. Stable Isotope Labelling with Amino Acids in Cell Culture (SILAC)

Protein quantitation employing Stable Isotope Labelling with Amino Acids in Cell culture (SILAC) involves the use of selected isotopically labelled amino acids added to cell culture media. Labelled amino acids can be incorporated into newly synthesised proteins in proliferating cells, enabling their selective detection and MS-based quantitation [123]. Typically, ^{14}N and ^{12}C atoms are replaced by ^{15}N and ^{13}C atoms in specific amino acids and are generally referred to as 'heavy' amino acids. By mixing heavy labelled samples with samples cultured in standard amino acid (light) media, comparisons between peptides abundances can be performed by mass spectrometry and relative protein concentrations determined. A representative SILAC workflow is shown in **Figure 1.9**. Cell cultures are typically grown in parallel, in light and heavy media, and once completely labelled; cells can be either subjected to an external perturbation or directly mixed in equal proportions prior to sample preparation and MS analysis. Therefore SILAC quantitation eliminates sample inconsistencies due to independent handling, and enables the multiplexing of at least two samples in the same experiment [124]. For proteomic workflows, which typically use trypsin to generate peptides, the use of lysine and arginine as labelled amino acids are well suited.

Following MS analysis of SILAC labelled peptides, quantitation of proteins is achieved by an integrated measurement of the MS precursor peptide peak. Heavy lysine labelled

peptides result in a 6 Da shift in *m/z* compared to the same peptide carrying a light label, while heavy arginine labelled peptides give rise to a 10 Da shift in *m/z* in the MS survey scan. Relative abundance can be determined by a calculated measurement of the areas for each light and heavy peptide as well as spectral counting [125]. Protein ratios can be calculated by a mean of all detected peptide ratios, or alternatively by an abundance based weighted average of detected peptides [121].

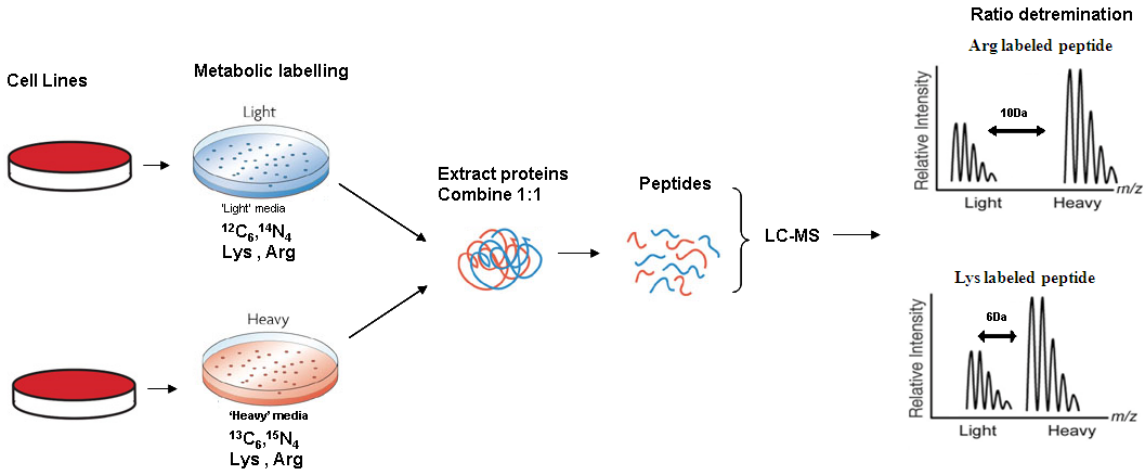

Figure 1.9: Schematic of a representative of a SILAC workflow. Different experimental cell types (or subjected to different perturbations) are grown in heavy or light media until >99% of the proteome is metabolically labelled. Following cell lysis, samples are mixed and analysed by LC-MS. Relative peptide ratios are determined by precursor ion peak integration. A heavy labelled arginine peptide exhibits a 10 Da shift in *m/z* when compared to the light arginine while a heavy labelled lysine exhibits a 6 Da shift in *m/z* when compared to light lysine.

Several advantages of SILAC include the sequential combination of identification and quantitation in one step, no adverse effects on growing cells or chemical additions that may affect MS analysis, and > 99 % proteome wide labelling of most cell lines grown in heavy amino acid supplemented medium after 6-8 passages [123]. However, some cell lines require careful measurement with respect to the amount of heavy arginine added to the medium in order to prevent excess arginine being converted to proline, complicating subsequent analysis [126].

1.5.2.1. SILAC analysis in Chemical proteomics

Several studies have efficiently integrated SILAC quantitation strategy with chemical proteomics to analyze quantitative changes of the protein targets captured by small molecule inhibitors [96, 98, 99]. Daub *et al.* combined kinase-selective affinity purification with SILAC based quantitative mass spectrometry to analyze the cell-cycle regulation of protein kinases. In their study, they demonstrated the capture of a large proportion of the protein kinase complement ("Kinome") of HeLa cells by serial drug affinity chromatography with five different immobilized kinase inhibitors (bisindolylmaleimide X, AX14596, SU6668, purvalanol B and VI16832) with distinct, overlapping kinase binding profiles. Further, they integrated the SILAC strategy to compare the expressed kinome from two different cell cycle stages (M and S) in a quantitative fashion. This proteomics approach enabled them to quantify 219 protein kinases from S and M phase-arrested human cancer cells. They also integrated a phosphoproteomic approach and identified more than 1000 phosphorylation sites on protein kinases, half of which were unregulated in mitosis. Their data also revealed numerous unknown M phase-induced phosphorylation sites on kinases with established mitotic functions.

Interestingly, Ong *et al.* used a SILAC based quantitative approach with kinase affinity enrichment strategies and reported improved sensitivity and specificity of unbiased affinity purification-based target identification methods [98]. They include three small molecule inhibitors, 2 selective kinase inhibitors, Ro-31-7549 and SB202190 and a broad-specificity kinase inhibitor, K252a, in their affinity enrichment studies. They creatively used SILAC to quantitatively differentiate the specific small molecule binders from the non-specific binders. The light labelled cell populations were lysed and incubated with the chemical probe immobilised beads along with free inhibitor. The heavy cell lysates were incubated with the chemical probe immobilised beads alone. Affinity purification and subsequent

MS-characterisation enabled them to comprehensively identify the specific SM binding proteins from the non-specific binders as shown in **Figure 1.10**.

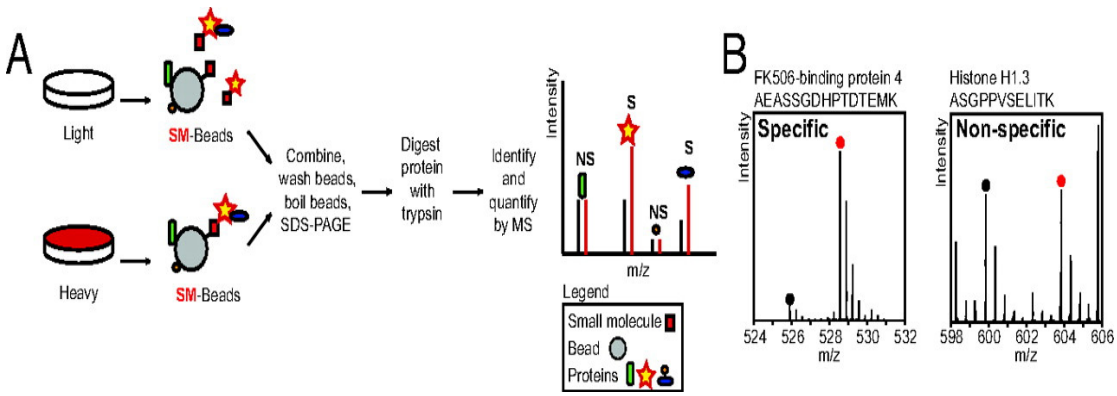

Figure 1.10: SILAC based identification of specific small molecule inhibitor-protein interactions. **(A)** Cell populations labelled with light (black) and heavy amino acids (red) were lysed and incubated either with small molecule inhibitor loaded beads (SM-Beads)+soluble small molecule (SM) competitor (light) or SM-Beads alone (heavy). Proteins interacting directly with the SM or via secondary and/or higher order interactions (marked "S" for specific) will be enriched in the heavy state over the light and will be identified with differential ratios. Nonspecific (NS) interactions of proteins will be enriched equally in both states and have ratios close to 1. **(B)** MS spectra of representative SILAC labelled peptides showing specific and non-specific binders, respectively. Adopted from ref [98].

1.5.3. Relative Quantification by Spectral Count

Relative protein quantification by spectral counting is a facile approach that is conducted by simply counting the number of identified MS/MS spectra from the same protein, and comparing this across multiple LC-MS/MS runs. An increase in protein abundance is typically reflected by an increase in the number of its proteolytic peptides, (and vice versa), and usually results in an increase in protein sequence coverage, the number of identified unique peptides, and the number of identified total MS/MS spectra (spectral count) for each protein [118]. Liu *et al*. conducted correlation studies between relative protein abundance and sequence coverage, peptide number, and spectral count [127]. They reported that among all the factors of identification, only spectral count showed strong linear correlation with relative protein abundance (r^2 = 0.9997) with a dynamic range over 2 orders of magnitude. Further, comparative studies using spectral counting-based method and $^{15}N/^{14}N$ isotope labelled, ion chromatographic method for relative quantification

revealed a strong correlation when the peptides with high signal-to-noise ratio in the extracted ion chromatogram were used in the comparison [128]. Furthermore, the run-to-run variability in quantification strategies was also accounted for, by suitable normalization and statistical analysis [129]. Moreover, a normalized spectral abundance factor (NSAF) has been defined to account for the effect of protein length on spectral count [130, 131]. For a recent review see [132].

1.6. Aims and Scope of the projects

The overall aim of this thesis was to develop a robust chemical proteomics method to characterise and quantitate cellular protein targets of a bisindolylmaleimide (Bis) chemical probe and apply it for biomedical investigation. The optimised chemical proteomics platform using the Bis-probe would be used to examine:

- Cell line model of basal breast cancer to examine the effect of phorbol ester stimulation.
- Tissue based mouse models of cancer cachexia to compare the liver of cachectic mice (high IL-6) with non-cachectic (low IL-6) and control mice (no tumour).
- Neural differentiation of human adipose derived stem cells.

Finally the use of a recently commercially available active-site directed ATP probe was used in a basal breast cancer cell line to compare and contrast results obtained with Bis-probe.

Chapter 2: Chemical Proteomics method development

This Chapter describes the characterisation of Bis-probes and optimisation of chemical proteomics methods. Bead washing conditions, effect of washing on protein interaction with the control probes and different elution protocols for affinity enrichment are determined. A method for mass spectrometry analysis was developed.

Syntheses of the Bis-probes were carried out by Ms. Qiang Xu and Dr. Fei Liu, Department of Chemistry and Biomolecular Science, Macquarie University. All other work was my own.

2.1. Methods

2.1.1. Synthesis of Bis-probes

Bisindolylmaleimide VIII acetate salt (Sigma-Aldrich, MO) (5 mg, 11 μM) was treated with 2 ml of 50 μM Na_2CO_3, solution and then extracted with dichloromethane (DCM) (3 x 2 ml). The combined organic layers were dried and dissolved in 1 ml of DMSO. TFP-PEO-biotin (Pierce Biotechnology, Rockford, IL) (10 mg, 11 μM) was added to the DMSO solution and stirred at 4˚C overnight. The resulting mixture was lyophilised and redissolved in methanol for reverse-phase HPLC purification (60% methanol / 40% H_2O with 0.1% TFA) to provide probe **1** (Bis-probe) in 62% yield (**Figure 2.1A**). **1** was characterised by LC-MS (calculated $C_{48}H_{63}N_8O_9S$ MH^+ *m/z* 927 and $C_{48}H_{64}N_8O_9S^{2+}$ MH_2^{2+} *m/z* 464; found MH^+ *m/z* 927 and MH_2^{2+} *m/z* 464).

For the synthesis of probe **2** (control-probe), I-PEO-biotin (Pierce Biotechnology, Rockford, IL) (11 mg, 20 μmol) was dissolved in DMF (300 μL), followed by the addition of isopropylamine (1.2 mg, 20 μM). The mixture was stirred overnight and then lyophilised. The crude mixture was purified by reverse phase preparative TLC (80% MeOH/20% H_2O) to provide **2** in 50% isolated yield (calculated $C_{21}H_{40}N_5O_5S$ MH^+ m/z 474; found 474) (**Figure 2.1B**).

A

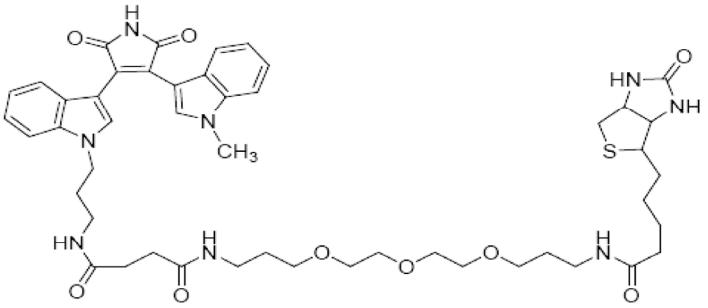

B

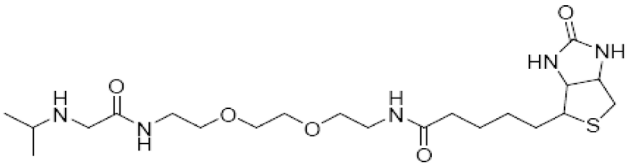

Figure 2.1: (A) Bisindolylmaleimide (Bis) probe (**1**) with polyethylene oxide linker and biotin affinity group, **(B)** Biotin linker control probe (**2**).

2.1.2. Characterisation of the Bis-probe

2.1.2.1. Competition assays

All competition studies were performed using 25 ηg of purified protein kinase C α (PKCα) (Sigma Aldrich). Purified PKCα was diluted to a final concentration of 10 ηg/µl using dilution buffer (10 mM HEPES, pH 7.4, 5 mM DTT, 0.01% Triton X-100) and was stored in ice. Ten different inhibitor concentrations ranging from 0.3 ηM to 10 µM for Bis-probe, control probe and Bis VIII were prepared in 10% DMSO. For each competition experiment 2.5 µl of PKCα solution was added to 15 µl of activation mix (20 mM HEPES, 10 mM $MgCl_2$, 0.1 mM $CaCl_2$) and 10 µl of lipid mix (100 µl of 10 mg/ml phosphatidylserine (PS) and 100 µl of 2 mg/ml diacylglycerol (DAG), dried and resuspend in 1 ml of resuspension buffer (10 mM HEPES, pH 7.4, 0.3% Triton X-100 at 40°C for 5 min). Appropriate concentration of inhibitor solutions and blanks along with MilliQ water were added to a final volume of 100 µl. The reaction was initiated by adding 5 ηM of γ^{32}P-ATP (PerkinElmer, MA) and incubating the assay tube at 37°C for 40 min.

2.1.2.2. Steady state kinase assays

For steady state kinase assays different concentrations of Bis-probe or Bis VIII (as described above) in 20 mM HEPES, 10 mM $MgCl_2$, 0.1 mM $CaCl_2$, 0.1 $mgmL^{-1}$ phosphatidylserine, 0.02 $mgmL^{-1}$ diacylglycerol, were added to histone H1 (5 μM) and PKCα (10 ηM). The reaction was initiated by adding ATP to a final concentration of 50 μM including approximately 0.2 $\mu Ci\mu L^{-1}$ γ^{32}P-ATP (PerkinElmer, MA) and terminated after incubation at 37°C for 40 min.

The assay for each inhibitor concentration for a particular inhibitor was conducted in duplicates and each assay had appropriate filter paper controls to measure the non-specific binding. The contents of each assay tube were filtered through a Whatman membrane after the reaction was terminated using 10% TCA (ice-cold). The membrane was then washed with 5% TCA (ice-cold) thrice before a final wash with ice-cold ethanol. The membranes were then transferred to scintillation vials and 5 ml of scintillation cocktail (PerkinElmer, MA) was added. The counts per minute (CPM) were determined with a Packard Tri-Carb liquid scintillation counter using the direct DPM programme.

After the CPM counts were obtained for each of the inhibitor concentrations in both the competition and steady state experiments, nonlinear regression analysis and competitive binding curve fitting was performed to determine K_i and relative IC_{50} for the different inhibitors using Prism software suite (version 5.03; GraphPad Software Inc, San Diego, California). IC_{50} values were defined to be the concentration of inhibitor at which CPM was 50% of the control sample, corrected by the background [117]. Competitive binding curves in the GraphPad Software are described by the following equation and nonlinear regression is used to fit the competitive binding curve to determine the log(IC_{50}).

$$Y = \text{Nonspecific} + \frac{(\text{Total} - \text{Nonspecific})}{1 + 10^{\log[D] - \log(IC50)}}$$

- Y is the total binding measured in the presence of various concentrations of the unlabeled drug. Y, Total and Nonspecific are allexpressed in the same units, such as cpm, fmol/mg, or sites/cell.
- log[D] is the logarithm of the concentration of competitor plotted on the X axis.
- Nonspecific is binding in the presence of a saturating concentration of D.
- Total is the binding in the absence of competitor.

The K_i is then determined from the IC_{50} using the equation of Cheng and Prusoff [133].

$$K_i = \frac{IC_{50}}{1 + \frac{[\text{radioligand}]}{K_d}}$$

- K_i is the equilibrium dissociation constant for binding of the unlabeled drug
- K_d is the affinity of the radioligand for the receptor
- [radioligand] is the concentration of the radioligand

2.1.3. Chemical Proteomics Method Development

The chemical proteomics method development using Bis-probes was performed using MDA-MB-231 cells. The growth, maintenance, phorbol ester (PMA) stimulation and SILAC labelling of cells along with Bis-probe Affinity pull down, MS sample preparation and Mass spectrometry are described in Chapter 3, Section 2 (Dolai *et al.*, Proteomics, Accepted [134]).

2.1.3.1. Effect of different elutions

The Bis-probe captured proteins in MDA-MB-231 cell lysates were affinity purified using avidin agarose beads and washed thrice with the wash buffer. For ATP elution, the beads

were incubated in 50 mM ATP in ammonium bicarbonate for 15 min twice and the eluate was pooled. Similar conditions were used for glycine elution with 100 mM glycine, pH 2.5. The pooled eluates from both ATP and glycine elution were separated on a 10% NuPAGE gel under reducing conditions and transferred onto a nitrocellulose membrane. Immunobloting was performed with 1:1000 dilution PKCα antibody. Control experiments using beads and control probe were also conducted.

2.1.3.2. Effect of washing condition

2.1.3.2.1. Beads

50 µl of avidin agarose beads (Sigma Aldrich, MO), with a binding capacity of 27 µg/ml, was incubated with MDA-MB-231 cell lysates for 1 h at 4°C. The beads were washed thrice with 500 µl of wash buffer (PBS containing 1% Triton X-100) for 5 min each on a rotor at 4ºC. Each time the beads were collected by centrifugation (1000 *g*, 5 min, and 4°C) and the bead captured proteins were eluted from the beads with 2 x LDS (65°C, 5 min). The proteins interacting with the beads were assessed by visualising the protein bands on a gel. The eluates were run in a 10% NuPAGE gel (Invitrogen, Carlsbad, CA) and stained with SYPRO Ruby protein gel stain (Molecular Probes, Eugene, OR, USA).

2.1.3.2.2. Control probes

MDA-MB-231 cell lysate sample was incubated with 10 µM of control probes (linker + biotin tag) and affinity purified with 50 µl of avidin agarose beads as described in Chapter 3, Section 2. The control probe captured proteins were eluted from the beads with 2 x LDS (65°C, 5 min) after every wash with the detergent based wash solution to assess the protein interaction with the linker and the biotin tags. The washing conditions were the same as described in Section 2.1.3.4.1. The eluates were run in a 10% NuPAGE gel (Invitrogen, Carlsbad, CA) and stained with SYPRO Ruby protein gel stain (Molecular Probes, Eugene,

OR, USA). Immunoblotting of the eluted sample after every wash was performed with PKC α antibody as described in Chapter 3, Section 2.

2.2. Results

2.2.1. Bis-probe

The Bis-probe harbours a Bisindolylmaleimide (Bis) reactive group for targeting protein kinases. Bisindolylmaleimides are strong inhibitors of serine-threonine family of protein kinases and kinase inhibition is through competitive interaction at the ATP binding site. For purification of the Bis-labelled proteins, a biotin tag is attached through a polyethylene oxide linker at a position that does not interfere with binding (**Figure 2.1A**). The spatial linker between the inhibitor and the biotin tag enables specific interaction between the inhibitor and the protein targets with limited steric hindrance and increases access of the tag for affinity purification. The choice of linker has a profound influence on the non-specific interaction [135] and hydrophilic spacers have been shown to improve sample quality [71, 136].

Similarly a control probe was designed containing only the linker and biotin affinity tag (**Figure 2.1B**). The control probe was used to assess all non-specific interactions that occur with the probe backbone. All Bis-probe pull down experiments described in this thesis had the control probes and beads as negative controls to assess non-specific binding.

2.2.2. Characterisation of the Bis-probes

2.2.2.1. Competition assays

The affinity of the Bis-probe for PKCα was initially assessed by allowing different concentrations of the probe to compete with a fixed concentration of the radioactive ligand γ^{32}P-ATP. The affinity of the receptor for the competing Bis-probe inhibitor was quantified by calculating the equilibrium dissociation constant, K_i. At 5 ηM γ^{32} P-ATP the affinity of

the Bis VIII inhibitor was 8.7 ηM (**Figure 2.2A**), while the affinity of Bis-probe for PKCα was calculated to be 82 ηM (**Figure 2.2B**). The affinity of the control probe was calculated to be 4.4 μM (**Figure 2.2C**). The affinity of the Bis-probe was 10 fold lower than the free inhibitor, consistent with literature [115].

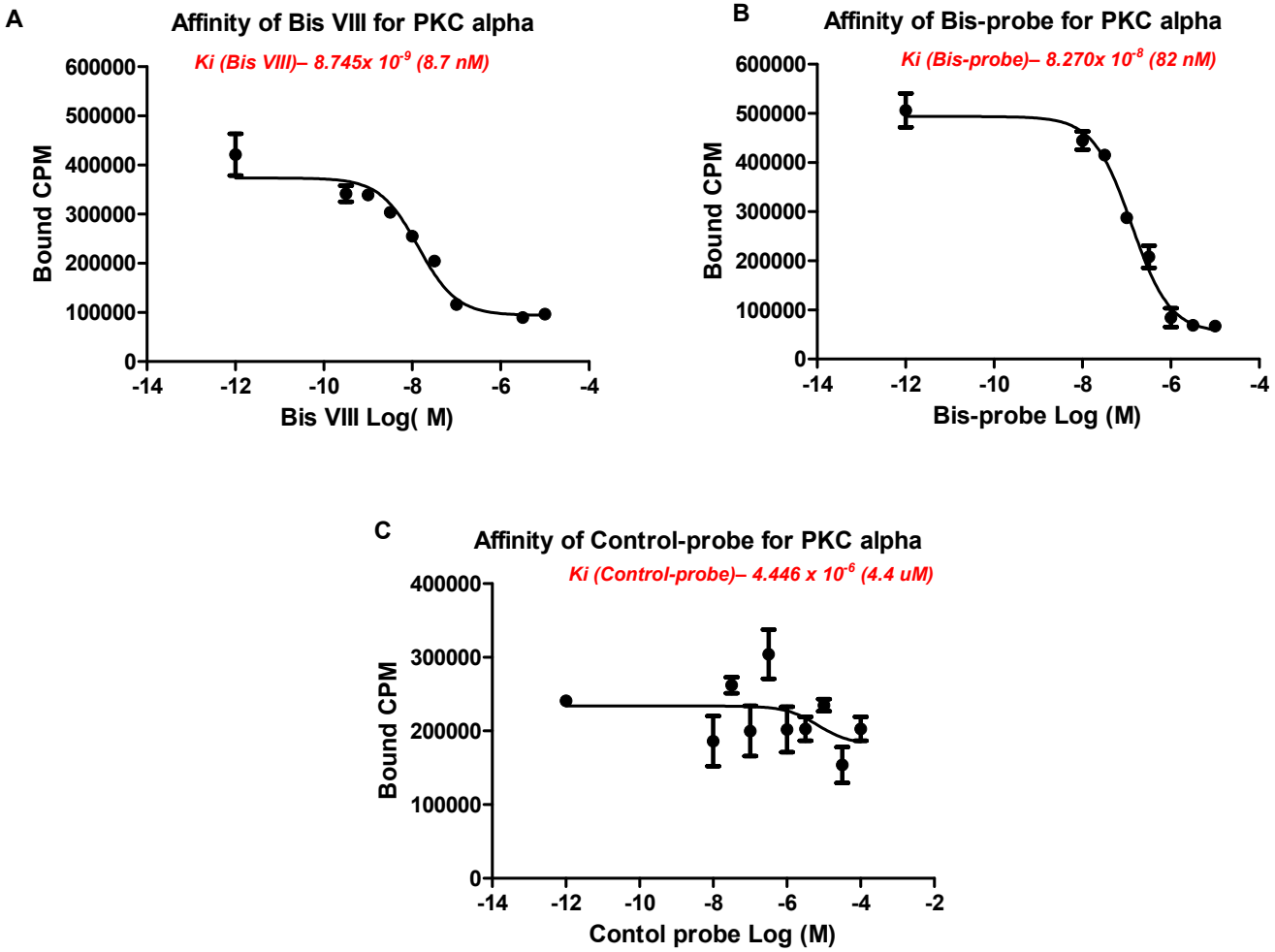

Figure 2.2: Non-linear regression analysis to determine the affinity (K_i) of the inhibitors for their receptor PKCα **(A)** Affinity (K_i) of commercially available Bis VIII inhibitor for PKCα **(B)** Affinity of Bis-probe for PKCα **(C)** Affinity of the control probe without the Bis- reactive group for PKCα. Note:-Prism software only reports error bars for data points with Standard Deviation >20%.

2.2.2.2. Steady state kinase assays

The relative PKCα inhibitory activity of the Bis-Probe with regards to Bis VIII (IC_{50}=53 nM) [137] was evaluated by a radioactive steady state kinase assay [138] using purified PKCα and introducing a substrate, Histone H1. The inhibitory enzyme activity was assessed by measuring the CPM of the phosphorylated histone substrate in steady state conditions.

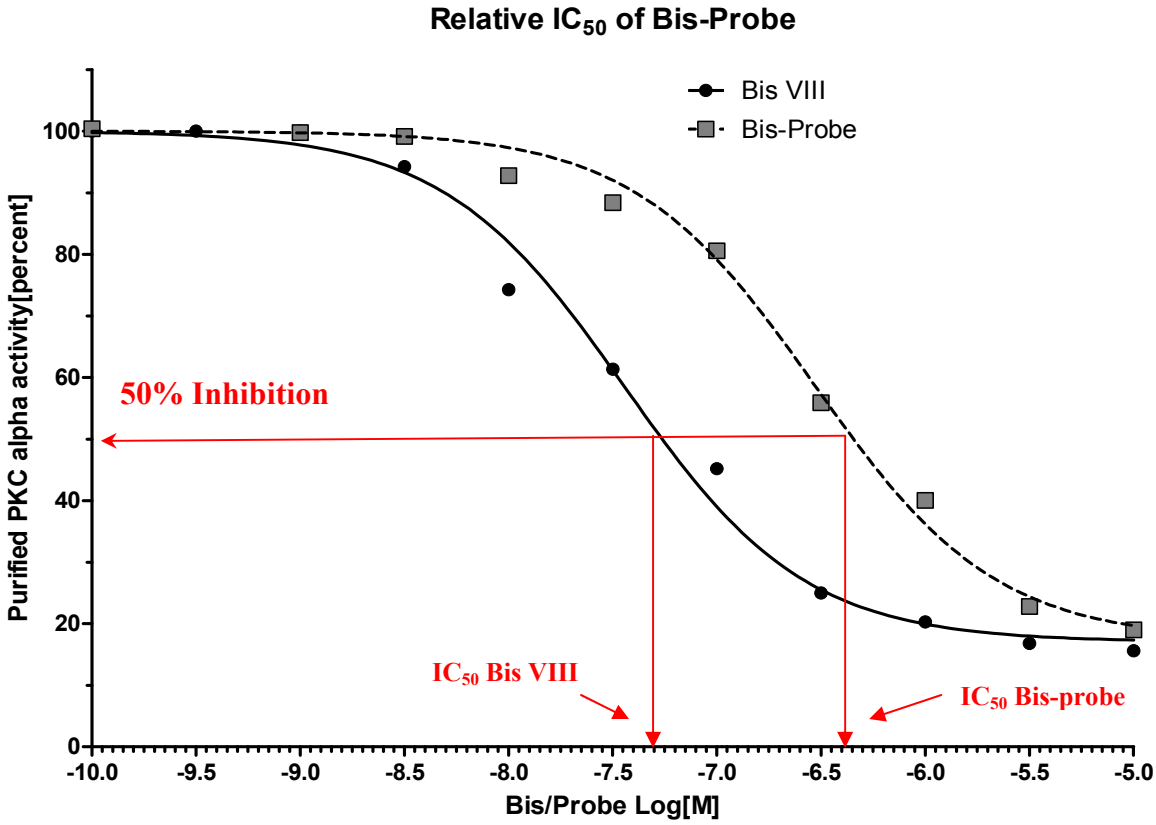

Figure 2.3: Non- regression analysis to determine the relative IC_{50} of the Bis-probe with regards to the free inhibitor Bis-VIII. IC_{50} values were defined to be the concentration of inhibitor at which CPM was 50% of the control sample, corrected by the background. Note:-Prism software only reports error bars for data points with Standard Deviation >20%.

IC_{50} values were defined to be the concentration of inhibitor at which CPM was 50% of the control sample, corrected by the background. The IC_{50} was determined to be 329 ηM and 40 ηM for Bis-probe and Bis VIII, respectively (**Figure 2.3**).

2.2.3. Chemical proteomics method development

The in-vitro testing of the Bis-probe in an *E.coli* based system and the effect of probe concentration on PKCα capture are described in Chapter 3, Section 3 (Dolai *et al.*, *Proteomics*, 2011, [134]). Other method optimization experiments not required to be included in the manuscript are described below.

2.2.3.1. Probe capture assessment by different elutions

The Bis-probe capture of its archetypal target, PKCα, was confirmed by ATP elution and glycine elution (**Figure 2.4A&B**). In the ATP elution strategy increasing concentration of ATP was used to compete with the Bisindolylmaleimide reactive group for the ATP binding sites of the probe captured proteins. With high ATP concentrations in the capture environment increasing amounts of Bis-bound proteins were eluted selectively without disrupting the probe binding to the beads. The basic principle of glycine elution is elution based on pH. The low pH (2.5) of glycine solution breaks the hydrophobic interactions of the protein and the probe reactive group, causing the bound proteins to unfold and be released. PKCα was undetected in the control experiment or on beads, which confirms specific enrichment by the Bis-probe and appropriate washing conditions had been established.

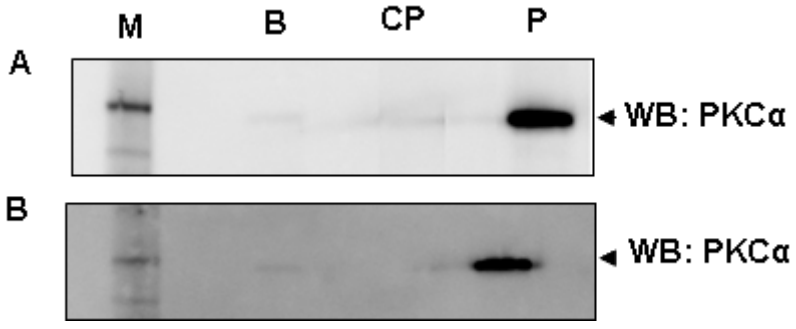

Figure 2.4: Immunoblot of PKCα capture by the Bis-probe by **(A)** ATP elution **(B)** Glycine elution. Molecular weight marker (**Lane M**), Bead controls (**Lane B**), Control probe affinity pull down (**Lane CP**), Bis-probe affinity pull down (**Lane P**).

2.2.3.2. Effect of washing conditions

2.2.3.2.1. Beads

Non-specific protein interaction with the affinity matrix beads is a key challenge in developing an effective chemical proteomic sample purification method. The nondenaturing conditions required for affinity purification allow many non-specific proteins to interact with the beads that must be dissociated by appropriate washing conditions.

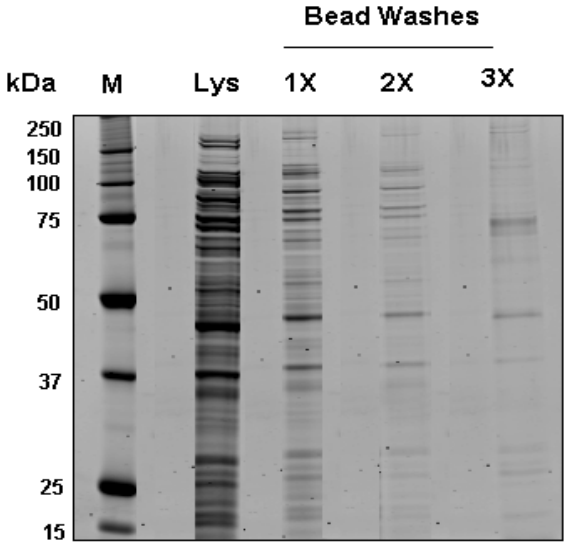

Figure 2.5: Sypro ruby stained gels showing optimal bead wash conditions. Molecular weight marker (**Lane M**), MDA-MB-231 cell lysates on beads after 1 h at 4°C, no wash (**Lane Lys**), eluates from beads after single wash with wash buffer (**lane 1X**), two time washed (**lane 2X**), three times washed (**lane 3X).**

The number of washing steps to discard non-specific binders of the affinity matrix was illustrated by gel staining. Clearly, at least three washes are required using a detergent based wash solution (1% TritonX-100 in PBS) for 5 min each at 4°C, to eliminate most non-specific binders (**Figure 2.5**). Western blotting was used to monitor recovery of the positive control (**Figure 2.6**).

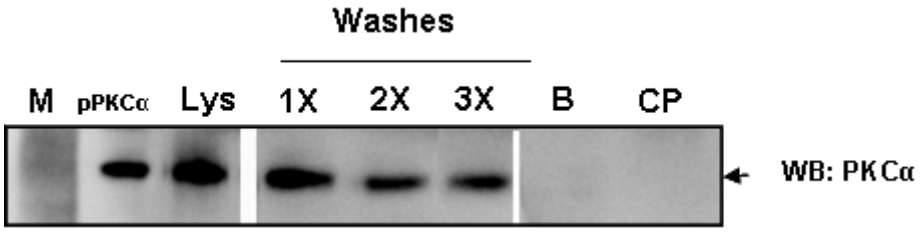

Figure 2.6: Immunoblot of PKCα capture by the Bis-probe at each washing step. Molecular weight marker (**Lane M**), purified PKCα (**Lane pPKCα**), MDA-MB-231 cell lysates (**Lane Lys**), probe captured eluates after single wash with wash buffer (**lane 1X**), two time washed (**lane 2X**), three times washed (**lane 3X),** Beads after three washes (**lane B**), Control probe after three washes (**lane CP**).

2.2.3.2.2. Control Probes

The contribution of the biotin tag and the PEO linker (Control probe) was then assessed. Washing conditions established in Section 2.3.2.1 were used, and then blots were probed with PKCα. The optimised washing conditions were sufficient to clear all loosely bound proteins to both the linker and the biotin tag as illustrated in **Figure 2.7A&B**. The minimal protein interaction which was observed with the control probe was evaluated by MS and is reported in Chapter 3 (Appendix A, **Table 2**).

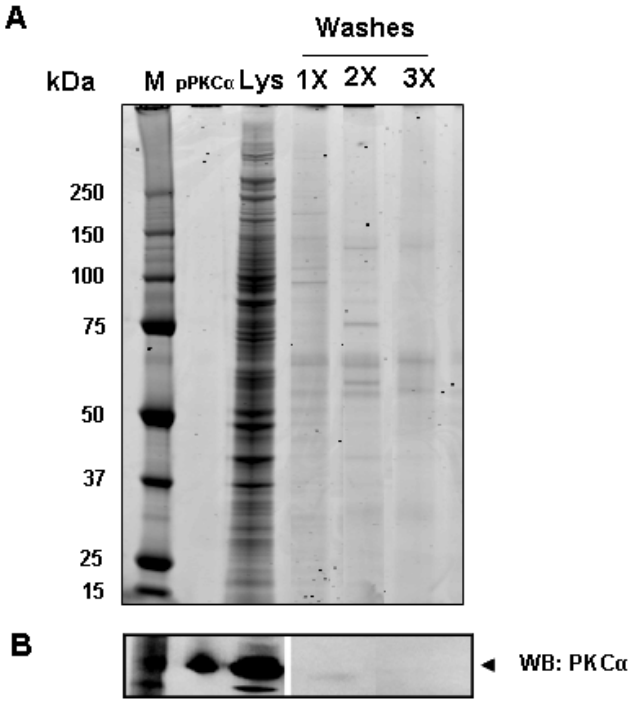

Figure 2.7: Evaluation of non-specific binding using control-probes. **(A)** Sypro ruby stained gels. Molecular weight marker (**Lane M**), purified PKCα (**Lane pPKCα**), MDA-MB-231 cell lysates (**Lane Lys**), eluates from affinity purification with control probes after single wash with wash buffer (**lane 1X**), two time washed (**lane 2X**), three times washed (**lane 3X). (B)** Immunoblot of PKCα capture by the control-probe after every wash.

Chapter 3: Quantitative chemical proteomics in small scale culture of basal breast cancer cells

The chapter describes the optimised chemical proteomics method developed using Bis-probes to characterise the binding targets in a basal breast cancer cell model (MDA-MB-231). SILAC based quantitation was applied to examine differential protein capture by the Bis-probe following phorbol ester (PMA) stimulation of the breast cancer cells. This chapter is now published in Proteomics, Dolai *et al*., *Proteomic* 2011, 11, 2683–2692**.**

Supplementary Figures 1A and 1B and Supplementary Tables 1A, 1B, 2 and 3 from this manuscript can be found in **Appendix A.**

A post examination addendum is included in page 55

Syntheses of the Bis-probes were carried out by Ms. Qiang Xu and Dr. Fei Liu, Department of Chemistry and Biomolecular Science, Macquarie University.

Pages 45-54 of this thesis have been removed as they contain published material under copyright. Removed contents published as:

Dolai, S., Xu, Q., Liu, F. and Molloy, M.P. (2011), Quantitative chemical proteomics in small-scale culture of phorbol ester stimulated basal breast cancer cells. *Proteomics*, vol. 11, no. 3, pp. 2683-2692. https://doi.org/10.1002/pmic.201000801

Addendum

1. Does 'activation of PKCα' (p 49) mean an increase in the amount of this protein?

The activation of PKCα means the opening of the ATP binding pocket upon binding of cofactors diacylglycerol (DAG) and phosphatidylserine (PS). This enables the enzyme to make itself available for interaction with ATP or ATP mimetic compounds. In its normal or unstimulated state, most of the kinase enzyme resides in the cytosol. In this state, the pseudo substrate sequence of the regulatory domain of PKC interacts with the catalytic domain and prevents access of the substrate to the catalytic site [1,2]. The activation of PKCα should not be confused with the increase in the amount of this protein, or activation due to phosphorylation/dephosphorylation.

2. How many isoforms of PKC are bound to the Bis-probe?

Two isoforms of PKC (α and θ) (Chapter 3, Figure 3 B&C) were detected in the study using Western Blotting. We did not look for other isoforms, so the possibility remains that other PKC isoforms may also interact with the Bis-probe. MS analysis of the Bis-bound proteins did not detect any PKC peptides.

3. 'Warburg effect' in cancers

Cancer cells rely on aerobic glycolysis to generate the energy needed for cellular process in contrast to normal differentiated cells, which rely primarily on mitochondrial oxidative phosphorylation [3]. This phenomenon is termed the Warburg effect and several studies have taken this into account to report an increase in glycolytic enzymes in cancer cells. These studies have been cited in Chapter 3, ref 41-43.

References:

1. Goldberg, E. M.; Zidovetzki, R., Synergistic effects of diacylglycerols and fatty acids on membrane structure and protein kinase C activity. *Biochemistry* **1998,** 37, (16), 5623-32.
2. Ichikawa, S.; Hatanaka, H.; Takeuchi, Y.; Ohno, S.; Inagaki, F., Solution structure of cysteine-rich domain of protein kinase C alpha. *J Biochem (Tokyo)* **1995,** 117, (3), 566-74.
3. Warburg, O., On the origin of cancer cells. *Science* **1956**, 123, 309-314.

Chapter 4: Chemical Proteomics of liver in a mouse model of cancer cachexia.

The ability of the Bis-probe to capture and quantify protein targets in a cell culture based model provided the foundation to conduct a study in a tissue based system. We chose to examine the liver proteome of a mouse model of cancer cachexia. This chapter adopted the chemical proteomic method developed in Chapter 3 and investigated the Bis-binding enzymes that were involved in various metabolic pathways in the liver of mice bearing a C26 adenocarcinoma with accompanying high IL-6 levels that induced cancer cachexia (cachectic), compared with mice bearing a C26 adenocarcinoma with low IL-6 levels that failed to induced cancer cachexia (non-cachectic) and control mice (no tumour). Spectral counting was used to quantify the relative abundance of the Bis-captured enzymes in these samples.

Livers from the mouse models of cancer cachexia and data shown in **Figure 4.1** were kindly provided by Ryland Taylor and Associate Professor Graham Robertson, ANZAC Research Institute, The University of Sydney, Australia.

The results of this study are being incorporated into a manuscript as part of a larger systems biology study with these samples, involving proteomics, glycomics and mRNA microarray analysis.

4.1. Introduction

The liver is a crucial organ responsible for a range of functions which include the processing of dietary amino acids, carbohydrates, lipids and vitamins; phagocytosis of particulate matter in the portal circulation; synthesis of serum proteins, biotransformation of circulating metabolites, detoxification and excretion of endogenous waste products and pollutant xenobiotics into the bile [139]. The central involvement of liver to regulate these important physiological functions makes it vulnerable to a wide range of metabolic, toxic, microbial, circulatory and neoplastic insults, which may result in inflammatory disorders of the liver. However, the liver plays host to number of enzymes from different hepatic cells that are actively involved in the breakdown of toxins and chemicals found in food and medicines, ultimately providing a detoxifier effect. There are a number of different cells that are involved in this range of processes going on in the liver; some of these include hepatocytes, stellate cells, endothelial cells, kuffer cells and epithelial cells.

Further, the liver also acts as a central organ of cytokine activity [140] . Hepatocytes make up 70-80% (w/w) of the cytoplasmic mass of the liver and are highly susceptible to the activity of cytokines in a variety of physiological and pathophysiological processes [140]. They bear cytokine receptors for interleukin 1 alpha (IL-1α), interleukin 1 beta (IL-1β), tumour necrosis factor alpha (TNFα) and interleukin-6 (IL-6), which may gain control over synthesis of plasma proteins that are produced mainly by hepatocytes. Cytokines are also important mediators of the acute phase response in the liver and are also responsible for the changes in the metabolic enzyme expression in the liver [141]. It is also reported that cytokines (IL-6, IL-1) are responsible for the changes in the synthesis of several plasma proteins in the liver, during the acute phase reactions [142]. A prominent feature of this reaction is the induction of acute phase proteins, which are involved in the restoration of metabolic homeostasis. The release of pro-inflammatory cytokines from tumours is often

known to initiate such hepatic acute phase responses along with liver inflammation. It has also been reported that the interaction of the pro-inflammatory cytokines with the liver can affect the cytokine signalling in the liver which can lead to reduced hepatic expression of cytochromes and ultimately to reduced drug clearance and increased chemotoxicity [143].

4.1.1. Colon 26 (C26) adenocarcinoma

The murine colon 26 xenograft adenocarcinoma is an undifferentiated colon carcinoma induced by the carcinogen *N*-nitroso-*N*-methylurethane [144]. The C26 adenocarcinoma Balb/c mouse model is useful for studying liver inflammation and cancer cachexia as very few animal transplantable tumours and tumour xenografts are able to induce inflammation, cachexia and disorders of homeostasis [144, 145]. In addition, harbouring this tumour in mice models has a major impact in the normal metabolic processes of the body and the liver [146]. The presence of a distal C26 adenocarcinoma has been shown to cause disorders in hepatic function that included protein metabolism, disorders of hepatic catalases and the decrease in drug metabolizing enzymes [145]. It is also capable of inducing inflammation and increasing levels of acute phase response proteins in the plasma such as fibrinogen, serum amyloid, α-1-antitrypsin and α-2-macroglobulin [147, 148]. In addition to the inflammatory effects, the C26 adenocarcinoma is a well investigated transplantable tumour that has been reported to induce cancer cachexia [145].

4.1.2. Cancer cachexia

Cancer cachexia is derived from the Greek words “kakos hexis” (meaning bad condition) and is found in any disease that involves the wasting of the host’s tissue [146, 149, 150]. Cachexia is defined as loss of muscle, with or without fat, frequently associated with anorexia, inflammation and insulin resistance [150]. Cachexia is often seen in patients with advanced stages of diseases such as cancer, autoimmunity and pulmonary diseases [151,

152]. The risk of death is also dramatically increased in cachectic patients as therapeutic intervention is further complicated by this condition. Cachectic cancer patients often exhibit increased energy expenditure, possibly due to increased thermogenesis and increased operation of the Cori cycle in the skeletal muscles [153]. The loss of skeletal muscle as a result of cachexia is mostly caused by the reduced protein synthesis and increased protein degradation by the ubiquitin-proteosome and the lysosomal pathways [154, 155]. The liver plays a central role in protein and amino acid metabolism, has a high rate of protein synthesis, and is a major contributor to whole body protein economy. Despite significant loss of lean body mass, cachectic cancer patients often have elevated liver protein synthesis, which is likely due to the augmented synthesis of acute phase proteins [156]. It has been speculated that the liver's demand for amino acids may drive the loss of protein mass from peripheral tissues such as skeletal muscle.

Abnormal protein, carbohydrate and lipid metabolism reported in cachexia, resulting in metabolic stress, has been linked to cytokines [146, 149, 157-159]. Numerous cytokines, including tumour necrosis factor α (TNFα), interleukin-1 (IL-1), interleukin-6 (IL-6), interferon gamma and leukaemia–inhibiting factor (LIF), have been postulated to play a role in causing muscle wasting in cancer cachexia leading to altered metabolism [160]. However, studies on the C26 adenocarcinoma models have revealed IL-6 as a critical factor related to maintenance of body mass during cachexia. Increasing levels of IL-6 in these mouse models has been reported to lead to cachexia [161]. More recently, Carson and Baltgalvis have reported IL-6 as a key regulator of muscle mass during cachexia [162]. In their theoretical model of IL-6 regulation of muscle wasting, they reported that increase in number and size of colon and intestinal tumours increases systemic inflammation and circulating IL-6. Further, the increasing IL-6 can act as a positive feedback signal to increase tumour growth and subsequent inflammation [162]. They also reported muscle

protein turnover to be influenced by increasing IL-6 through suppression of protein synthesis and activation of protein degradation. Further IL-6 can also have indirect effects through the induction of adipose tissue lipolysis that causes more metabolic stress in the cachectic mice [162]. These altered metabolic events directly affect the liver causing it to alter its metabolic pathway to adapt to the new demands imposed on it. The over expression of IL-6 has also been reported to cause severe inflammation of the liver [163] along with increased hepatic protein synthesis of acute phase proteins, lipolysis and fatty acid synthesis [164, 165]. Similarly studies on the clonal variants of the colon-26 tumour with low serum IL-6 levels have been reported not to induce weight loss [166] and the corresponding stress on the body was not seen.

In this study, the chemical proteomics method developed in Chapter 3 was adopted to profile the hepatic Bis-binding proteome in mice bearing a C26 adenocarcinoma with accompanying high IL-6 levels that induced cancer cachexia (cachectic), in mice bearing a C26 adenocarcinoma with low IL-6 levels that failed to induce cancer cachexia (non-cachectic) and control mice. We also used spectral counting to quantitate the relative abundance of the Bis-captured enzymes in these samples. Liver, as the centre of metabolism is the host to number of enzymes that are involved in various metabolic pathways and is an important target for study of cachexia. Further, chemical proteomics target proteins, particularly enzymes that utilise cofactors such as ATP, NAD/FAD and nucleotides for their activity. This provides a mechanism to profile many proteins involved in metabolism that are often not recovered in general shotgun proteomic methods. The study of the liver proteome using a chemical proteomics approach could help determine the changes in potentially important biological and metabolic pathways that occur during tumour induced liver inflammation and cancer cachexia.

4.2. Methods

4.2.1. Tumour transplantation

Eight to ten week old transgenic BALB/c male mice (n=3) were aseptically inoculated using a 14-gauge needle with 0.3 mL suspension of mouse colon 26 adenocarcinoma cells (containing 10^6 cells) in 0.9% (w/v) PBS. Reduced food intake was observed after 9 to 10 days with no apparent loss of weight. Tumour mass reached approximately 3 g or 10% (w/w) total body weight over 14 to 16 days, where approximately 20% (w/w) of weight was lost in cachectic mice. Tumour and control mice were euthanized and livers were harvested. All animal work was approved by the Concord Repatriation General Hospital local area health service Animal Ethics Committee.

4.2.2. Liver Sample preparation

Mice liver tissue (10 mg w/w) of the cachectic, non-cachectic and the control groups was homogenised in 1 ml of modified radioimmuno-precipitation (RIPA) buffer containing 50 mM Tris-HCl, pH7.4, 150 mM NaCl, 1% Triton X-100 plus protease inhibitors (1 mM phenylmethylsulfonyl fluoride, 1 mM EDTA, 1 µg/ml aprotinin, 1 µg/ml leupeptin, 1 µg/ml pepstatin) and phosphatase inhibitors (1 mM sodium fluoride and 1 mM sodium orthovanadate) using an Omni TH homogenizer (Omni International Inc., VA, USA) for 2 min at room temperature.

The homogenized tissue was then centrifuged at 2000 *g* for 20 min at 4°C. The supernatant was then assayed for relative protein concentration using bicinchoninic acid (BCA) assay. 100 µg of protein was then volume adjusted to 500 µl with modified–RIPA buffer and was used as starting material for affinity pull-down experiments. Three mice from each group (cachectic, non-cachectic and control) were analysed. Further, two independent pull-downs were conducted for each sample and each analysed by MS independently.

4.2.3. Affinity pull down and MS analysis

Affinity pull down and MS analysis was carried out as described in Chapter 3, Section 2.

4.2.4. Protein Identification and Data Analysis

Spectra files were processed and searched as described in Chapter 3, Section 2. MS/MS spectra were searched against the SwissProt *Mus musculus* database (release 56.8 of February 10, 2009). The proteins identified for all the replicates for each of the three groups was further filtered using two criteria. Every protein was retained as a true identification if it was found in at least 2 of the three biological replicates and the protein should have a total spectral count > 4. After this filtering the peptide and protein false discovery rates (FDR) were calculated. Peptide FDR was calculated as 2 x (total number of peptides representing reversed protein hits in the list/total number of peptides representing all proteins in the list) x 100 and protein FDR was calculated as (number of reverse protein hits in a list/total number of proteins in the list) x 100.

4.2.5. Calculation of protein Normalized Spectral Abundance Factor (NSAF)

Normalized spectral abundance factors (NSAF) were calculated for each protein in all the groups using the formula: NSAF = (Spc/L)/$\sum$ (Spc/L) described by Zybailov *et al.* [131, 167], where Spc refers to the spectral count (total number of MS/MS spectra) identifying a given protein, L is the length of the protein and $\sum$ (Spc/L) refers to the summation of spectral count/length of all the proteins identified in the experiment. Protein identifications were only included in NSAF data analysis if a given protein was identified in at least 2 of the 3 biological replicates. Further a spectral fraction of 0.5 was added to all values to compensate for null values [131]. Statistical analysis of the abundance levels of the proteins present in all the groups was analysed by a one-way ANOVA analysis of the log

NSAF data. To examine the natural log NSAF data, overlapped Kernel plots were generated and this assured the normal distribution of data for each group.

4.3. Results

4.3.1. Protein targets captured by the Bis-probe from cachectic, non-cachectic and control mice livers

The chemical proteomics method developed and described in Chapter 3 using Bis-probe was used to capture, identify and quantify proteins in the liver of mice bearing a C26 adenocarcinoma with high IL-6 levels that induced cancer cachexia (cachectic), mice bearing a C26 adenocarcinoma with low IL-6 levels that failed to induce cancer cachexia (non-cachectic) and mice bearing no tumour (control). **Figure 4.1** shows the increasing IL-6 levels in the control and C26 adenocarcinoma transplanted mice along with their body weight change. Using a linear ion trap mass spectrometer 338 proteins were identified in control mice liver samples, 348 in cachectic mice liver samples and 354 in non-cachectic mice samples (**Figure 4.1**). The proteins identified in each group were reproducibly present in at least 2 of the 3 biological replicates for each group.

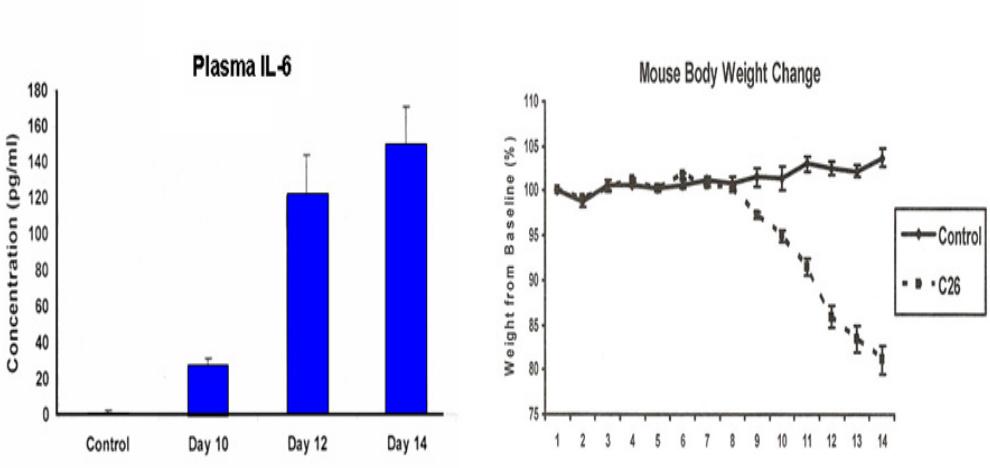

Figure 4.1: Increasing plasma IL-6 levels and body weight changes in mice transplanted with colon C 26 adenocarcinoma cells**.**

Figure 4.2 shows the distribution of Bis-binding proteins captured in the livers from cachectic, non-cachectic and control mice. The majority of proteins (260) that were

common to all three liver samples (~75% of all captured were common). However, 37, 21 and 25 proteins were unique to cachectic, non-cachectic and control mice livers respectively. Additionally, 15 were common to the cachectic and control groups only, 38 were common to the non-cachectic and control groups only and 35 proteins were common between the cachectic and the non-cachectic group only.

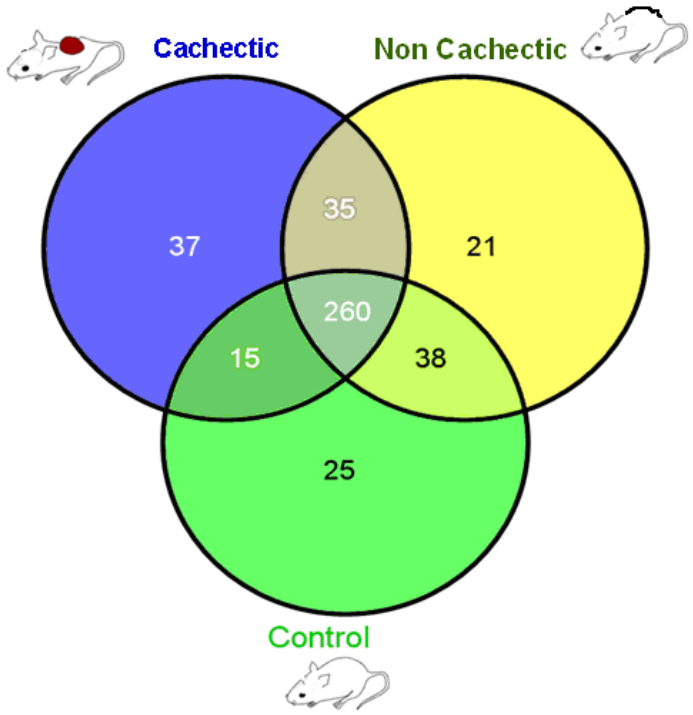

Figure 4.2: Proteins captured by the Bis-probe in cachectic, non-cachectic and control mouse liver samples with the unique and common subsets**.**

A summary of protein identification data of the Bis-probe captured proteins for each of mice groups along with their redundant peptide counts, peptide False Discovery Rate (FDR) and protein FDR are shown in **Table 4.1**. The average number of peptides from proteins that were captured by the Bis-probe and that were consistently identified in all 3 mouse groups varied from 12275 in the cachectic to 12585 in the non-cachectic with the control being 12448 and the ±RSD were 5.3%, 3.3% and 9.9% respectively indicating high reproducibility of peptide counts within as well as among the different groups.

MICE	Redundant Count of peptides						Peptide FDR (%)						Average Peptide FDR(%) (± SD)	No of proteins common to AllRep	Protein FDR(%)
	R1	R2	R3	R4	R5	R6	R1	R2	R3	R4	R5	R6			
Control	13509	13127	13038	12175	10090	12750	0.12	0.03	0.21	0.10	0.12	0.19	0.13±0.07	338	1.46
Cachectic	13147	12510	11552	11468	12422	12552	0.21	0.29	0.14	0.14	0.13	0.08	0.16±0.07	348	1.42
Non-Chachectic	13277	12486	12576	12390	12755	12030	0.17	0.16	0.22	0.23	0.13	0.23	0.19±0.04	354	1.95

Table 4.1: Peptide and protein counts captured by the Bis-probe in each of the cachectic, control and Non-cachectic mouse livers. R1, R2, R3, R4, R5 and R6 are the six replicates in each group. FDR denotes False Discovery Rate and SD standard deviation.

4.3.2. Gene Ontology (GO) analysis

The identified proteins were then grouped using Gene Ontology (GO) annotation and categorised based on their binding function (**Figure 4.3**). GO mapping of the comprehensive list of non-redundant proteins captured by the Bis-probe in cachectic, non-cachectic and control mouse liver samples illustrated that there was a similar distribution of protein binding groups in all the three mice groups. On average 34% of the Bis-probe bound proteins that were identified in our study had reported ATP-binding and 23% reported NAD/FAD binding functions in all the three mice groups. Similarly, in all the three groups, 5% of the Bis-bound proteins were reported as protein binding and only 1% was reported as Lipid binding. A further 3% reported DNA/RNA/Nucleotide binding functions in the control and the non-cachectic groups, which was double (7%) in the cachectic group. Furthermore, the Bis-bound proteins that reported metal (Zinc, Calcium, Iron/heme and Selenium) binding function totalled 9% in cachectic, 13% in non-cachectic and 12 % in the control mouse liver proteins. All the three groups had ~23% proteins which did not have any designated ligand binding ability and were categorised as others.

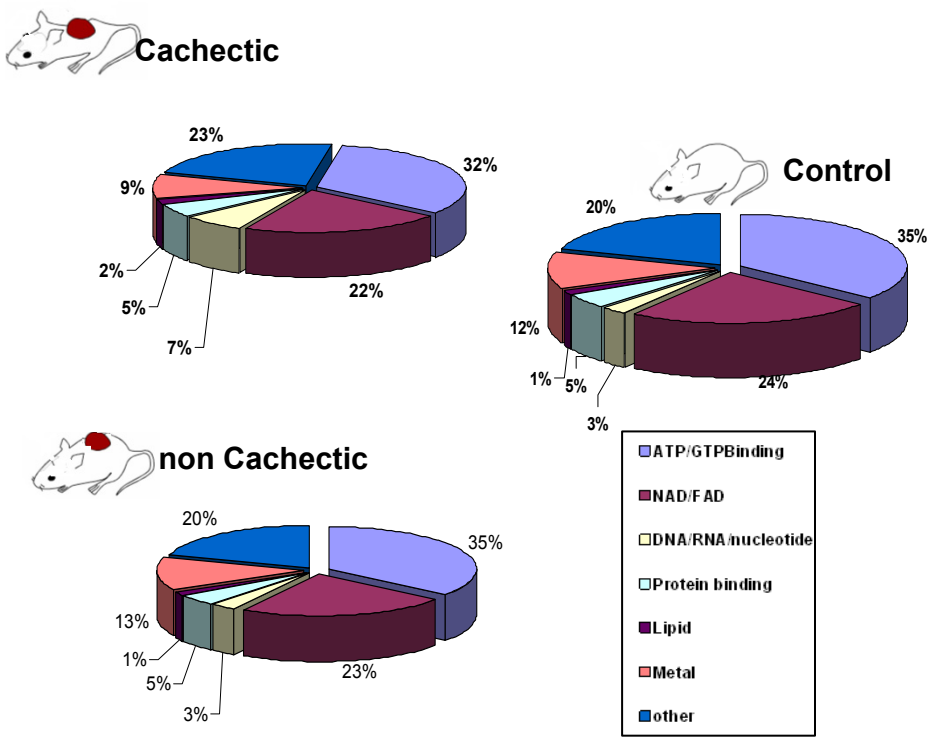

Figure 4.3: Bis-probe binding proteins in cachectic, non-cachectic and control mouse livers categorised according to their binding functions based on Gene Ontology (GO).

4.3.3. Biological Pathways

Analysis with the Skypainter reactome programme was then performed to evaluate the biological reactions and/or pathways of the Bis-captured proteins in the cachectic, control and non-cachectic mice livers. Based on the identity of the proteins, Skypainter categorised the Bis-bound proteins to be mainly involved in lipids and lipoprotein metabolism, protein metabolism, amino acid metabolism, carbohydrate metabolism, pyruvate metabolism including TCA cycle, diabetes pathway, biological oxidation, and gene expression (**Figure 4.4**). As seen in the mice reactome map, the biological events that the Bis-captured proteins correspond to were grossly similar for all the three groups, although differences did exist. We then analysed the number of Bis-bound proteins that contributed to a particular biological event in all the three mice groups (**Figure 4.4**).

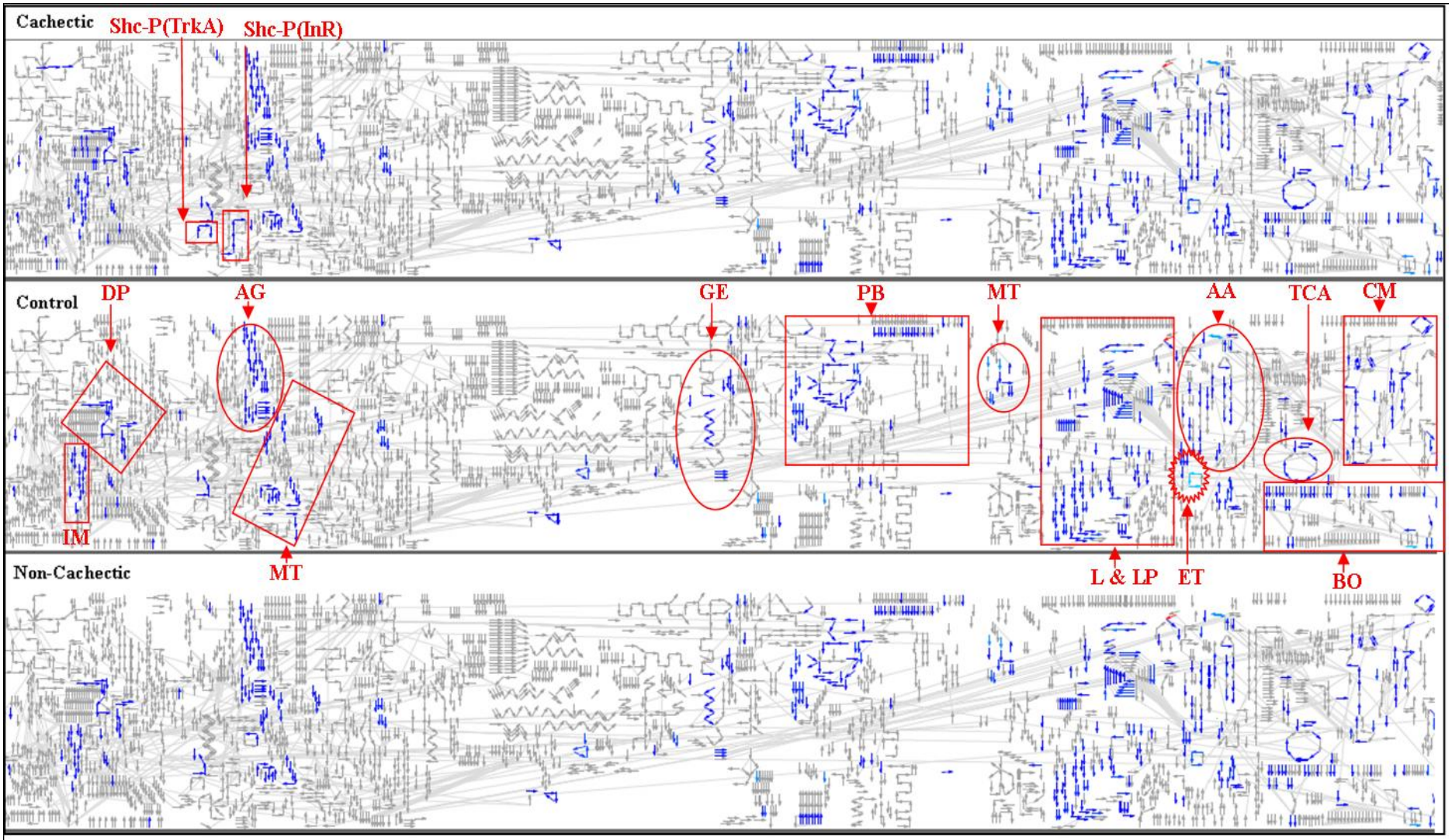

Figure 4.4: Reactome Skypainter Analysis of Bis-bound proteins in mice liver. Arrows represent all the biological events (reactions and/or pathways) present in the mouse system and the coloured arrows represent the Bis-captured proteins involved in a particular event. Highlighted pathways:- CM- Carbohydrate Metabolism; BO-Biological Oxidation; TCA-TCA cycle; AA-Amino acid Metabolism; ET-Electrone transport; L&LP- Lipid and Lipoprotein Metabolism; MT-Membrane Trafficking; PB- Protein Biosynthesis; GE- Gene Expression; AG-Axon Guidance; DP- Diabetes Pathway; IM- Immune System Signalling; Nerve growth factor signalling events unique to cachectic groups:- Shc-P (TrkA)-SHC phosphorylation via tyrosine kinase A and Shc-P (InR)-SHC phosphorylation via Insulin receptors.

4.3.4. Spectral Count Quantitation

Next, the relative abundance of the Bis-captured proteins in cachectic, non-cachectic and control liver samples was determined by calculating the NSAF values for each of the identified proteins. Further, natural log was applied to the NSAF values to normalize the distribution, which allowed significance testing and quantitation of proteins that were low in abundance (**Figure 4.5**). We calculated the NSAF values for all the Bis-captured proteins in each of the six replicates for each mouse group and determined the average. Proteins that were confidently identified in at least 2 of the 3 biological replicates were examined. ANOVA analysis of the average NSAF values of the Bis-captured proteins revealed 46 proteins with the greatest different abundance levels in the cachectic, control and non-cachectic mice livers ($p \leq 0.05$). These differentially expressed proteins were then clustered on the basis of relative abundance (**Figure 4.6**).

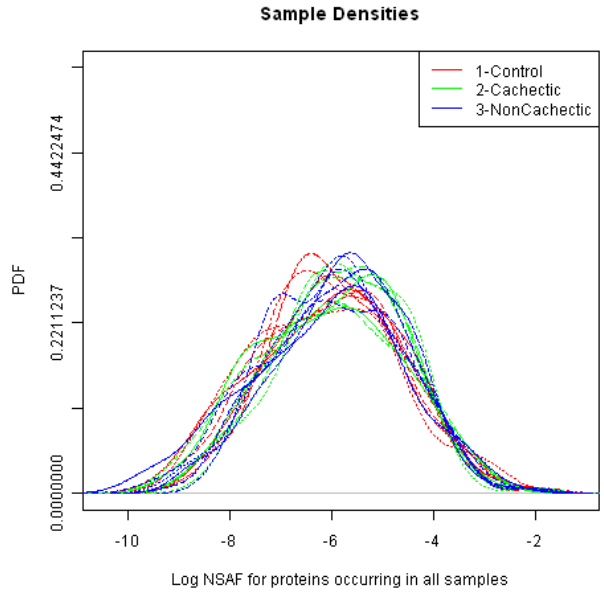

Figure 4.5: Log NSAF values of all the proteins that were captured by the Bis-probe in control, non-cachectic and cachectic mouse liver samples. Applying natural log to the NSAF values normalizes the distribution as shown by the sample densities. This allows quantitation and statistical analyses.

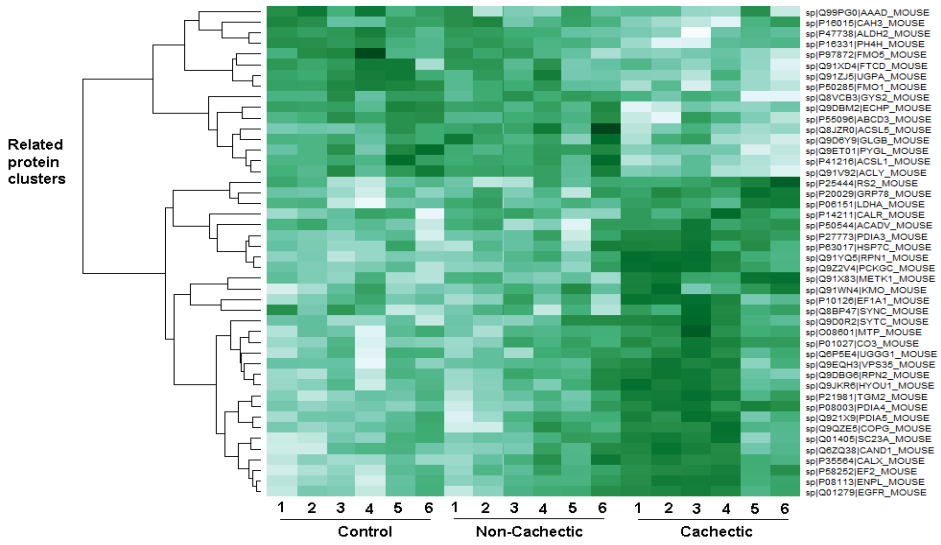

Figure 4.6: Heat map of the proteins that were differentially captured by the Bis-probe in cachectic, non-cachectic and control liver samples.

4.3.5. Protein abundance levels of Bis-probe binding proteins in the cachectic and control mice liver samples.

We identified 107 proteins captured by the Bis-probe that were significantly different ($p \leq 0.05$) in their relative abundance in the cachectic mouse livers compared to the controls (**Table 4.2**). However, in the comparison of the non-cachectic to the controls, only 24 proteins were significantly different in abundance ($p \leq 0.05$) (**Table 4.3**). In the cachectic Vs control groups, of the 107 differentially captured proteins, the relative abundance of 69 proteins was higher in the cachectic group than the control and 38 proteins were more abundant in the control groups. The proteins captured by the Bis-probe that were high in abundance in cachectic were primarily involved in protein metabolism, UTR mediated translation, signal recognisation (preprolacin) and membrane trafficking events and the proteins that were relatively abundant in the control groups were involved in biological oxidation, lipid metabolism and amino acid metabolism events (**Figure 4.7**). The abundance levels of majority of the proteins captured by the Bis-probe in the non-cachectic and control groups was similar. However, the relative abundance of 24 proteins were significantly different ($p \leq 0.05$) in the non-cachectic mouse livers compared to the controls (**Table 4.3**). The abundance level of 16 proteins was higher and 8 proteins were lower in

the non-cachectic group compared to the controls. The Skypainter molecular function analysis of these differentially abundant proteins in the non-cachectic and control groups revealed that the proteins captured by the Bis-probe that were high in abundance in non-cachectic were primarily involved in protein metabolism, Diabetes pathways, immune system signalling and gene expression. The low in abundance Bis-captured protein in the non-cachectic group were primarily involved in Biological oxidation and amino acid metabolism (**Figure 4.8**).

Table 4.2: Protein abundance levels of Bis-probe binding proteins that were significantly different in cachectic and control mice liver samples.

Identifier	Description	Fold Change	pValue	Avg No. of pep Cac	Avg No. of pep Con	Average NSAF Cachectic	SD NSAF Cachectic	Average NSAF Control	SD NSAF Control
Q64459	Cytochrome P450 3A11	-80	0.00	0	43	4.73E-05	9.29E-06	0.003801	0.001102
P00186	Cytochrome P450 1A2	-50	0.00	0	45	7.91E-05	7.96E-05	0.003937	0.001013
P11714	Cytochrome P450 2D9	-18	0.02	1	21	0.000103	5.97E-05	0.001812	0.001351
P50285	Dimethylaniline monooxygenase 1	-9.3	0.00	2	25	0.000242	0.000208	0.002246	0.000752
Q91WL5	Cytochrome P450 4A12A	-7	0.00	2	14	0.000184	0.00018	0.001323	0.000264
P97494	Glutamate--cysteine ligase catalytic subunit	-6	0.01	0	5	6.34E-05	6.38E-05	0.00039	0.000238
Q91ZJ5	UTP--glucose-1-phosphate uridylyltransferase	-5.4	0.01	3	22	0.000382	0.000339	0.002051	0.000986
Q63836	Selenium-binding protein 2	-5.4	0.05	9	58	0.000986	0.000746	0.005294	0.003636
P16331	Phenylalanine-4-hydroxylase	-4.8	0.00	6	30	0.000608	0.00054	0.002903	0.001278
P40936	Indolethylamine N-methyltransferase	-5	0.00	4	18	0.000666	0.000947	0.003125	0.001597
P56657	Cytochrome P450 2C40	-5	0.04	1	5	9.87E-05	0.000116	0.000447	0.000397
Q9DBM2	Peroxisomal bifunctional enzyme	-4.3	0.01	24	103	0.001619	0.000825	0.007031	0.002529
P53395	Branched-chain alpha-keto acid dehydrogenase E2	-4	0.03	3	11	0.000302	0.000298	0.001064	0.000739
Q91V92	ATP-citrate synthase	-3.4	0.02	11	40	0.000553	0.000291	0.001871	0.000895
Q3ULD5	Methylcrotonoyl-CoA carboxylase beta chain	-3	0.05	1	4	0.000131	0.000169	0.000428	0.000336
Q9ET01	Glycogen phosphorylase, liver form	-2.8	0.03	48	133	0.002772	0.00099	0.007669	0.004255
P16015	Carbonic anhydrase 3	-2.7	0.00	36	89	0.005602	0.006566	0.015121	0.009039
Q64458	Cytochrome P450 2C29	-3	0.05	8	22	0.000683	0.00093	0.001835	0.001652
Q8VCB3	Glycogen synthase, liver	-2.5	0.04	4	11	0.000314	0.000258	0.000797	0.000415
P41216	Long-chain-fatty-acid--CoA ligase 1	-2.2	0.02	57	134	0.004046	0.001176	0.009036	0.003251
Q99PG0	Arylacetamide deacetylase	-2.2	0.02	5	12	0.000626	0.000433	0.001393	0.000515
P55096	ATP-binding cassette sub-family D member 3	-2.2	0.03	15	37	0.001193	0.000902	0.002618	0.000637
P24456	Cytochrome P450 2D10	-2.1	0.02	19	40	0.001623	0.001162	0.003468	0.001728
O08749	Dihydrolipoyl dehydrogenase, mitochondrial	-2	0.02	2	4	0.000197	0.000187	0.000408	0.000204
Q9D0M3	Cytochrome c1, heme protein, mitochondrial	-2.0	0.02	3	6	0.000453	0.000444	0.00092	0.000598
P17717	UDP-glucuronosyltransferase 2B5	-2.0	0.04	19	40	0.001625	0.000824	0.003286	0.001311
P47738	Aldehyde dehydrogenase, mitochondrial	-2.0	0.02	99	195	0.008791	0.00348	0.017521	0.003758
P51174	Long-chain specific acyl-CoA dehydrogenase	-1.9	0.03	8	15	0.000813	0.000832	0.001555	0.001045
P61922	4-aminobutyrate aminotransferase, mitochondrial	-2	0.04	2	4	0.000184	0.000152	0.000341	0.000247
Q9EQ20	Methylmalonate-semialdehyde dehydrogenase	-1.7	0.03	49	84	0.004267	0.002181	0.007458	0.001871

Q91XD4	Formimidoyltransferase-cyclodeaminase	-1.7	0.05	30	56	0.002829	0.000743	0.004822	0.00144
P16460	Argininosuccinate synthase	-1.7	0.05	207	352	0.023042	0.012962	0.038963	0.011961
P97872	Dimethylaniline monooxygenase 5	-1.6	0.01	50	88	0.004548	0.00053	0.007495	0.002115
Q63880	Liver carboxylesterase 31	-1.6	0.00	69	118	0.006169	0.00385	0.010125	0.004922
P70694	Estradiol 17 beta-dehydrogenase 5	-1.6	0.04	25	35	0.003026	0.003828	0.004771	0.003186
Q8BW75	Amine oxidase B	-1.5	0.01	14	23	0.001386	0.001015	0.002126	0.001157
Q8BWT1	3-ketoacyl-CoA thiolase, mitochondrial	-1.5	0.01	151	213	0.01712	0.012468	0.025065	0.010698
P32020	Non-specific lipid-transfer protein	-1.4	0.04	69	107	0.006397	0.001821	0.009165	0.003627
P11499	Heat shock protein HSP 90-beta	1.3	0.05	178	142	0.01168	0.002501	0.008916	0.001858
P07901	Heat shock protein HSP 90-alpha	1.3	0.03	117	92	0.00762	0.001974	0.005681	0.001444
Q9D0F9	Phosphoglucomutase-1	1.3	0.05	11	9	0.001069	0.000442	0.000795	0.000363
P14211	Calreticulin	1.5	0.04	101	69	0.01128	0.002377	0.007286	0.002653
Q4LDG0	Bile acyl-CoA synthetase	1.6	0.03	65	42	0.004801	0.00218	0.002985	0.000909
Q8BHN3	Neutral alpha-glucosidase AB	1.6	0.03	43	26	0.00229	0.000758	0.001416	0.000786
P62267	40S ribosomal protein S23	1.6	0.01	3	2	0.001121	0.000886	0.000682	0.000642
P62830	60S ribosomal protein L23	1.7	0.02	9	6	0.00323	0.001558	0.001945	0.00199
Q9R0H0	Peroxisomal acyl-coenzyme A oxidase 1	1.7	0.04	48	28	0.003218	0.001567	0.001901	0.000659
P10126	Elongation factor 1-alpha 1	1.7	0.01	91	57	0.010202	0.003338	0.005965	0.001419
O08601	Microsomal triglyceride transfer protein large subunit	1.8	0.04	96	56	0.005318	0.001353	0.003016	0.000985
P63017	Heat shock cognate 71 kDa protein	1.8	0.01	121	71	0.009186	0.001785	0.005143	0.001448
P50544	Very long-chain specific acyl-CoA dehydrogenase	1.9	0.01	46	26	0.003518	0.000792	0.001814	0.000696
P68040	Guanine nucleotide-binding protein subunit beta-2-like 1	2.1	0.01	21	9	0.003237	0.001609	0.001507	0.000963
P47962	60S ribosomal protein L5	2.2	0.04	23	10	0.003985	0.002629	0.001812	0.001931
Q01405	Protein transport protein Sec23A	2.2	0.01	26	12	0.00171	0.000733	0.000773	0.000369
Q3UPL0	Protein transport protein Sec31A	2.2	0.05	31	14	0.001366	0.00074	0.000611	0.000445
P23116	Eukaryotic translation initiation factor 3 subunit A	2.3	0.05	10	4	0.000367	0.000281	0.000163	0.000107
P47911	60S ribosomal protein L6	2.3	0.00	10	4	0.001606	0.001279	0.000711	0.000929
Q9WVD5	Mitochondrial ornithine transporter 1	2.3	0.05	16	7	0.002708	0.00197	0.00118	0.000693
P27659	60S ribosomal protein L3	2.4	0.03	44	19	0.005546	0.003271	0.002359	0.001839
P62908	40S ribosomal protein S3	2.4	0.00	15	6	0.002897	0.001149	0.001202	0.000777
P08113	Endoplasmin	2.4	0.00	274	113	0.016259	0.003694	0.006664	0.002633
P08249	Malate dehydrogenase, mitochondrial	2.5	0.05	3	1	0.000397	0.000347	0.000159	0.000145
Q9Z1Z0	General vesicular transport factor p115	2.5	0.03	7	3	0.000426	0.000256	0.000167	0.000165
Q9CR57	60S ribosomal protein L14	2.6	0.05	4	1	0.000895	0.000581	0.000344	0.000371
Q9D0I9	Arginyl-tRNA synthetase, cytoplasmic	2.6	0.05	3	1	0.000244	0.000171	9.34E-05	9.1E-05
P37040	NADPH--cytochrome P450 reductase	2.8	0.03	18	6	0.001228	0.000714	0.000444	0.000222

P58252	Elongation factor 2	2.8	0.00	87	31	0.004973	0.000853	0.001784	0.000832
P07759	Serine protease inhibitor A3K	2.8	0.01	6	2	0.000682	0.000249	0.00024	0.000217
Q9DBG6	Dolichyl-diphosphooligosaccharide--protein glycosyltransferase subunit 2	2.9	0.02	42	15	0.00352	0.001858	0.00123	0.000627
P20029	78 kDa glucose-regulated protein	2.9	0.00	106	36	0.0074	0.002261	0.00255	0.001018
P62242	40S ribosomal protein S8	2.9	0.04	13	4	0.003223	0.002063	0.001099	0.001312
Q91YQ5	Dolichyl-diphosphooligosaccharide--protein glycosyltransferase subunit 1	2.9	0.00	62	23	0.005049	0.001634	0.001718	0.00028
Q9JKR6	Hypoxia up-regulated protein 1	3.0	0.01	50	17	0.002583	0.001205	0.000866	0.000384
P62281	40S ribosomal protein S11	3.0	0.02	6	2	0.002026	0.000912	0.000676	0.00055
Q8K010	5-oxoprolinase	3.0	0.04	26	9	0.001154	0.000776	0.000381	0.000255
Q8CIB5	Fermitin family homolog 2	3.1	0.01	6	2	0.000457	0.000297	0.000149	0.000134
P25444	40S ribosomal protein S2	3.2	0.03	5	1	0.000854	0.000584	0.000269	0.000164
O55143	Sarcoplasmic/endoplasmic reticulum calcium ATPase 2	3.3	0.03	20	6	0.001057	0.000666	0.000315	0.000239
Q9EQH3	Vacuolar protein sorting-associated protein 35	3.5	0.02	8	2	0.00053	0.000269	0.00015	7.52E-05
P06151	L-lactate dehydrogenase A chain	3.6	0.00	49	13	0.006546	0.003245	0.001839	0.00128
Q6P5E4	UDP-glucose:glycoprotein glucosyltransferase 1	3.6	0.05	18	5	0.00062	0.000387	0.000173	0.000134
Q6ZWY3	40S ribosomal protein S27-like	3.9	0.05	6	1	0.003733	0.003017	0.000963	0.00106
Q9Z2V4	Phosphoenolpyruvate carboxykinase, cytosolic	4.0	0.01	79	22	0.006414	0.002664	0.001592	0.000525
Q8BU30	Isoleucyl-tRNA synthetase, cytoplasmic	4.1	0.04	6	1	0.00026	0.000204	6.33E-05	6.42E-05
Q9D0R2	Threonyl-tRNA synthetase, cytoplasmic	4.1	0.02	16	4	0.001141	0.000593	0.000276	0.00012
Q9QZE5	Coatomer subunit gamma	4.6	0.04	13	3	0.000827	0.000578	0.00018	0.000122
Q921X9	Protein disulfide-isomerase A5	4.6	0.03	15	3	0.001536	0.001015	0.000333	0.000235
Q78XF5	Oligosaccharyltransferase complex subunit OSTC	4.7	0.01	3	0	0.000984	0.000576	0.000209	0.000126
Q91X83	S-adenosylmethionine synthetase isoform type-1	4.9	0.01	147	30	0.016781	0.006879	0.003416	0.002074
P62754	40S ribosomal protein S6	5.0	0.00	6	1	0.001128	0.000316	0.000226	0.000171
Q6ZQ38	Cullin-associated NEDD8-dissociated protein 1	5.0	0.01	10	2	0.000455	0.000303	9.12E-05	6.61E-05
P35980	60S ribosomal protein L18	5.1	0.05	3	0	0.000806	0.000693	0.000158	7.88E-05
P21981	Protein-glutamine gamma-glutamyltransferase 2	5.2	0.00	37	7	0.002801	0.001224	0.000542	0.000293
Q91YW3	DnaJ homolog subfamily C member 3	5.2	0.05	3	0	0.000321	0.000252	6.13E-05	3.68E-05
Q923B6	Metalloreductase STEAP4	5.5	0.01	3	0	0.000276	0.000148	5.02E-05	1.03E-05
Q8VCM7	Fibrinogen gamma chain	5.6	0.05	3	0	0.0003	0.000227	5.39E-05	1.1E-05
P61620	Protein transport protein Sec61 subunit alpha isoform 1	5.8	0.00	3	0	0.000409	0.000154	7.1E-05	5.41E-05
P35487	Pyruvate dehydrogenase E1 component subunit alpha	5.8	0.05	4	0	0.000454	0.000383	7.86E-05	3.92E-05
Q9EQK5	Major vault protein	6.1	0.04	16	2	0.001065	0.000821	0.000175	0.000209
P14148	60S ribosomal protein L7	7.1	0.05	5	0	0.000776	0.000645	0.000109	5.42E-05
Q91WG8	Bifunctional UDP-N-acetylglucosamine 2-epimerase/N-acetylmannosamine kinase	7.4	0.04	9	1	0.000707	0.000498	9.53E-05	7.08E-05

P27046	Alpha-mannosidase 2	8.7	0.04	3	0	0.000176	0.000135	2.03E-05	4.12E-06
Q01279	Epidermal growth factor receptor	8.9	0.01	21	2	0.000902	0.000469	0.000101	0.000101
Q8CFX1	GDH/6PGL endoplasmic bifunctional protein	9.5	0.00	10	1	0.000603	0.000188	6.33E-05	4.81E-05
P08003	Protein disulfide-isomerase A4	10.0	0.00	20	2	0.00149	0.000493	0.000149	5.44E-05
P01029	Complement C4-B	10.5	0.04	10	1	0.000315	0.000266	3E-05	4.1E-05
P01027	Complement C3	14.8	0.01	61	4	0.00187	0.000995	0.000127	0.000132

Table 4.3: Protein abundance levels of Bis-probe binding proteins that were significantly different in non-cachectic and control mice liver samples.

Identifier	Description	Fold change	pvalue	Avg No. of pep NCac	Avg No. of pep Con	Average NSAF Non-Cachectic	SD NSAF Non-Cachectic	Average NSAF Control	SD NSAF Control
P50285	Dimethylaniline monooxygenase	-2.4	0.03	10	25	0.000932	0.000524	0.002246	0.000752
Q99J08	SEC14-like protein 2	-2.3	0.04	14	2	0.000102	0.000111	0.000238	0.00018
P00186	Cytochrome P450 1A2	-2.0	0.01	21	45	0.001929	0.000546	0.003937	0.001013
O08749	Dihydrolipoyl dehydrogenase	-2.0	0.02	2	4	0.000204	0.000125	0.000408	0.000204
Q99PG0	Arylacetamide deacetylase	-1.9	0.00	6	12	0.00072	0.000464	0.001393	0.000515
Q91WL5	Cytochrome P450 4A12A	-1.8	0.01	8	14	0.000739	0.000212	0.001323	0.000264
Q64459	Cytochrome P450 3A11	-1.6	0.03	26	43	0.002447	0.001046	0.003801	0.001102
P16331	Phenylalanine-4-hydroxylase	-1.5	0.05	19	30	0.001944	0.000855	0.002903	0.001278
P08113	Endoplasmin	1.5	0.04	166	113	0.009769	0.002787	0.006664	0.002633
P20029	78 kDa glucose-regulated protein	1.5	0.03	52	36	0.003806	0.001868	0.00255	0.001018
Q91WN4	Kynurenine 3-monooxygenase	1.5	0.00	5	3	0.000511	0.000242	0.000335	0.000213
Q91YQ5	Dolichyl-diphosphooligosaccharide--protein glycosyltransferase subunit 1	1.5	0.03	33	23	0.002647	0.000739	0.001718	0.00028
Q8JZR0	Long-chain-fatty-acid--CoA ligase 5	1.6	0.02	34	22	0.002427	0.001074	0.001512	0.000436
Q9DBG6	Dolichyl-diphosphooligosaccharide--protein glycosyltransferase subunit 2	1.7	0.04	25	15	0.00208	0.001158	0.00123	0.000627
Q9EQH3	Vacuolar protein sorting-associated protein 35	1.7	0.04	4	2	0.000258	0.000121	0.00015	7.52E-05
P58252	Elongation factor 2	1.7	0.01	54	31	0.003069	0.000919	0.001784	0.000832
P35564	Calnexin	1.7	0.02	33	20	0.002732	0.001011	0.001575	0.000292
P06151	L-lactate dehydrogenase A chain	1.8	0.03	23	13	0.003258	0.001341	0.001839	0.00128
Q9EQK5	Major vault protein	1.8	0.05	5	0	0.000319	0.00032	0.000175	0.000209
Q9QYC7	Vitamin K-dependent gamma-carboxylase	2.6	0.01	3	0	0.000211	0.000135	8.14E-05	5.81E-05
Q6ZWN5	40S ribosomal protein S9	2.7	0.05	1	0	0.000317	0.000198	0.000118	2.41E-05
P01027	Complement C3	3.9	0.05	16	4	0.000492	0.000373	0.000127	0.000132
P35487	Pyruvate dehydrogenase	4.2	0.02	2	0	0.000329	0.000147	7.86E-05	3.92E-05
P01029	Complement C4-B	6.2	0.01	6	0	0.000185	0.000126	3E-05	4.1E-05

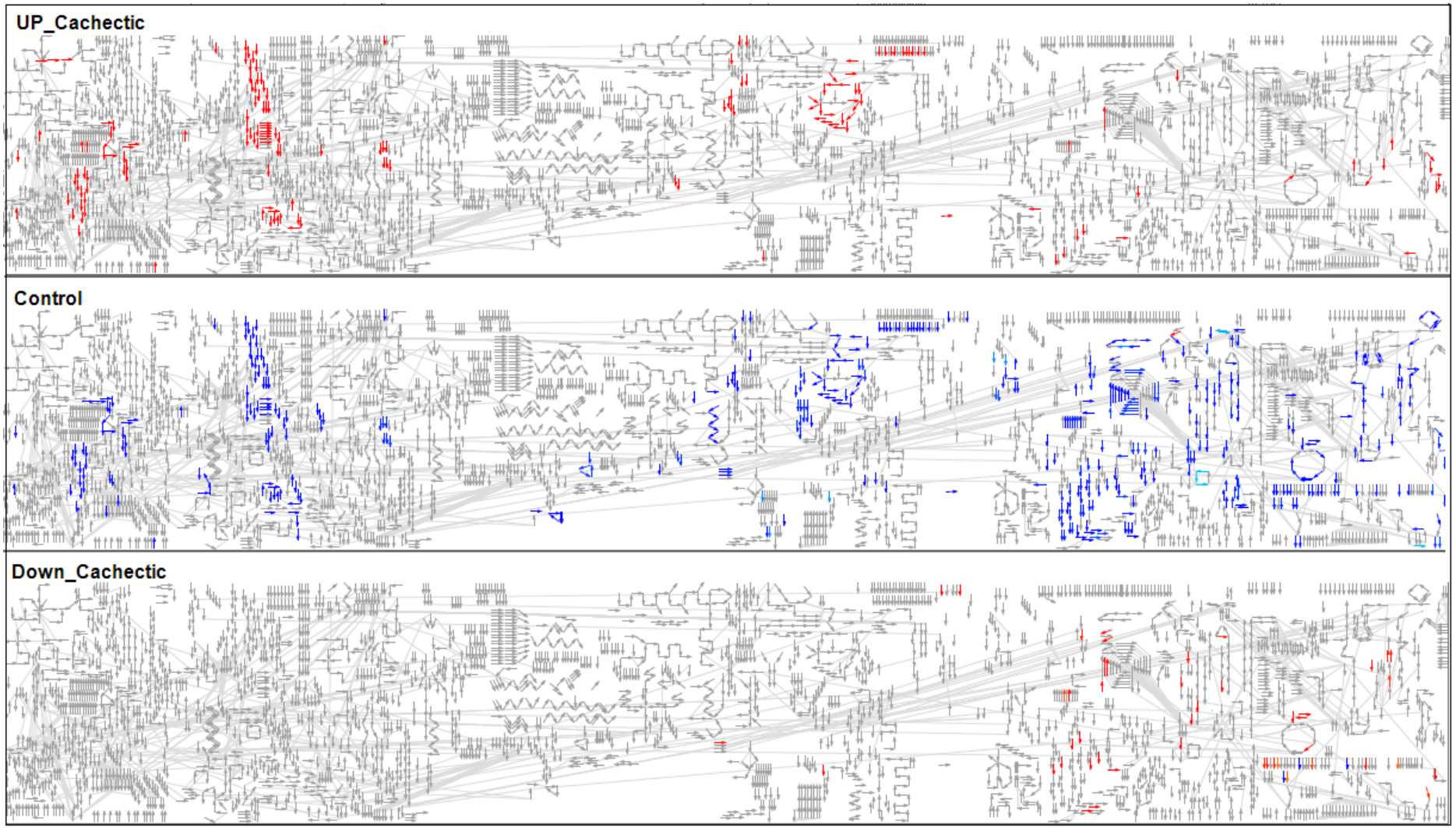

Figure 4.7: The up and down regulated Bis-probe captured proteins (Red arrows) in the cachectic mice liver samples compared to the control (Blue arrows) in the reactome map of mice.

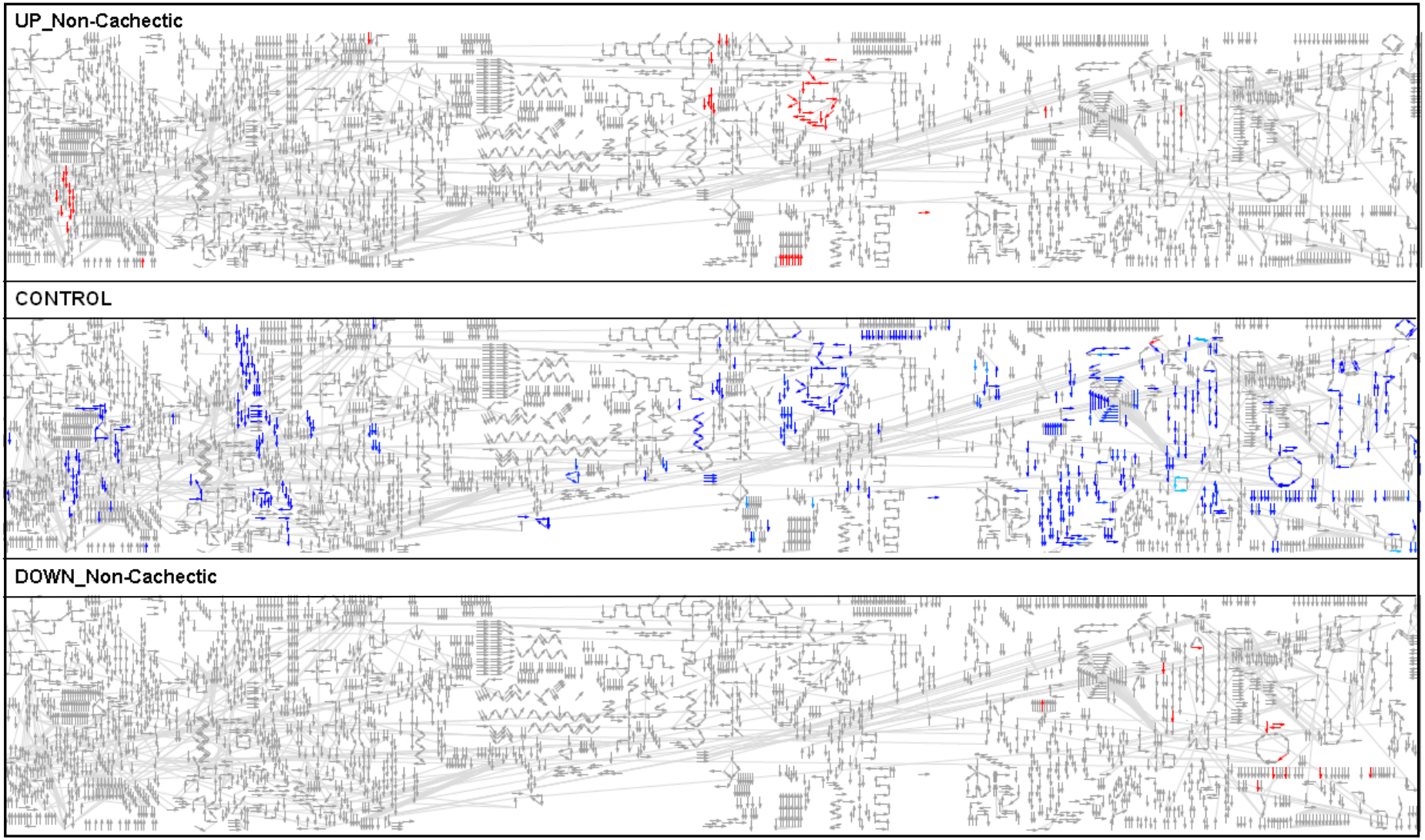

Figure 4.8: The up and down regulated Bis-probe captured proteins (Red arrows) in the non-cachectic mice liver samples compared to the control (Blue arrows) in the reactome map of mice.

4.3.5.1. Pathway Analysis.

4.3.5.1.1. Protein Biosynthesis

The Bis-probe captured 8 proteins involved in the protein biosynthesis pathway that were significantly upregulated in the cachectic mice liver samples compared to the control (**Figure 4.9**). In the cachectic mice livers the capture of two ATP-dependent aminoacyl synthetases, threonyl-tRNA synthetase and isoleucyl-tRNA synthetase, were approximately 4 fold higher (**Figure 4.9**). Similarly, the GTP dependent translational elongation enzymes; elongation factor 1α and elongation factor 2 were of greater abundance in the cachectic mice liver. Interestingly, the Bis-probe also pulled down many RNA-binding 40S and 60S ribosomal proteins involved in the protein biosynthesis pathway and the capture of these proteins varied from 1.5 fold to approximately 7.5 fold in the cachectic mice livers compared to the control mice livers (**Figure 4.10**). Of the 5 proteins that were involved in protein metabolism and upregulated in the non-cachectic group, vitamin K dependent gamma carboxylase showed the highest fold change (2.5 fold) (**Figure 4.9**) and only one 40S ribosomal protein (S9) was identified with a significant difference of 2.7 fold (**Figure 4.10**).

4.3.5.1.2. Amino acid metabolism.

In the amino acid metabolism pathway, the abundance of enzymes captured by the Bis-probe was down regulated in the cachectic mice liver samples compared to the control. In our study we identified 6 enzymes involved in amino acid degradation, which were differentially captured by the Bis-probe (**Figure 4.11**). The Bis-captured enzymes in this pathway are primarily components of the branched-chain alpha-keto acid dehydrogenase complex and their relative abundance was lower in the cachectic mice livers, except for mitochondrial ornithine transporter which showed a 2 fold increase (**Figure 4.11**). Similarly, in the non-cachectic samples the relative abundance of 2 out of 3 Bis-captured

proteins involved in amino acid metabolism was lower compared to the control samples (**Figure 4.11**)

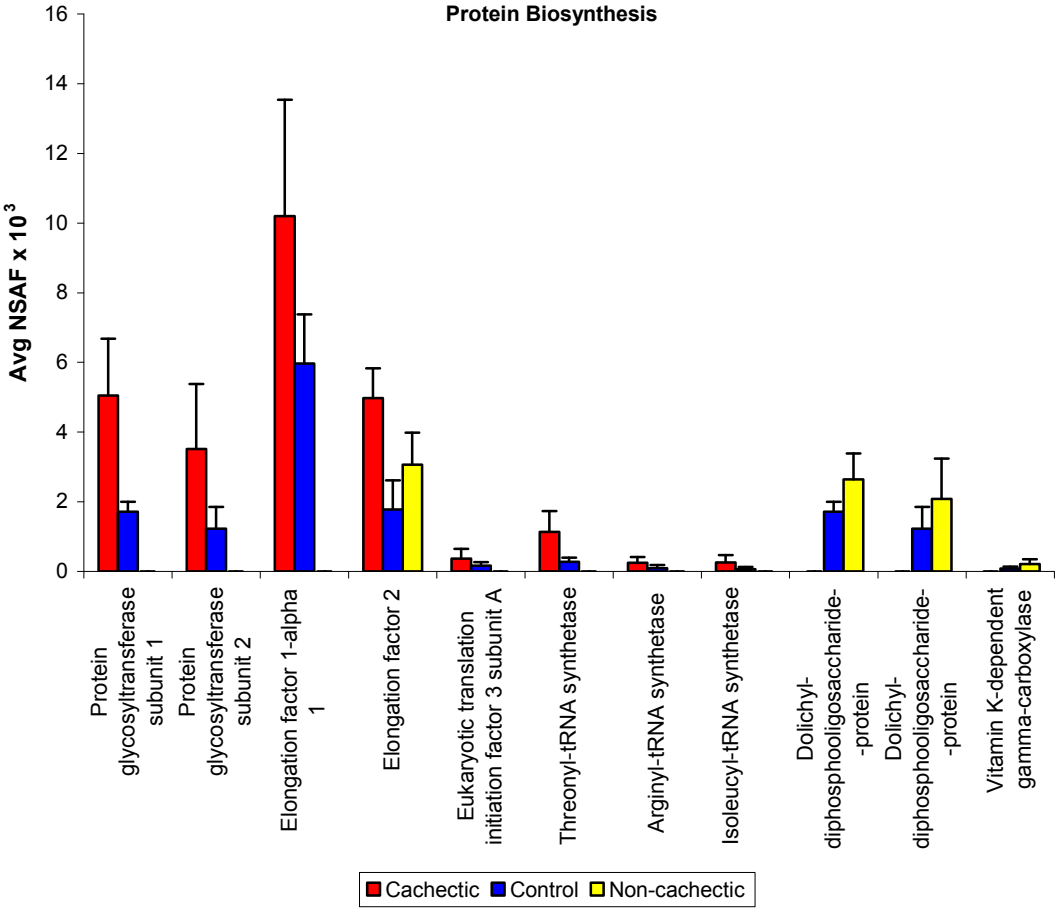

Figure 4.9: Average NSAF values and relative fold change of enzymes involved in Protein Biosynthesis, captured by the Bis-probe in cachectic, non-cachectic and control mouse liver samples.

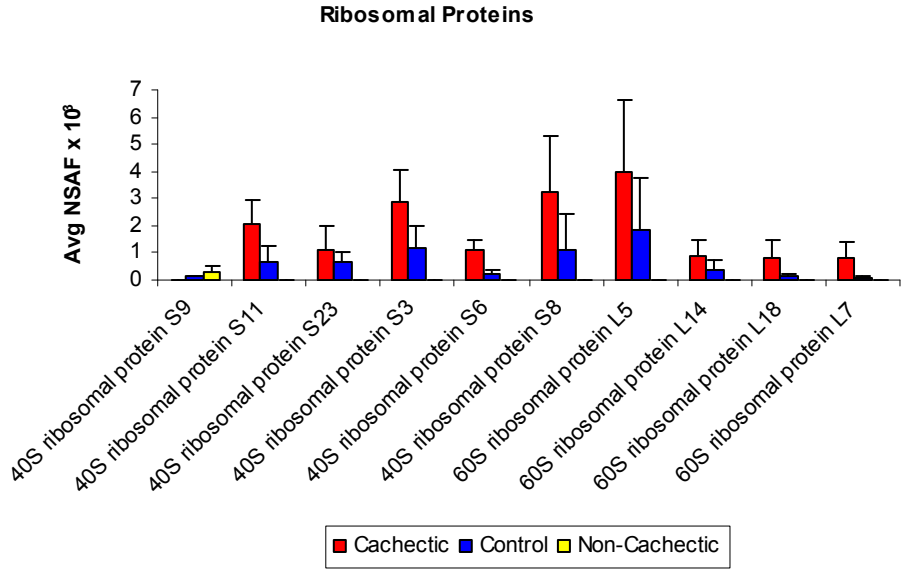

Figure 4.10: Average NSAF values and relative fold change of 40S and 60S ribosomal proteins involved in Protein Biosynthesis, captured by the Bis-probe in cachectic, non-cachectic and control mouse liver samples**.**

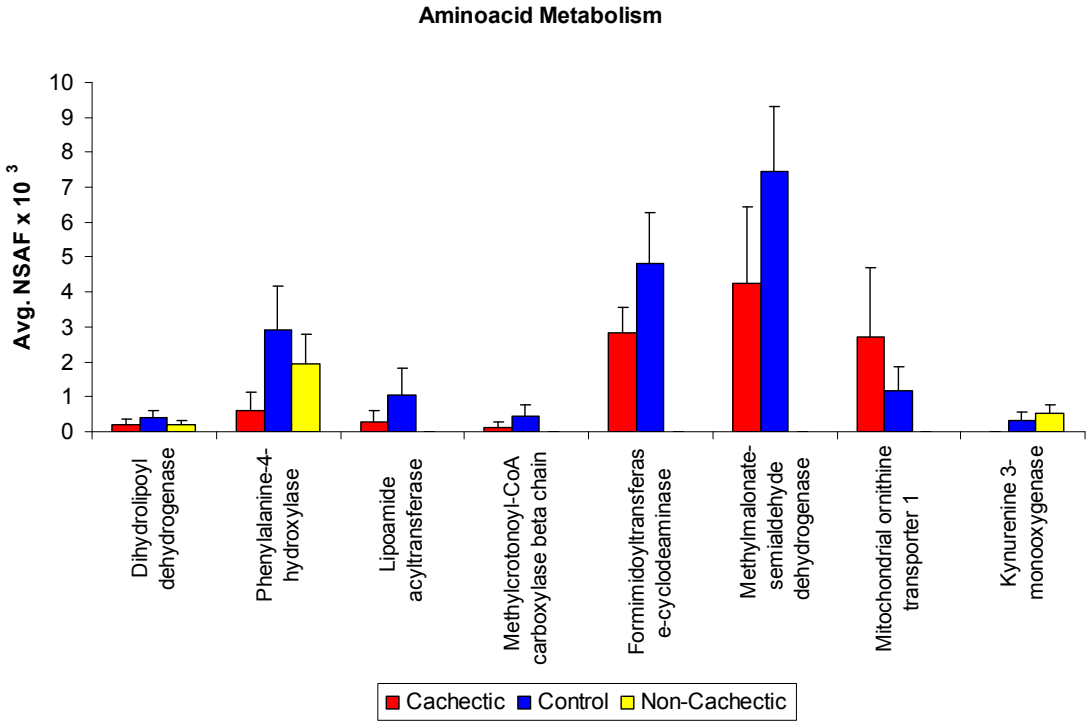

Figure 4.11: Average NSAF values of enzymes involved in amino acid metabolism, captured by the Bis-probe in cachectic, non-cachectic and control mouse liver samples.

4.3.5.1.3. Lipid metabolism.

The Bis-probe captured 9 key enzymes involved in β-oxidation of fatty acids and lipid biosynthesis that were significantly different in their abundance level in cachectic and control mice liver samples (**Figure 4.12**). The abundance level of very long-chain specific acyl-CoA dehydrogenase was almost double in the cachectic samples compared to that of the control (**Figure 4.12**). However, in the control samples the structurally and functionally related enzyme, long-chain specific acyl-CoA dehydrogenase, was almost 2 fold higher in abundance compared to the cachectic group. Similarly, long chain fatty acid-CoA ligase 1 responsible for the activation of long-chain fatty acids for both cellular lipid synthesis and degradation via β- oxidation was almost 2 fold lower in abundance in the cachectic samples compared to the controls. A sharp reduction in abundance level (3.4 fold) in the cachectic samples was also observed for ATP- citrate synthase, the primary enzyme responsible for cytosolic acetyl CoA synthesis.

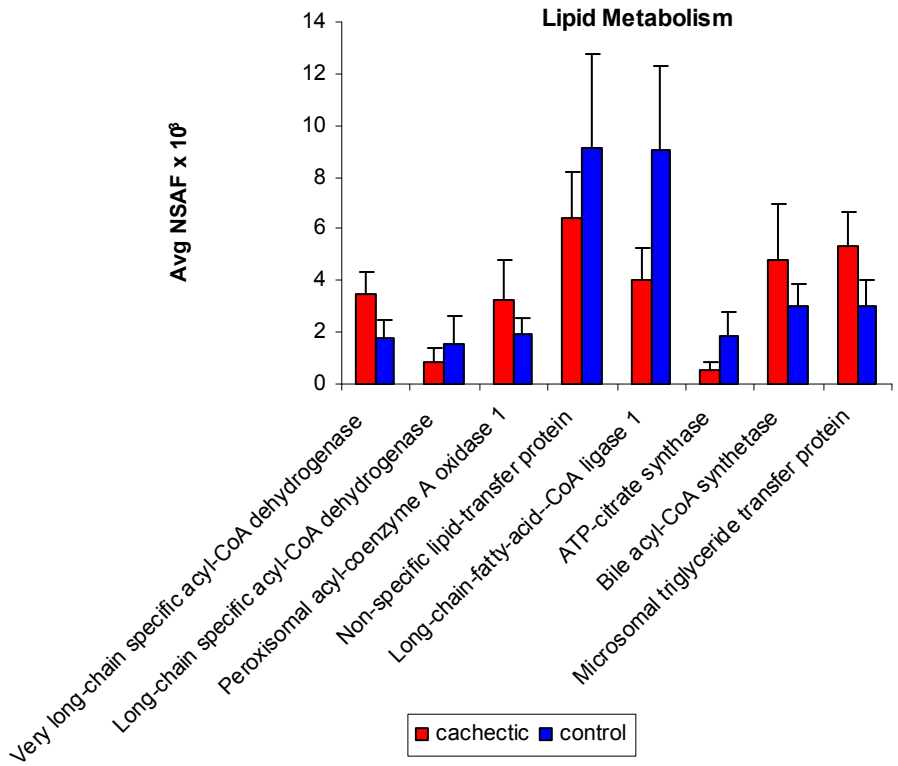

Figure 4.12: Average NSAF values of enzymes involved in Lipid metabolism, captured by the Bis-probe in cachectic and control mouse liver samples.

4.3.5.1.4. Carbohydrate metabolism.

Six Bis-bound enzymes were identified that were involved in carbohydrate metabolism and were significantly different in abundance levels in the cachectic and control mice groups (**Figure 4.13**). In the cachectic mice liver samples the abundance level of phosphoenol pyruvate carboxykinase and malate dehydrogenase, were upregulated by 4 fold and 2.5 fold respectively. However, the abundance level of two of the key glycogenesis enzymes, glycogen synthase and UTP-glucose-1-phosphate uridylyltransferase, were significantly lower in cachectic mice livers by 2.5 and 5.4 fold respectively. There was no significant difference in the abundance levels of Bis-captured enzymes in the non-cachectic and control groups.

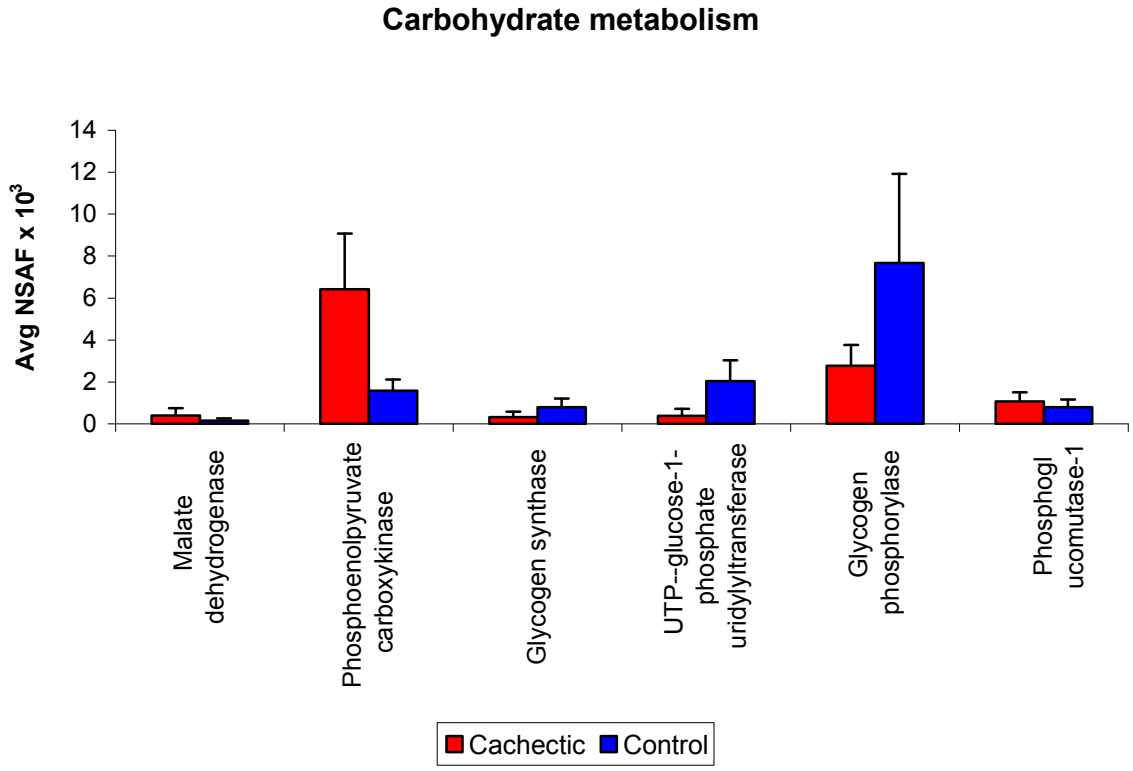

Figure 4.13: Average NSAF values of enzymes involved in carbohydrate metabolism, captured by the Bis-probe in cachectic and control mouse liver samples.

4.3.5.1.5. Biological Oxidation.

The study identified 5 Bis-bound enzymes that were significantly different in their abundance levels in the cachectic and control mouse livers (**Figure 4.14**). The abundance levels of all the enzymes involved in biological oxidation was lower in the cachectic groups except for s-adenosylmethionine synthase isoform type 1, which was 5 fold more abundant (**Figure 4.14**). The abundance levels of amine oxidase B involved in the oxidative deamination of biogenic and xenobiotic amines was almost 1.5 fold down and the enzyme involved in the n-oxidation of aldehydes, aldehyde dehydrogenase, was 2 fold lower in abundance.

Further, the Bis-probe also captured 6 Cytochrome P450s (CYP) with abundance levels significantly different in the cachectic and control samples (**Figure 4.15**). The abundance levels of these heme-thiolate monooxygenases involved in drug metabolism and oxidation of steroids, fattyacids and xenobiotics were significantly lower in the cachectic group.

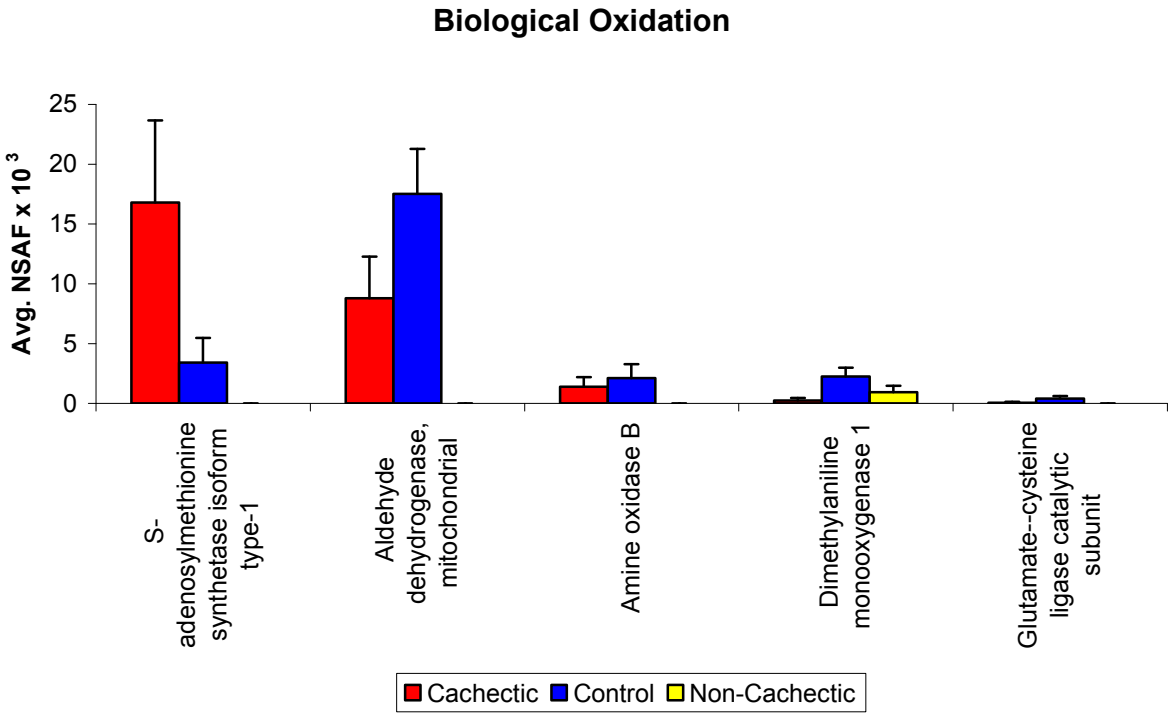

Figure 4.14: Average NSAF values of enzymes involved in Biological oxidation, captured by the Bis-probe in cachectic, non-cachectic and control mouse liver samples

Similarly, in the non-cachectic and the control groups, dimethyl monooxygenase 1 was significantly down regulated by 2.4 fold. As observed in the cachectic and the control group comparison the CYP 1A2 and CYP 4A12A were also down regulated in the non-cachectic and control group comparisions (**Figure 4.15**). However, both the proteins were only down regulated by 2 fold in the non-cachectic group in contrast to the overwhelmingly large decreases observed in cachectic mice (50 and 7 fold).

4.3.5.1.6. Membrane Trafficking.

In the cachectic mice liver samples 4 Bis-captured proteins were identified that were involved in membrane trafficking and had significant difference in abundance levels to the control group (**Figure 4.16**).

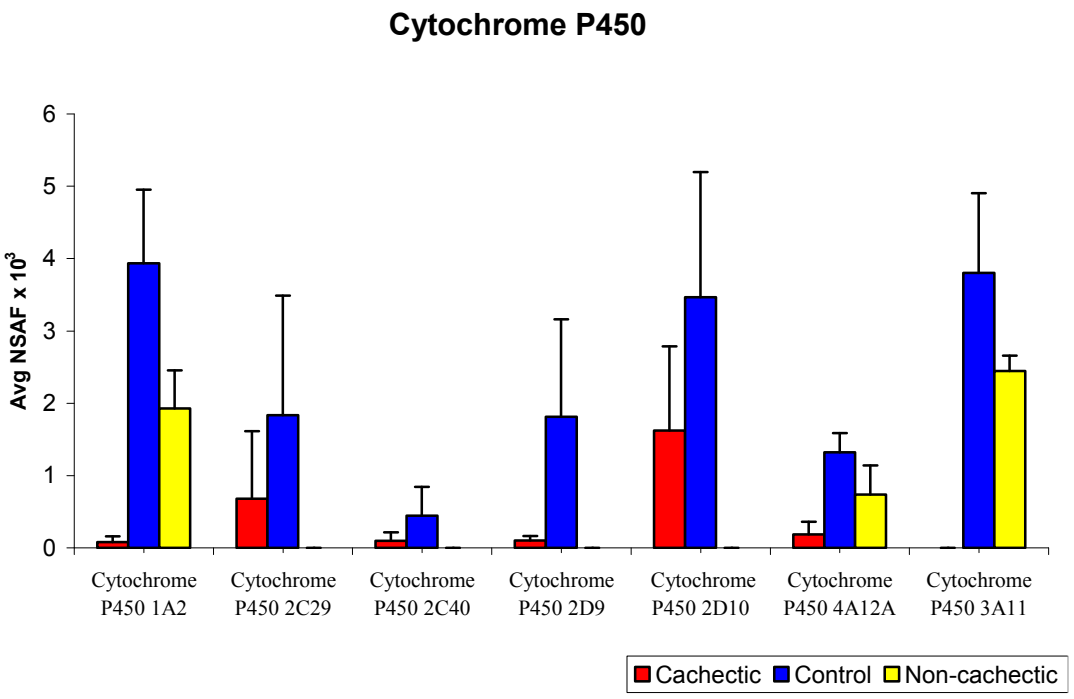

Figure 4.15: Average NSAF values of enzymes involved in Biological oxidation, captured by the Bis-probe in cachectic, non-cachectic and control mouse liver samples.

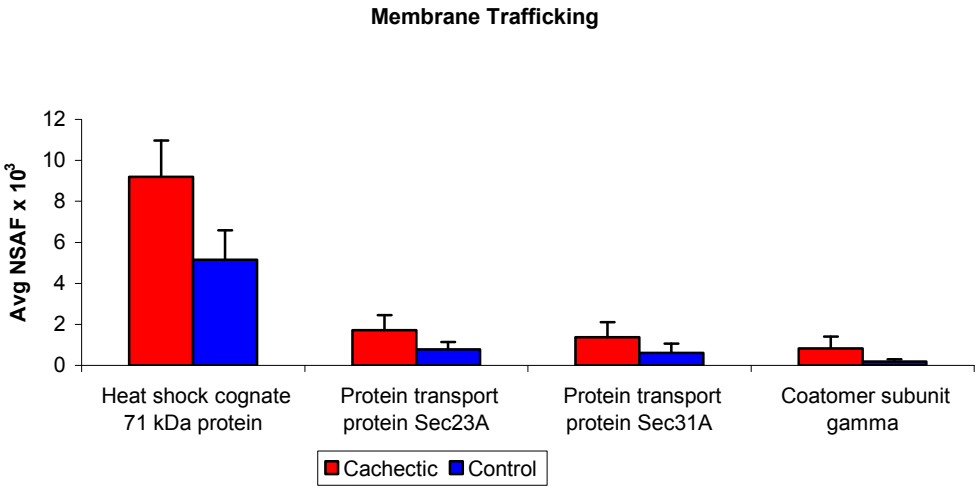

Figure 4.16: Average NSAF values of enzymes involved in Membrane Trafficking, captured by the Bis-probe in cachectic and control mouse liver samples.

The Sec 23A and Sec 31A proteins responsible for ER-Golgi protein trafficking were 2 fold higher in abundance in the cachectic group. Similarly, the coatomer subunit gamma was also higher by 4.5 fold and the heatshock 71 kDa protein by 1.8 fold. There was no significant difference in the abundance levels of Bis-captured enzymes in the non-cachectic and control groups.

4.4. Discussion

The study employed a Bis-probe to capture a broad spectrum of enzyme classes that utilized ATP or structurally related analogues as cofactor for catalysis in the liver of C26 adenocarcinoma mouse models. The method was used to compare liver enzymes in tumour free control mice, tumour bearing mouse models with high circulating IL-6 causing cachexia and tumour bearing non-cachexic models. This approach allowed us to identify and quantitate the relative abundance of many Bis-bound enzymes in the liver of cachectic and non-cachectic mice involved in protein biosynthesis, amino acid metabolism, lipid metabolism, carbohydrate metabolism and biological oxidation. This provided the opportunity to study the effects of cachexia on the liver of mice bearing C-26 adenocarcinoma.

Our approach used only 100 μg of protein from the mouse livers to identify the Bis-bound proteins and quantitate the relative abundance of the captured enzymes. This approach has provided valuable information towards more thorough understanding of the biochemical pathways that are involved in cancer cachexia.

4.4.1. Carbohydrate Metabolism

Six Bis-bound enzymes involved in gluconeogenesis, glycogenesis and glycogenolysis pathways were identified with differential abundance levels in cachectic mice livers compared to the controls. The relative abundance levels of phosphoenol pyruvate carboxykinase, which catalyses the rate limiting step in hepatic gluconeogensis was 4 times higher in the cachectic mice livers. The increased presence of this enzyme is an indication of hepatic lactate recycling via the Cori Cycle, which is one of the main metabolic disturbances associated with cancer cachexia [168]. The high IL-6 secreting C-26 adenocarcinomas have been reported to influence tumour growth and directly

influencing liver metabolism. Tumours are known to consume huge amounts of glucose aerobically and once the supply of oxygen becomes too low for complete aerobic dissimilation, the tumours anaerobic dissimilation is activated to generate energy. This anaerobic dissimilation not only results in massive release of lactate into the host circulation but also uncouples the glycolysis and TCA cycles maintaining the increased lactic acid concentration in the circulation [153]. Lactate is then recycled via a very inefficient metabolic process consuming 6 moles of ATP.

Similarly, the abundance of malate dehydrogenase was also upregulated by 2.5 fold in the cachectic mice livers compare to controls. Malate dehydrogenase is a highly stereo specific NAD requiring enzyme involved in production of glucose by catalysing the conversion of malate to oxaloacetate and vice versa. However, the abundance levels of 2 glycogenesis enzymes glycogen synthase and UTP-glucose-1-phosphate uridylyltransferase were significantly lower in cachectic mice livers by 2.5 and 5.4 fold respectively. Similarly, the abundance levels of the glycogenolytic enzyme, glycogen phosphorylase, which catalyses the rate limiting step in the degradation of glycogen was 3 fold lower in the cachectic mice liver samples. Blood glucose levels are important indicators and sensors of hepatic glycogenesis and glycogenolysis [169]. The decrease in the glycogenesis enzyme levels in the cachectic mice livers may be attributed to the decreased glucose levels in the host circulation, meaning the absence of glucose that could be transported into the liver for glycogen synthesis. In normal livers, unused circulating glucose blocks hepatic glycogenolysis and promote glycogenesis and vice versa [169]. However, the decreased abundance level of glycogen phosphorylase indicates a depletion of liver glycogen in cachectic mice livers. Studies on cachexia inducing colonic adenocarcinomas (MAC16) have showed a progressive decrease in liver glycogen in direct proportion to the loss of body weight [170]. Similarly, loss of liver glycogen has also been reported by Schulze *et*

al. in Walker Carcinoma 256 bearing rats inducing cachexia [171]. They found the activity of liver phosphorylase was reduced in advanced tumour cachexias. However, the comparison of abundance levels of Bis-bound enzymes in non-cachectic and control mouse liver did not find any enzymes involved in carbohydrate metabolism to be significantly different, indicating that disrupted carbohydrate metabolism is a hallmark of cancer cachexia.

4.4.2. Protein biosynthesis

The relative abundance of Bis-bound enzymes involved in hepatic protein biosynthesis was higher in the cachectic mice liver samples compared to the controls. However, in the non-cachectic mouse liver with low IL-6 levels the abundance levels of enzymes involved in hepatic protein biosynthesis were relatively similar to that of the control mouse liver samples.

IL-6 is known to induce increased hepatic synthesis of acute phase proteins [164, 172, 173]. Acute phase proteins are the export plasma proteins that are synthesised in the hepatocytes in response to an inflammatory stimulus and are often considered as an index of pro-inflammatory cytokine activity [174]. The synthesis of acute phase reactants both positive (e.g. C-reactive protein, fibrinogen) and negative (e.g. albumin, transferrin) in human hepatocytes is reported to be strongly influenced by IL-6 [172]. Significantly higher levels of C-reactive protein (CRP) and fibrinogen has also been reported in lung cancer patients with high serum IL-6 levels compared to those without serum IL-6 levels or having benign lung diseases [164]. Further, studies have also reported a massive increase in hepatic protein synthesis rate as a result of IL-6 exposure [172]. In our study, ATP dependent aminoacyl synthetases involved in the activation phase of protein translation and the GTP dependent elongation enzymes were higher in relative abundance in the

cachectic mice livers compared to the controls, indicating the potential for increased acute phase hepatic protein synthesis in cachexia. Further, as expected, the abundance level of 40S and 60S ribosomes was also high in the cachectic livers to facilitate the increased demand of acute phase protein synthesis. Similarly in the non-cachexic mice livers there was no significant difference in the abundance levels of the ribosomes compared to the controls, with the exception of 40S ribosomal protein S9 (+2.7 fold).

4.4.3. Amino acid Metabolism

The abundance levels of Bis-bound enzymes involved in the hepatic degradation of amino acids was lower in the cachectic mice livers compared to the controls. Interestingly, two enzymes (dihydrolipoyl dehydrogenase and lipoamide acyl transferase) of branched-chain alpha-keto acid dehydrogenase complex (BCKDH) were observed to be down regulated in the cachectic mice livers. The BCKDH complex is a key regulatory and rate limiting enzyme in the catabolism of branched-chain amino acids (BCAAs) [175]. The catabolic pathway of BCAAs involves two important steps. The first step is the reversible transamination to form branched-chain α-keto acids (BCKAs), which is catalysed by branched-chain aminotransferase (BCAT). The second step is the irreversible oxidative decarboxylation of the BCKAs, which is catalysed by the (BCKDH) complex [176] . The complex consists of three catalytic components: a branched-chain α-keto acid decarboxylase (E1; heterotetramer of α and β subunits), a dihydrolipoyl transacylase (E2), and a dihydrolipoyl dehydrogenase (E3) [177]. The activity of the BCKDH complex is primarily regulated through a reversible phosphorylation (inactivation) and dephosphorylation (activation) of the E1 component of the complex by the BCDH kinase and phosphatase, respectively [178, 179]. **Figure 4.17** summarises the activity of BCKDH complex.

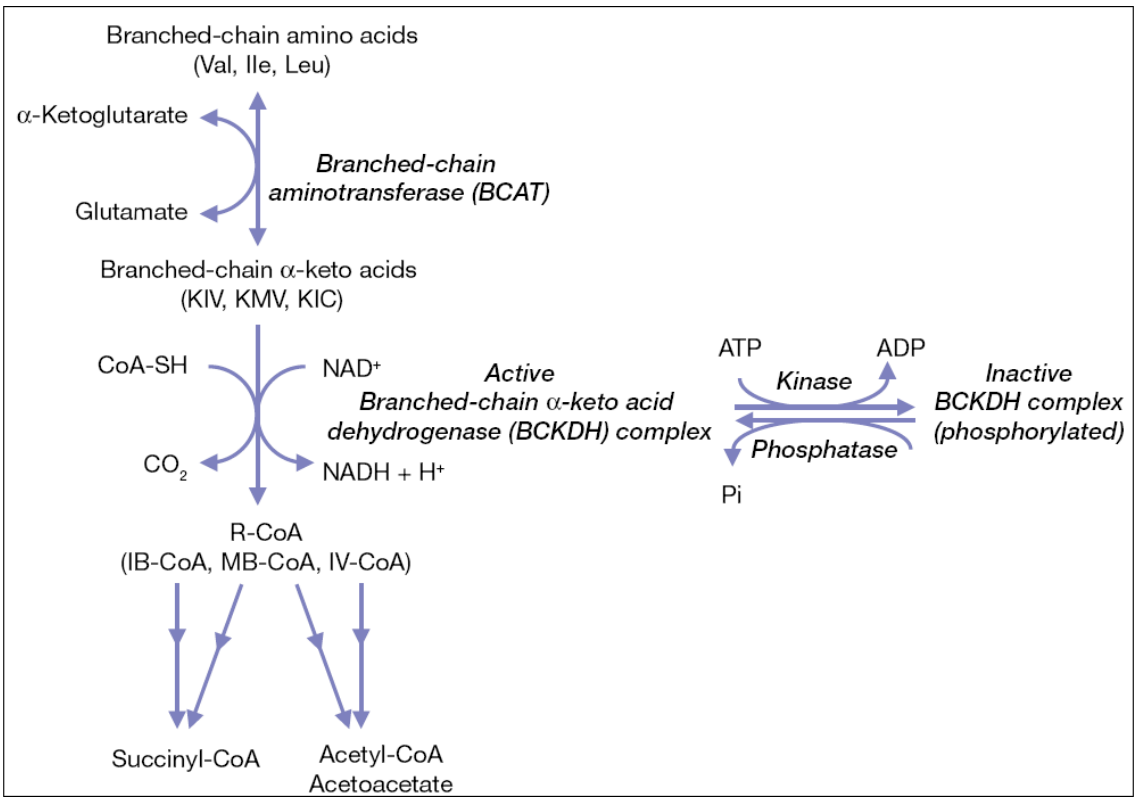

Figure 4.17 Activity of BCKDH complex.

Most previous studies have focused on the rat liver because BCKDH activity is markedly higher in liver in comparison to other organs [180]. The liver lacks or expresses lower levels of BCAT activity leaving the initial step in BCAA degradation to tissues other than liver [181]. So in hepatocytes, the absence of the BCAT isozyme and high activity of BCKDH favours liver oxidation of circulating BCKAs and account for the low concentrations of BCKAs found in liver [182]. However, there are no studies that profiled the hepatic BKCDH complex in cancer cachexia or studied the effect of mice bearing distal C26 adenocarcinoma on liver BCKDH activity. It would be very interesting and useful to enrich BCDH kinase using specific probes and study the relative abundance in cachectic mice livers, which would further elucidate the decreased hepatic branched chain amino acid degradation in cancer cachexia.

4.4.4. Lipid Metabolism

The Bis-probe captured three key enzymes involved in the first step of β-oxidation that were differentially abundant in the cachectic and control mice livers. Fatty acid oxidation occurs in both mitochondria and peroxisomes. When the fatty acids are too long to be handled by the mitochondria for degradation, they are processed via the peroxisomes. A key enzyme involved in the peroxisomal oxidation is the peroxisomal acyl-coenzyme A oxidase 1, which was upregulated in the cachectic mice livers by 1.7 fold. After the initial oxidation in the peroxisomes the shortened fatty acids are then directed to the mitochondria for further oxidation. The first committed step in the mitochondrial β-oxidation of the very long chain fatty acids is carried out by very long-chain specific acyl-CoA dehydrogenase (VLCAD). Our studies revealed that this Bis-bound enzyme was also two times more abundant in the cachectic mice livers compared to the controls. However, this enzyme has very little activity for substrates which are less than 12 carbon atoms long and these are handled by long-chain specific acyl-CoA dehydrogenase (LCAD). LCAD are also key enzyme involved in the mitochondrial β-oxidation of unsaturated fatty acids [183]. However, the abundance level of this enzyme was two fold lower in the cachectic livers. The reduced abundance of this enzyme in the cachectic livers implicates the reduction in further shortening of the fatty acid chain and ultimately limiting the available pool of produced acetyl-CoA. The hepatic content of acetyl-CoA was also found to be low in the host livers of mice bearing cachexia-inducing colon adenocarcinoma MAC16 or related tumour MAC13 [184]. Further, the enzyme, long-chain-fatty-acid-CoA ligase 1, responsible for the activation of the long chain fatty acids for degradation via β-oxidation and propanoyl-CoA C-acyl transferase, involved in the final step of β- oxidation was lower in abundance in the cachectic samples by 2 fold and 1.4 fold.

4.4.5. Xenobiotic Metabolism

Cytochrome P450 (CYP) mixed function oxidase system play a key role in the modification phase (Phase-1) of xenobiotic metabolism by introducing reactive and polar groups into their substrates by hydroxylation. The reaction mechanism of the P-450 oxidases proceeds through the reduction of cytochrome-bound oxygen and the generation of a highly-reactive oxyferryl species [185]. Subsequently the activated xenobiotic metabolites are then conjugated with charged species such as glutathione (GSH), sulphate, glycine or glucoronic acids. The activated xenobiotic conjugates are then further metabolised and subsequently excreted from the body. Pro-inflammatory cytokines are reported to effect the cytokine signalling in the liver, which can lead to reduce hepatic expression of cytochromes and ultimately to reduced drug clearance and increased chemotoxicity [143]. A decreased expression of hepatic cytochrome P450 drug metabolism in advanced cancer cases associated with increased plasma concentration of interleukin-6 (IL-6) and C-reactive protein is also reported [186, 187]. Further, the relationship between inflammation and repression of CYP activity has been extensively studied in various in vitro and animal models of acute inflammation, including infection and trauma, but also following administration of endotoxin or individual cytokines. These studies have shown that the inflammatory response leads to reduced CYP mRNA and protein synthesis [188, 189]. Further, the reduced CYP levels consequently results in decreased microsomal metabolism and CYP-mediated drug clearance.

Six cytochrome CYP enzymes (CYP1A2, CYP2C29, CYP2C40, CYP2D9, CYP2D10 and CYP4A12A) were identified using Bis-probe. The relative abundance of all the cytochrome P450 enzymes was significantly down regulated in the cachectic mice liver samples compared to the controls. Reduced abundance of CYP1A2 and CYP4A12A was also observed along with CYP3A11 in the non-cachectic group compared to the controls.

CYP3A11 is part of the CYP3A subclass of cytochrome P450 enzymes and is responsible for the phase I metabolism of 45%-60% of clinically administered drugs [190]. The CYP1A2 catalyses the metabolism of many xenobiotics, including the oxygenation of polycyclic aromatic hydrocarbons (PAH). Induction of CYP1A enhances the metabolism of PAHs, and therefore, represents an adaptive response to chemical exposure in mammalian cells [191]. CYP1A2 was almost 50 times down regulated in the cachectic mice livers and 2 times in the non-cachectic livers, indicating the vulnerability of both these groups to chemical exposure compared to the controls. Similarly, the other cytochrome P450 enzymes of CYP2C and CYP2D subclass those were determined to be down regulated in the cachectic mouse livers has been described to be functionally related to fattyacid metabolism and steroid production, suggesting the reduced hormone synthesis and metabolite clearing during cachexia.

The use of Bis-probe to capture liver enzymes in mouse model of cancer cachexia has shed light on the involvement of various metabolic pathways. The overall carbohydrate metabolism is reduced, the hepatic acute phase protein synthesis is induced, branched chain amino acid degradation and lipid metabolism is significantly reduced. Further, the marked reduction in the cytochrome P450 enzymes reflected the impaired xenobiotic metabolism and the subsequent chemotoxicity encountered in cancer cachexia. It would be of interest to examine these livers by chemical proteomics using other probe architecture to possibly capture enzymes missing from the analysis. A specific kinase enrichment probe to understand the kinase activation in these liver samples would add to the completeness of the study.

Supplementary Figure 1:
Enlarged Figure 4.4

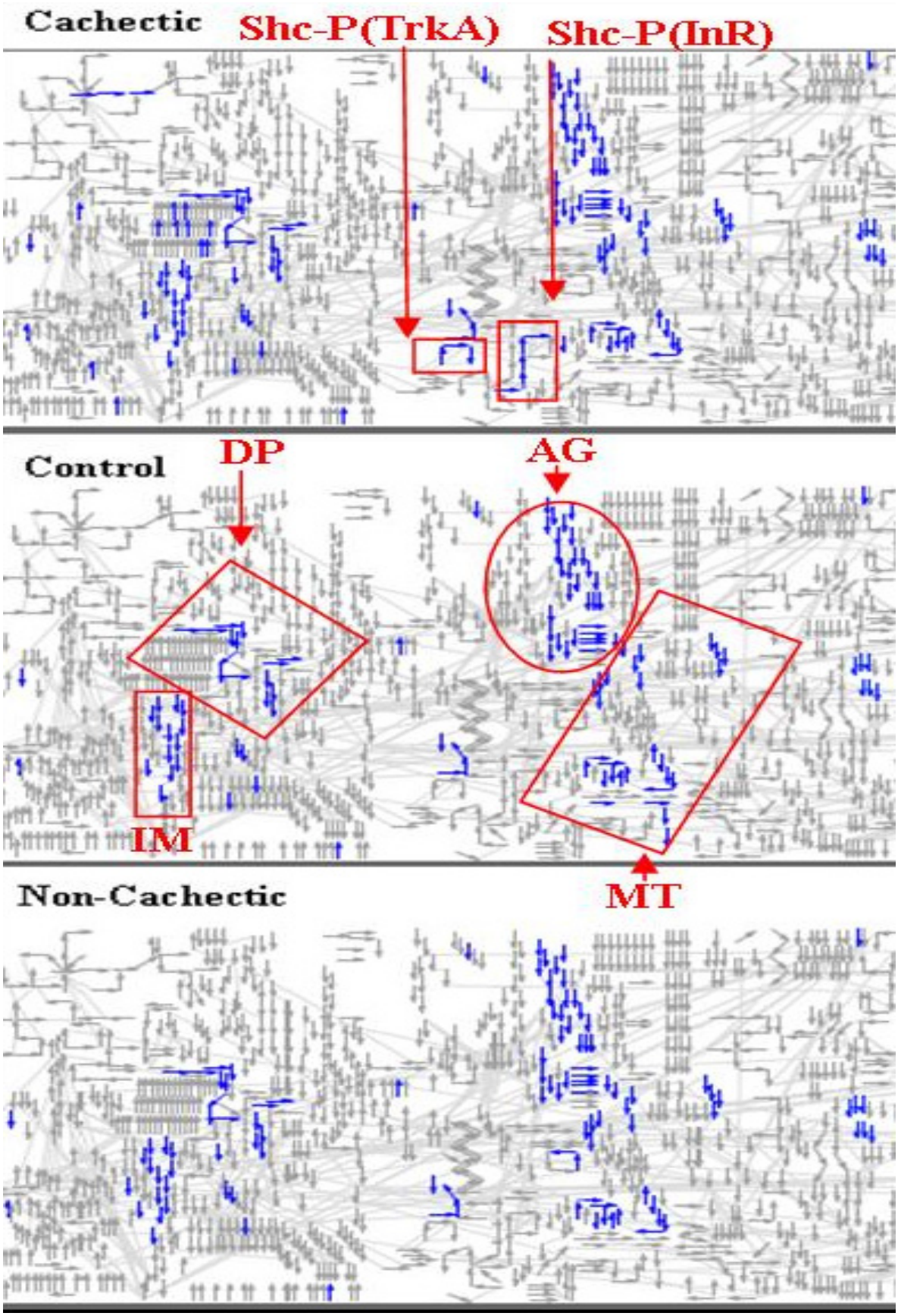

Figure 4.4 Section 1: Reactome Skypainter Analysis of Bis-bound proteins in mice liver. Arrows represent all the biological events (reactions and/or pathways) present in the mouse system and the coloured arrows represent the Bis-captured proteins involved in a particular event. Highlighted pathways:- MT-Membrane Trafficking; AG-Axon Guidance; DP- Diabetes Pathway; IM- Immune System Signalling; Nerve growth factor signalling events unique to cachectic groups:- Shc-P (TrkA)-SHC phosphorylation via tyrosine kinase A and Shc-P (InR)-SHC phosphorylation via Insulin receptors.

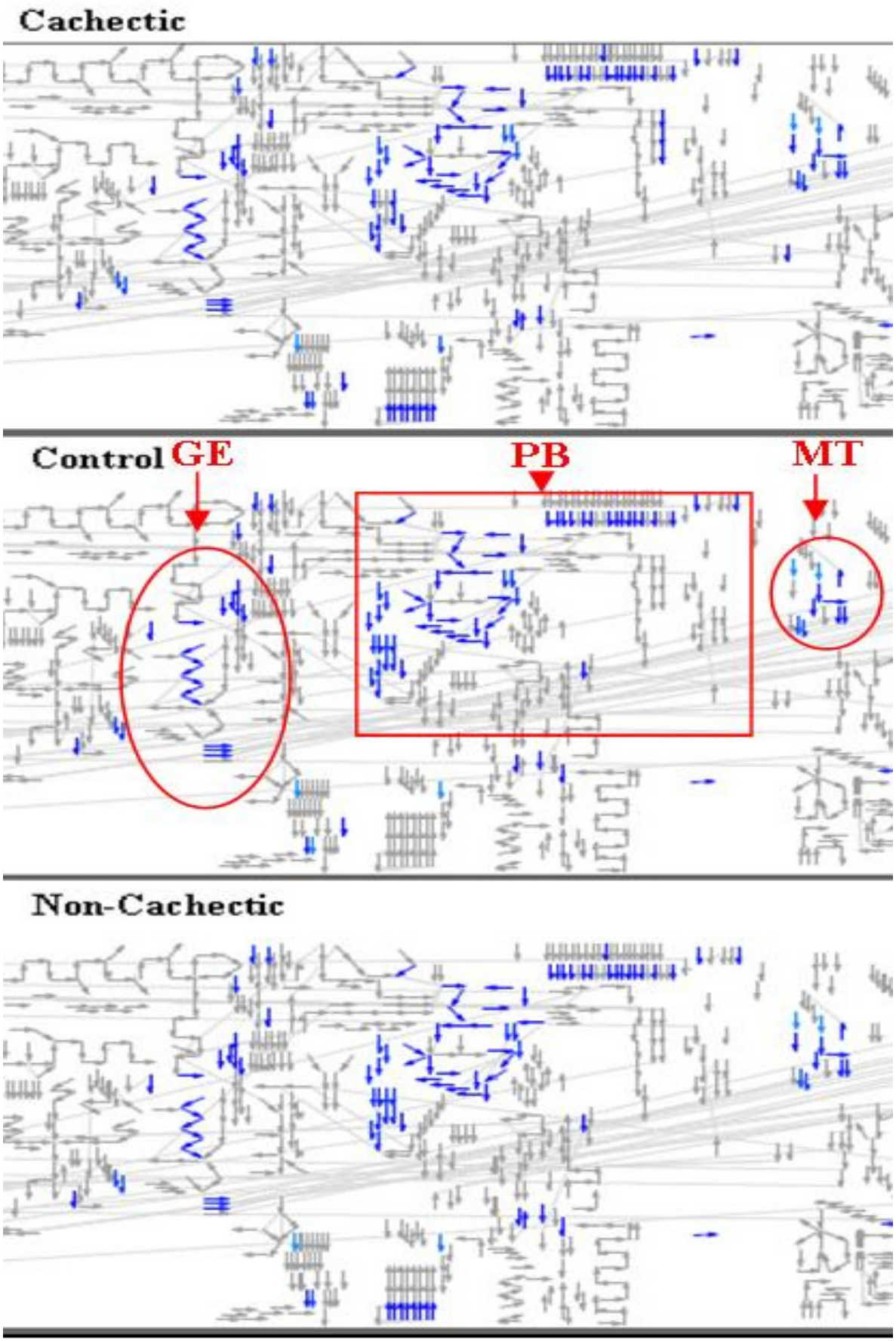

Figure 4.4 Section 2: Reactome Skypainter Analysis of Bis-bound proteins in mice liver. Arrows represent all the biological events (reactions and/or pathways) present in the mouse system and the coloured arrows represent the Bis-captured proteins involved in a particular event. Highlighted pathways: - MT-Membrane Trafficking; GE- Gene Expression and PB- Protein Biosynthesis.

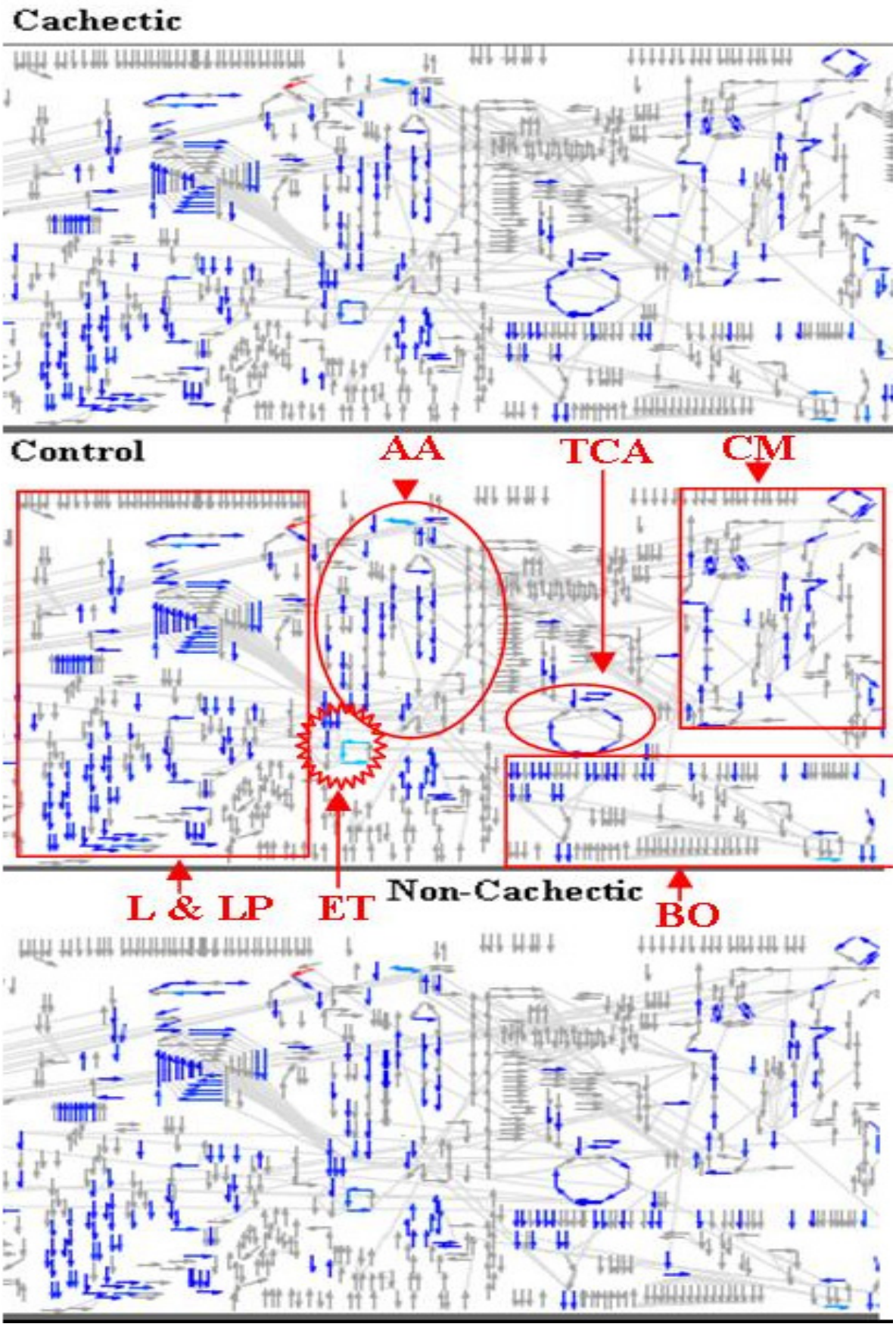

Figure 4.4 Section 3: Reactome Skypainter Analysis of Bis-bound proteins in mice liver. Arrows represent all the biological events (reactions and/or pathways) present in the mouse system and the coloured arrows represent the Bis-captured proteins involved in a particular event. Highlighted pathways: - CM- Carbohydrate Metabolism; BO-Biological Oxidation; TCA-TCA cycle; AA-Amino acid Metabolism; ET-Electrone transport; L&LP- Lipid and Lipoprotein Metabolism.

Supplementary Figure 2:
Enlarged Figure 4.7

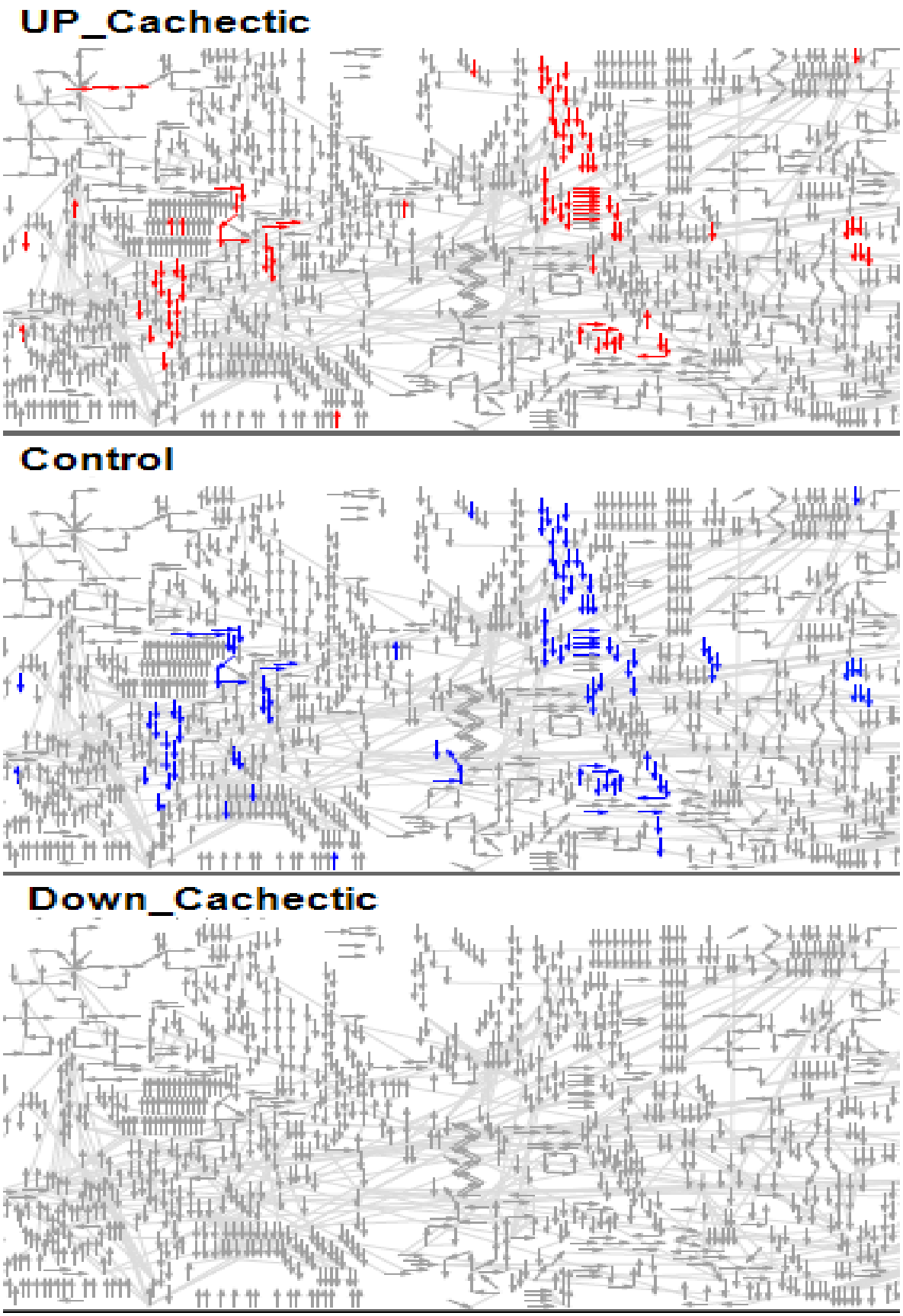

Figure 4.7 Section 1: The up and down regulated Bis-probe captured proteins (Red arrows) in the cachectic mice liver samples compared to the control (Blue arrows) in the reactome map of mice. Pathways:- Membrane Trafficking; Axon Guidance; Diabetes Pathway; Immune System Signalling; Nerve growth factor signalling events unique to cachectic groups:- Shc-P (TrkA)-SHC phosphorylation via tyrosine kinase A and Shc-P (InR)-SHC phosphorylation via Insulin receptors.

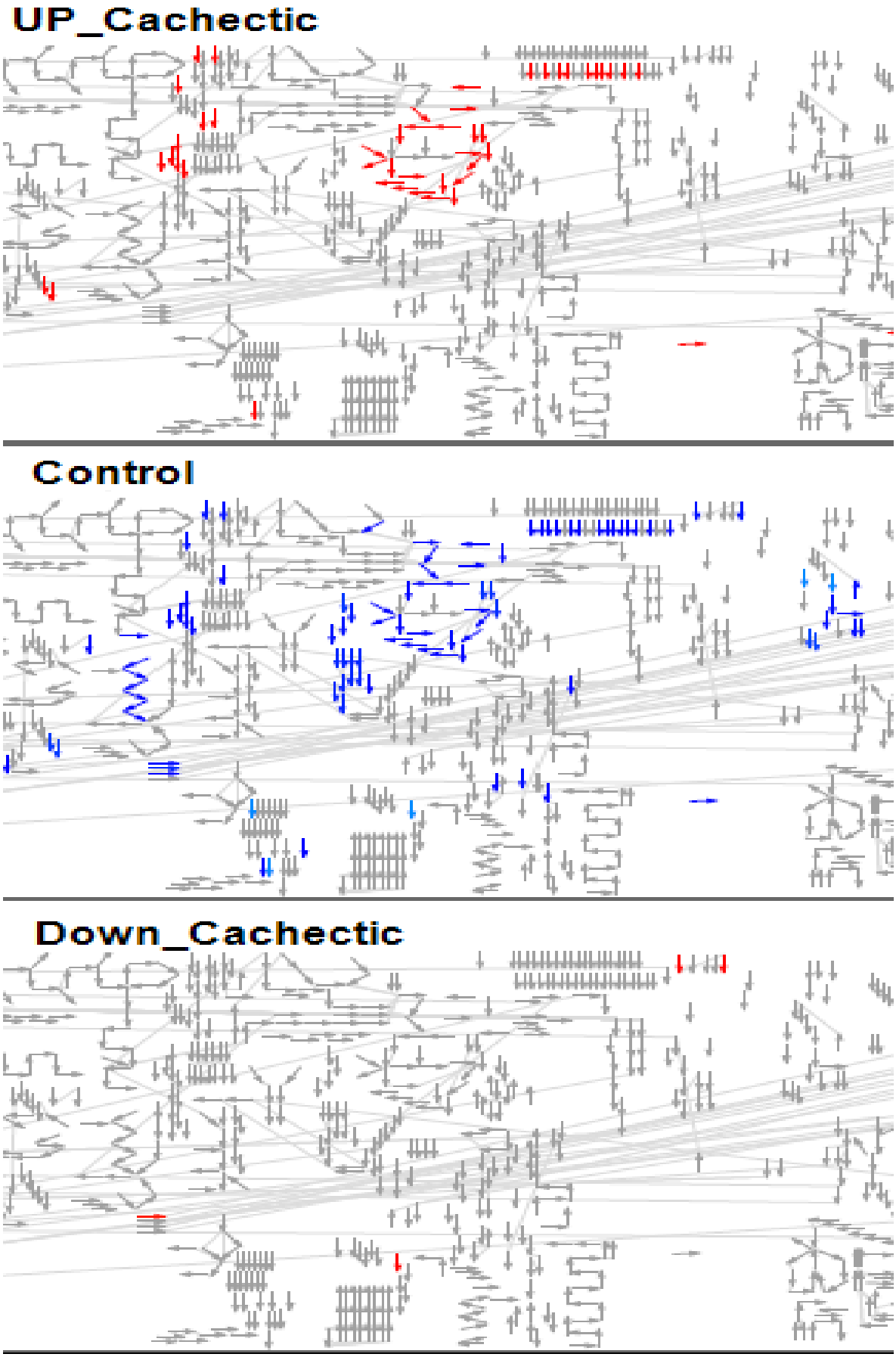

Figure 4.7 Section 2: The up and down regulated Bis-probe captured proteins (Red arrows) in the cachectic mice liver samples compared to the control (Blue arrows) in the reactome map of mice. Pathways: - Membrane Trafficking; Gene Expression and Protein Biosynthesis.

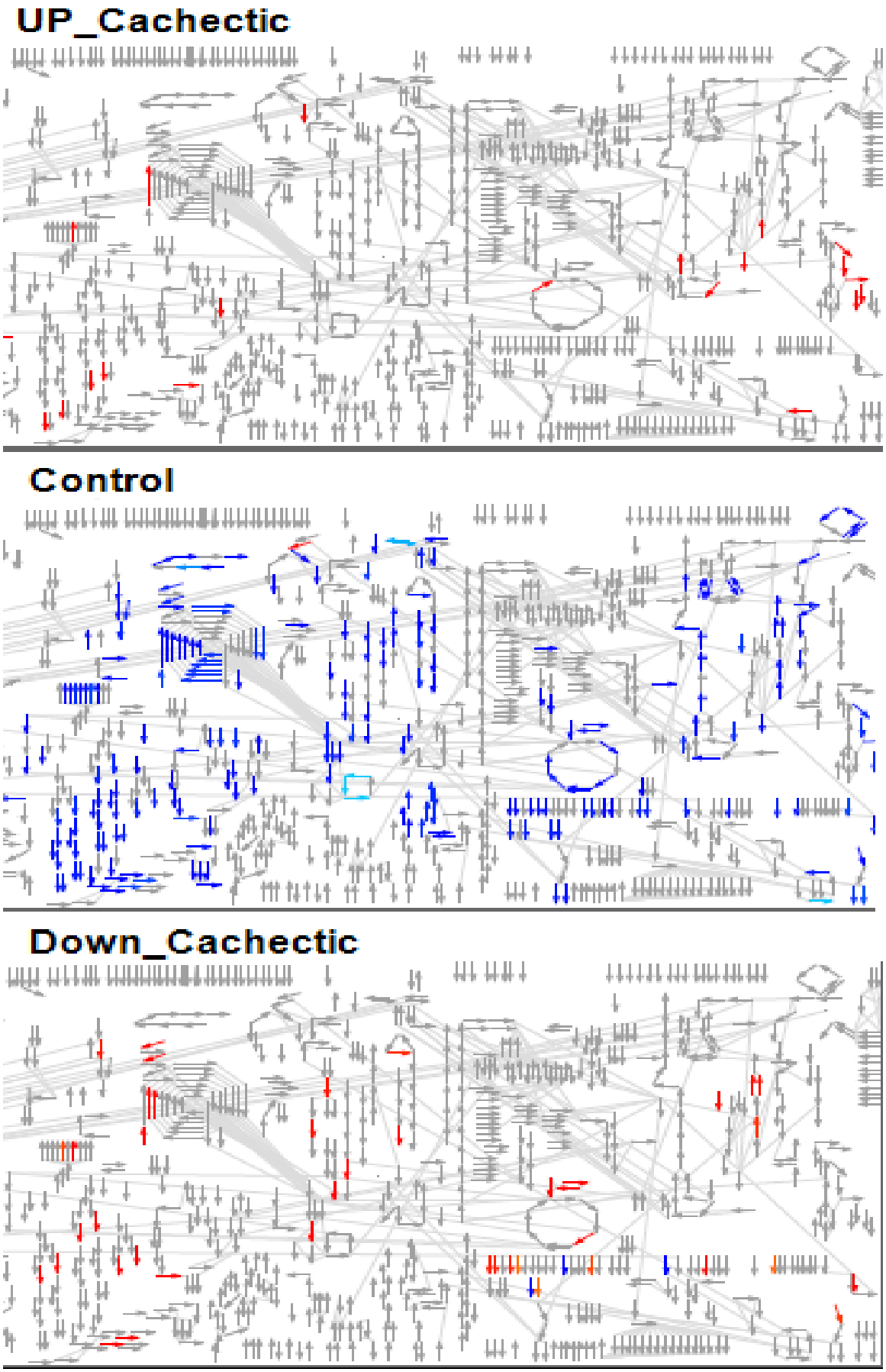

Figure 4.7 Section 3: The up and down regulated Bis-probe captured proteins (Red arrows) in the cachectic mice liver samples compared to the control (Blue arrows) in the reactome map of mice. Pathways: - Carbohydrate Metabolism; Biological Oxidation; TCA cycle; Amino acid Metabolism; Electrone transport; Lipid and Lipoprotein Metabolism.

Supplementary Figure 3:
Enlarged Figure 4.8

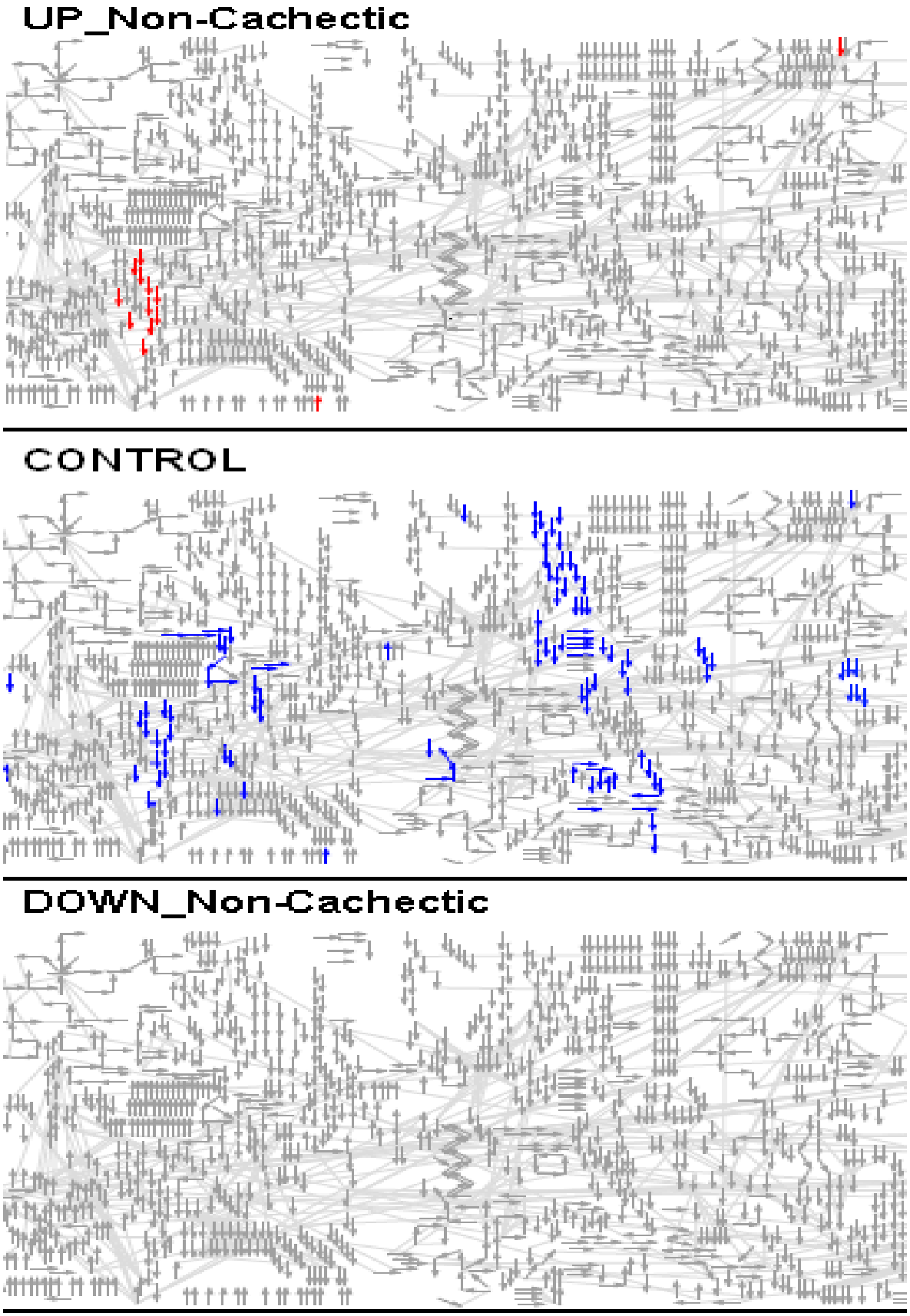

Figure 4.8 Section 1: The up and down regulated Bis-probe captured proteins (Red arrows) in the non-cachectic mice liver samples compared to the control (Blue arrows) in the reactome map of mice. pathways:- Membrane Trafficking; Axon Guidance; Diabetes Pathway; Immune System Signalling; Nerve growth factor signalling events unique to cachectic groups:- Shc-P (TrkA)-SHC phosphorylation via tyrosine kinase A and Shc-P (InR)-SHC phosphorylation via Insulin receptors.

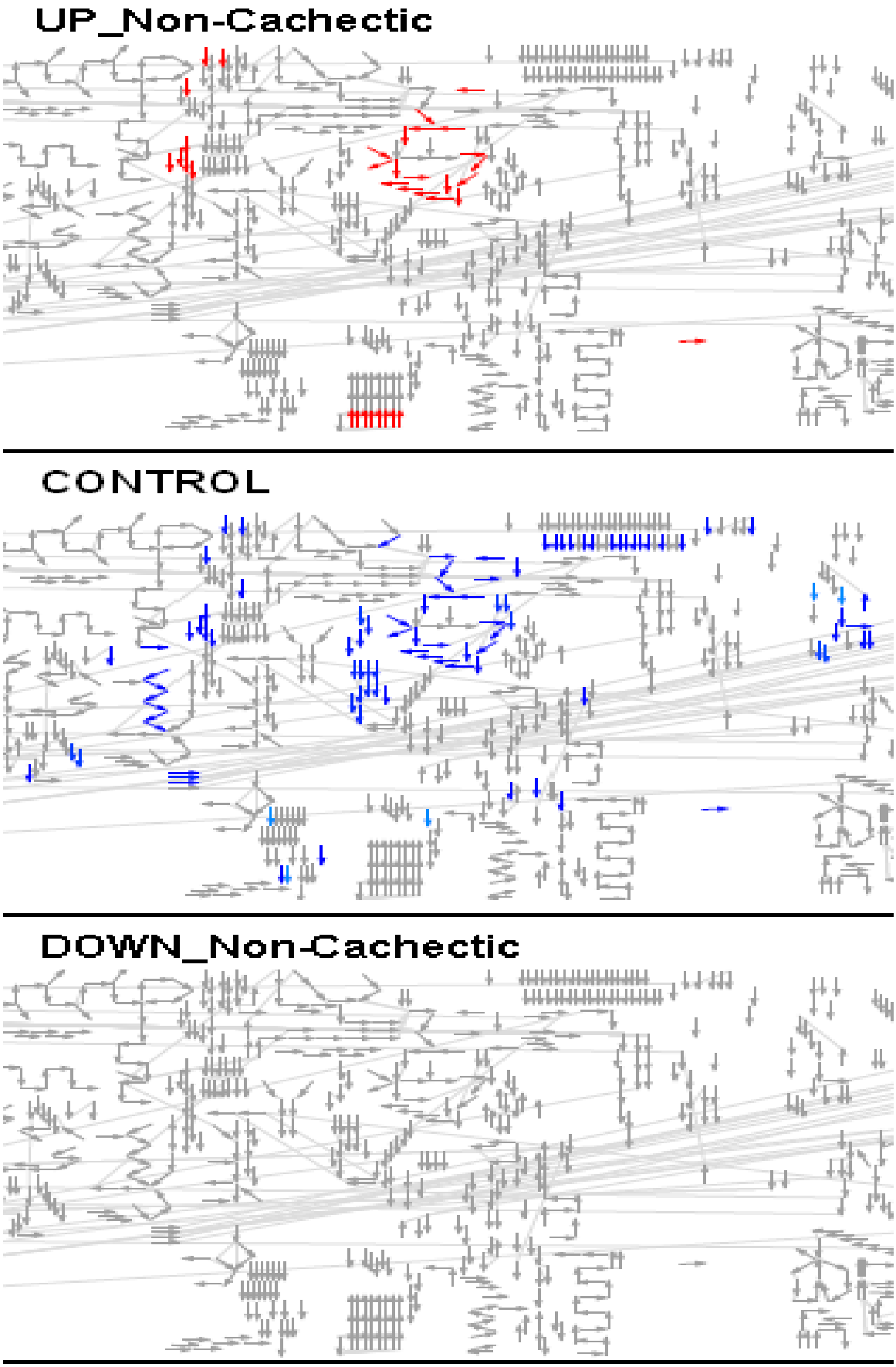

Figure 4.8 Section 2: The up and down regulated Bis-probe captured proteins (Red arrows) in the non-cachectic mice liver samples compared to the control (Blue arrows)in the reactome map of mice. Pathways: - Membrane Trafficking; Gene Expression and Protein Biosynthesis.

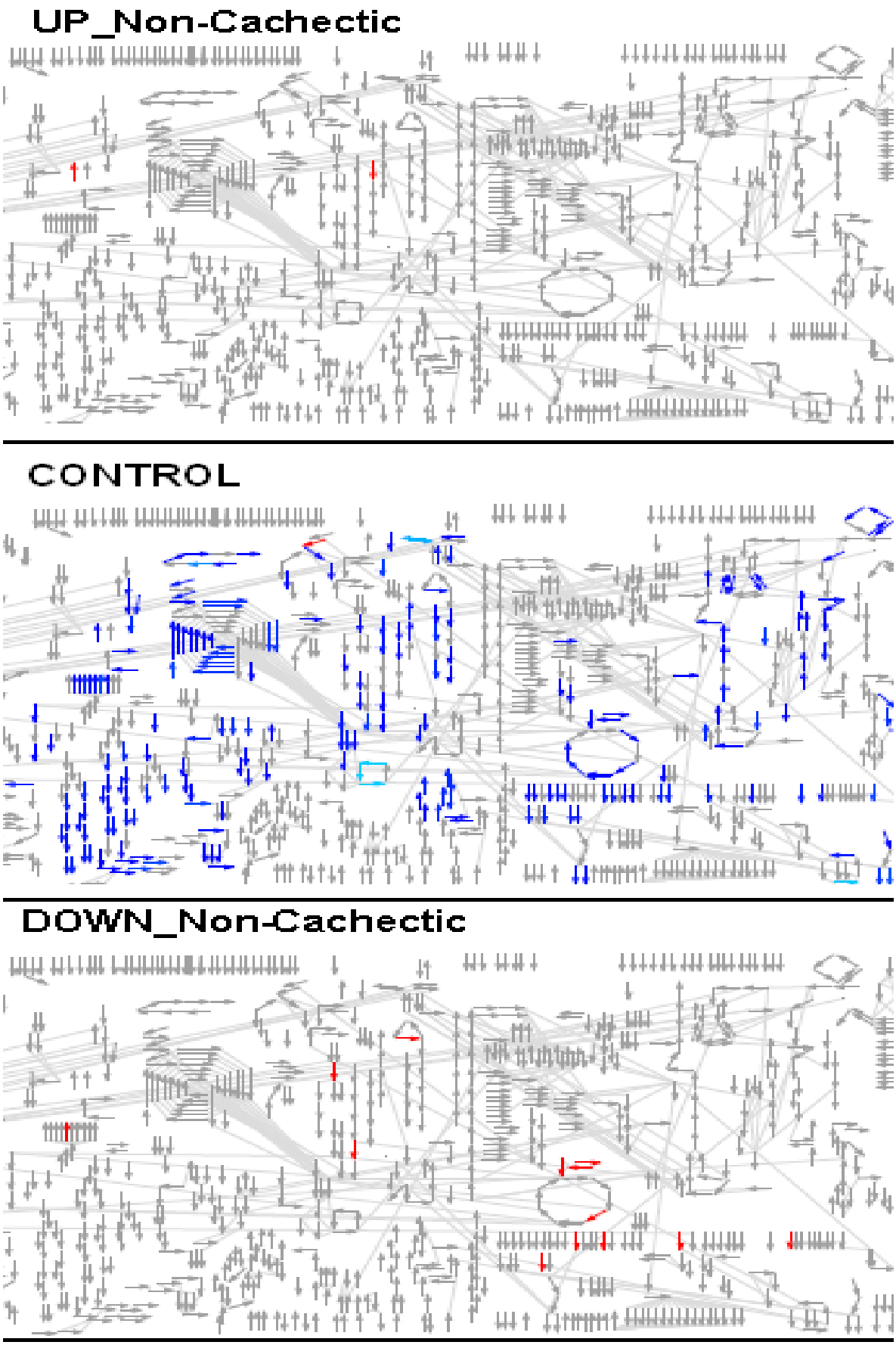

Figure 4.8 Section 3: The up and down regulated Bis-probe captured proteins (Red arrows) in the non-cachectic mice liver samples compared to the control (Blue arrows) in the reactome map of mice. pathways: - Carbohydrate Metabolism; Biological Oxidation; TCA cycle; Amino acid Metabolism; Electrone transport; Lipid and Lipoprotein Metabolism.

Chapter 5: Chemical proteomic profiling of neural differentiated human adipose-derived stem cells using Bis-probe.

This study describes the application of Bis-probe based Chemical proteomics to profile the neural differentiation of human adipose derived stem cells (hADSC). A neural induction protocol using β-mercaptoethanol (2BME) was employed for neuronal differentiation in hADSC's. The protein binding profile of the Bis-probes was assessed in early stage (1 h and 6 h) and late stage (12 h) neural differentiation and was compared with the pre-induced control hADSC prior to neural induction. Spectral counting was used to quantitate the relative abundance of the Bis-captured proteins in these samples.

This investigation was a collaboration with Mr. Jerran Naidoo and Dr. Ben Herbert (Chemistry and Biomolecular Science, Macquarie University). Mr Jerran Naidoo wrote aspects of Section 5.3.1 (Description of neurogenic differentiation in hADSC) and Section 5.3.5 (Interaction network analysis). The interaction networks data shown in **Figure 5.9** in this thesis is produced by Jerran. All other written work was my own.

5.1. Introduction

5.1.1. Human adipose derived stem cells (hADSC)

Mesenchymal stem cells are multipotent adult stem cells that have innate potential for self renewal and the ability to divide and create a specialized cell, phenotypically more differentiated than the parent. Over the last 50 years, most adult stem cells for research and therapeutics have been harvested from peripheral blood and bone marrow. In the last decade adipose tissue has been identified as a major source of mesenchymal adult stem cells. Adipose tissue contains a stromal vascular fraction (SVF), akin to bone marrow, containing pluripotent mesenchymal adult stem cells. The SVF is rich in adult mesenchymal stem cells, termed adipose-derived stem cells (ADSCs). ADSCs numbers are a thousand fold greater than that derived from bone marrow. In recent years adult stem cells have been successfully used to treat joint and muscle injuries in humans and animals [192-195]. However, regenerative therapies have yet to be developed for organs such as the brain and central nervous system. These stem cell therapies have the potential to revolutionise human healthcare and medicine.

5.1.2. Effect of β- mercaptoethanol on neurogenic differentiation of hADSC

Numerous studies show ADSCs as well as other adult MSCs have been induced toward a neural differentiated population *in vitro* [196-198]. The various research groups adopted one of two main strategies. Woodbury *et al.* [196] applied simple chemical compounds as media additives to induce differentiation. Sanchez-Ramos *et al.* investigated cytokine and growth factor media additives [199]. Interestingly the two methods vary considerably for the time MSCs spend in culture. The Woodbury method takes mere hours for more than 75% of MSCs to adopt neural morphology as well as express neural specific markers such as NeuN, MAP-2, and tubulin III. Conversely, the Sanchez-Ramos method takes several weeks for MSCs to assume neural morphological and marker traits, however the

percentage of differentiated cells is significantly lower. Barnabe *et al.* [200] argue that these cells are non-functional. While others believe the cells are at pre-neural stage or immature neuroblasts that can be further differentiated into glial, oligodendrocytes, astrocytes including myelin sheath forming Schwann cells that are functional [201-206].

In this study the Bis-probe based Chemical proteomics strategy (Chapter 3) was applied to characterise the binding proteome of human adipose derived stem cells (hADSC) and to profile protein changes associated with neural differentiation. A neural induction protocol using β-mercaptoethanol (2BME) was employed for neuronal differentiation in hADSC's. Differentiation was induced in the pre-induced control hADSCs (S0) with 10 mM 2BME treatment for 1 h (N1), 6 h (N6) and 12 h (N12).The protein binding profile of the Bis-probes was assessed in early stage (1 h and 6 h) and late stage (12 h) of neural differentiation and was compared with the pre-induced control hADSC's. Spectral counting was used to quantitate the relative abundance of the Bis-captured proteins in these samples.

5.2. Methods

5.2.1. Cell Culture

STEMPRO Human adipose derived stem cells (hADSCs) were obtained from Invitrogen, Carlsbad, CA and were cultured in DMEM supplemented with 10% FBS, 10 mM glutamax and 1% antibiotic (penicillin, 100 μg/mL and streptomycin, 100 μg/mL) at 37°C in the presence of 5% CO_2. For each passage the cells were plated at about 5000 cells/cm^2 and grown to 90% confluency.

5.2.2. Neurogenic Differentiation

Sub confluent hADSCs at passage 3 were cultured for 24 h in a medium made up of DMEM/10%FBS/1 mM β-mercaptoethanol (2BME). Neuronal differentiation was then induced for up to 12 h in a neuronal induction media (DMEM/10 mM 2BME), according to an established protocol by Woodbury *et al.*, 2000.

5.2.3. Sample preparation

Three independent populations of control (S0) and neuronal induced cells at three different time points post neuronal induction 1 h (N1), 6 h (N6) and 12 h (N12) were harvested. After rinsing in PBS, the control and neuronal induced cells were lysed in Pierce IP lysis buffer (Thermo Scientific/Pierce Biotechnology, CA, USA) containing 25 mM Tris-HCl, pH 7.4, 150 mM NaCl, 1% NP-40, 1 mM EDTA and 5% glycerol plus protease inhibitors (1 mM phenylmethylsulfonyl fluoride, 1 mM EDTA, 1 µg/ml aprotinin, 1 µg/ml leupeptin, 1 µg/ml pepstatin) and phosphatase inhibitors (1 mM sodium fluoride and 1 mM sodium orthovanadate). Cell lysates were vortexed and cleared by centrifugation at 14000 rpm for 5 min at 4ºC. The cleared lysates were filtered through Zeba Spin Desalting Coloumns (Thermo Scientific/Pierce Biotechnology, CA, USA) into fresh lysis buffer. The cell lysates were desalted to remove endogenous nucleotides, particularly ATP which competes with the probe for the ATP binding sites of target proteins. Relative protein concentration was determined using the bicinchoninic acid (BCA) assay.

5.2.4. Synthesis of Bis-probe, Affinity pull down, In-gel clean up and Digestion

The Bis-Probe synthesised and characterised in Chapter 3 was used for chemical proteomics. For affinity pull down experiments, 100 µg protein from each independent population of pre-induced cells (S0) and neuronal induced cells at three different time points 1 h (N1), 6 h (N6) and 12 h (N12) was volume adjusted to 500 µl with Pierce IP

lysis buffer. The remaining affinity pull down steps, In-gel clean up and digestion steps were essentially as previously described (Chapter 3).

5.2.5. Mass Spectrometry, Protein Identification and Data Analysis

The tryptic peptide samples obtained for each of the independent biological replicates S0, N1, N6 and N12 were analyzed by nanoLC-MS/MS using a LTQ XL linear ion-trap mass spectrometer (Thermo, CA, USA) as described previously (Chapter 3, Section 2). Spectra files were processed and searched against the SwissProt *Human* database (release 56.8 of February 10, 2009) using the global proteome machine (GPM) software (version 2.1.1) and the X!Tandem algorithm. The search modifications and parameters were the same as described previously (Chapter 3, Section 2). The proteins identified for all the replicates for each of the four groups was further filtered using the criteria that every protein that was retained as a true identification only if it was found in at least two of the three biological replicates. After this filtering the peptide and protein false discovery rates (FDR) were calculated. Peptide FDR was calculated as 2 x (total number of peptides representing reversed protein hits in the list/total number of peptides representing all proteins in the list) x 100 and protein FDR was calculated as (number of reverse protein hits in a list/ total number of proteins in the list) x 100.

5.2.6. Calculation of protein Normalized Spectral Abundance Factor (NSAF)

Normalized spectral abundance factors (NSAF) were calculated for each protein in all the groups; control hADSCs (S0), 1 h, 6 h and 12 h neural differentiated hADSC's as described in Chapter 4, Section 4.2.5.

5.3. Results

5.3.1. Cell culture and Neurogenic differentiation of hADSCs

Cultures prior to neuronal differentiation were placed in a medium of 1 mM beta-marcaptoethanol, one-tenth the strength of the differentiation media concentration. This initiates the necessary differentiation pathway without shocking and killing cells which a full strength differentiation medium would do. The treatment also increases the viability of cells for the differentiation media [207, 208]. **Figure 5.1A** shows the growth of base group (S0) hADSCs. An hour after placing the differentiation media onto the cells (group N1), considerable changes was apparent throughout the culture with significant cellular remodelling observable (**Figure 5.1B**). The cellular remodelling most notably affects the membrane which retracts giving the cells a narrower appearance. The culture appears less confluent with larger area between cells this is due to the decreased surface area of each cell. The cell population numbers remain relatively unchanged compared to S0. The cell membranes exhibit retraction with the majority of cells forming a spindle-like bipolar structure. Within 6 hours of differentiation (group N6) the total cell population were quite distinct compared to the base group S0 (**Figure 5.1C**). The spindle-like cells have dense and highly refractive nuclei with multiple neurite extensions reaching between cells. At 12 hours (group N12) all cells appear neuronal-like in morphology greatly resembling primary neurites or astrocytes (**Figure 5.1D**). Cell neurite extensions were observed linking multiple cells in succession.

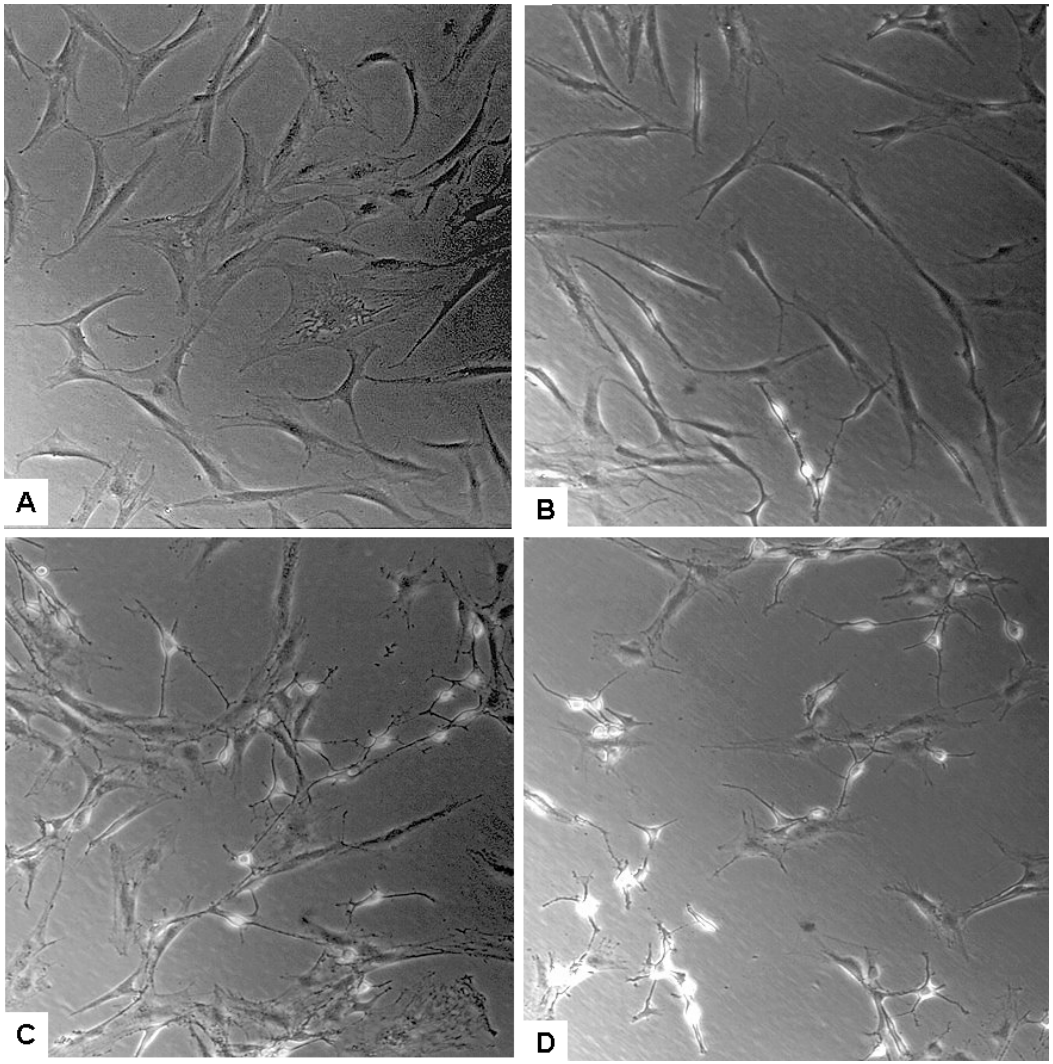

Figure 5.1: hADSCs treated with 2BME at different time points. (**A**) Pre-induced control group (S0) (**B**) neuronal induction with 10mM BME for 1 h (N1) (**C**) induction for 6 h (N6) (**D**) induction for 12 h (N12).

5.3.2. MS characterisation of the binding targets of the Bis-probe

The Bis-probe was used to characterise the Bis-binding proteome of hADSCs and to profile protein changes associated neural differentiation. Differentiation was induced in the hADSCs (S0) with 10 mM 2BME treatment for 1 h (N1), 6 h (N6) and 12 h (N12). We applied spectral counting to analyse the differential expression patterns in the Bis-binding proteome following stimulation of these cells with the neural differentiating agent 2BME. The number of proteins that were enriched by the Bis-probe and were reproducibly present in at least two of the three biological replicates were 133 in group S0, 118 in group N1, 126 in group N6 and 89 in group N12. **Table 5.1** shows the peptide and protein false discovery rate (FDR) of the identified proteins in each of the groups. **Figure 5.2** shows the distribution of the Bis-binding proteins captured at different time points of neuronal differentiation. In comparison to the control hADSCs (S0), the protein targets captured in 2BME treated cells for 1 h (N1), 6 h (N6) and 12 h (N12) had 73%, 65% and 46% proteins in common.

Groups	#Proteins	Protein FDR (%)	Peptide FDR (%)
S0	133	0.12	0.01
N1	118	0.18	0.01
N6	126	0.16	0.01
N12	89	0.12	0.01

Table 5.1: Number of proteins captured by the Bis-probe in S0, N1, N6 and N12 groups with their protein and peptide false discovery rates (FDR).

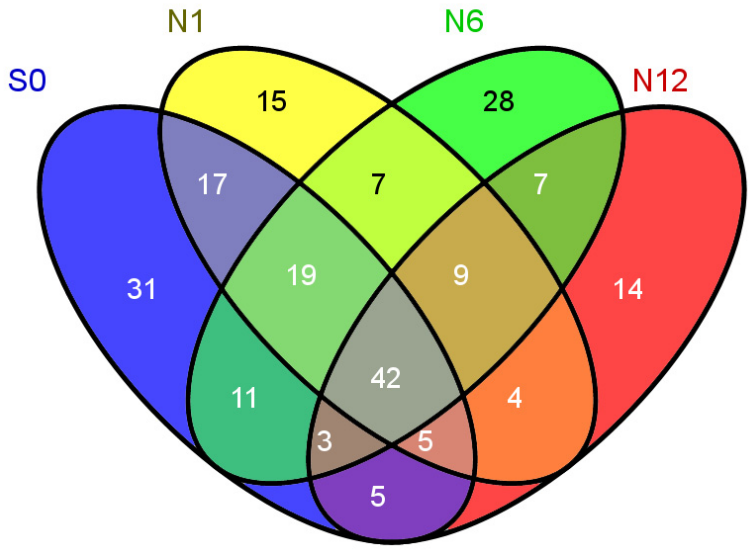

Figure 5.2: Bis-binding proteins captured in neural differentiated hADSCs in S0, N1, N6 and N12 groups with the unique and common subsets.

The proteins captured by the Bis- probe were further partitioned into categories based on the presence and or absence in the each time points of 2BME treatment. 42 proteins were identified that were common to the control and all the time points (**Table 5.2**). The probe captured 14% (31 proteins) unique proteins in the S0 group, 7% (15 proteins) in the N1 group, 13% (29 proteins) in the N6 group and 7% (14 proteins) in the N12 group across the entire data set of 217 distinct proteins (**Table 5.2 A, B, C, D,** and **Figure 5.2**).

Table 5.2: Proteins captured by Bis-probe common to all groups S0, N1, N6, and N12. # Total number of peptides.

UniProt Accn.	Protein	S0		N1		N6		N12	
		#peptides	Avg. NSAF	#peptides	Avg. NSAF	#peptides	Avg. NSAF	#peptides	Avg. NSAF
RL18_HUMAN	60S ribosomal protein L18	18	0.0024	20	0.0027	8	0.0010	14	0.0021
RL4_HUMAN	60S ribosomal protein L4	18	0.0011	17	0.0011	24	0.0012	13	0.0009
RL6_HUMAN	60S ribosomal protein L6	21	0.0017	12	0.0011	7	0.0006	10	0.0010
ACTB_HUMAN	Actin, cytoplasmic 1	698	0.0399	699	0.0438	1382	0.0743	141	0.0108
ACTG_HUMAN	Actin, cytoplasmic 2	658	0.0368	594	0.0364	1377	0.0738	146	0.0111
ADAS_HUMAN	Alkyldihydroxyacetonephosphate synthase	4	0.0002	9	0.0004	8	0.0003	3	0.0002
ACTN1_HUMAN	Alpha-actinin-1	22	0.0006	36	0.0010	54	0.0012	19	0.0006
ACTN4_HUMAN	Alpha-actinin-4	28	0.0008	35	0.0010	51	0.0011	20	0.0006
BORG5_HUMAN	Cdc42 effector protein 1	2	0.0002	4	0.0004	3	0.0003	6	0.0006
COPA_HUMAN	Coatomer subunit alpha	16	0.0003	12	0.0003	5	0.0001	13	0.0003
CO1A1_HUMAN	Collagen alpha-1(I) chain	3	0.0001	6	0.0001	6	0.0001	5	0.0001
CRUM1_HUMAN	Crumbs homolog 1	19	0.0004	22	0.0004	21	0.0003	33	0.0007
K2C1_HUMAN	Cytokeratin-1	1025	0.0437	964	0.0415	1223	0.0419	1309	0.0592
K1C10_HUMAN	Cytokeratin-10	682	0.0328	665	0.0324	887	0.0341	976	0.0494
K1C14_HUMAN	Cytokeratin-14	82	0.0047	58	0.0033	126	0.0055	109	0.0065
K2C5_HUMAN	Cytokeratin-5	143	0.0066	113	0.0052	176	0.0064	181	0.0087
K2C6A_HUMAN	Cytokeratin-6A	111	0.0057	58	0.0030	112	0.0043	161	0.0081
CKAP4_HUMAN	Cytoskeleton-associated protein 4	70	0.0029	49	0.0021	41	0.0014	64	0.0028
EF1A1_HUMAN	Elongation factor 1-alpha 1	39	0.0019	43	0.0022	79	0.0036	15	0.0010
ENPL_HUMAN	Endoplasmin	19	0.0006	13	0.0004	11	0.0003	4	0.0002
FLNA_HUMAN	Filamin-A	85	0.0008	227	0.0020	363	0.0028	173	0.0018
GSK3A_HUMAN	Glycogen synthase kinase-3 alpha	16	0.0009	8	0.0005	14	0.0007	8	0.0005
HS90B_HUMAN	Heat shock protein HSP 90-beta	20	0.0007	17	0.0006	13	0.0004	12	0.0005
HNRPL_HUMAN	Heterogeneous nuclear ribonucleoprotein L	6	0.0003	12	0.0006	17	0.0007	19	0.0010
K22E_HUMAN	Keratin, type II cytoskeletal 2 epidermal	505	0.0219	521	0.0230	655	0.0227	437	0.0204
LDB3_HUMAN	LIM domain-binding protein 3	4	0.0002	4	0.0002	4	0.0002	4	0.0002
MAP1B_HUMAN	Microtubule-associated protein 1B	2	0.0000	7	0.0001	14	0.0001	10	0.0001
MYH10_HUMAN	Myosin-10	782	0.0086	1029	0.0124	1100	0.0108	924	0.0117
MYH11_HUMAN	Myosin-11	418	0.0047	596	0.0073	621	0.0062	567	0.0072
MYH9_HUMAN	Myosin-9	4391	0.0496	5669	0.0687	6258	0.0621	5106	0.0652

MYO1B_HUMAN	Myosin-Ib	25	0.0005	70	0.0015	82	0.0014	42	0.0009
MYO1C_HUMAN	Myosin-Ic	87	0.0018	261	0.0058	202	0.0037	186	0.0044
MYO1D_HUMAN	Myosin-Id	6	0.0002	44	0.0011	60	0.0012	36	0.0009
NUCL_HUMAN	Nucleolin	11	0.0005	14	0.0005	27	0.0008	12	0.0005
PLEC_HUMAN	Plectin	6	0.0000	121	0.0005	359	0.0015	149	0.0008
DDX17_HUMAN	Probable ATP-dependent RNA helicase DDX17	5	0.0002	5	0.0002	8	0.0003	9	0.0004
SPA13_HUMAN	Putative serpin A13	4	0.0004	10	0.0010	8	0.0006	12	0.0012
KPYM_HUMAN	Pyruvate kinase isozymes M1/M2	47	0.0022	35	0.0017	52	0.0020	42	0.0022
IQGA1_HUMAN	Ras GTPase-activating-like protein IQGAP1	6	0.0001	19	0.0003	15	0.0002	6	0.0001
RHDF2_HUMAN	Rhomboid family member 2	6	0.0002	5	0.0002	6	0.0002	8	0.0003
ECHA_HUMAN	Trifunctional enzyme subunit alpha	13	0.0005	10	0.0004	5	0.0002	13	0.0005
VIME_HUMAN	Vimentin	24	0.0013	24	0.0012	75	0.0031	7	0.0005

Table 5. 2A: Proteins captured by Bis-probe unique to S0.

UniProt Accn.	Protein	S0	
		# Peptides	Avg. NSAF
RS11_HUMAN	40S ribosomal protein S11	13	0.0019
RS13_HUMAN	40S ribosomal protein S13	7	0.0012
RS14_HUMAN	40S ribosomal protein S14	4	0.0008
RS15_HUMAN	40S ribosomal protein S15	5	0.0009
RS15A_HUMAN	40S ribosomal protein S15a	15	0.0027
RS3A_HUMAN	40S ribosomal protein S3a	8	0.0008
RS4X_HUMAN	40S ribosomal protein S4, X isoform	16	0.0014
RS5_HUMAN	40S ribosomal protein S5	5	0.0007
CH60_HUMAN	60 kDa heat shock protein, mitochondrial	4	0.0003
RL10A_HUMAN	60S ribosomal protein L10a	6	0.0007
RL17_HUMAN	60S ribosomal protein L17	3	0.0006
RL18A_HUMAN	60S ribosomal protein L18a	7	0.0010
RL19_HUMAN	60S ribosomal protein L19	8	0.0010
RL21_HUMAN	60S ribosomal protein L21	9	0.0014
RL27_HUMAN	60S ribosomal protein L27	6	0.0011
RL27A_HUMAN	60S ribosomal protein L27a	2	0.0005
RL31_HUMAN	60S ribosomal protein L31	3	0.0008
RL32_HUMAN	60S ribosomal protein L32	4	0.0009
RL36_HUMAN	60S ribosomal protein L36	2	0.0011
RL3L_HUMAN	60S ribosomal protein L3-like	4	0.0003
RL5_HUMAN	60S ribosomal protein L5	4	0.0004
RL9_HUMAN	60S ribosomal protein L9	6	0.0008
ADT1_HUMAN	ADP/ATP translocase 1	6	0.0006
DYH17_HUMAN	Dynein heavy chain 17, axonemal	3	0.0000
HNRPM_HUMAN	Heterogeneous nuclear ribonucleoprotein M	4	0.0002
H2A1A_HUMAN	Histone H2A type 1-A	4	0.0010
PDZD2_HUMAN	PDZ domain-containing protein 2	3	0.0000
MYCB2_HUMAN	Probable E3 ubiquitin-protein ligase MYCBP2	3	0.0000
THADA_HUMAN	Thyroid adenoma-associated protein	4	0.0001
VP13B_HUMAN	Vacuolar protein sorting-associated protein 13B	3	0.00003

Table 5.2B: Proteins captured by Bis-probe unique to N1.

UniProt Accn	Protein	N1	
		# Peptides	Avg. NSAF
RS16_HUMAN	40S ribosomal protein S16	4	0.0009
RS24_HUMAN	40S ribosomal protein S24	3	0.0008
RS6_HUMAN	40S ribosomal protein S6	4	0.0005
DDX1_HUMAN	ATP-dependent RNA helicase DDX1	8	0.0003
COF1_HUMAN	Cofilin-1	6	0.0012
EF2_HUMAN	Elongation factor 2	6	0.0002
CNNM1_HUMAN	Metal transporter CNNM1	3	0.0001
MCRS1_HUMAN	Microspherule protein 1	3	0.0002
MYH7B_HUMAN	Myosin-7B	14	0.0002
MYO6_HUMAN	Myosin-VI	6	0.0001
HELZ_HUMAN	Probable helicase with zinc finger domain	4	0.0001
TERA_HUMAN	Transitional endoplasmic reticulum ATPase	3	0.0001

TPM4_HUMAN	Tropomyosin alpha-4 chain	4	0.0005
ZN687_HUMAN	Zinc finger protein 687	3	0.0001
ZRAB2_HUMAN	Zinc finger Ran-binding domain-containing protein 2	2	0.0003

Table 5.2C: Proteins captured by Bis-probe unique to N6.

UniProt Accn	Protein	N6	
		# Peptides	Avg. NSAF
RS18_HUMAN	40S ribosomal protein S18	3	0.0006
RS25_HUMAN	40S ribosomal protein S25	7	0.0014
RL23_HUMAN	60S ribosomal protein L23	6	0.0011
RL29_HUMAN	60S ribosomal protein L29	3	0.0006
K6PP_HUMAN	6-phosphofructokinase type C	3	0.0001
ARP2_HUMAN	Actin-related protein 2	4	0.0003
DDX3X_HUMAN	ATP-dependent RNA helicase DDX3X	4	0.0002
CALD1_HUMAN	Caldesmon	7	0.0002
CLH1_HUMAN	Clathrin heavy chain 1	10	0.0001
EF1G_HUMAN	Elongation factor 1-gamma	3	0.0002
CAZA1_HUMAN	F-actin-capping protein subunit alpha-1	7	0.0006
FNDC1_HUMAN	Fibronectin type III domain-containing protein 1	3	0.0001
FILA2_HUMAN	Filaggrin-2	4	0.0000
FLNC_HUMAN	Filamin-C	25	0.0002
ALDOA_HUMAN	Fructose-bisphosphate aldolase A	5	0.0004
ADDG_HUMAN	Gamma-adducin	3	0.0001
HNRPK_HUMAN	Heterogeneous nuclear ribonucleoprotein K	4	0.0002
ILF3_HUMAN	Interleukin enhancer-binding factor 3	5	0.0001
K1C17_HUMAN	Keratin, type I cytoskeletal 17	33	0.0016
PTRF_HUMAN	Polymerase I and transcript release factor	12	0.0007
POTEF_HUMAN	POTE ankyrin domain family member F	563	0.0104
MUT7_HUMAN	Probable exonuclease mut-7 homolog	3	0.0001
RAB21_HUMAN	Ras-related protein Rab-21	3	0.0004
SERPH_HUMAN	Serpin H1	26	0.0013
TLN1_HUMAN	Talin-1	14	0.0001
THOC1_HUMAN	THO complex subunit 1	3	0.0001
TPP2_HUMAN	Tripeptidyl-peptidase 2	3	0.0001
TMOD3_HUMAN	Tropomodulin-3	21	0.0013

Table 5.2D: Proteins captured by Bis-probe unique to N12.

UniProt Accn	Protein	N12	
		# Peptides	Avg. NSAF
GA2L2_HUMAN	GAS2-like protein 2	3	0.0001
SYG_HUMAN	Glycyl-tRNA synthetase	3	0.0002
VAV3_HUMAN	Guanine nucleotide exchange factor VAV3	3	0.0001
GBX1_HUMAN	Homeobox protein GBX-1	4	0.0004
K1C28_HUMAN	Keratin, type I cytoskeletal 28	50	0.0031
K2C3_HUMAN	Keratin, type II cytoskeletal 3	42	0.0021
LYSC_HUMAN	Lysozyme C	4	0.0010
KPCT_HUMAN	Protein kinase C theta type	3	0.0002
DHX57_HUMAN	Putative ATP-dependent RNA helicase DHX57	3	0.0001
TRY3_HUMAN	Trypsin-3	23	0.0024

CP074_HUMAN	Uncharacterized protein C16orf74	3	0.0020
XPP1_HUMAN	Xaa-Pro aminopeptidase 1	5	0.0003
XRCC6_HUMAN	X-ray repair cross-complementing protein 6	6	0.0003
ZN292_HUMAN	Zinc finger protein 292	3	0.00004

5.3.3. Gene Ontology (GO) Analysis of Bis-probe bound proteins

The identified proteins in each treatment were grouped using Gene Ontology (GO) annotation and categorised on the basis of molecular function (**Figure 5.3**). In the S0 group, approximately 70% of the Bis-probe bound proteins had reported purine binding functions and 30% had either protein/lipid or metal binding functions and were categorised as others (**Figure 5.3A**). Majority of the purine binders had RNA/DNA binding function (34%) and 14% had ATP/GTP binding functions. The protein kinase binding function was reported as 9% and a further 8% had ATPase/GTPase activity. The remaining 4% of the identified purine binders had NAD/FAD binding function. Similarly, in the N1 group 64% of the Bis-bound proteins were reported to have purine binding functions of which 20% each had ATP/GTP and RNA/DNA binding functions (**Figure 5.3B**). The Protein kinase and NAD/FAD binding functions were similar to the control group where as the ATPase/GTPase activity was increased to 12% compared to the control group (S0). In the N6 group, 68% of the Bis-bound proteins had purine binding functions with 21% ATP/GTP binding and 22% RNA/DNA binding function (**Figure 5.3C**). The protein kinase binding and ATPase/GTPase activity of the purine binders was 12% and 10% respectively, with NAD/FAD binding functions (3%) similar to the control group. Finally, in the N12 group 63% of the Bis-bound proteins were reported to have purine binding functions majority of which had ATP/GTP binding function (29%) (**Figure 5.3D**).

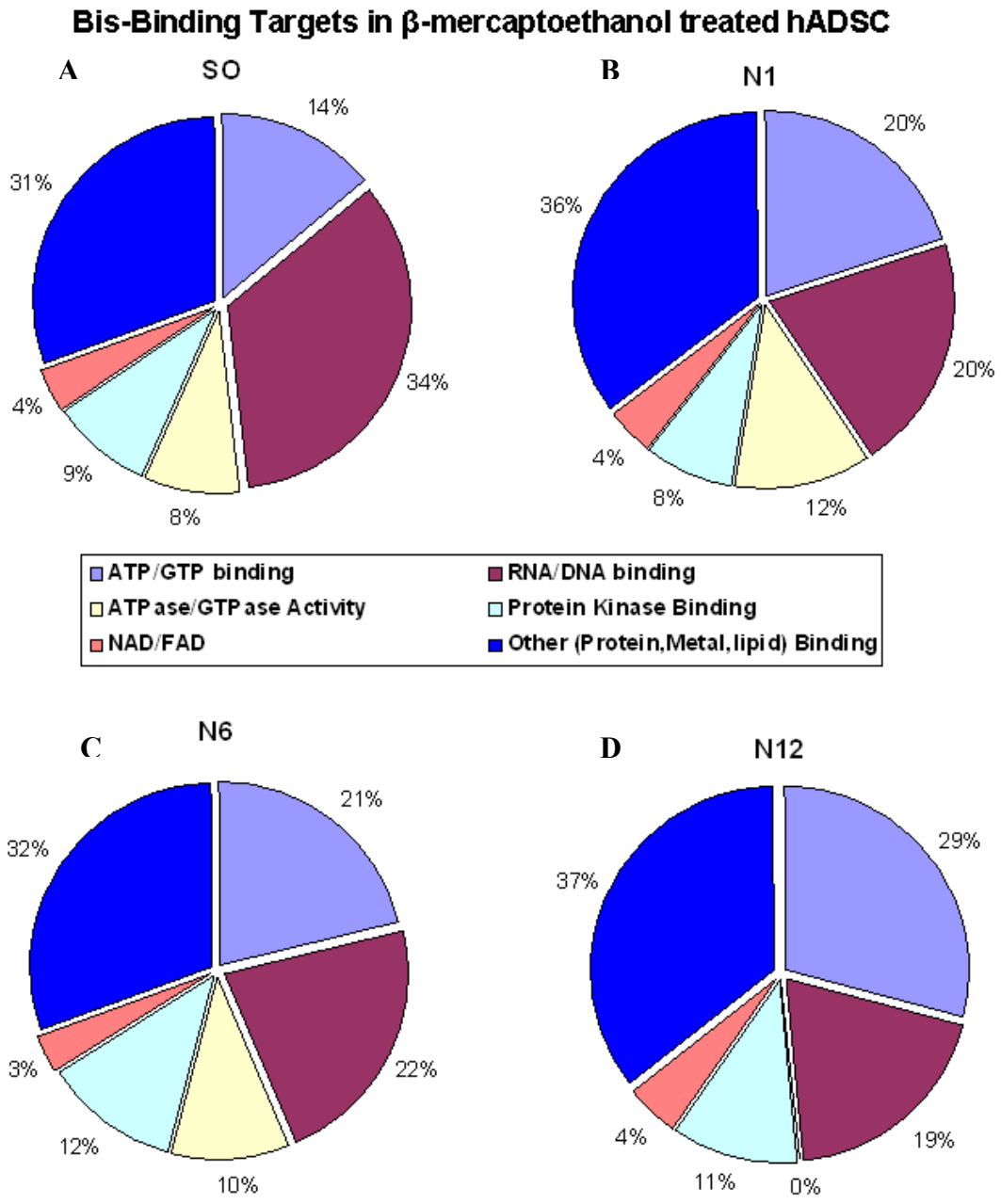

Figure 5.3: Bis-probe binding proteins in S0, N1,N6 and N12 categorised according to their binding functions based on Gene Ontology.

19% of the purine binders had RNA/DNA binding and 11% had protein kinase binding functions. NAD/FAD binding functions of the purine binders were similar to the control group. Interestingly, no ATPase/GTPase activity was reported in this group.

5.3.4. Enzymes Captured by the Bis-probe

We also evaluated the captured proteins at each time point of 2BME treatment to identify different enzymes. The Bis-probe captured 46 distinct enzymes that were identified in the entire data set (S0, N1, N6 and N12). 20 enzymes were identified in the control group, 23 in the N1 group, 22 in the N6 group and 24 enzymes were identified in the N12 group (**Figure 5.4**). The relative abundance of the Bis-captured enzymes in S0, N1, N6 and N12 was determined by calculating the NSAF values for each of the identified proteins.

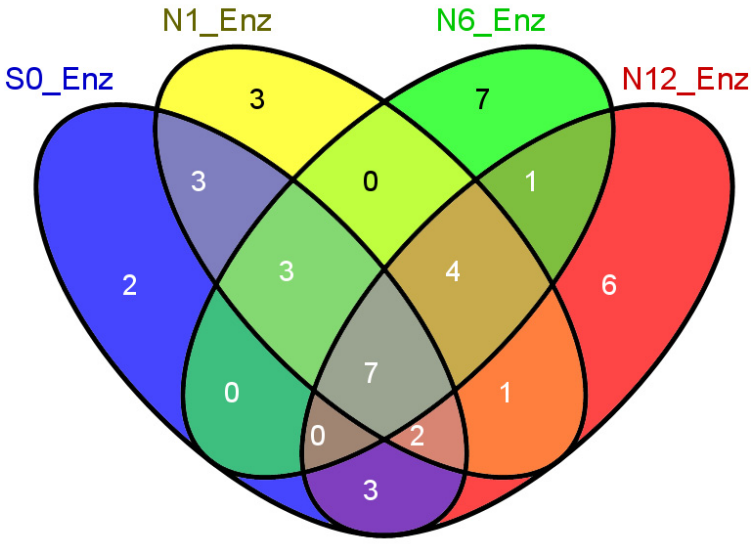

Figure 5.4: Enzymes captured by the Bis-probe in each treatment group.

5.3.4.1. Enzymes present in all four groups

The analysis identified seven enzymes that were captured by the Bis-probe in all the different groups (**Figure 5.5**). These included neurite growth promoting enzymes Ras GTPase-activating-like protein IQGAP1, glycogen synthase kinase-3 alpha and Cdc42 effector protein 1. The Bis-probe also captured metabolic enzymes pyruvate kinase isozymes M1/M2, alkyldihydroxyacetonephosphate synthase and trifunctional enzyme subunit alpha in all the groups. However, no significant change was observed in the

relative abundance of these Bis-bound enzymes across the various groups using anova analysis of the log NSAF values.

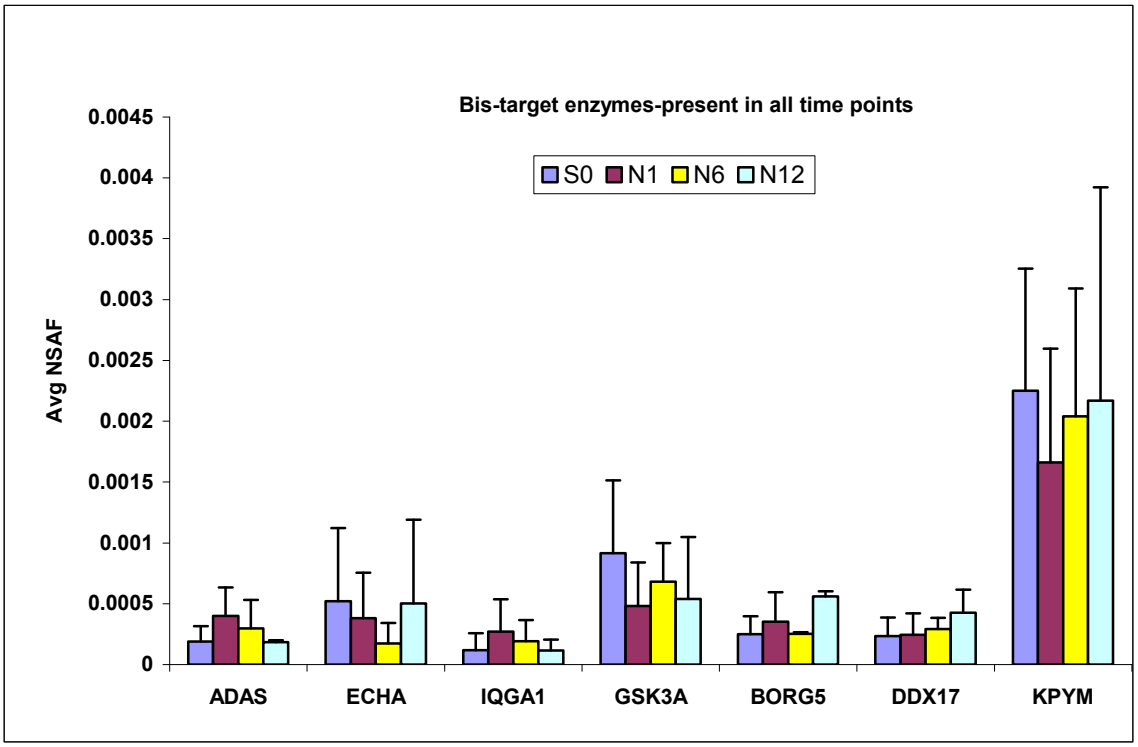

Figure 5.5: Enzymes captured by the Bis-probe in all the groups.

5.3.4.2. Enzymes Unique to a time point

Among the distinct enzymes captured by the Bis-probe, probable E3 ubiquitin-protein ligase and ADP/ATP translocase 1 were unique to the control group, S0. Similarly, ATP-dependent RNA helicase DDX1, transitional endoplasmic reticulum ATPase and probable helicase with zinc finger domain enzymes were uniquely identified in the N1 group. The N6 and the N12 groups had 7 and 6 unique enzymes respectively that were captured by the Bis probe.

The unique enzymes identified in the group N6 were fructose-bisphosphate aldolase A, tripeptidyl-peptidase 2, interleukin enhancer-binding factor 3, 6-phosphofructokinase type C, ATP-dependent RNA helicase DDX3X, polymerase I and transcript release factor and

probable exonuclease mut-7 homolog enzyme. In the group N12, protein kinase C theta, lysozyme C, x-ray repair cross-complementing protein 6, xaa-Pro aminopeptidase 1, putative ATP-dependent RNA helicase DHX57 and glycyl-tRNA synthetase were uniquely captured by the Bis-probe (**Figure 5.6**).

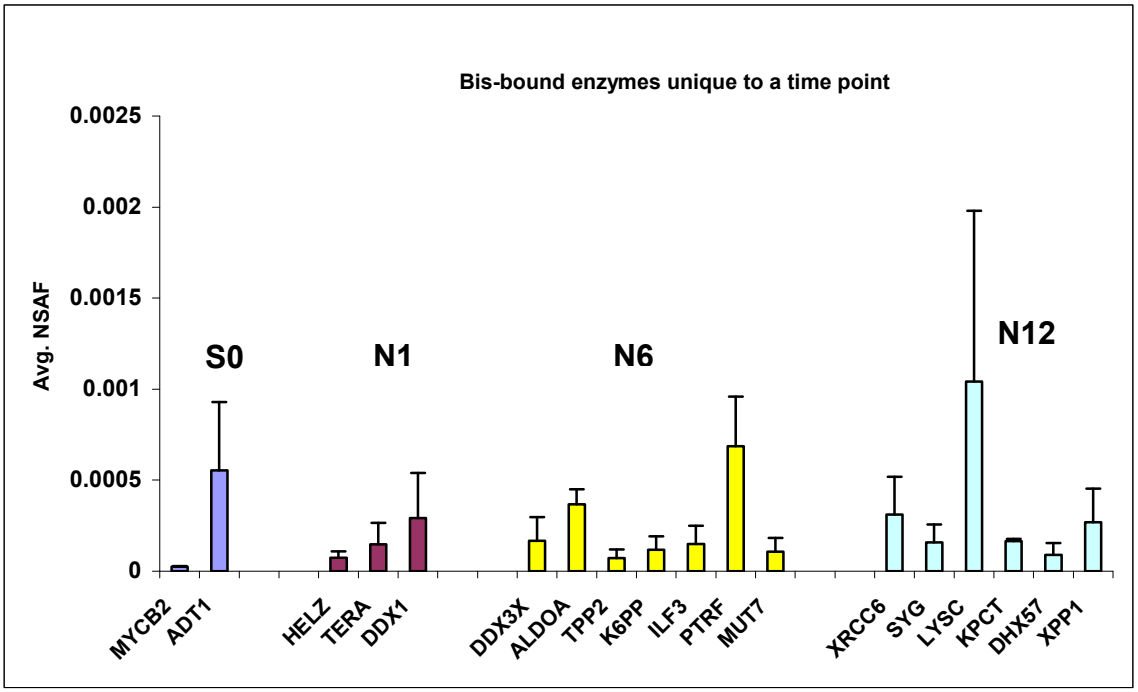

Figure 5.6: Bis bound enzymes unique to a time point.

5.3.4.3. Enzymes present in any three time points

The analysis revealed 9 enzymes that were captured by the Bis-probe in three different time points of 2BME treatment and were absent in one (**Figure 5.7**). Of these nine enzymes glyceraldehyde 3-phosphate dehydrogenase (GAPDH), alpha enolase and glycogen synthase kinase -3 beta were identified only in the control (S0), N1 and N6 groups but were absent in the N12 group. The relative abundance of these proteins was similar in the S0 and the N6 groups and the N1 group had the lowest abundance of GAPDH.

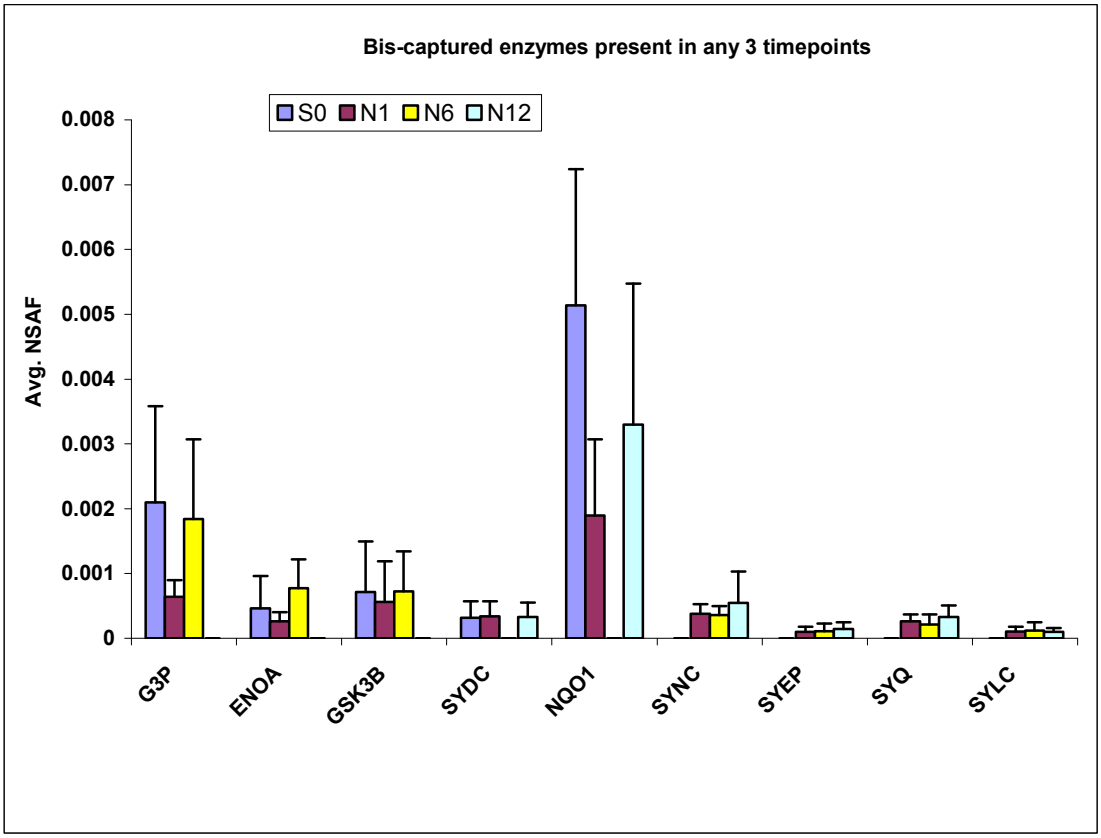

Figure 5.7: Bis bound enzymes present in any three time points.

Similarly, aspartyl-tRNA synthetase and NAD (P) H dehydrogenase were only captured in the S0, N1 and N12 groups and were absent in the N6 groups. Interestingly, most of the enzymes involved in protein biosynthesis, asparaginyl-tRNA synthetase, bifunctional aminoacyl-tRNA synthetase, glutaminyl-tRNA synthetase, leucyl-tRNA synthetase, that were captured by the Bis-probe were present only in the N1, N6, N12 groups and were absent in the control group, indicating modulation of molecular activity upon initiation of cellular differentiation.

5.3.4.4. Enzymes with known roles of neurogenic differentiation

Further categorisation of the Bis-captured enzymes revealed 18 enzymes known roles in neurogenic differentiation. Of these Ras GTPase-activating-like protein IQGAP1, Cdc42 effector protein 1, glycogen synthase kinase-3 alpha and probable ATP-dependent RNA helicase DDX17 were identified in all the time points without any significant difference in

their relative abundance (**Figure 5.8A**). Glycogen synthase kinase-3 beta and alpha-enolase were found consistently in S0, N1 and N6 groups but not observed in the N12 group where as NAD(P)H dehydrogenase 1 was present only in the S0, N1 and N12 but was absent in the N6 group (**Figure 5.8B**). Further, peroxiredoxin-1 and ribosyldihydronicotinamide dehydrogenase 2 were only identified in early differentiation (S0 and N1). In contrast, D-3-phosphoglycerate dehydrogenase was only present in later time points (N6 and N12). The Bis-probe also captured enzymes that were uniquely observed only at a particular time point and was absent in the rest of the treatments (**Figure 5.8C**). These included probable E3 ubiquitin-protein ligase MYCBP2, transitional endoplasmic reticulum ATPase and protein kinase C theta type that were found only in group S0, N1 and N12 respectively. The N6 group had majority of the enzymes involved in neurogenic differentiation that were unique to this group. Five enzymes ATP-dependent RNA helicase DDX3X, fructose-bisphosphate aldolase A, tripeptidyl-peptidase 2, 6-phosphofructokinase type C and interleukin enhancer-binding factor 3 were captured by the Bis-probe that were unique to the N6 group and have been reported to be involved in neurogenic differentiation [209-213].

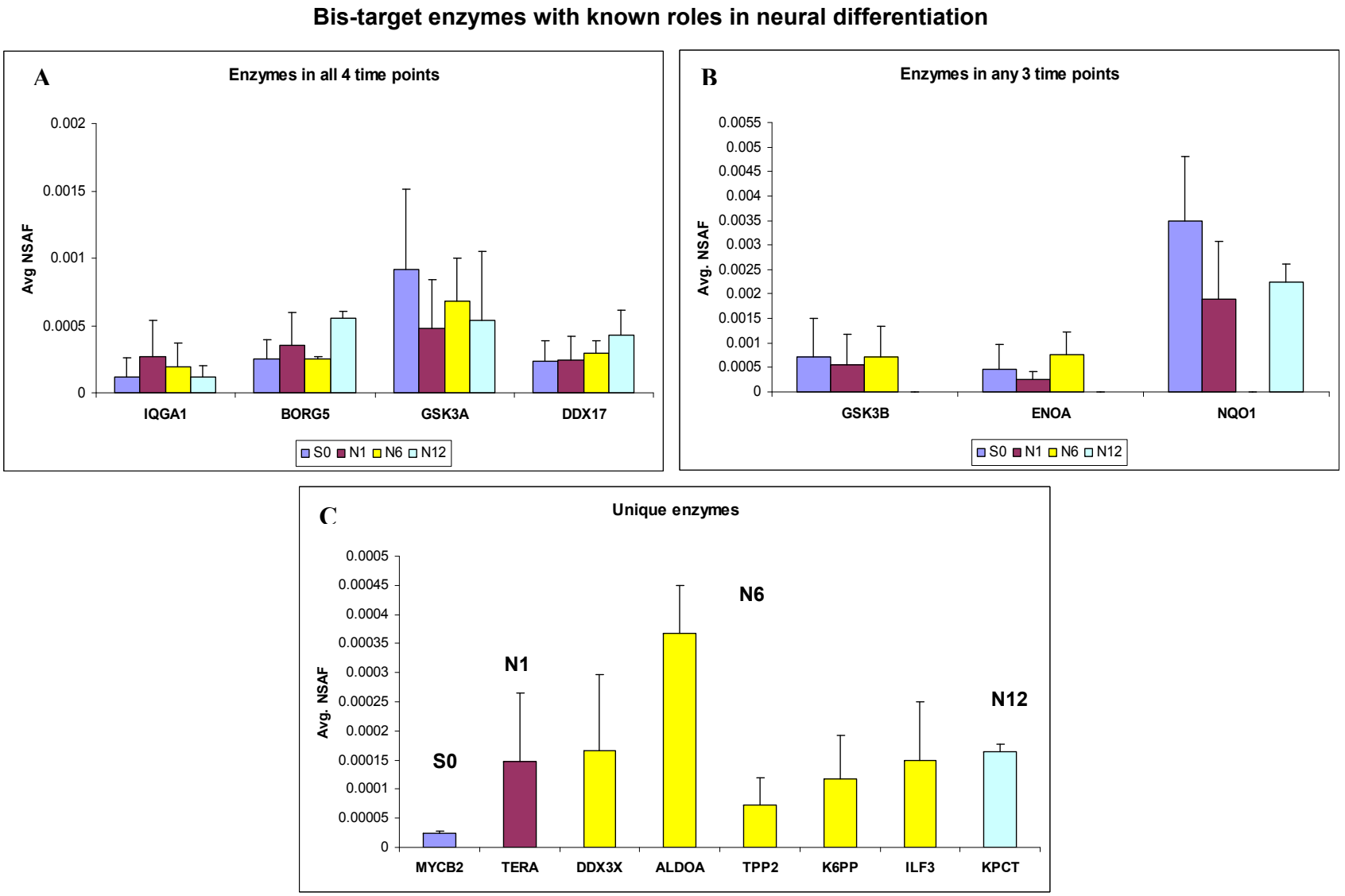

Figure 5.8: Bis-target enzymes involved in neurogenic differentiation. (**A**) Enzymes present in all four time points (**B**) Enzymes present in any three time points (**C**) Unique enzyme.

5.3.5. Protein-protein interaction network analysis of Bis-enriched hADSC and Neural differentiated proteomes

The confirmed Bis-probe captured proteins were constructed in an interaction network software Cytoscape (v.2.8.0) [214] to evaluate their interactive role in the differentiation process. Data input was searched against well maintained open access databases Gene Ontology, SwissProt, Ensembl, TrEMBL, UniProt, PDB, EBI, ENTREZ and RCSB. The visualised result was constructed as an interactive graphical layout (**Figure 5.9**). Proteins within the interaction network are represented as nodes and the interactions linking the nodes are lines known as edges. The organic layout utilised applies a force-directed algorithm model which treats each node within the network as a physical object with attraction and repulsion forces dependent on node proximity [214, 215]. This evenly distributes nodes and limits overlapping edge intersections allowing unambiguous edge analysis [216]. The organic layout shows biological clustering structure of a graph. Each group's uniquely expressed protein nodes at the time points S0, N1, N6 and N12 were designated a specific colour red, green, yellow and purple respectively for an interaction network differential display. The temporal progression of the networks allows the carryover of time specific nodes throughout all networks. Proteins not present at later time point data sets were no longer visualised in the networks. Each network was directionally aligned and overlayed for differential network analysis. Different clusters intercept a significant number of interactions across the network via several hub proteins. The time point specific expressed protein nodes have varying affects on the overall layout of each network, dependent on the types of interactions formed.

Bis-enriched protein interaction network

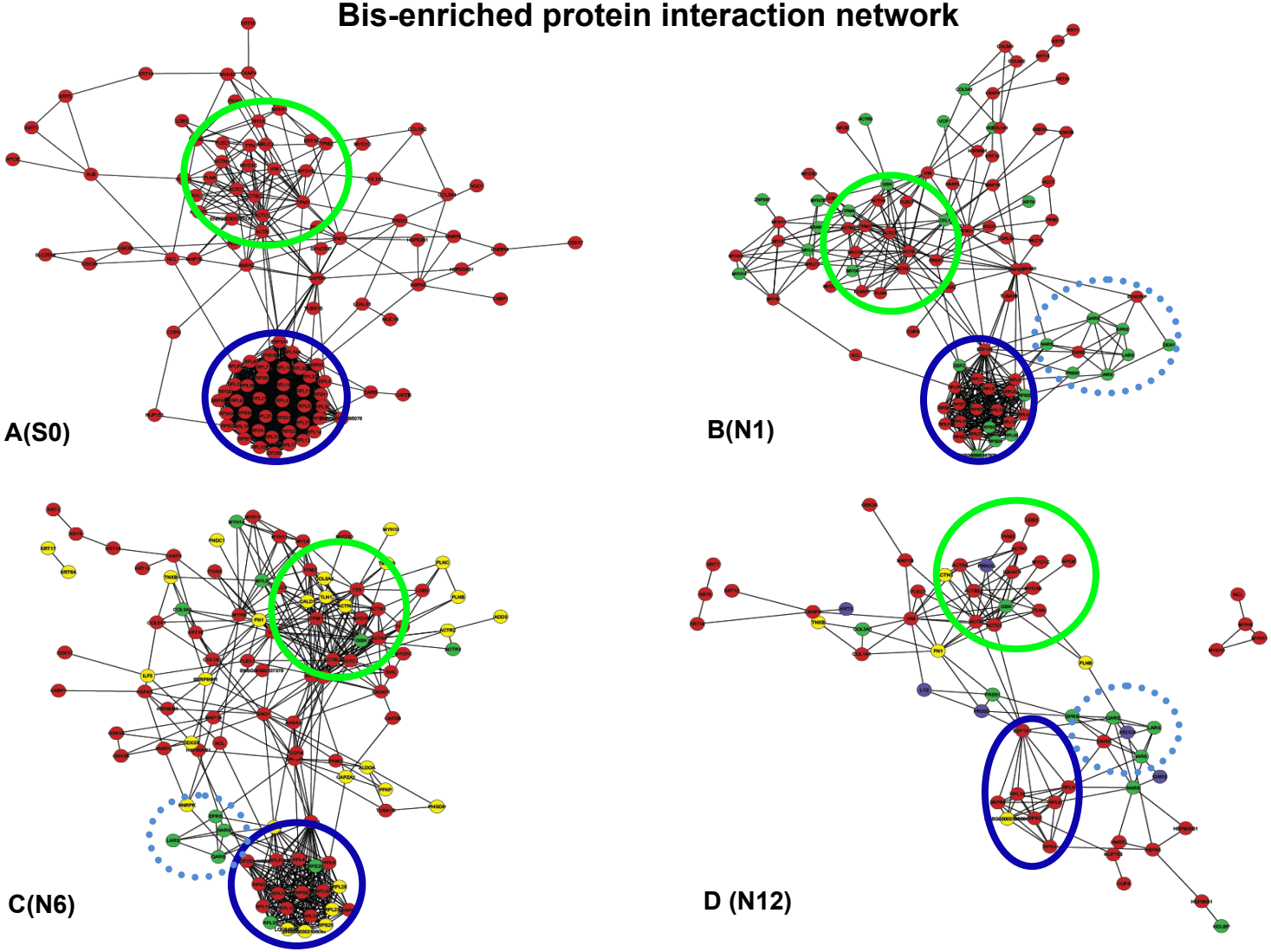

Figure 5.9: (A) Pre-induction media 1hr (S0). Proteins are represented by coloured circular nodes. 105 Red nodes denote S0 specific proteins. Connecting lines between each node indicate annotated interactions between identified proteins. *Ribosomal cluster* is encircled blue and the *structural cluster* is encircled green. **(B) hADSCs differentiation media 1hr (N1).** Proteins are represented by coloured circular nodes. 65 Red nodes denote shared S0 proteins from 10A. 27 Green nodes denote N1 specific proteins. Connecting lines between each node indicate annotated interactions between identified proteins. *Ribosomal cluster* is encircled navy blue and the *structural cluster* is encircled green. **(C) hADSCs differentiation media 6hrs (N6)** Proteins are represented by coloured circular nodes. 68 Red nodes shared S0 proteins from 10A. 11 Green nodes shared N1 proteins from 10B. 29 Yellow nodes are N6 specific proteins. Connecting lines between each node indicate annotated interactions between identified proteins. *Ribosomal cluster* is encircled blue and the *structural cluster* is encircled green. **(D) hADSCs differentiation media 12hrs (N12).** Proteins are represented by coloured circular nodes. Red nodes shared S0 proteins from 9A. Green nodes shared N1 proteins from 9B. 29 Yellow nodes are shared N6 proteins from 9C. Purple nodes are N12 specific proteins. Connecting lines between each node indicate annotated interactions between identified proteins. *Ribosomal cluster* is encircled blue and the *structural cluster* is encircled green.

5.3.5.1. S0 Interaction Networks

Network S0 (**Figure 5.9A**) contains 105 protein nodes from the 134 probe captured proteins. The remaining 29 proteins are not visualised as they do not have database confirmed interactions within this dataset. From the 105 nodes there are 1009 annotated confirmed edge interactions across the network. The '*ribosomal'* and *'structural'* clusters are encircled blue and green respectively are focal points of the network. Elongation factor-1 alpha 1 (EEF1A1) and dolichyldiphosphooligosaccharide protein glycosyltransferase (RPN1) interact beyond the ribosomal cluster and are linked to eleven hub proteins most notably the enzymes glyceraldehyde-3-phosphate dehydrogenase (GAPDH), alpha-enolase (ENO1) and the structural proteins beta-actin (ACTB), gamma-actin (ACTG1) and tropomyosin-1 alpha chain (TPM1) all of which have in excess of 20 interactions per node. The eleven hub nodes are functional linkers situated between ribosomal to structural clusters also serving numerous functional roles across the network. The structural cluster is much more diffuse containing 21 nodes and 111 adjacent edges; it is constituted of various actins, tubulins and myosins. There are four identified direct interactions between structural cluster nodes and the ribosomal cluster nodes. GAPDH, ENO1, TPM1, ANAX2 and NCL associated hub nodes relay as secondary edges between the clusters interacting with 59 separate nodes network wide.

5.3.5.2. N1 Interaction Networks

The overall network logistics of N1 is altered somewhat relative to S0 in that there are 92 nodes with 425 associated edges of which 194 are new (**Figure 5.9B**). The N1 network shares only 65 proteins with S0, a difference of 40 red nodes are no longer expressed. There are however, 27 new N1 specific nodes detected. The introduction of these N1 nodes influences the organic layout due to the fluctuated number of connections. The structural cluster tends directionally toward the left of the network due to losing 12 S0 nodes and including 6 new actin and myosin related members forming 36 new interactions. The ribosomal cluster has significantly decreased size missing 26 ribosomal related proteins. However the introduction of RPL35, EEF2, RPS 6, 16, 20, 24 proteins forms 105 new interactions with direct links to the pathway altering enzyme hubs GAPDH, IARS, PRDX1 and the structural hub ACTG1. A N1-specific 8 node enzymatic modular cluster has formed contiguously to the ribosomal cluster. Encircled by the blue dashed ring the modular cluster comprises of 6 synthases NARS, DARS, QARS, IARS, LARS, EPRS, a trypsin-1 precursor and an ATP-dependent RNA helicase with the majority of the 31 edges linked directly to the ribosomal cluster.

5.3.5.3. N6 Interaction Networks

The variation of Bis-captured proteins again affects network wide layout. The N6 network (**Figure 5.9C**) contains 103 nodes a minuscule change from 105 node S0 network. However N6, confirmed at 488 edges, has less than half the interactions of S0. The carryover of only 63-S0 and 11-N1 shared proteins, including 29 new yellow N6-specific nodes reveals an altered organic layout. The structural cluster is significantly different than S0, comprised of a total of 17 nodes with 170 edges. The cluster is derived from 12 S0 nodes, 1 N1 node and 4 N6 nodes which form 40 new interactions. The newly introduced peripheral nodes ACTR2, ACTR3, ACTN3, CALD1, COL8A2, FN1, FNDC1, FLNB,

FLNC, ADD3, MYL6, MYH10, MYH13, MYO1D, TLN1, TMOD3 now visualised within the purple dashed ring extend structural cluster changes. The greater proportion of newly formed interactions of structure altering and binding related peripheral nodes, reveal a greater trend in cytoskeleton modification in the cells. Further dramatic decrease of ribosomal cluster is reduced to 22 proteins, 14 of the original S0, 2 from N1 and 6 N6 specific. The 6 new nodes EEF1G, RPS18, RPS25, RPL23, RPL29 and ubiquitin form 101 unique edges. The synthase modular cluster observed in N1 has migrated, flanking the ribosomal cluster on the left due to alternate interactions with adjacent proteins. The enzymes phosphofructokinase type C (PFKP), ATP-dependent RNA helicase (DDX3Y), D-3-phosphoglycerate dehydrogenase (PHGDH) and fructose-bisphosphate aldolase A (ALDOA) are linked both directly and indirectly to either cluster in tandem.

5.3.5.4. N12 Interaction Networks

Network N12 (**Figure 5.9D**) shows a 42.8% reduction in visualised nodes to 60 Bis-captured proteins and 85.9% reduction of edges to 142 annotated interactions. The structural cluster is reduced to 15 nodes of which only one, PKCθ, is unique to this time point. Within the N12 network PKCθ interacts with beta-actin (ACTB), gamma-actin (ACTG), filamin-A (FLNA) and pyruvate kinase isozyme (PKM2). The ribosomal cluster has decreased to only 8 members with 7 S0 shared nodes and 1 N6 shared node. EEF1A1 is the sole direct link between the two dominant ribosomal and structural clusters. Some indirect links are associated via the modular cluster which at N12 has the equal number of node members as the ribosomal cluster. The modular cluster contains DARS from S0 and EPRS, IARS, LARS, NARS, QARS from N6 with the new additions glycyl-tRNA synthetase (GARS) and ATP-dependent DNA helicase 2 subunit 1 (XRCC6). GARS shares 2 edges with 2 modular nodes, while XRCC6 interacts with filamin-B (FLNB) and 78 kDa glucose-regulated protein precursor (HSPA5) revealing an indirect links of the

structural and ribosomal through the modular cluster. Proximal to the modular cluster are a group of nodes COPA, HDLBP, HNRPL, HSP90AB1, HSP90B1, HSPA5 and NUP153 which in all previous networks were extensively associated with both major clusters. At N12 this group shares 4 interactions equally between the ribosomal and minor modular cluster. The dissociated quartet of NCL, MYH9, MYH10 and MYH11 no longer share any links with the rest of the network as their functional partners do not exist at this time point.

5.4. Discussion

The study employed the Bis-probe to capture a broad spectrum of purine binding enzymes in hADSCs treated with the neuron inducing chemical agent 2BME. The use of chemical proteomic probes has the benefit of selecting subsets of the proteome with specific molecular attributes. In this study we chose to examine purine binders as these proteins are effective enzymes and thus play a central role in cellular processes directing differentiation. We are the first to report the MS-based characterisation of the binding targets of bisindolylmaleimide in neural differentiated hADSCs. Studies were conducted on hADSCs treated with 2BME for 1 h, 6 h and 12 h durations, utilising as little as 100 µg of protein. This enabled rapid investigation of stem cell proteomics using Bis-probes. Further the successful integration of label free quantitation technique into our small scale quantitative chemical proteomics method enabled us to quantitate the relative abundance of the Bis-captured proteins in 2BME treated hADSCs. This approach allowed a rapid quantitative evaluation of chemical probes in stem cell models, where protein yields after chemical treatment for neurogenic differentiation are considerably low, unlike aggressively growing cancer cell models.

Consistent with the promiscuous nature of the Bis-probe for kinase target selectivity as noted in previous studies [27, 85, 217] (Dolai *et al.*,[134]), the Bis-probe interacted with

many kinase and other non-kinase, purine binding proteins with related structural binding pockets in hADSCs. Almost 70% of the enriched proteome was from purine binders at each of the different time points of 2BME treatment. Majority of the kinase and non-kinase targets that were reported [27, 115] and confirmed (Dolai *et al.*, [134]) previously as Bis-binding proteins were also identified in the 2 BME treated hADSCs.

The previously identified Bis-target kinases GSK3α/β were both identified in the hADSCs. The alpha isoform was identified in all the different groups of 2BME treatment where as the beta isoform was absent in the N12 groups. The presence and different roles of both these isoforms has been previously reported in differentiating Murine Bone marrow derived mesenchymal stem cells [218]. In their study, Cho *et al.* reported the over expression of GSK3β to be potentially responsible for cardiomyocyte differentiation of mesenchymal stem cells and the over expression of GSK3α to induce markers of neuronal differentiation. This could be one of the possible reasons for the capture of the α isoform in all the time point of 2BME treatment. **Figure 5.9A** indicates GSK3α/β are functionally linked to ADP/ATP translocase 1, microtubule-associated protein 1B (MAP 1B) and ATP-citrate synthase. GSK3α/β acquires ATP from the translocase at the mitochondrial membrane. The subsequent phosphorylation of MAP1B by GSK3α/β initiates microtubule assembly and cytoskeletal changes that are implicated neurite extension an essential step in neurogenesis [219]. Gene knockout studies by Lie *et al.* support MAP1B's role in development and function of the nervous system [220]. The phosphorylation of citrate synthase by GSK3β to ATP-citrate synthase is found to be abundant in developing nervous tissue and is involved in the biosynthesis of acetylcholine a neurotransmitter. Although, varying level of GSK3α was captured in different groups on the basis of average NSAF values, the relative abundance of the protein at different time points was not statistically significant. GSK3β is associated with Wnt stimulation and has been found to promote self-

renewal and regeneration of nervous system cells, thus thought to be implicated in the neuro-differentiation of hADSCs [220]. Further, in neuronal stem cells derived from rat sub ventricular zone, Maurer *et al.* reported that GSK3β is a central regulator for differentiation and cell survival of adult neuronal stem cells [221]. They used proteomic approaches to study the inhibitory effect of GSK3β on neuronal differentiation and concluded that GSK3β inhibition results in participation of Wnt/β-catenin signalling pathways for enhanced neuronal differentiation and activates the transcription of β-catenin target genes. They also reported decreased apoptosis of neural stem cells due to GSK3β inhibition. Interesting, GSK3β showed lower relative abundance compared to GSK3α observed at S0, N1 and N6 and was absent in the N12 group, consistent with [221] its function in neural differentiation.

Similarly, we also identified PKC isoenzyme, PKCθ as a Bis-binding target consistently in all the three biological replicates of the N12 group. PKCθ has been previously identified to be enriched by Bis-probes in our study of basal breast cancer cells (Chapter 3). Presently, there are no studies that reported the role of PKCθ in neural differentiated hADSCs. However, there is evidence for changes in PKCθ distribution and molecular properties during the neuronal differentiation of a rat pheochromocytoma PC12 cell line [222]. This study also reported PKCθ involvement in the long term programme of neuronal differentiation. Further, PKCθ was also reported to be associated with the reorganisation of cytoskeletal networks during differentiation of PC12 cells towards the neuron like non proliferating phenotypes. In **Figure 5.9D** PKCθ has annotated interactions with pyruvate kinase isozymes M2 (PKM2), beta-actin, gamma-actin and filamin-A (FLNA). Although PKM2 is a muscle isoform it is widely expressed in some differentiated tissues including brain tissue and nervous cells [223] the role of PKM2 in these tissue remains to be elucidated. Contrastingly, the hydrolysation of the non-muscle type β and γ type actin

allows their polymerisation forming microfilaments in various tissues. The axonal transport of β-actin mRNA in both primary and transformed neuronal cell lines has been identified in the development of neuronal growth cones [224]. Moreover γ-actin plays a role in the chemotaxis migration of the axon growth cone. Studies reveal defects in γ-actin yield damaged neural receptors in the inner ear and nerve pathways to the brain [225] suggesting a greater involvement of enzyme linked interactions to structural proteins in the differentiation process. The interaction between PKCθ and FLNA is also implicated in neuroblast migration and neuronal orientation [226]. FLNA is known to promote branching and anchoring of actin filaments in cytoskeleton remodelling. Another study in neuroblastomas and Jurkat cells, have reported the role of PKCθ in apoptotic induction [227]. In addition, apoptosis rates are also known to have increased over induction time during chemical induction using 2BME in adult rat bone marrow MSCs [228]. Thus the identification of PKCθ only in the N12 group could be related to the onset of apoptosis in the 12 h 2BME treated hADSCs.

Small GTPases, IQGAP 1 is a known Bis-binding protein and has been previously reported in HeLa cells [115]. In eukaryotic cells IQGAP1 binds to and alters the function of several proteins including actin, E-cadherin, β-catenin, CDC42 and RAC1. Studies have reported IQGAP1 as a major regulatory protein that interacts with the actin cytoskeleton [229] and the effect is mediated both by a direct interaction with actin and indirectly via Cdc42 and Rac1 [230]. Although no reports are available on its detection and cytoskeletal regulation in neural differentiated hADSCs, Li *et al.* were the first to report the presence of IQGAP1 in neuronal cells [231]. Their study demonstrated the expression of IQGAP1 in hippocampal neurons from E17 rat embryos and revealed the ubiquitous presence of this enzyme throughout the cells, along the neurites and the developing axon as well as the growth cone. Further, they confirmed the ability and over expression of this enzyme to

promote neurite outgrowth by regulating the neuronal cytoskeleton. Neurite outgrowth requires the interplay of all the three major types of protein filaments that form the cytoskeleton; actin filaments, microtubules and intermediate filaments and precise regulation of cytoskeletal dynamics is important for neurite outgrowth through reorganization of cytoskeleton components [232, 233]. The overexpression of IQGAP1 has also been demonstrated to increase the amount of endogenous active Cdc42 in mammalian cells, resulting in morphological changes with the production of filopodia and microspikes [230]. Studies have also suggested a role of IQGAP1 as a molecular link between active Cdc42 and the actin cytoskeleton [234, 235]. Consistent with these findings, the Bis-probe captured both IQGAP1 and Cdc42 in all the time points on neuronal differentiation of hADSCs, including S0.

Apart from the kinases and the GTPases, the Bis-probe also captured the previously reported [27, 115] (Dolai *et al.*, [134]) non kinases target of bisindolylmaleimides, ribosyldihydronicotinamide dehydrogenase (NQO2) in the group S0 and N1. In addition NAD(P)H dehydrogenase 1 (NQO1) was also identified as a Bis-binding target in the S0, N1 and N12 groups. The relative abundance of the NQO1 dehydrogenase was comparatively higher than that of the NQO2 dehydrogenase. Neurogenic differentiation agents are known to induce oxidative stress, which activates transcription factors like Nrf2 and its target gene NQO1 to counteract redox imbalance and eliminate the harmful reactive species [236]. The differentiating agent 2BME has been reported to cause oxidative stress in bone marrow stromal cells [237], which provides a possible explaination for the identification of NQO1 in 2BME treated hADSCs. However, whether NQO1 has any role in neuronal differentiation has not yet been investigated. Zhao *et al.* have reported that the over expression of Nrf2 promoted neuronal differentiation in neuroblastoma cell line SH-SY5Y.

Similarly the Bis-probe also captured another dehydrogenase D-3 phosphoglycerate dehydrogenase (3PGDH) that was observed only in the N6 and N12 groups. 3PGDH is an initial step enzyme for de-novo L-serine biosynthesis in animal cells. L-serine is synthesised from glycolytic intermediate 3-phosphoglycerate and is an indispensable precursor for the synthesis of proteins, membrane lipids, nucleotides and neuroactive amino acids D-serine and glycine [238]. Yamasaki *et al.* has investigated the cellular expression of 3PGDH and have also reported over expression of 3PGDH in neuroepithelial stem cells. Further, emerging evidence indicates that the non-essential amino acid L-serine plays an essential role in neuronal development and function. Capture of this enzyme by the Bis-probe at N6 and N12 time points of neurogenic differentiation of hADSCs may indicate an active synthesis of this neuronal development amino acid.

Similarly, we also identified the antioxidant enzyme peroxiredoxin 1 (Prdx-1) in S0 and N1 groups, which were previously reported as Bis-target in HeLa cells [115]. Prdx-1 are widely expressed hydrogen peroxide scavenger proteins best known for their role in detoxifying reactive oxygen species, protecting against oxidative stress, DNA damage, cancer and also been suggested to act in cellular signalling and as molecular chaperones [239, 240]. This Bis-target has also been recently reported to be involved in a thiol redox signalling cascade that is known to induce neuronal differentiation [241]. They were the first to identify a new role of Prdx-1 in regulating neuronal differentiation. The cascade identified by Yan *et al.* is mediated by the transmembrane protein glycerophosphodiester phosphodiesterase (GDE2) and the antioxidant protein Prdx1 that controls the timing of motor neuron differentiation in the spinal cord. They issued an innovative proteomic screening approach to demonstrate the direct binding of Prdx-1 to GDE2 and serves as an activating cofactor that promotes neuronal differentiation.

The application of Bis-probe to capture enzymes in neural differentiated hADSCs provided a platform for rapid quantitative evaluation of the effect of chemical induction in stem cell models. The study revealed several unreported enzymes in hADSCs that were expressed and involved in key protein interaction networks for neurogenic differentiation. The differential expression of the enzymes at different time points of neurogenic induction by 2BME has not been studied previously and sheds lights into the regulatory pathways that are involved in neural differentiation of hADSCs. Our results indicate the involvement of kinases related signalling events in the regulation of neural differentiation and the use of a kinase specific probe to study these signalling events in treated and resting stem cells would contribute immensely to the stem cell research field.

Chapter 6: Chemical proteomics of Desthiobiotin ActivX® Probes in Basal breast cancer cells

In this chapter, ActivX® Desthiobiotin (DB) ATP probes were used to study the enriched proteomes of phorbol ester treated MDA-MB-231 basal breast cancer cells. Two different approaches to purify probe bound protein targets were employed. First, a shotgun proteomics technique combined with affinity enrichment was applied to study the binding proteomes of the DB-ATP probes. Second, a MS-based assessment of active-site labelling of the enriched peptides was carried out using the Desthiobiotin ATP probes in 30 min phorbol ester (PMA) treated and was compared with the enriched peptides of resting MDA-MB-231 basal breast cancer cells.

ActivX® Desthiobiotin (DB) ATP probes were a gift from Thermo Fisher Scientific, Rockford, IL, USA.

6.1. Introduction

Probe-based chemical proteomic technologies using synthetic small molecule probes to selectively capture and enrich particular classes of proteins from complex biological samples have been successfully used for enrichment of low copy number metabolic enzymes [242-244]. More recently, gel free chemical proteomics enrichment strategies have been applied to these technologies that specifically target and enrich the binding site peptide of enzyme classes, thus limiting interference from non-specific and more abundant proteins [40, 245]. This active-site peptide profiling technique relies on the principle that activity based chemical probes react selectively with a single active-site amino acid on the probe-binding site of the target enzymes. So analysis of the probe labelled peptides from digested proteomic sample, rather than the intact proteins would allow high resolution analysis [245]. Further the mass spectrometric characterisation of only the labelled peptides would enable the identification of the labelled protein along with the precise site of labelling. This provides valuable information about probe selectivity and mechanism of labelling.

6.1.1. Active-site peptide profiling

Active-site peptide profiling has been used for profiling protein kinases using acyl phosphate ATP and ADP probes that are uniquely capable of profiling broad range of protein kinases along with other nucleotide binding proteins [40]. The probes have also been rigorously studied using MS based technologies to elucidate the binding mechanism and the precise site of labelling [246]. These probes act by covalently modifying the conserved lysine residue in the ATP binding pocket of protein kinases enabling the analysis of the active-site peptides. Patricelli *et al.* reported the most comprehensive study of protein kinase enrichment using acyl phosphate ATP probes and active-site peptide profiling [40]. Several previous studies have also used ATP analogues for the affinity

enrichment of ATP binding proteins and protein kinases. One of the earliest studies used immobilised γ-phosphate linked ATP sepharose for the affinity purification of mitogen-activated protein kinase kinase (MAPKK) from rabbit skeletal muscle [90]. Immobilised ATP was used by Wong *et al.* along with cAMP and cGMP for the affinity enrichment of ATP binding proteins in platelet proteins [247]. Similarly, studies have also utilised ATP analogues, 5'-fluorosulfonylbenzoyl 5'-adenosine (FSBA) as activity based probes and reported the covalent modification of the conserved lysine in the ATP binding pocket of ALK5 and CDK2 [248]. Further a gel free chemical proteomics strategy has also been reported using FSBA for the enrichment and identification of nucleotide binding sites in human Jurkat cell lysate [249]. They reported the identification of six kinases along with the characterisation of the FSBA labelled sites. Haibo *et al.* demonstrated the utility of affinity labelled ATP-acyl phosphate probe with MS in elucidating protein structure and probing nucleotide binding sites [246]. They also applied the probe in HeLa and WM-266-4 cell lysates to establish the potential application of these probes to capture the nucleotide binding proteins in whole cell lysates.

In this chapter, active-site peptide profiling strategy was applied, to enrich the ATP binding metabolic enzymes and kinases in PMA stimulated and resting MDA-MB-231 basal breast cancer cells. Further, the precise site of labelling of all the distinct kinases that were identified in the treated and resting cells was characterised. Studies were conducted to characterise the binding targets of the DB-ATP probes using CCCP MS based protein profiling strategy. Additionally, comparative analysis of the active-site enrichment strategy and CCCP protein profiling study in PMA treated basal breast cancer cells was performed using DB-ATP probes.

6.2. Methods

6.2.1. Probe Design

The DB-ATP probe was a gift from Thermo Fisher Scientific, Rockford, IL, USA. The probe is designed to selectively label and enrich enzymes that utilise ATP/ADP as cofactor for their activity. These include kinases, chaperones and metabolic enzymes. The probe is an adenine nucleotide derivative that covalently modifies the active-site of enzymes at conserved lysine residues in the nucleotide binding sites. The probe architecture is designed to harbour a nucleotide (ATP) binding group which is attached to a desthiobiotin affinity tag through a linker by a labile acyl-phosphate bond (**Figure 6.1A**). The nucleotide group acts as a recognition element and binds to the specific binding sites (Active-site) of enzyme classes, which allows the acyl phosphate reactive group to be placed in close proximity of the conserved lysine residue in the active-site. This results in a covalent amide bond to be formed between the affinity tag and the highly conserved lysine and the ATP group is released (**Figure 6.1B**). The desthiobiotin affinity tags allow the detection of the labelled proteins. This biotin analogue binds less tightly to biotin binding proteins, which is easily reversed by biotin displacement, low pH or heat denaturation.

6.2.2. Cell culture and sample preparation

MDA-MB-231 cells (1.8×10^7 cells) were grown and PMA stimulated as described in Chapter 3, Section 2. Three independent populations of resting and PMA treated cells were harvested. After rinsing in PBS, the cells were lysed in Pierce IP lysis buffer (Thermo Scientific/Pierce Biotechnology, CA, USA) containing 25 mM Tris-HCl, pH 7.4, 150 mM NaCl, 1% NP-40, 1 mM EDTA and 5% glycerol plus protease inhibitors (1 mM phenylmethylsulfonyl fluoride, 1 mM EDTA, 1 μg/ml aprotinin, 1 μg/ml leupeptin, 1 μg/ml pepstatin) and phosphatase inhibitors (1 mM sodium fluoride and 1 mM sodium orthovanadate).

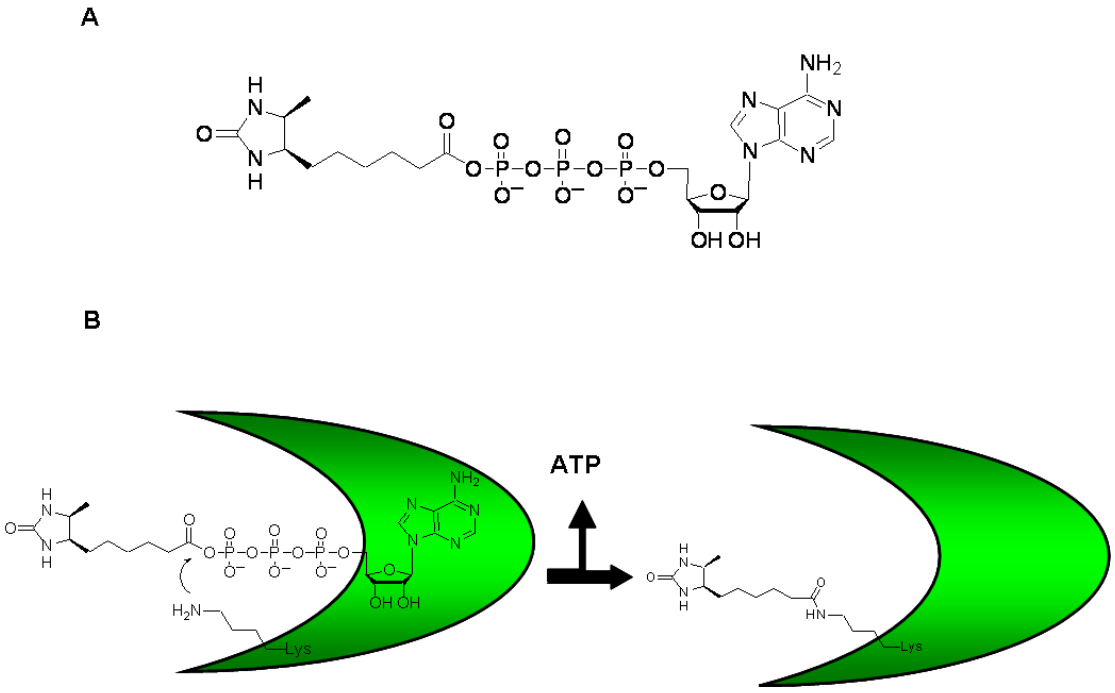

Figure 6.1: Structure and labelling mechanism of Desthiobiotin probes. **(A)** Structure of Desthiobiotin ATP probe. The probes contain an ATP binding group which is linked to a Desthiobiotin affinity tag through an acyl phosphate linkage. **(B)** Mechanism of labelling. The nucleotide analogue of the probe first binds to the active-site (ATP binding site) of ATP binding proteins/protein kinases. Upon binding, the acyl phosphate reactive group will be placed in the proximity of a conserved lysine residue in the active-site. The ε- amino group of the lysine residue then attacks the carbonyl carbon of the probe (arrow), releasing ATP, and irreversibly transferring the affinity tag to highly conserved lysine through an amide bond.

Cell lysates were vortexed and cleared by centrifugation at 14000 rpm for 5 min at 4ºC. The cleared lysates were filtered through Zeba Spin Desalting Coloumns (Thermo Scientific/Pierce Biotechnology, CA, USA) into fresh lysis buffer. The cell lysates were desalted to remove endogenous nucleotides, particularly ATP which competes with the probe for the ATP binding sites of target proteins. Relative protein concentration was determined using the bicinchoninic acid (BCA) assay.

6.2.2.1. DB-ATP probes Protein Profiling

For CCCP based protein profiling studies (**Figure 6.2**), desalted cell lysates of two independent biological replicates of PMA treated MDA-MB-231 cells were volume adjusted to 500 µl with Pierce IP lysis buffer and was labelled with DB-ATP probe at 10 µM, for 10 min at RT. Labelled proteins were affinity purified with high capacity

streptavidin agarose beads and eluted at 65°C with 2 x LDS. Eluates were gel purified and MS sample preparation of the gel pieces was performed as described in Chapter 3, Section 2.

6.2.2.2. Active-site enrichment using DB ATP probes

For active-site peptide enrichment (**Figure 6.2**), 1 mg desalted resting or PMA treated cell lysates were labelled with DB-ATP as described in Section 6.2.2.1. Labelled samples were reduced with 10 mM DTT and alkylated with 55 mM iodoacetamide for 30 min in the dark. The samples were then filtered through Zeba Spin Desalting Coloumns (Thermo Scientific/Pierce Biotechnology, CA, USA) into digestion buffer (2 M Urea/20 mM Tris, pH 8.0). The desalted and labelled samples were digested with 10 µg of trypsin for 2 h at 37°C and the probe labelled peptides were isolated with high capacity streptavidin agarose beads (Pierce, catalog no. 20357). Afterwards, the beads were washed thrice with 500 µl of Pierce IP lysis buffer, four times with 500 µl of PBS and four times with LCMS-grade water. The captured peptides were eluted thrice with 50% acetonitrile/water mixture with 0.1% TFA. The combined eluate was dried under vaccum to 10 µl and was directly injected onto a LTQ XL linear ion-trap mass spectrometer (Thermo, CA, USA) for LC-MS/MS analysis.

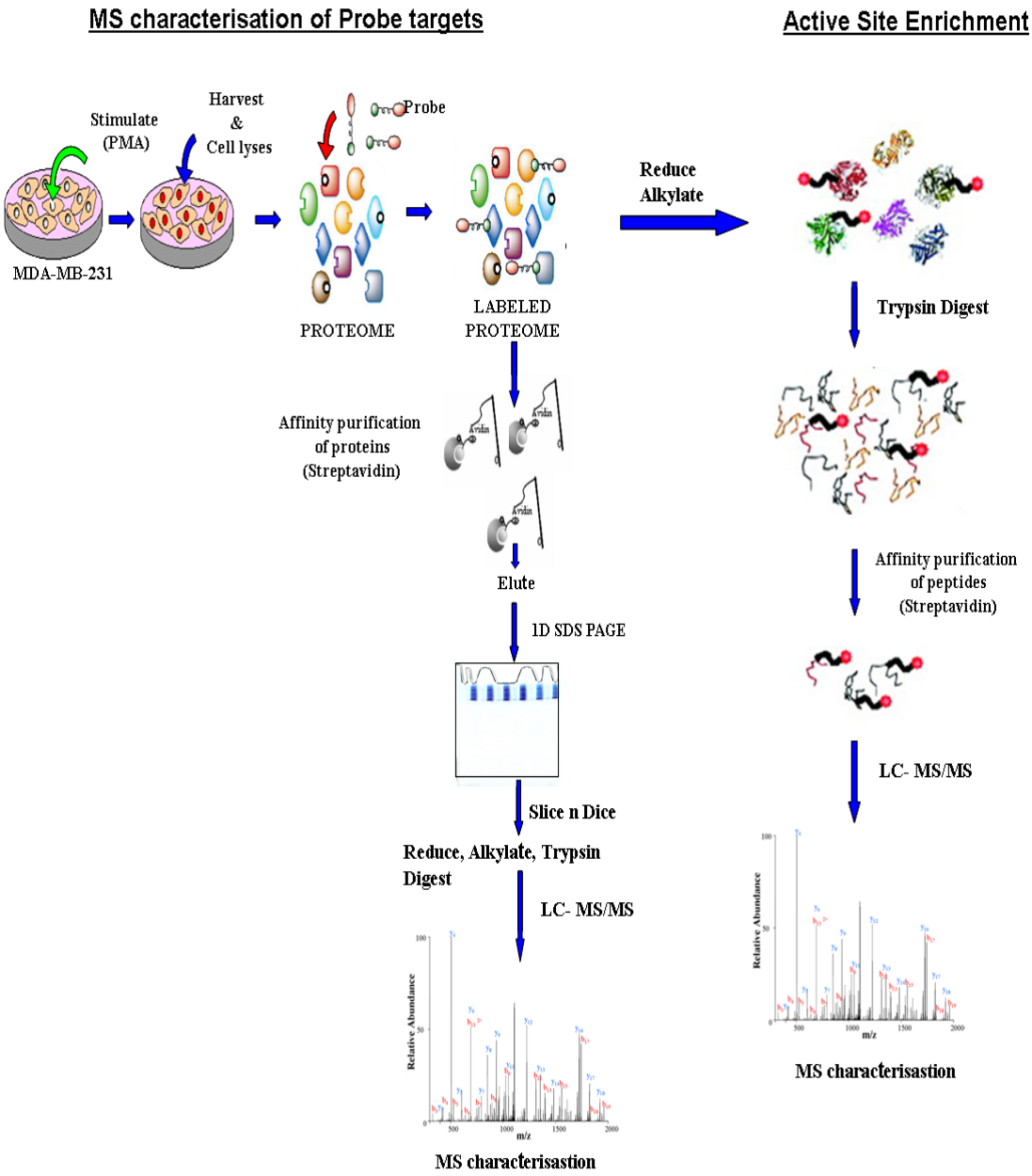

Figure 6.2: CCCP based protein profiling and active-site peptide enrichment using chemical probes. In protein profiling experiments the probe labelled proteins are first affinity purified and then reduced, alkylated and trypsin digested prior to MS analysis. In active-site enrichment analysis the labelled proteins are first reduced, alkylated and trypsin digested. The labelled tryptic peptides are then affinity purified and characterised by MS.

6.2.2.3. Mass spectrometry and Data analysis

Samples were analysed by LC-MS/MS on LTQ XL linear ion-trap mass spectrometer (Thermo, CA, USA) as described previously in Chapter 3, Section 2. The LC-MS/MS data were searched against the Swissprot *Human* database ver. 57.4 by using the MASCOT algorithm (Ver.2.3, Matrix Science, London) with the following search criteria, enzyme

(trypsin), allowed missed cleavages (2), fixed modifications (carbamidomethyl cysteine), variable modifications (oxidation methionine), peptide charge (1+, 2+ and 3+), instrument (ESI-TRAP), peptide tolerance (1.3 Da) and fragment tolerance (0.6 Da). In addition a modification mass of 196.1212 Da was used as a variable modification on lysine for search purposes.

Spectra acquired from the CCCP based protein profiling experiments on the LTQ XL linear ion trap mass spectrometer were identified using Mascot Distiller (Matrix Science). The .raw Xcalibur (Thermo) spectra files were submitted into Mascot Distiller and default peak picking was performed on all submitted scans followed by Mascot protein identification search against the Swissprot Human database ver. 57.4 with the same search parameters as described above.

6.3. Results

6.3.1. Active-site peptide enrichment using DB-ATP probe

The adenine nucleotide interacting proteome of the DB-ATP probe was assessed by labelling phorbol ester treated MDA-MB-231 basal breast cancer cell lysates. Proteins harvested from each of the biological triplicates of the 30 min PMA treated cells were labelled with DB-ATP probes, followed by reduction, alkylation, trypsin digestion and purification of the probe-labelled peptides with streptavidin-agarose beads. Using a linear ion trap mass spectrometer the labelled peptides were analysed to determine the identity of the protein and the precise site of labelling. Further, differential analysis of the active-site enrichment by the DB-ATP probes was carried out in resting MDA-MB-231 basal breast cancer cell lysates. Proteins that were confidently identified with peptide FDR<1% and present in at least 2 of the 3 biological replicates were examined. In the PMA treated MDA-MB-231 cell lysates 69 proteins and in the resting cells 65 proteins were identified

that were captured by the DB-ATP probe. Of these 49 proteins were common to both the treated and resting cell lysates, 20 proteins were unique to the PMA treated group and 16 proteins were unique to the resting cells (**Table 6.1A,B and C**). The labelling site of DB-ATP probe on all the distinct kinases identified in both the groups was characterised. The sequence of the captured peptide of each of the kinase was identified with a lysine residue that was acylated due to probe binding (**Table 6.2**). Additionally, 12 of the peptide sequences exactly matched to the previously identified active-site peptides of acylated ATP probes (BHAcATP) [40], which yielded stronger evidence that the probes are acting by the predicted labelling mechanism.

6.3.2. Gene Ontology (GO) analysis

GO analysis annotated two-thirds of the identified targets in both the PMA treated and the resting MDA-MB-231 cells as ATP binding, which included 23 protein kinases (**Figure 6.3A**). Of the identified protein kinases 16 were common to both the groups and 7 protein kinases each were unique to the PMA treated samples and the resting cells (**Table 6.1**). The remaining ATP binding proteins totalled to 28% in the PMA treated group and 23% in the resting group. The probe captured equal number of GTP binding (5 proteins) and NAD binding enzymes (4 proteins) in both the groups. Both the groups had ~13% DNA/RNA binding enzymes and 13 % proteins that did not have any designated ligand binding ability, categorised as others.

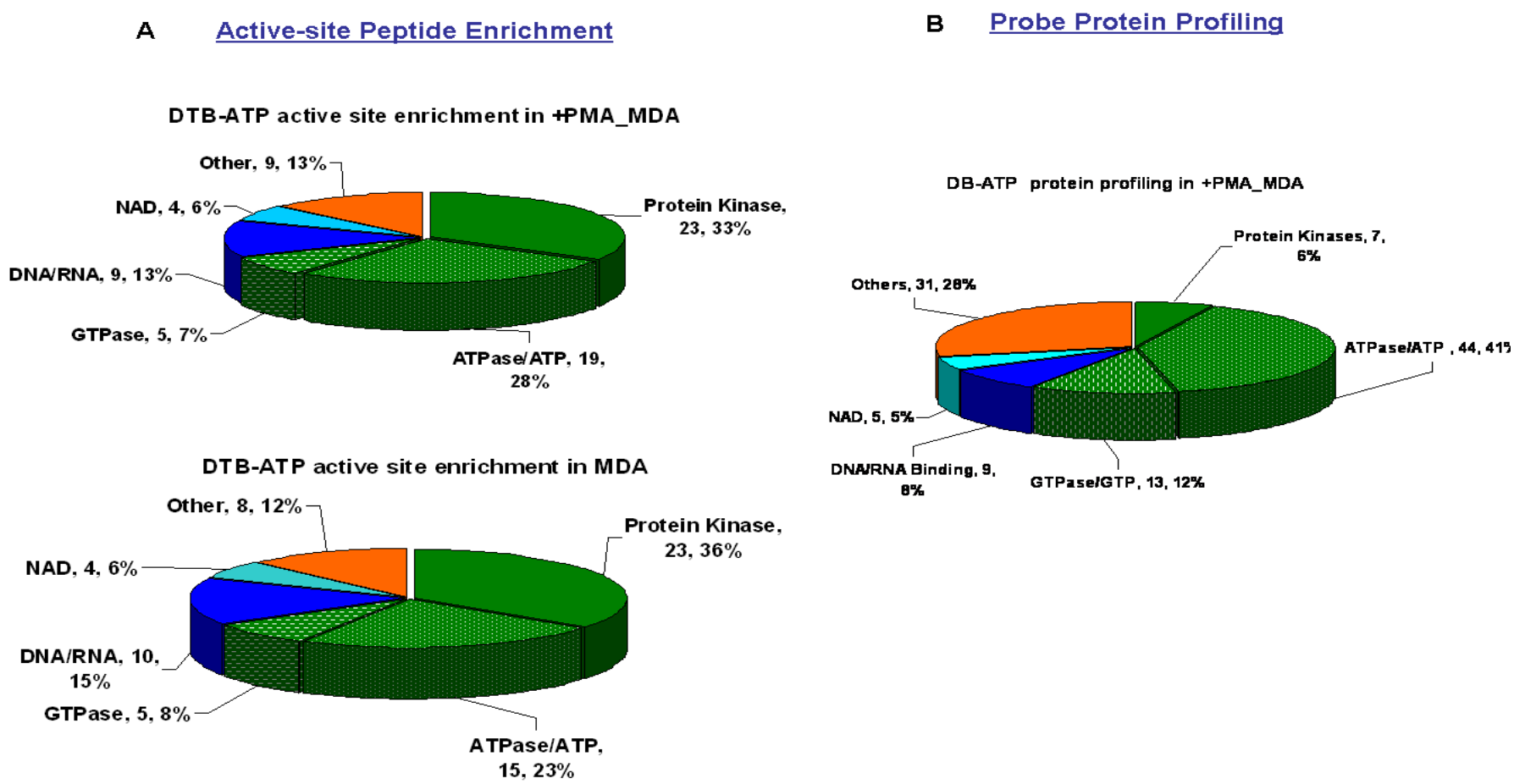

Figure 6.3: (A) Active-site peptide enrichment in PMA treated and resting MDA-MB-231 basal breast cancer cells. **(B)** CCCP protein profiling studies of DB-ATP probe in PMA treated MDA-MB-231 basal breast cancer cells. Identified protein targets categorised according to their binding functions based on Gene Ontology (GO).

6.3.3. CCCP based protein profiling of DB-ATP probes

Comparative analysis of the active-site enrichment technique with CCCP based protein profiling of DB-ATP probes demonstrated a clear enrichment of protein kinases by the former. Protein profiling using DB-ATP probes in PMA treated MDA-MB-231 revealed 111 proteins as DB-ATP protein targets that were identified in both the replicates (**Table 6.3**). GO analysis of the probe captured proteome revealed 6% (7 proteins) of the captured targets as protein kinases, 41% (44 proteins) as ATP binding proteins, 12% (13 proteins) as GTP binding and 8% (9 proteins) as DNA/RNA binding (**Figure 6.3B**). The enrichment of NAD utilising enzymes (5%, 5 proteins) was similar to the active-site enrichment technique. Further, the probe reported ~30% of protein capture that are well characterised but had no known nucleotide recognition ability. Many proteins in this group are abundant proteins and there is a possibility that the probe may have interacted in a non-selective manner with the surface lysines of these proteins.

6.4. Discussion

The active-site peptide profiling method based on novel DB-probe showed a distinct advantage in enrichment of protein kinases and enabled the characterisation of the precise site of covalent modification confirming the predicted mechanism of labelling of the probe. The covalent modification by the probe at a conserved lysine residue in the ATP binding site of metabolic enzymes/kinases and subsequent affinity enrichment of the labelled active-site peptides resulted in specific enrichment for low-copy number enzymes without interference from more abundant proteins. The most striking feature of the data was a massive percentage increase of ~300% in kinase enrichment compared to CCCP based protein profiling experiment. Further, the analysis of DB-ATP labelled peptides from digested proteomic samples, rather than intact proteins allowed more specific and enhanced enrichment of kinases. For example, only 7 protein kinases were enriched in the

CCCP based protein profiling experiments, where as in the active-site enrichment 23 protein kinases were enriched (**Figure 6.3**).

Interference in MS detection of kinases in specific probe based technologies is primarily caused by highly abundant ATP-binding proteins such as actin and heat shock proteins. The advantage of active-site analysis is that only labelled peptides are enriched and affinity purified for MS analysis, which significantly diminishes the background noise of unlabelled peptides and the subsequent masking effect on low copy number kinases [40, 245, 246]. This was eloquently demonstrated, when 30 peptides of actin that were identified in protein profiling studies reduced to identification of only 5 peptides in the active-site analysis. Similarly, the detection of heat shock proteins (HSP90-β) was reduced from 22 peptides in protein profiling studies to 3 peptides in active-site analysis. Further, the co-purification of abundant proteins with low probe affinity and non-specific targets that co-elute due to protein-protein interactions was also significantly reduced. This was evident from a ~90% specific enrichment of binding sites with conserved lysine in the active-site analysis compared to the protein profiling studies. Further, comparative active-site analysis of phorbol ester treated and resting breast cancer cells revealed an enrichment of 29 kinases in both with a 75 % overlap and 25 % unique kinases. The differential capture potentially provides a powerful tool for specific quantitative kinase studies using SILAC.

Additionally, 12 of the peptide sequences and probe labelled sites exactly matched to the previously identified active-site peptides of acylated ATP probes (Biotin-Hex-Acyl-ATP) [40], which yielded stronger evidence that the probes are acting by the predicted labelling mechanism by covalently modifying the conserved lysine residue located in the proximity of the γ-phosphate of ATP. The results obtained from our study with the DB-ATP probe

are comparable with other acylated ATP probes which reported a two third enrichment of ATP binding proteins [40]. In addition, the release of the large ATP binding group in the reaction leaving the uncharged biotin analogue on the protein is an added advantage, facilitating MS analysis. Moreover, the reduced binding ability of desthiobiotin to biotin binding proteins minimised non-specific biotin interactions. Finally, the additional modification mass of the attached probe to labelled peptides with the DB-ATP probes added up to 196.12 Da, which facilitated the MS analysis of even large peptides. Usually probe fragments with higher additional mass results in observation of +4 and +5 charge states for larger peptides which complicates searching of MS spectra [245].

.

Table 6.1A: Proteins identified by active-site peptide enrichment using Desthiobiotin (DB) ATP probes in both PMA stimulated and resting MDA-MB-231 basal breast cancer cell lines. R1, R2, R3 are the independent biological replicates. † Number of peptide observations. Number in parentheses indicates number of unique peptide sequences. No parentheses mean only unique peptides.

UniProt Accession	Protein	+PMA_MDA						MDA					
		MASCOT Prot_Scores			Peptide Counts†			MASCOT Prot_Scores			Peptide Counts		
		R1	R2	R3	R1	R2	R3	R1	R2	R3	R1	R2	R3
CH10_HUMAN	10 kDa heat shock protein, mitochondrial	53	85	79	1	3 (2)	2 (1)	88	76	_	2 (1)	2 (1)	_
1433F_HUMAN	14-3-3 protein eta	_	50	51	_	1	1	54	_	89	1	_	2 (1)
PRS10_HUMAN	26S protease regulatory subunit 10B	64	190	61	1	3 (1)	1	57	68	68	1	1	1
PRS6A_HUMAN	26S protease regulatory subunit 6A	80	_	40	3 (1)	_	1	_	62	47	_	1	1
PRS6B_HUMAN	26S protease regulatory subunit 6B	114	127	99	2 (1)	3 (1)	3 (1)	52	_	68	1	_	1
RSSA_HUMAN	40S ribosomal protein SA	67	_	44	2 (1)	_	1	81	94	82	2 (1)	3 (1)	3 (1)
ACTA_HUMAN	Actin, aortic smooth muscle	346	331	239	9 (5)	10 (5)	6 (4)	124	229	_	4 (4)	7 (4)	_
KAD2_HUMAN	**Adenylate kinase 2, mitochondrial**	156	102	215	2 (1)	3 (1)	4 (1)	126	190	212	2 (1)	3 (1)	4 (1)
KAD1_HUMAN	**Adenylate kinase isoenzyme 1**	262	94	172	4 (1)	1	3 (1)	127	132	87	2 (1)	2 (1)	1
AL1A3_HUMAN	Aldehyde dehydrogenase family 1 member A3	_	90	90	_	2 (1)	2 (1)	71	_	73	2 (1)	_	2 (1)
A16A1_HUMAN	Aldehyde dehydrogenase family 16 member A1	74	47	100	2 (1)	1	2 (1)	103	121	_	2 (1)	3 (1)	_
ENOA_HUMAN	Alpha-enolase	_	49	71	_	1	2 (1)	40	49	_	1	1	_
ANXA2_HUMAN	Annexin A2	_	47	96	_	1	3 (2)	45	54	_	1	1	_
ABCF3_HUMAN	ATP-binding cassette sub-family F member 3	_	68	66	_	1	1	129	73	93	2 (1)	1	2 (1)
KCC2G_HUMAN	**Calcium/calmodulin-dependent proteinkinasetype II gamma**	61	_	84	1	_	2 (1)	69	58	_	1	1	_
PRKDC_HUMAN	**DNA-dependent protein kinase catalytic subunit**	51	68	55	1	1	1	85	_	59	1	_	1
MP2K3_HUMAN	**Dual specificity mitogen-activated protein kinase kinase 3**	187	270	230	4 (2)	5 (1)	5 (2)	182	213	215	3 (1)	4 (1)	4 (1)
EF1A1_HUMAN	Elongation factor 1-alpha 1	117	240	279	6 (5)	7 (5)	9 (6)	107	160	126	3 (2)	4 (3)	3 (2)
ENPL_HUMAN	Endoplasmin	363	444	188	12 (3)	14 (4)	7 (2)	268	425	156	9 (4)	14 (3)	4 (2)
EGFR_HUMAN	**Epidermal growth factor receptor**	78	169	96	3 (2)	5 (3)	3 (2)	42	78	45	1	3 (2)	1
ESYT2_HUMAN	Extended synaptotagmin-2	129	95	74	2 (1)	1	1	75	136	53	1	2 (1)	1
FLNB_HUMAN	Filamin-B	64	44	81	1	1	2 (1)	61	140	_	1	4 (1)	_
ALDOA_HUMAN	Fructose-bisphosphate aldolase A	74	_	134	1	_	2 (1)	_	72	76	_	1	1
G3P_HUMAN	Glyceraldehyde-3-phosphate dehydrogenase	220	138	91	8 (2)	5 (3)	3	46	165	54	1	6 (3)	1
HSP7C_HUMAN	Heat shock cognate 71 kDa protein	42	198	197	1	5 (1)	4 (3)	78	72	54	2 (1)	2 (1)	1
TRAP1_HUMAN	Heat shock protein 75 kDa, mitochondrial	40	36	59	1	1	1	102	37	61	2	1	2 (1)
HS90A_HUMAN	Heat shock protein HSP 90-alpha	104	143	_	4 (2)	5 (4)	_	115	113	81	5 (4)	4 (2)	2 (1)
HS90B_HUMAN	Heat shock protein HSP 90-beta	167	186	97	6 (3)	8 (5)	3	179	197	115	7 (5)	9 (3)	3
IMDH2_HUMAN	Inosine-5~-monophosphate dehydrogenase 2	78	60	_	1	1	_	_	35	121	_	1	2 (1)
LDHA_HUMAN	L-lactate dehydrogenase A chain	74	145	90	2	2	2	90	60	57	2 (1)	1	1
MK01_HUMAN	**Mitogen-activated protein kinase 1**	111	_	37	3 (1)	_	1	49	118	_	2 (1)	3 (1)	_
MK03_HUMAN	**Mitogen-activated protein kinase 3**	111	_	37	3 (1)	_	1	49	118	_	2 (1)	3 (1)	_
MYH9_HUMAN	Myosin-9	39	135	78	1	4 (3)	2 (1)	70	157	116	2	3 (2)	4 (3)

AHNK_HUMAN	Neuroblast differentiation-associated protein AHNAK	_	45	83	_	1	2 (1)	38	55	70	1	1	2 (1)
NPM_HUMAN	Nucleophosmin	_	67	123	_	2 (1)	3 (2)	41	130	_	1	3 (2)	_
UBB_HUMAN	Polyubiquitin-B	73	47	92	2 (1)	1	3 (1)	51	55	64	1	1	2 (1)
PROF1_HUMAN	Profilin-1	311	149	186	10 (3)	5 (4)	7 (5)	99	360	137	3 (2)	10 (5)	5 (3)
TMSL1_HUMAN	Putative thymosin beta-4-like protein 1	_	67	45	_	2 (1)	1	46	_	62	1	_	2 (1)
PRPS1_HUMAN	**Ribose-phosphate pyrophosphokinase 1**	188	173	164	4 (1)	3 (1)	3 (1)	58	141	96	1	3 (1)	2 (1)
PRPS2_HUMAN	**Ribose-phosphate pyrophosphokinase 2**	204	98	101	4 (1)	2	2	118	240	76	2 (1)	4 (1)	1
KS6A3_HUMAN	**Ribosomal protein S6 kinase alpha-3**	_	89	71	_	3 (2)	1	86	163	87	2	5 (2)	2 (1)
STK3_HUMAN	**Serine/threonine-protein kinase 3**	_	72	91	_	1	2 (1)	112	128	146	2 (1)	3 (1)	3 (1)
NEK7_HUMAN	**Serine/threonine-protein kinase Nek7**	52	82	86	1	2 (1)	2 (1)	94	94	_	2 (1)	2 (1)	_
S12A4_HUMAN	Solute carrier family 12 member 4	44	37	61	1	1	2 (1)	39	41	58	1	1	2 (1)
TNIK_HUMAN	**TRAF2 and NCK-interacting protein kinase**	189	128	_	3 (1)	2 (1)	_	93	124	121	1	2 (1)	2 (1)
TERA_HUMAN	Transitional endoplasmic reticulum ATPase	251	101	84	9 (3)	3 (2)	2 (1)	291	344	237	7 (1)	8 (2)	7 (2)
PUR2_HUMAN	Trifunctional purine biosynthetic protein adenosine-3	139	94	171	5 (1)	3 (2)	5 (2)	152	201	115	5 (2)	6 (2)	5 (2)
CSK_HUMAN	**Tyrosine-protein kinase CSK**	120	106	105	2 (1)	2	2	106	91	_	3 (2)	2	_
KCY_HUMAN	**UMP-CMP kinase**	52	171	65	1	6 (1)	2 (1)	147	69	_	3 (1)	2 (1)	_

Table 6.1B: Proteins identified by active-site peptide enrichment using Desthiobiotin (DB) ATP probes unique to PMA stimulated MDA-MB-231 basal breast cancer cell lines. R1, R2, R3 are the independent biological replicates. † Number of peptide observations. Number in parentheses indicates number of unique peptide sequences. No parentheses mean only unique peptides.

UniProt Accession	Protein	+PMA_MDA					
		MASCOT Prot_Scores			Peptide Counts†		
		R1	R2	R3	R1	R2	R3
PDE12_HUMAN	2~,5~-phosphodiesterase 12	_	65	50	_	2 (1)	1
PRS4_HUMAN	26S protease regulatory subunit 4	72	46	48	1	1	1
PRS8_HUMAN	26S protease regulatory subunit 8	85	_	51	2 (1)	_	1
RS13_HUMAN	40S ribosomal protein S13	_	66	40	_	1	1
RS17_HUMAN	40S ribosomal protein S17	39	38	_	1	1	_
AAPK1_HUMAN	**5~-AMP-activated protein kinase catalytic subunit alpha-1**	67	41	41	2 (1)	1	1
ABCF2_HUMAN	ATP-binding cassette sub-family F member 2	61	64	_	1	1	_
KCC1D_HUMAN	**Calcium/calmodulin-dependent protein kinase type 1D**	_	36	51	_	1	1
KCC4_HUMAN	**Calcium/calmodulin-dependent protein kinase type IV**	62	_	40	2 (1)	_	1
COF1_HUMAN	Cofilin-1	44	_	67	1	_	2 (1)
MP2K2_HUMAN	**Dual specificity mitogen-activated protein kinase kinase 2**	_	96	101	_	4 (2)	4 (2)
EZRI_HUMAN	Ezrin	_	41	37	_	1	1
HSP71_HUMAN	Heat shock 70 kDa protein 1A/1B	63	80	_	2 (1)	2 (1)	_
ILK_HUMAN	**Integrin-linked protein kinase**	91	55	_	2 (1)	1	_
MLKL_HUMAN	**Mixed lineage kinase domain-like protein**	39	_	37	1	_	1
PSB10_HUMAN	Proteasome subunit beta type-10	50	56	118	1	1	2 (1)
S10AA_HUMAN	Protein S100-A10	45	_	37	1	_	1
TYB10_HUMAN	Thymosin beta-10	_	88	72	_	3 (3)	2 (1)
FER_HUMAN	**Tyrosine-protein kinase Fer**	84	143	77	1	2 (1)	2 (1)
XRCC5_HUMAN	X-ray repair cross-complementing protein 5	_	50	83	_	1	2 (1)

Table 6.1C: Proteins identified by active-site peptide enrichment using Desthiobiotin (DB) ATP probes unique to Resting MDA-MB-231 basal breast cancer cell lines. R1, R2, R3 are the independent biological replicates. † Number of peptide observations. Number in parentheses indicates number of unique peptide sequences. No parentheses mean only unique peptides.

UniProt Accession	Protein	MDA					
		MASCOT Prot_Scores			Peptide Counts		
		R1	R2	R3	R1	R2	R3
CH60_HUMAN	60 kDa heat shock protein, mitochondrial	59	84	_	2	2 (2)	_
ANXA6_HUMAN	Annexin A6	39	_	86	1	_	1
KCC2D_HUMAN	**Calcium/calmodulin-dependent proteinkinasetype II delta**	65	_	57	2 (1)	_	1
MP2K1_HUMAN	**Dual specificity mitogen-activated protein kinase kinase 1**	37	36	_	1	1	_
HNRPU_HUMAN	Heterogeneous nuclear ribonucleoprotein U	44	_	40	1	_	1
HNRL1_HUMAN	Heterogeneous nuclear ribonucleoprotein U-like protein 1	51	78	_	1	3 (2)	_
PGAM1_HUMAN	Phosphoglycerate mutase 1	70	250	57	1	6 (1)	1
PMVK_HUMAN	**Phosphomevalonate kinase**	80	57	51	2 (1)	1	1
RIR1_HUMAN	Ribonucleoside-diphosphate reductase large subunit	42	34	_	1	1	_
STK24_HUMAN	**Serine/threonine-protein kinase 24**	65	69	98	1	1	2 (1)
BRAF_HUMAN	**Serine/threonine-protein kinase B-raf**	58	_	42	2 (1)	_	1
SLK_HUMAN	**STE20-like serine/threonine-protein kinase**	70	79	_	1	1	_
THIO_HUMAN	Thioredoxin	40	54	40	1	1	1
TOR1B_HUMAN	Torsin-1B	_	55	46	_	2 (1)	1
PRPK_HUMAN	**TP53-regulating kinase**	_	132	60	_	3 (1)	2 (1)
TBA1A_HUMAN	Tubulin alpha-1A chain	48	118	_	1	2 (1)	_

Table 6.2: Active-site peptide sequences identified for the protein kinases present in both PMA treated and resting MDA-MB-231 cell lysates. An asterisk denotes the lysine (bold red) acetylated by the probes. The sequences that matched to the kinase sequences identified by Patricelli *et al.* 2007 [40]using BHAcATP probes are underlined.

FOUND IN BOTH (MDA/PMA)		
Uniprot Accession	**Protein**	***Identified peptides***
CSK_HUMAN	Tyrosine-protein kinase CSK	K.VSDFGLT**K***EASSTQDTGK.L
KAD1_HUMAN	Adenylate kinase isoenzyme 1	K.IIFVVGGPGSG**K***GTQCEK.I
KAD2_HUMAN	Adenylate kinase 2, mitochondrial	R.AVLLGPPGAG**K***GTQAPR.L
KCC2G_HUMAN	Calcium/calmodulin-dependent protein kinase type II subunit gamma	K.TSTQEYAA**K***IINTK.K
KCY_HUMAN	UMP-CMP kinase	.MKPLVVFVLGGPGAG**K***GTQCAR.I
KS6A3_HUMAN	Ribosomal protein S6 kinase alpha-3	R.DL**K***PENILLDEEGHIK.L
MK01_HUMAN	Mitogen-activated protein kinase 1	R.DL**K***PSNLLLNTTCDLK.I
MK03_HUMAN	Mitogen-activated protein kinase 3	R.DL**K***PSNLLINTTCDLK.I
MP2K3_HUMAN	Dual specificity mitogen-activated protein kinase kinase 3	R.HAQSGTIMAV**K***R.I
NEK7_HUMAN	Serine/threonine-protein kinase Nek7	R.DI**K***PANVFITATGVVK.L
PRKDC_HUMAN	DNA-dependent protein kinase catalytic subunit	K.**K***GGSWIQEINVAEK.N
PRPS1_HUMAN	Ribose-phosphate pyrophosphokinase 1	R.NCTIVSPDAGGA**K***R.V
PRPS2_HUMAN	Ribose-phosphate pyrophosphokinase 2	K.NCIIVSPDAGGA**K***R.V
STK3_HUMAN	Serine/threonine-protein kinase 3	R.DI**K***AGNILLNTEGHAK.L
TNIK_HUMAN	TRAF2 and NCK-interacting protein kinase	R.DI**K***GQNVLLTENAEVK.L
ONLY FOUND IN PMA		
AAPK1_HUMAN	5~-AMP-activated protein kinase catalytic subunit alpha-1	K.VAV**K***ILNR.Q
FER_HUMAN	Tyrosine-protein kinase Fer	R.QEDGGVYSSSGL**K***QIPIK
ILK_HUMAN	Integrin-linked protein kinase	R.ISMADV**K***FSFQCPGR.M
KCC1D_HUMAN	Calcium/calmodulin-dependent protein kinase type 1D	K.LFAV**K***CIPK.K
KCC4_HUMAN	Calcium/calmodulin-dependent protein kinase type IV	R.DL**K***PENLLYATPAPDAPLK.I
MLKL_HUMAN	Mixed lineage kinase domain-like protein	R.APVAI**K***VFK.K
MP2K2_HUMAN	Dual specificity mitogen-activated protein kinase kinase 2	R.DV**K***PSNILVNSR.G
ONLY FOUND IN MDA		
BRAF_HUMAN	Serine/threonine-protein kinase B-raf	R.DL**K***SNNIFLHEDLTVK.I
KCC2D_HUMAN	Calcium/calmodulin-dependent protein kinase type II subunit delta	K.IPTGQEYAA**K***IINTK.K
MP2K1_HUMAN	Dual specificity mitogen-activated protein kinase kinase 1	R.DV**K***PSNILVNSR.G
PMVK_HUMAN	Phosphomevalonate kinase	K.SG**K***DFVTEALQSR.L
PRPK_HUMAN	TP53-regulating kinase	R.FLSGLELV**K***QGAEAR.V
SLK_HUMAN	STE20-like serine/threonine-protein kinase	R.DL**K***AGNILFTLDGDIK.L
STK24_HUMAN	Serine/threonine-protein kinase 24	R.DI**K***AANVLLSEHGEVK.L

Table 6.3: Protein targets of DB-ATP characterised in PMA treated MDA-MB-231 cell lysates by protein profiling studies.

UniProt Accession	Protein	PMA_MDA_DB-ATP			
		EXPT-1		Expt-2	
		Mascot score	Peptide	Mascot score	Peptide
PSMD2_HUMAN	26S proteasome non-ATPase regulatory subunit 2	98	2	41	3
PSMD3_HUMAN	26S proteasome non-ATPase regulatory subunit 3	108	3	53	3
RS3_HUMAN	40S ribosomal protein S3	72	2	71	3
K6PP_HUMAN	**6-phosphofructokinase type C**	102	4	241	3
K6PF_HUMAN	**6-phosphofructokinase, muscle type**	42	1	46	3
ACTC_HUMAN	Actin, alpha cardiac muscle 1	661	28	618	29
ACTB_HUMAN	Actin, cytoplasmic 1	805	30	640	29
ANXA6_HUMAN	Annexin A6	167	3	39	4
SYNC_HUMAN	Asparaginyl-tRNA synthetase, cytoplasmic	38	1	41	1
ACLY_HUMAN	ATP-citrate synthase	107	4	131	2
DHX9_HUMAN	ATP-dependent RNA helicase A	116	3	80	2
SYEP_HUMAN	Bifunctional aminoacyl-tRNA synthetase	96	2	73	2
C1TC_HUMAN	C-1-tetrahydrofolate synthase, cytoplasmic	509	16	587	16
CAN2_HUMAN	Calpain-2 catalytic subunit	44	1	115	16
ZW10_HUMAN	Centromere/kinetochore protein zw10 homolog	42	1	60	1
CLH1_HUMAN	Clathrin heavy chain 1	38	1	73	2
CLPT1_HUMAN	Cleft lip and palate transmembrane protein 1	44	1	47	2
COPA_HUMAN	Coatomer subunit alpha	52	2	169	1
COPB_HUMAN	Coatomer subunit beta	102	1	111	1
CND3_HUMAN	Condensin complex subunit 3	78	2	46	1
QCR1_HUMAN	Cytochrome b-c1 complex subunit 1, mitochondrial	113	1	52	1
DYHC1_HUMAN	Cytoplasmic dynein 1 heavy chain 1	256	6	396	1
P5CS_HUMAN	Delta-1-pyrroline-5-carboxylate synthase	42	1	66	1
MCM2_HUMAN	DNA replication licensing factor MCM2	90	2	95	1
MCM7_HUMAN	DNA replication licensing factor MCM7	39	1	39	1
PRKDC_HUMAN	**DNA-dependent protein kinase catalytic subunit**	370	11	218	1
EF1A1_HUMAN	Elongation factor 1-alpha 1	52	1	90	1
EF1G_HUMAN	Elongation factor 1-gamma	64	2	63	1
EF2_HUMAN	Elongation factor 2	168	5	191	1
ENPL_HUMAN	Endoplasmin	409	15	660	1

EGFR_HUMAN	**Epidermal growth factor receptor**	148	2	72	16
IF4A1_HUMAN	Eukaryotic initiation factor 4A-I	210	5	282	2
EIF3L_HUMAN	Eukaryotic translation initiation factor 3 subunit L	64	1	91	2
RRP44_HUMAN	Exosome complex exonuclease RRP44	109	1	80	2
XPO1_HUMAN	Exportin-1	147	4	129	2
ESYT1_HUMAN	Extended synaptotagmin-1	38	1	80	2
FAS_HUMAN	Fatty acid synthase	430	17	341	10
FLNA_HUMAN	Filamin-A	199	6	190	10
FLNB_HUMAN	Filamin-B	116	4	146	10
GFPT1_HUMAN	Glucosamine--fructose-6-phosphate aminotransferase	94	2	93	2
G3P_HUMAN	Glyceraldehyde-3-phosphate dehydrogenase	350	11	333	2
PYGB_HUMAN	Glycogen phosphorylase, brain form	111	3	218	2
PYGL_HUMAN	Glycogen phosphorylase, liver form	82	1	67	2
GUAA_HUMAN	GMP synthase [glutamine-hydrolyzing]	142	5	73	2
GBLP_HUMAN	Guanine nucleotide-binding protein subunit beta-2-like 1	207	2	176	1
HSP74_HUMAN	Heat shock 70 kDa protein 4	143	4	92	7
HSP7C_HUMAN	Heat shock cognate 71 kDa protein	54	1	78	7
HS105_HUMAN	Heat shock protein 105 kDa	83	3	107	7
TRAP1_HUMAN	Heat shock protein 75 kDa, mitochondrial	60	1	52	7
HS90A_HUMAN	Heat shock protein HSP 90-alpha	454	15	598	7
HS90B_HUMAN	Heat shock protein HSP 90-beta	651	22	736	7
HXK1_HUMAN	**Hexokinase-1**	244	6	317	7
HYOU1_HUMAN	Hypoxia up-regulated protein 1	92	2	102	3
IMB1_HUMAN	Importin subunit beta-1	48	1	39	6
IPO5_HUMAN	Importin-5	300	8	195	6
IPO7_HUMAN	Importin-7	96	2	98	6
IMDH2_HUMAN	Inosine-5~-monophosphate dehydrogenase 2	127	4	270	6
SYIC_HUMAN	Isoleucyl-tRNA synthetase, cytoplasmic	86	2	120	2
SYIM_HUMAN	Isoleucyl-tRNA synthetase, mitochondrial	125	2	76	2
LPPRC_HUMAN	Leucine-rich PPR motif-containing protein, mitochondrial	192	8	201	5
SYLC_HUMAN	Leucyl-tRNA synthetase, cytoplasmic	76	3	121	5
LDHA_HUMAN	L-lactate dehydrogenase A chain	200	8	213	5
MYOF_HUMAN	Myoferlin	101	4	85	2
MYH9_HUMAN	Myosin-9	755	19	425	2
MYO1C_HUMAN	Myosin-Ic	81	2	134	2
NCKP1_HUMAN	Nck-associated protein 1	106	3	48	2

AHNK_HUMAN	Neuroblast differentiation-associated protein AHNAK	137	6	130	1
GANAB_HUMAN	Neutral alpha-glucosidase AB	119	4	203	1
PUR4_HUMAN	Phosphoribosylformylglycinamidine synthase	65	1	78	1
PLEC_HUMAN	Plectin	44	1	80	2
PCBP2_HUMAN	Poly(rC)-binding protein 2	42	1	80	2
PDC6I_HUMAN	Programmed cell death 6-interacting protein	84	2	47	7
PCNA_HUMAN	Proliferating cell nuclear antigen	97	3	69	7
PPCE_HUMAN	Prolyl endopeptidase	107	2	53	7
ANM1_HUMAN	Protein arginine N-methyltransferase 1	97	2	191	7
DIAP1_HUMAN	Protein diaphanous homolog 1	102	1	103	7
SC23A_HUMAN	Protein transport protein Sec23A	77	1	62	7
KPYM_HUMAN	**Pyruvate kinase isozymes M1/M2**	640	19	566	1
RUVB2_HUMAN	RuvB-like 2	49	1	77	2
ALBU_HUMAN	Serum albumin	80	3	61	1
SYSC_HUMAN	Seryl-tRNA synthetase, cytoplasmic	60	2	45	1
AT1A1_HUMAN	Sodium/potassium-transporting ATPase subunit alpha-1	81	1	66	2
SND1_HUMAN	Staphylococcal nuclease domain-containing protein 1	101	2	92	1
SLK_HUMAN	**STE20-like serine/threonine-protein kinase**	66	1	42	1
SMC2_HUMAN	Structural maintenance of chromosomes protein 2	83	2	77	1
SMC4_HUMAN	Structural maintenance of chromosomes protein 4	38	1	138	1
SAE2_HUMAN	SUM	49	1	66	1
TLN1_HUMAN	Talin-1	87	1	67	2
TCPA_HUMAN	T-complex protein 1 subunit alpha	206	5	168	6
TCPD_HUMAN	T-complex protein 1 subunit delta	64	1	104	6
TCPH_HUMAN	T-complex protein 1 subunit eta	116	1	432	6
TCPG_HUMAN	T-complex protein 1 subunit gamma	168	3	72	6
TCPQ_HUMAN	T-complex protein 1 subunit theta	109	1	129	6
TCPZ_HUMAN	T-complex protein 1 subunit zeta	162	3	108	6
ECHA_HUMAN	Trifunctional enzyme subunit alpha, mitochondrial	175	4	114	1
PUR2_HUMAN	Trifunctional purine biosynthetic protein adenosine-3	92	2	177	1
NSUN2_HUMAN	tRNA (cytosine-5-)-methyltransferase NSUN2	80	1	57	1
TBA1B_HUMAN	Tubulin alpha-1B chain	612	16	637	1
TBB5_HUMAN	Tubulin beta chain	113	5	359	1
TBB2C_HUMAN	Tubulin beta-2C chain	242	7	519	1
TBB3_HUMAN	Tubulin beta-3 chain	120	4	182	1
TBB4_HUMAN	Tubulin beta-4 chain	221	6	391	1

TBB6_HUMAN	Tubulin beta-6 chain	119	3	226	1
UBA1_HUMAN	Ubiquitin-like modifier-activating enzyme 1	101	3	52	1
GALE_HUMAN	UDP-glucose 4-epimerase	85	1	71	1
VPS35_HUMAN	Vacuolar protein sorting-associated protein 35	64	2	81	1
SYVC_HUMAN	Valyl-tRNA synthetase	178	6	88	1
VDAC1_HUMAN	Voltage-dependent anion-selective channel protein 1	112	2	139	1
VDAC2_HUMAN	Voltage-dependent anion-selective channel protein 2	229	3	151	1
VDAC3_HUMAN	Voltage-dependent anion-selective channel protein 3	49	1	47	1
XRCC5_HUMAN	X-ray repair cross-complementing protein 5	120	3	48	1

Chapter 7: Summary and Future Directions

The most important findings of this thesis are summarised and discussed. Directions for future research are suggested.

7.1. Overview

The overall objective of the research presented in this thesis was to develop a MS based quantitative chemical proteomics method using a Bisindolylmaleimide probe (Bis-probe) to selectively enrich Bis-binding proteins in complex biological systems. First, radioactive binding assays were used to characterise the Bis-probe for its binding affinity and inhibitory activity. The K_i and IC_{50} of the Bis-probe were determined. A sample enrichment method was optimised, appropriate for proteomic characterisation of binders (Chapter 2). The optimised method was first applied to characterise the Bis-binding protein targets in the MDA-MB-231 basal breast cancer cell model. Two novel kinase targets (SRPK1 and PKR) and several metabolic enzymes were identified in phorbol ester treated (PMA) breast cancer cells (Chapter 3). Additionally, differential capture of Bis-probe binding proteome in resting and PMA stimulated cells was demonstrated using SILAC.

The optimised chemical proteomic method was then utilised in a tissue based mouse model of cancer cachexia. Bis-binding enzymes in various metabolic pathways in the liver of mice bearing a C26 adenocarcinoma with accompanying high IL-6 levels that induced cancer cachexia (cachectic) was compared with mice bearing a C26 adenocarcinoma with low IL-6 levels (non-cachectic) and control mice. The quantitative changes in the relative abundance of the Bis-captured enzymes in these samples were determined using spectral counting by MS (Chapter 4). The use of Bis-probe to capture liver enzymes in mouse model of cancer cachexia shed light on the involvement of hepatic amino acid, protein, carbohydrate and lipid metabolic pathways in cachexia. Further, the analysis revealed impaired xenobiotic metabolism which in cancer cachexia patients, may exacerbate chemotoxicity associated with drug treatment.

The application of the Bis-probe based chemical proteomic method was further diversified to examine human adipose derived stem cells (hADSCs) undergoing chemically induced, neural differentiation. The analysis revealed several critical enzymes involved in the morphological changes in initial stages of neuron development. The relative protein abundance at different stages of differentiation was also quantified using the spectral counting method (Chapter 5). Finally, active-site peptide enrichment studies were conducted to specifically enrich the binding site peptide of probe labelled enzymes using a recent commercially available desthiobiotin-acyl-ATP (DB-ATP) probe in the MDA-MB-231 cancer cell models (Chapter 6). Peptides of the kinase active-site could be readily identified by MS due to acylation of the active-site lysine residue. These peptides provide direct evidence for the interaction of kinases with the chemical probe.

Affinity enrichment strategies using synthetic small molecules have been frequently applied in proteomic profiling to increase the proteome coverage and identify novel proteins and peptides, particularly those at lower abundance levels [66-69]. However, only recently, the combination of probe based technologies with modern high-resolution mass spectrometry analysis and advanced bioinformatics tools has provided further avenues for enrichment of low copy number metabolic enzymes [242-244]. In this thesis, the characterisation of specific enzyme classes enriched by the Bis-probe in diverse proteomes provided evidence for the utility of MS coupled chemical probe based enrichment to detect proteins which would have normally escaped detection due to their low expression had conventional proteomic methods been applied [250].

7.2. Affinity enrichment of Bis-Probe binding targets in breast cancer cell models

The utility of probe based enrichment technology and the subsequent MS characterisation of the binding targets was demonstrated in this study to affinity purify specific enzyme

classes using the Bis probe in basal breast cancer cells (Chapter 3). A robust chemical proteomics method was developed compatible with batch-mode analysis of protein obtained from small-scale culture (150 cm^2 flask), demonstrating utility of the method with as little as 100 μg of protein. This enabled rapid investigation of cell proteomics using chemical probes and is in contrast to most previous studies that typically used >10 times greater protein amount for related experiments [27, 98, 115]. While the above studies have shown the utility of Bis-probes to identify interacting proteins in various cancer cell types, this study was the first to report the cellular proteins that interact with Bis in basal breast cancer cells in response to stimulation by a suitable PKC activator, such as PMA. Using mass spectrometry 174 proteins were identified that were captured by the Bis-probe in phorbol ester (PMA) stimulated cells. Gene ontology analysis broadly categorised these proteins as ATP binding (42%), GTP binding (6%) and having nucleoside-triphosphatase activity (21%). Of the 64 enzymes captured by the Bis-probe, the majority had either ATP and/or nucleotide binding functions. Affinity enrichment of the ATP binding class of proteins using the chemical proteomics method was evident with an increase in 135% of the ATP binding proteome compared to the non enriched MDA-MB-231 cell lysates. Many of the previously reported kinase (GSK3α, GSK3β, PKCα and MARK2) and non-kinase (NOQ1) Bis-targets were characterised in this study confirming the mechanism of interaction of the Bis-group with the ATP binding pocket in protein targets. Additionally, two previously unreported Bis binding protein kinases, serine/arginine-rich protein-specific kinase 1 (SRPK1) and interferon induced RNA-dependent protein kinase (PKR) were observed. The Bis-probe chemical proteomics study was the first to provide orthogonal evidence of PMA activated PKC promoting activation of downstream kinases SRPK1 and PKR in MDA-MB-231 cells. Further a SILAC quantitation strategy was coupled to the chemical proteomics method to examine the proteins that were differentially captured by the Bis-probe following 30 min and 60 min PMA stimulation. This provided novel

evidence for PMA regulation of the enzymes glyceraldehyde-3-phosphate dehydrogenase, nucleolar RNA helicase 2 and heterogeneous nuclear ribonucleoprotein M.

7.3. Application in tissue based animal models of cancer

After demonstrating the utility of the Bis-probe chemical proteomics method in the breast cancer cell line model, it was of interest to investigate the compatibility of the developed method with tissue based systems. The application of the method in the liver of C 26 adenocarcinoma mouse models demonstrated the capture of a broad spectrum of enzyme classes that utilized ATP or structurally related analogues as cofactors for catalysis. Additionally, the method was coupled to a spectral counting quantitation strategy to compare liver enzymes in tumour bearing mouse models with high circulating IL-6 causing cachexia, tumour bearing non-cachexic models and tumour free control mice. This approach allowed us to identify and quantitate the relative abundance of many Bis-bound enzymes involved in carbohydrate metabolism, protein biosynthesis, amino acid metabolism, lipid metabolism and biological oxidation (Chapter 4).

The altered carbohydrate metabolism was reflected by the differential abundance levels of several critical enzymes involved in gluconeogenesis, glycogenesis and glycogenolysis pathways in cachectic mice livers compared to the controls. The findings confirmed previously studied effects of high IL-6 secreting C26 adenocarcinomas that affect tumour growth and directly influence liver metabolism [153, 168, 170]. Interestingly, the relative abundance levels of phosphoenol pyruvate carboxykinase, which catalyses the rate limiting step in hepatic gluconeogensis was 4 time higher in the cachectic mice livers. The increased presence of this enzyme is an indication of hepatic lactate recycling via Cori Cycle, which is one of the main metabolic disturbances associated with cancer cachexia [168]. Additionally, the comparison of abundance levels of Bis-bound enzymes in non-

cachectic and control mouse liver did not find any enzymes involved in carbohydrate metabolism to be significantly different, indicating that disrupted carbohydrate metabolism is a hallmark of cancer cachexia.

Similarly, the study revealed the enzymes involved in the hepatic acute phase protein synthesis to be significantly higher in the cachectic mice livers compared to the controls. ATP dependent aminoacyl synthetases involved in the activation phase of protein translation and the GTP dependent elongation enzymes were higher in relative abundance in the cachectic mice livers, indicating the potential for increased acute phase hepatic protein synthesis in cachexia. These results confirmed previous studies that reported an induction in hepatic protein synthesis of acute phase proteins with exposure to increased IL-6 levels in cachectic mice [164, 172, 173].

Further the study also reported the impaired hepatic amino acid degradation and lipid metabolism in cachectic mice. The abundance levels of the Bis-bound enzymes involved in lipid metabolism revealed interesting mechanisms involved in the β oxidation of fatty acids in cachectic mice livers. In the cachectic mice livers, the abundance levels of the enzymes involved in the preliminary processing of very long chain (VLC) and long chain (LC) fatty acids in both the mitochondria and peroxisomes were high in comparison to the control livers. However, interestingly the relative abundance of the enzymes that regulate the fatty acid β-oxidation are down-regulated, which ultimately limits the available pool of hepatic acetyl-COA. Although, previous studies have also reported low hepatic acetyl-CoA levels in the host livers of mice bearing cachexia-inducing colon adenocarcinoma MAC16 or related tumour MAC13 [184], the Bis-enriched study was able to elucidate the peroxisomal and mitochondrial regulation of VLC fatty acids.

Furthermore, the relative abundance of all the cytochrome P450 (CYP) enzymes was significantly down regulated in the cachectic mice liver samples compared to the controls. Pro-inflammatory cytokines are reported to effect the cytokine signalling in the liver, which can lead to reduce hepatic expression of cytochromes and ultimately to reduced drug clearance and increased chemotoxicity [143]. A decreased expression of hepatic cytochrome P450 drug metabolism in advanced cancer cases associated with increased plasma concentration of interleukin-6 (IL-6) and C-reactive protein is also reported [186, 187]. Reduced abundance of CYP1A2 and CYP4A12A was observed along with CYP3A11 in the non-cachectic group compared to the controls. The marked reduction in the cytochrome P450 enzymes reflected the impaired xenobiotic metabolism and is consistent with the subsequent chemotoxicity often encountered in cancer cachexia. The exact reason for CYP binding to the Bis-probe is unknown, given the lack of a defined ATP binding pocket. CYPs are primarily known to bind to heme groups. However, a recent X-ray crystallography study of CYP119A2 has revealed a sufficiently large heme pocket for NAD(P)H binding [251]. This observation provides a novel rationale for Bis-binding to CYPs. A crystallography study of Bis-bound CYPs is an avenue for further studies to substantiate this possibility. In summary, the use of Bis-probe to capture liver enzymes in the mouse model of cancer cachexia has shed light on the involvement of various metabolic pathways and provided valuable information towards thorough understanding of the biochemical pathways in the liver that are involved in cancer cachexia.

7.4. Bis-probe enrichment analysis in neural differentiated stem cells

Stem cell research is one of the most exciting new frontiers in modern biomedical science. Having demonstrated the use of the Bis-probe in cancer cell lines and mouse liver tissue it was of interest to test the Bis-probe with stem cells. The method was applied to profile

chemically induced neural differentiation of hADSCs. Further, neural differentiation of hADSCs with 2BME induction has been a subject of debate with studies arguing that these cells are non-functional as neurons [200]. While others believe the cells are at pre-neural stage or immature neuroblasts that can be further differentiated into functional glial, oligodendricytes or astrocytes, including myelin sheath forming Schwann cells [201-206]. Hence, studies elucidating the exact biochemical pathways involved in neurogenic differentiation become imperative for stem cell research. To date, stem cell proteomic studies have been primarily focused on 2D gel-based separations followed by MS characterisation of proteins [252-254] and due to low protein yields of pluripotent stem cells in culture, large scale culture is challenging. The small scale chemical proteomics method developed in this thesis, allowed rapid quantitative evaluation of neurogenic differentiation in hADSCs with as little as 100 μg proteins.

The study described in this thesis is the first to demonstrate the application of Bis-probe based chemical proteomics strategy to characterise the binding proteome of hADSCs and to profile protein changes associated with neural differentiation (Chapter 6). The protein binding profile of the Bis-probe was assessed in early stage (1 h and 6 h) and late stage (12 h) of neural differentiation and was compared with pre-induced control hADSCs. The relative abundance of the Bis-captured proteins in these samples was also quantitated using spectral counting.

Consistent with studies on breast cancer cell model and mice liver tissue model, ~70% of the Bis-enriched proteome was reported as purine binders in control hADSC and following each of the different time points of 2BME treatment. The majority of the kinase and non-kinase targets that were reported [27, 115] and confirmed (Chapter 3) previously as Bis-binding proteins were also identified in the 2BME treated hADSCs. The study revealed

novel regulation of GSK3α/β in neural differentiation of hADSCs. Additionally, interaction network analysis reported an interplay of this kinase with ADP/ATP translocase 1, microtubule-associated protein 1B (MAP 1B) and ATP-citrate synthase, which are subsequently phosphorylated and contribute in the initiation of microtubule assembly and cytoskeletal changes that implicated neurite extension, an essential step in neurogenesis [219]. Further, the role of small GTPases IQGAP1 and its binding partner CDC42 in their ability to promote neurite outgrowth by regulating the neuronal cytoskeleton were highlighted in this study. In addition, the new role of dehydrogenases (NQO1, 3PGDH) and antioxidant enzymes (PRDX-1) in regulating neuronal differentiation were also revealed. In conclusion, the study revealed several previously unreported enzymes that were expressed and involved in key protein interaction networks for neurogenic differentiation of hADSCs. The differential expression of the enzymes at different time points of neurogenic induction by 2BME has not been studied previously and sheds new light into the regulatory pathways that are involved in neural differentiation of hADSCs. Further, work in this area needs a different quantitation method as not many peptides were detected due to low number of cells. A SILAC strategy would perhaps prove to be a valuable method for quantitative chemical proteomic studies with hADSCs.

7.5. Active-site peptide enrichment

Finally, this thesis reports the use of a gel free chemical proteomics enrichment strategy (active-site peptide profiling) that specifically targets and enriches the binding site peptides of enzyme that require ATP for catalysis. Desthiobiotin-ATP (DB-ATP) probes were used in phorbol ester treated breast cancer cells (MDA-MB-231) to enrich the active-site peptides of probe binding enzymes. The covalent modification by the probe at a conserved lysine residue in the ATP binding site of metabolic enzymes/kinases and subsequent affinity enrichment of the acylated peptides resulted in specific enrichment of these

enzymes and elimination of background interference from more abundant cellular proteins. The most striking feature of the data was a ~300% increase in kinase enrichment compared to a compound centric protein profiling experiment (**Figure 7.1**). The large increase was observed regardless of the RG used in CCCP. The Bis-probe identified 6 kinases in the phorbol ester stimulated breast cancer cells, where as the active-site enrichment using DB-ATP probe identified 23 kinases. However, the kinase enrichment was similar in the CCCP studies using DB-ATP probes and Bis-probe, with 7 and 6 kinases respectively identified by each of the probes. Interestingly, there was minimal overlap between the kinases identified by the two different enrichment strategies using two different probes, except for protein kinase M1/M2 which was identified by both the probes in CCCP. **Figure 7.1** summarises the kinase enrichment by the Bis-probe and DB-ATP probes by two different enrichment strategies. Additionally, the novel Bis-probe targets (SRPK1, PKR) and previously known kinase targets of Bis (GSK3α/β) were not identified in the active-site enrichment with DB-ATP probes. These findings highlight the distinct kinase targets and specific subproteomes that can be enriched based on the RG of a chemical probe. On one hand, the finding reflects the advantage of using active-site peptide enrichment for enhanced retrieval of specific protein targets such as kinases. On the other hand, use of RG with higher binding affinity can provide greater selectivity (e.g. GSK3α/β using Bis).

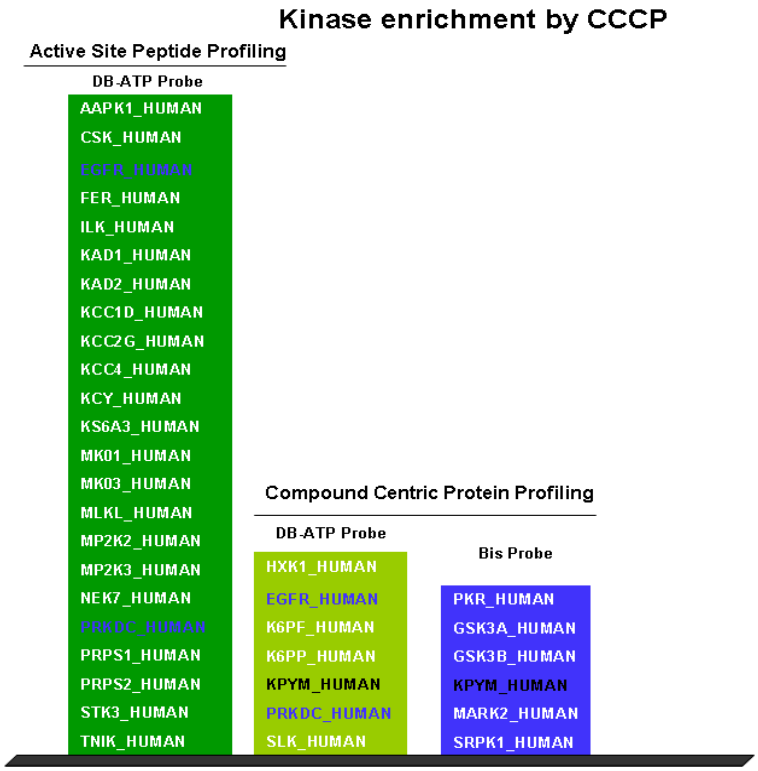

Figure 7.1: Kinase enrichment by CCCP using Bis-probe and DB-ATP probes and active-site enrichment of kinase targets by DB-ATP probes. Highlighted kinases show overlap.

Highly abundant ATP-binding proteins such as actin and heat shock proteins are problematic in CCCP as their detection can limit or prevent detection of less abundant target proteins in the MS. The advantage of active-site analysis is that only labelled peptides are enriched and affinity purified for MS analysis, which significantly diminishes the background of unlabelled peptides and the subsequent masking effect on low copy number kinases [40, 245, 246]. This was clearly demonstrated in Chapter 6, when 30 peptides of actin that were identified in using the CCCP protein profiling studies, but was reduced to only 5 peptides in the active-site analysis. Similarly, the detection of heat shock proteins (HSP90-β) was reduced from 22 peptides in CCCP studies to 3 peptides in active-site analysis. The reduction in MS sequencing time allotted to abundant proteins increases the opportunity to detect less abundant proteins. Further, the co-purification of abundant proteins with low probe affinity and non-specific targets that co-elute due to protein-protein interactions was also significantly reduced. This was evident from a ~90% specific enrichment of peptides with conserved lysine in the active-site analysis compared to the

CCCP protein profiling studies. Furthermore, comparative active-site analysis of phorbol ester treated and resting breast cancer cells revealed an enrichment of 29 kinases in both with a 75 % overlap and 25 % unique kinases. Because only a single peptide is usually recovered in active-site peptide profiling, spectral counting is not recommended for quantitation. However, coupling active-site peptide profiling with SILAC could provide a powerful tool for specific quantitative kinase studies.

7.6. Challenges encountered

7.6.1. Quantity of biological specimen

One of the chief limitations of chemical proteomics, despite its obvious advantages, is the relatively high amount of starting material required for enrichment based experiments. In most previous contemporary studies, binding target proteins were characterised by the use of large number of cells (up to 2.5 x 10^9 cells [27, 97]) or up to 10 g of wet weight cells [115] as starting material. Experiments of this magnitude require considerable labour, cost and time considerations and are often impractical to implement for rapid evaluation of chemical probes. Further, in studies involving primary stem cell cultures, such as hADSCs it becomes an unsurmountable task to achieve high protein yields considering the loss of pluripotency in these cells with increasing passage numbers.

In this thesis, considerable amount of preliminary studies were conducted to optimise enrichment of Bis-targets by downscaling the amount of starting material to 100 µg that could be easily harvested from a single flask (150 cm^2). With the starting material at 100 µg different probe concentrations and washing conditions were used to obtain optimum enrichment. Different elution strategies were also followed to monitor specific and maximum recovery of the bound targets after affinity purification. Additionally, the use of

a fast scanning LTQ XL linear ion trap mass spectrometer enabled the detection of many enriched peptides from a small amount of starting material.

7.6.2. Non-specific interactions

Non-specific interaction and co-elution of proteins without the specific binding site for the inhibitor is a key challenge to minimise in chemical proteomics involving affinity purification protocols. The extraordinarily high affinity for biotin makes streptavidin conjugated beads a preferred choice for affinity pull downs. However, the non-denaturing conditions in the affinity purification protocols allow many proteins to interact with the beads through weak affinity interactions. These interactions are particularly problematic in the case of cellular proteins expressed at high levels (e.g. ribosomes). However, from the studies conducted in this thesis it appears that majority of the background proteins usually do not stem from interaction with the bead matrix and are usually from low affinity interaction with probe components (linker, biotin tag) or with specific interactions with probe-bound protein target (**Appendix A, Table 2**).

To overcome these challenges, rigorous and optimal washing conditions were used and the effects of these conditions were individually assessed in beads and the control probes. This ensured minimal non-specific binding to the beads and probe components (linker, biotin tag). Additionally, all the studies reported in this thesis had appropriate bead and probe negative controls. Further, the minimal protein interaction, which was observed with the control probe, was also evaluated mass spectrometrically to characterise the non-specific binders.

An alternate strategy to resolve the specificity issue and address the non-specific binders would be to elute the probe-binders with increasing concentrations of free inhibitor, as investigated for the specific binders of natural product FK506 [255]. Such a strategy with

ATP and glycine elution was assessed in preliminary studies in this thesis but it required relatively high concentrations of the free ATP/glycine that cannot necessarily be reached for complete elution owing to limited solubility in aqueous buffers. Another interesting approach that may be considered involves the application of linker molecules that are cleavable with proteases [256], acids [257, 258], reducing agents [259-261] and UV light [262]. Further, quantitative strategies such as SILAC have also been reported to address the specificity issue [98].

7.6.3. Validation

Immunoblotting was used to confirm some of the MS characterised binding targets of Bis-probe reported in this thesis. For some of the differentially captured SILAC labelled probe targets in treated and resting cells validation by immunoblotting was attempted. However, given the semi quantitative nature of immunoblotting, it was difficult to objectively confirm the small fold changes reported by SILAC MS. Further, the low copy number enzymes which were enriched by probes in small scale studies can be difficult to visualise using chemiluminescence. The sensitivity issue was addressed by using fluorescent tagged secondary antibodies and visualising with the Odyssey (Li-Cor) system that provides low background noise due to imaging in the Infra Red spectrum.

A possible alternative to validation by immunoblotting of probe enriched targets is with techniques such as Surface Plasmon Resonance (SPR). SPR confirms the direct interaction between the activity-associated structure and the selected proteins enabling validation of specific targets by a probe. Despite this being a low throughput method, Oda *et al.* have reported the use of SPR for the validation of malate dehydrogenase as an E7070 target [82]. Another attractive validation option in the case of highly specific probes is to obtain three-dimensional structural information of protein-ligand pairs by NMR or

cocrystallisation. Indeed, NMR has been used as a validation tool to confirm specific kinase targets of, Roscovitine (CYC202), a selective inhibitor of cyclin-dependent kinases [71]. However, both these techniques required specialised equipment and method development and could not be used as a validation method in Bis-probe enrichment studies. As an alternative to immunoblotting, selected reaction monitoring (SRM) may also be considered to confirm the concentrations of differentially captured protein targets in probe based enrichment studies. Confirmation of differentially expressed proteins in this thesis was not assessed by SRM due to extensive assay development required for their specific and sensitive detection, which was beyond the scope of this thesis.

7.7. Future Directions

The research presented here provides a chemical proteomics platform with its application demonstrated in diverse biological systems. One of the interesting uses of the developed method is in the application of "kinomics". Protein kinases are currently one of the most prominently investigated drug target classes, with implications ranging from cancer to autoimmune disorders [80, 263]. Selectivity in kinase enrichment is one of the most critical issues as majority of the kinase inhibitors target the ATP binding pocket, conserved among the more than 500 known human protein kinases. Several previous studies have investigated kinase profiling using specific drug inhibitors and reported the enrichment of several known kinases [26, 27, 61, 85]. However, these studies also identified a large number of unexpected targets for each of the inhibitors, challenging the specificity of known kinase inhibitors for specific kinase enrichment. Bantscheff *et al.* have also demonstrated the successful application of a mixed broad specificity kinase inhibitor matrix ("kinobeads") to comprehensively profile kinase targets using seven different kinase inhibitors in the K562 cell line [94]. By far Patricelli *et al.* reported the most comprehensive study of protein kinase enrichment using acyl phosphate ATP probes and

active-site peptide profiling and reported enrichment of 394 protein kinases in various cell and tissue samples [40], although this required 4000 MS runs in more than 100 human, mouse, rat and dog proteomes.

It would be worthwhile to integrate and use kinase inhibitory matrix with acyl phosphate ATP probes and probes with related analogue (ADP, GTP and GDP), such as the "kinobeads" model and affinity enrich the kinome of a biological model by active-site peptide profiling. Indeed, preliminary studies on kinase enrichment using ATP probes and active-site peptide profiling have been reported in this thesis and would be interesting to study the comprehensive profiling with mixed nucleotide probes. Further, such an enrichment strategy using ATP related analogues coupled to beads can be integrated to inhibitor profiling with specific kinase inhibitors (e.g. Staurosporin) to observe changes in kinase activity due to presence of a drug or inhibitor. To further investigate the role of kinases in disease progression and signal transduction appropriate quantitation strategies can be integrated to this kinase enrichment strategy.

Another interesting avenue for the application of the developed chemical proteomics platform is the use of natural products as reactive groups rather than synthetically derived compounds. Majority of the novel natural products that are purified from their source are usually tested for antibacterial or anticancer activity. This leaves an entire unexplored territory for their use as drugs, the binding partners of which in biological pathways could be effectively elucidated using chemical proteomics. Identification of cellular targets and mode of action of natural products can accentuate drug development process. Several studies have used a chemical proteomics approach to characterise natural products interaction to biological molecules [264] and the field is increasingly gaining attention.

Hence, rapid characterisation of binding targets of natural products in biological systems would be of value.

7.8. Integrated approaches towards understanding drug action using chemical proteomics

The field of chemical proteomics represents the crossroads of several disciplines that, when applied together, are well suited to advance our understanding of biology and drug development. Comprehensive knowledge about small molecule inhibitor selectivity creates new rationales for drug development and allows its molecular interactions with biological systems to be defined. However, a prerequisite for deriving the benefits of such a systems approach is an integration of chemical proteomics to the 'omics' field of study including proteomics, glycomics, transcriptomics, metabolomics and interactomics. For example, Bantscheff *et al.* have combined a chemical and phosphoproteomics approach to characterise kinase inhibitors, their targets and their effects on downstream signalling components [94]. Further, Daub *et al.* have also innovatively integrated chemical proteomics as a preparative tool for the fractionation and enrichment of phosphopeptides in the investigation of phosphorylation changes during mitosis [96].

It is increasingly evident from the use of broad specificity kinase inhibitors as affinity probes that these inhibitors/drugs enrich unexpected targets. Probably many of these proteins are directly interacting with the intended drug target by protein-protein interactions and are an essential component of biological activity. In fact, observations of remodelling of the BCR-ABL complex [265] upon drug treatment revealed that drug target is not always only a single polypeptide but can also be an entire molecular functional unit. Thus, integration of chemical proteomics with other proteomic approaches may elucidate the entire drug target binding mechanism. One such approach could be characterisation of drug target protein complex by tandem affinity purification (TAP) [266, 267]. The novel

drug targets characterised by chemical proteomics can be used as a bait to characterise the drug target protein complex in the presence of the drug and compared when the drug is absent. These studies would also provide valuable insight into downstream drug effects.

More recently, Nomura *et al.* [47] have demonstrated the use of a chemical proteomics based integrated approach with large-scale metabolomics and proteomics profiling methods, in the discovery and functional characterization of deregulated enzymatic pathways in cancer using activity based probes [32, 243, 268]. Ultimately, it is evident that chemical proteomics with its synergy with many current technologies will become an essential tool to decipher molecular mechanism of action of drugs, and when integrated with other 'omics' fields of study it can provide a compelling, systems-level understanding of biochemical networks that are important for the development and progression of disease.

References

[1] Patterson, S. D., Aebersold, R. H., Proteomics: the first decade and beyond. *Nat Genet* 2003, *33 Suppl*, 311-323.
[2] Phizicky, E., Bastiaens, P. I., Zhu, H., Snyder, M., Fields, S., Protein analysis on a proteomic scale. *Nature* 2003, *422*, 208-215.
[3] Saghatelian, A., Cravatt, B. F., Assignment of protein function in the postgenomic era. *Nat Chem Biol* 2005, *1*, 130-142.
[4] Sieber, S. A., Cravatt, B. F., Analytical platforms for activity-based protein profiling--exploiting the versatility of chemistry for functional proteomics. *Chem Commun (Camb)* 2006, 2311-2319.
[5] Oh, P., Li, Y., Yu, J., Durr, E.*, et al.*, Subtractive proteomic mapping of the endothelial surface in lung and solid tumours for tissue-specific therapy. *Nature* 2004, *429*, 629-635.
[6] Lopez, M. F., Berggren, K., Chernokalskaya, E., Lazarev, A.*, et al.*, A comparison of silver stain and SYPRO Ruby Protein Gel Stain with respect to protein detection in two-dimensional gels and identification by peptide mass profiling. *Electrophoresis* 2000, *21*, 3673-3683.
[7] Santoni, V., Molloy, M., Rabilloud, T., Membrane proteins and proteomics: un amour impossible? *Electrophoresis* 2000, *21*, 1054-1070.
[8] Corthals, G. L., Wasinger, V. C., Hochstrasser, D. F., Sanchez, J. C., The dynamic range of protein expression: a challenge for proteomic research. *Electrophoresis* 2000, *21*, 1104-1115.
[9] Rabilloud, T., Chevallet, M., Luche, S., Lelong, C., Two-dimensional gel electrophoresis in proteomics: Past, present and future. *J Proteomics* 2010, *73*, 2064-2077.
[10] Gygi, S. P., Corthals, G. L., Zhang, Y., Rochon, Y., Aebersold, R., Evaluation of two-dimensional gel electrophoresis-based proteome analysis technology. *Proc Natl Acad Sci U S A* 2000, *97*, 9390-9395.
[11] Aebersold, R., Mann, M., Mass spectrometry-based proteomics. *Nature* 2003, *422*, 198-207.
[12] Walther, T. C., Mann, M., Mass spectrometry-based proteomics in cell biology. *J Cell Biol* 2010, *190*, 491-500.
[13] Baggerman, G., Vierstraete, E., De Loof, A., Schoofs, L., Gel-based versus gel-free proteomics: a review. *Comb Chem High Throughput Screen* 2005, *8*, 669-677.
[14] Rabilloud, T., Two-dimensional gel electrophoresis in proteomics: old, old fashioned, but it still climbs up the mountains. *Proteomics* 2002, *2*, 3-10.
[15] Anderson, N. L., Anderson, N. G., The human plasma proteome: history, character, and diagnostic prospects. *Mol Cell Proteomics* 2002, *1*, 845-867.
[16] Anderson, L., Hunter, C. L., Quantitative mass spectrometric multiple reaction monitoring assays for major plasma proteins. *Mol Cell Proteomics* 2006, *5*, 573-588.
[17] Qian, W. J., Jacobs, J. M., Liu, T., Camp, D. G., 2nd, Smith, R. D., Advances and challenges in liquid chromatography-mass spectrometry-based proteomics profiling for clinical applications. *Mol Cell Proteomics* 2006, *5*, 1727-1744.
[18] Huber, L. A., Pfaller, K., Vietor, I., Organelle proteomics: implications for subcellular fractionation in proteomics. *Circ Res* 2003, *92*, 962-968.
[19] Jung, E., Heller, M., Sanchez, J. C., Hochstrasser, D. F., Proteomics meets cell biology: the establishment of subcellular proteomes. *Electrophoresis* 2000, *21*, 3369-3377.
[20] Bouwmeester, T., Bauch, A., Ruffner, H., Angrand, P. O.*, et al.*, A physical and functional map of the human TNF-alpha/NF-kappa B signal transduction pathway. *Nat Cell Biol* 2004, *6*, 97-105.
[21] Speers, A. E., Cravatt, B. F., Profiling enzyme activities in vivo using click chemistry methods. *Chem Biol* 2004, *11*, 535-546.
[22] Retooling chemical probes. *Nat Chem Biol* 2010, *6*, 157.
[23] Frye, S. V., The art of the chemical probe. *Nat Chem Biol* 2010, *6*, 159-161.

[24] Han, S. Y., Hwan Kim, S., Introduction to chemical proteomics for drug discovery and development. *Arch Pharm (Weinheim)* 2007, *340*, 169-177.
[25] Jeffery, D. A., Bogyo, M., Chemical proteomics and its application to drug discovery. *Curr Opin Biotechnol* 2003, *14*, 87-95.
[26] Godl, K., Wissing, J., Kurtenbach, A., Habenberger, P.*, et al.*, An efficient proteomics method to identify the cellular targets of protein kinase inhibitors. *Proc Natl Acad Sci U S A* 2003, *100*, 15434-15439.
[27] Brehmer, D., Godl, K., Zech, B., Wissing, J., Daub, H., Proteome-wide identification of cellular targets affected by bisindolylmaleimide-type protein kinase C inhibitors. *Mol Cell Proteomics* 2004, *3*, 490-500.
[28] Rix, U., Superti-Furga, G., Target profiling of small molecules by chemical proteomics. *Nat Chem Biol* 2009, *5*, 616-624.
[29] Evans, M. J., Cravatt, B. F., Mechanism-based profiling of enzyme families. *Chem Rev* 2006, *106*, 3279-3301.
[30] Sadaghiani, A. M., Verhelst, S. H., Bogyo, M., Tagging and detection strategies for activity-based proteomics. *Curr Opin Chem Biol* 2007, *11*, 20-28.
[31] Kidd, D., Liu, Y., Cravatt, B. F., Profiling serine hydrolase activities in complex proteomes. *Biochemistry* 2001, *40*, 4005-4015.
[32] Liu, Y., Patricelli, M. P., Cravatt, B. F., Activity-based protein profiling: the serine hydrolases. *Proc Natl Acad Sci U S A* 1999, *96*, 14694-14699.
[33] Patricelli, M. P., Giang, D. K., Stamp, L. M., Burbaum, J. J., Direct visualization of serine hydrolase activities in complex proteomes using fluorescent active site-directed probes. *Proteomics* 2001, *1*, 1067-1071.
[34] Greenbaum, D., Medzihradszky, K. F., Burlingame, A., Bogyo, M., Epoxide electrophiles as activity-dependent cysteine protease profiling and discovery tools. *Chem Biol* 2000, *7*, 569-581.
[35] Kato, D., Boatright, K. M., Berger, A. B., Nazif, T.*, et al.*, Activity-based probes that target diverse cysteine protease families. *Nat Chem Biol* 2005, *1*, 33-38.
[36] Li, Y. M., Xu, M., Lai, M. T., Huang, Q.*, et al.*, Photoactivated gamma-secretase inhibitors directed to the active site covalently label presenilin 1. *Nature* 2000, *405*, 689-694.
[37] Chan, E. W., Chattopadhaya, S., Panicker, R. C., Huang, X., Yao, S. Q., Developing photoactive affinity probes for proteomic profiling: hydroxamate-based probes for metalloproteases. *J Am Chem Soc* 2004, *126*, 14435-14446.
[38] Saghatelian, A., Jessani, N., Joseph, A., Humphrey, M., Cravatt, B. F., Activity-based probes for the proteomic profiling of metalloproteases. *Proc Natl Acad Sci U S A* 2004, *101*, 10000-10005.
[39] Sieber, S. A., Niessen, S., Hoover, H. S., Cravatt, B. F., Proteomic profiling of metalloprotease activities with cocktails of active-site probes. *Nat Chem Biol* 2006, *2*, 274-281.
[40] Patricelli, M. P., Szardenings, A. K., Liyanage, M., Nomanbhoy, T. K.*, et al.*, Functional interrogation of the kinome using nucleotide acyl phosphates. *Biochemistry* 2007, *46*, 350-358.
[41] Hekmat, O., Kim, Y. W., Williams, S. J., He, S., Withers, S. G., Active-site peptide "fingerprinting" of glycosidases in complex mixtures by mass spectrometry. Discovery of a novel retaining beta-1,4-glycanase in Cellulomonas fimi. *J Biol Chem* 2005, *280*, 35126-35135.
[42] Vocadlo, D. J., Hang, H. C., Kim, E. J., Hanover, J. A., Bertozzi, C. R., A chemical approach for identifying O-GlcNAc-modified proteins in cells. *Proc Natl Acad Sci U S A* 2003, *100*, 9116-9121.
[43] Salisbury, C. M., Cravatt, B. F., Activity-based probes for proteomic profiling of histone deacetylase complexes. *Proc Natl Acad Sci U S A* 2007, *104*, 1171-1176.

[44] Adam, G. C., Sorensen, E. J., Cravatt, B. F., Proteomic profiling of mechanistically distinct enzyme classes using a common chemotype. *Nat Biotechnol* 2002, *20*, 805-809.
[45] Barglow, K. T., Cravatt, B. F., Discovering disease-associated enzymes by proteome reactivity profiling. *Chem Biol* 2004, *11*, 1523-1531.
[46] Jessani, N., Liu, Y., Humphrey, M., Cravatt, B. F., Enzyme activity profiles of the secreted and membrane proteome that depict cancer cell invasiveness. *Proc Natl Acad Sci U S A* 2002, *99*, 10335-10340.
[47] Nomura, D. K., Dix, M. M., Cravatt, B. F., Activity-based protein profiling for biochemical pathway discovery in cancer. *Nat Rev Cancer* 2010, *10*, 630-638.
[48] Simon, G. M., Cravatt, B. F., Activity-based proteomics of enzyme superfamilies: serine hydrolases as a case study. *J Biol Chem* 2010, *285*, 11051-11055.
[49] Graves, P. R., Kwiek, J. J., Fadden, P., Ray, R.*, et al.*, Discovery of novel targets of quinoline drugs in the human purine binding proteome. *Mol Pharmacol* 2002, *62*, 1364-1372.
[50] Krugmann, S., Anderson, K. E., Ridley, S. H., Risso, N.*, et al.*, Identification of ARAP3, a novel PI3K effector regulating both Arf and Rho GTPases, by selective capture on phosphoinositide affinity matrices. *Mol Cell* 2002, *9*, 95-108.
[51] Gharbi, S. I., Zvelebil, M. J., Shuttleworth, S. J., Hancox, T.*, et al.*, Exploring the specificity of the PI3K family inhibitor LY294002. *Biochem J* 2007, *404*, 15-21.
[52] Scholten, A., Poh, M. K., van Veen, T. A., van Breukelen, B.*, et al.*, Analysis of the cGMP/cAMP interactome using a chemical proteomics approach in mammalian heart tissue validates sphingosine kinase type 1-interacting protein as a genuine and highly abundant AKAP. *J Proteome Res* 2006, *5*, 1435-1447.
[53] Schulze, W. X., Deng, L., Mann, M., Phosphotyrosine interactome of the ErbB-receptor kinase family. *Mol Syst Biol* 2005, *1*, 2005 0008.
[54] Hanke, S., Mann, M., The phosphotyrosine interactome of the insulin receptor family and its substrates IRS-1 and IRS-2. *Mol Cell Proteomics* 2009, *8*, 519-534.
[55] Thornberry, N. A., Peterson, E. P., Zhao, J. J., Howard, A. D.*, et al.*, Inactivation of interleukin-1 beta converting enzyme by peptide (acyloxy)methyl ketones. *Biochemistry* 1994, *33*, 3934-3940.
[56] Betley, J. R., Cesaro-Tadic, S., Mekhalfia, A., Rickard, J. H.*, et al.*, Direct screening for phosphatase activity by turnover-based capture of protein catalysts. *Angew Chem Int Ed Engl* 2002, *41*, 775-777.
[57] Wang, Q., Dechert, U., Jirik, F., Withers, S. G., Suicide inactivation of human prostatic acid phosphatase and a phosphotyrosine phosphatase. *Biochem Biophys Res Commun* 1994, *200*, 577-583.
[58] Bogyo, M., Verhelst, S., Bellingard-Dubouchaud, V., Toba, S., Greenbaum, D., Selective targeting of lysosomal cysteine proteases with radiolabeled electrophilic substrate analogs. *Chem Biol* 2000, *7*, 27-38.
[59] Daub, H., Characterisation of kinase-selective inhibitors by chemical proteomics. *Biochim Biophys Acta* 2005, *1754*, 183-190.
[60] Tong, L., Pav, S., White, D. M., Rogers, S.*, et al.*, A highly specific inhibitor of human p38 MAP kinase binds in the ATP pocket. *Nat Struct Biol* 1997, *4*, 311-316.
[61] Godl, K., Gruss, O. J., Eickhoff, J., Wissing, J.*, et al.*, Proteomic characterization of the angiogenesis inhibitor SU6668 reveals multiple impacts on cellular kinase signaling. *Cancer Res* 2005, *65*, 6919-6926.
[62] Rix, U., Hantschel, O., Durnberger, G., Remsing Rix, L. L.*, et al.*, Chemical proteomic profiles of the BCR-ABL inhibitors imatinib, nilotinib, and dasatinib reveal novel kinase and nonkinase targets. *Blood* 2007, *110*, 4055-4063.
[63] Borodovsky, A., Kessler, B. M., Casagrande, R., Overkleeft, H. S.*, et al.*, A novel active site-directed probe specific for deubiquitylating enzymes reveals proteasome association of USP14. *EMBO J* 2001, *20*, 5187-5196.

[64] Borodovsky, A., Ovaa, H., Kolli, N., Gan-Erdene, T., *et al.*, Chemistry-based functional proteomics reveals novel members of the deubiquitinating enzyme family. *Chem Biol* 2002, *9*, 1149-1159.
[65] Wilchek, M., Bayer, E. A., Introduction to avidin-biotin technology. *Methods Enzymol* 1990, *184*, 5-13.
[66] Cuatrecasas, P., Wilchek, M., Anfinsen, C. B., Selective enzyme purification by affinity chromatography. *Proc Natl Acad Sci U S A* 1968, *61*, 636-643.
[67] Harding, M. W., Galat, A., Uehling, D. E., Schreiber, S. L., A receptor for the immunosuppressant FK506 is a cis-trans peptidyl-prolyl isomerase. *Nature* 1989, *341*, 758-760.
[68] Crews, C. M., Collins, J. L., Lane, W. S., Snapper, M. L., Schreiber, S. L., GTP-dependent binding of the antiproliferative agent didemnin to elongation factor 1 alpha. *J Biol Chem* 1994, *269*, 15411-15414.
[69] Knockaert, M., Gray, N., Damiens, E., Chang, Y. T., *et al.*, Intracellular targets of cyclin-dependent kinase inhibitors: identification by affinity chromatography using immobilised inhibitors. *Chem Biol* 2000, *7*, 411-422.
[70] Lolli, G., Thaler, F., Valsasina, B., Roletto, F., *et al.*, Inhibitor affinity chromatography: profiling the specific reactivity of the proteome with immobilized molecules. *Proteomics* 2003, *3*, 1287-1298.
[71] Bach, S., Knockaert, M., Reinhardt, J., Lozach, O., *et al.*, Roscovitine targets, protein kinases and pyridoxal kinase. *J Biol Chem* 2005, *280*, 31208-31219.
[72] Cohen, P., Protein kinases--the major drug targets of the twenty-first century? *Nat Rev Drug Discov* 2002, *1*, 309-315.
[73] Whartenby, K. A., Calabresi, P. A., McCadden, E., Nguyen, B., *et al.*, Inhibition of FLT3 signaling targets DCs to ameliorate autoimmune disease. *Proc Natl Acad Sci U S A* 2005, *102*, 16741-16746.
[74] Bhagwat, S. S., Kinase inhibitors for the treatment of inflammatory and autoimmune disorders. *Purinergic Signal* 2009, *5*, 107-115.
[75] Solinas, G., Vilcu, C., Neels, J. G., Bandyopadhyay, G. K., *et al.*, JNK1 in hematopoietically derived cells contributes to diet-induced inflammation and insulin resistance without affecting obesity. *Cell Metab* 2007, *6*, 386-397.
[76] Smith, W. W., Pei, Z., Jiang, H., Dawson, V. L., *et al.*, Kinase activity of mutant LRRK2 mediates neuronal toxicity. *Nat Neurosci* 2006, *9*, 1231-1233.
[77] Catapano, L. A., Manji, H. K., Kinases as drug targets in the treatment of bipolar disorder. *Drug Discov Today* 2008, *13*, 295-302.
[78] Manning, G., Whyte, D. B., Martinez, R., Hunter, T., Sudarsanam, S., The protein kinase complement of the human genome. *Science* 2002, *298*, 1912-1934.
[79] Haystead, T. A., The purinome, a complex mix of drug and toxicity targets. *Curr Top Med Chem* 2006, *6*, 1117-1127.
[80] Zhang, J., Yang, P. L., Gray, N. S., Targeting cancer with small molecule kinase inhibitors. *Nat Rev Cancer* 2009, *9*, 28-39.
[81] Brehmer, D., Greff, Z., Godl, K., Blencke, S., *et al.*, Cellular targets of gefitinib. *Cancer Res* 2005, *65*, 379-382.
[82] Oda, Y., Owa, T., Sato, T., Boucher, B., *et al.*, Quantitative chemical proteomics for identifying candidate drug targets. *Anal Chem* 2003, *75*, 2159-2165.
[83] Inagaki, M., Watanabe, M., Hidaka, H., N-(2-Aminoethyl)-5-isoquinolinesulfonamide, a newly synthesized protein kinase inhibitor, functions as a ligand in affinity chromatography. Purification of Ca2+-activated, phospholipid-dependent and other protein kinases. *J Biol Chem* 1985, *260*, 2922-2925.
[84] Engh, R. A., Girod, A., Kinzel, V., Huber, R., Bossemeyer, D., Crystal structures of catalytic subunit of cAMP-dependent protein kinase in complex with isoquinolinesulfonyl

protein kinase inhibitors H7, H8, and H89. Structural implications for selectivity. *J Biol Chem* 1996, *271*, 26157-26164.
[85] Wissing, J., Godl, K., Brehmer, D., Blencke, S.*, et al.*, Chemical proteomic analysis reveals alternative modes of action for pyrido[2,3-d]pyrimidine kinase inhibitors. *Mol Cell Proteomics* 2004, *3*, 1181-1193.
[86] Nagar, B., Bornmann, W. G., Pellicena, P., Schindler, T.*, et al.*, Crystal structures of the kinase domain of c-Abl in complex with the small molecule inhibitors PD173955 and imatinib (STI-571). *Cancer Res* 2002, *62*, 4236-4243.
[87] Nagar, B., Hantschel, O., Young, M. A., Scheffzek, K.*, et al.*, Structural basis for the autoinhibition of c-Abl tyrosine kinase. *Cell* 2003, *112*, 859-871.
[88] Winger, J. A., Hantschel, O., Superti-Furga, G., Kuriyan, J., The structure of the leukemia drug imatinib bound to human quinone reductase 2 (NQO2). *BMC Struct Biol* 2009, *9*, 7.
[89] Lombardo, L. J., Lee, F. Y., Chen, P., Norris, D.*, et al.*, Discovery of N-(2-chloro-6-methyl- phenyl)-2-(6-(4-(2-hydroxyethyl)- piperazin-1-yl)-2-methylpyrimidin-4-ylamino)thiazole-5-carboxamide (BMS-354825), a dual Src/Abl kinase inhibitor with potent antitumor activity in preclinical assays. *J Med Chem* 2004, *47*, 6658-6661.
[90] Haystead, C. M., Gregory, P., Sturgill, T. W., Haystead, T. A., Gamma-phosphate-linked ATP-sepharose for the affinity purification of protein kinases. Rapid purification to homogeneity of skeletal muscle mitogen-activated protein kinase kinase. *Eur J Biochem* 1993, *214*, 459-467.
[91] Davies, S. P., Hawley, S. A., Woods, A., Carling, D.*, et al.*, Purification of the AMP-activated protein kinase on ATP-gamma-sepharose and analysis of its subunit structure. *Eur J Biochem* 1994, *223*, 351-357.
[92] Wymann, M. P., Bulgarelli-Leva, G., Zvelebil, M. J., Pirola, L.*, et al.*, Wortmannin inactivates phosphoinositide 3-kinase by covalent modification of Lys-802, a residue involved in the phosphate transfer reaction. *Mol Cell Biol* 1996, *16*, 1722-1733.
[93] Kim, S. Y., Chang, K. H., Doh, H. J., Jung, J. A.*, et al.*, Rapid purification and characterization of nucleoside diphosphate kinase isoforms using ATP-sepharose affinity column chromatography. *Mol Cells* 1997, *7*, 630-634.
[94] Bantscheff, M., Eberhard, D., Abraham, Y., Bastuck, S.*, et al.*, Quantitative chemical proteomics reveals mechanisms of action of clinical ABL kinase inhibitors. *Nat Biotechnol* 2007, *25*, 1035-1044.
[95] Scholten, A., van Veen, T. A., Vos, M. A., Heck, A. J., Diversity of cAMP-dependent protein kinase isoforms and their anchoring proteins in mouse ventricular tissue. *J Proteome Res* 2007, *6*, 1705-1717.
[96] Daub, H., Olsen, J. V., Bairlein, M., Gnad, F.*, et al.*, Kinase-selective enrichment enables quantitative phosphoproteomics of the kinome across the cell cycle. *Mol Cell* 2008, *31*, 438-448.
[97] Aye, T. T., Mohammed, S., van den Toorn, H. W., van Veen, T. A.*, et al.*, Selectivity in enrichment of cAMP-dependent protein kinase regulatory subunits type I and type II and their interactors using modified cAMP affinity resins. *Mol Cell Proteomics* 2009, *8*, 1016-1028.
[98] Ong, S. E., Schenone, M., Margolin, A. A., Li, X.*, et al.*, Identifying the proteins to which small-molecule probes and drugs bind in cells. *Proc Natl Acad Sci U S A* 2009, *106*, 4617-4622.
[99] Sharma, K., Weber, C., Bairlein, M., Greff, Z.*, et al.*, Proteomics strategy for quantitative protein interaction profiling in cell extracts. *Nat Methods* 2009, *6*, 741-744.
[100] Toullec, D., Pianetti, P., Coste, H., Bellevergue, P.*, et al.*, The bisindolylmaleimide GF 109203X is a potent and selective inhibitor of protein kinase C. *J Biol Chem* 1991, *266*, 15771-15781.

[101] Hannun, Y. A., Loomis, C. R., Merrill, A. H., Jr., Bell, R. M., Sphingosine inhibition of protein kinase C activity and of phorbol dibutyrate binding in vitro and in human platelets. *J Biol Chem* 1986, *261*, 12604-12609.
[102] Kobayashi, E., Nakano, H., Morimoto, M., Tamaoki, T., Calphostin C (UCN-1028C), a novel microbial compound, is a highly potent and specific inhibitor of protein kinase C. *Biochem Biophys Res Commun* 1989, *159*, 548-553.
[103] Hidaka, H., Inagaki, M., Kawamoto, S., Sasaki, Y., Isoquinolinesulfonamides, novel and potent inhibitors of cyclic nucleotide dependent protein kinase and protein kinase C. *Biochemistry* 1984, *23*, 5036-5041.
[104] Loomis, C. R., Bell, R. M., Sangivamycin, a nucleoside analogue, is a potent inhibitor of protein kinase C. *J Biol Chem* 1988, *263*, 1682-1692.
[105] Tamaoki, T., Nomoto, H., Takahashi, I., Kato, Y.*, et al.*, Staurosporine, a potent inhibitor of phospholipid/Ca++dependent protein kinase. *Biochem Biophys Res Commun* 1986, *135*, 397-402.
[106] Dray, A., Bettaney, J., Forster, P., Perkins, M. N., Bradykinin-induced stimulation of afferent fibres is mediated through protein kinase C. *Neurosci Lett* 1988, *91*, 301-307.
[107] Sako, T., Tauber, A. I., Jeng, A. Y., Yuspa, S. H., Blumberg, P. M., Contrasting actions of staurosporine, a protein kinase C inhibitor, on human neutrophils and primary mouse epidermal cells. *Cancer Res* 1988, *48*, 4646-4650.
[108] Watson, S. P., McNally, J., Shipman, L. J., Godfrey, P. P., The action of the protein kinase C inhibitor, staurosporine, on human platelets. Evidence against a regulatory role for protein kinase C in the formation of inositol trisphosphate by thrombin. *Biochem J* 1988, *249*, 345-350.
[109] Meyer, T., Regenass, U., Fabbro, D., Alteri, E.*, et al.*, A derivative of staurosporine (CGP 41 251) shows selectivity for protein kinase C inhibition and in vitro anti-proliferative as well as in vivo anti-tumor activity. *Int J Cancer* 1989, *43*, 851-856.
[110] Ruegg, U. T., Burgess, G. M., Staurosporine, K-252 and UCN-01: potent but nonspecific inhibitors of protein kinases. *Trends Pharmacol Sci* 1989, *10*, 218-220.
[111] Eastman, A., Kohn, E. A., Brown, M. K., Rathman, J.*, et al.*, A novel indolocarbazole, ICP-1, abrogates DNA damage-induced cell cycle arrest and enhances cytotoxicity: similarities and differences to the cell cycle checkpoint abrogator UCN-01. *Mol Cancer Ther* 2002, *1*, 1067-1078.
[112] Davis, P. D., Hill, C. H., Lawton, G., Nixon, J. S.*, et al.*, Inhibitors of protein kinase C. 1. 2,3-Bisarylmaleimides. *J Med Chem* 1992, *35*, 177-184.
[113] Bit, R. A., Davis, P. D., Elliott, L. H., Harris, W.*, et al.*, Inhibitors of protein kinase C. 3. Potent and highly selective bisindolylmaleimides by conformational restriction. *J Med Chem* 1993, *36*, 21-29.
[114] Swanson, K. D., Taylor, L. K., Haung, L., Burlingame, A. L., Landreth, G. E., Transcription factor phosphorylation by pp90(rsk2). Identification of Fos kinase and NGFI-B kinase I as pp90(rsk2). *J Biol Chem* 1999, *274*, 3385-3395.
[115] Saxena, C., Zhen, E., Higgs, R. E., Hale, J. E., An immuno-chemo-proteomics method for drug target deconvolution. *J Proteome Res* 2008, *7*, 3490-3497.
[116] Knighton, D. R., Zheng, J. H., Ten Eyck, L. F., Ashford, V. A.*, et al.*, Crystal structure of the catalytic subunit of cyclic adenosine monophosphate-dependent protein kinase. *Science* 1991, *253*, 407-414.
[117] Debreczeni, J. E., Bullock, A. N., Atilla, G. E., Williams, D. S.*, et al.*, Ruthenium half-sandwich complexes bound to protein kinase Pim-1. *Angew Chem Int Ed Engl* 2006, *45*, 1580-1585.
[118] Washburn, M. P., Wolters, D., Yates, J. R., 3rd, Large-scale analysis of the yeast proteome by multidimensional protein identification technology. *Nat Biotechnol* 2001, *19*, 242-247.

[119] Zhang, B., VerBerkmoes, N. C., Langston, M. A., Uberbacher, E.*, et al.*, Detecting differential and correlated protein expression in label-free shotgun proteomics. *J Proteome Res* 2006, *5*, 2909-2918.
[120] Ross, P. L., Huang, Y. N., Marchese, J. N., Williamson, B.*, et al.*, Multiplexed protein quantitation in Saccharomyces cerevisiae using amine-reactive isobaric tagging reagents. *Mol Cell Proteomics* 2004, *3*, 1154-1169.
[121] Bantscheff, M., Schirle, M., Sweetman, G., Rick, J., Kuster, B., Quantitative mass spectrometry in proteomics: a critical review. *Anal Bioanal Chem* 2007, *389*, 1017-1031.
[122] Zieske, L. R., A perspective on the use of iTRAQ reagent technology for protein complex and profiling studies. *J Exp Bot* 2006, *57*, 1501-1508.
[123] Ong, S. E., Blagoev, B., Kratchmarova, I., Kristensen, D. B.*, et al.*, Stable isotope labeling by amino acids in cell culture, SILAC, as a simple and accurate approach to expression proteomics. *Mol Cell Proteomics* 2002, *1*, 376-386.
[124] Rigbolt, K. T., Blagoev, B., Proteome-wide quantitation by SILAC. *Methods Mol Biol* 2010, *658*, 187-204.
[125] Mueller, L. N., Brusniak, M. Y., Mani, D. R., Aebersold, R., An assessment of software solutions for the analysis of mass spectrometry based quantitative proteomics data. *J Proteome Res* 2008, *7*, 51-61.
[126] Ong, S. E., Kratchmarova, I., Mann, M., Properties of 13C-substituted arginine in stable isotope labeling by amino acids in cell culture (SILAC). *J Proteome Res* 2003, *2*, 173-181.
[127] Liu, H., Sadygov, R. G., Yates, J. R., 3rd, A model for random sampling and estimation of relative protein abundance in shotgun proteomics. *Anal Chem* 2004, *76*, 4193-4201.
[128] Zybailov, B., Coleman, M. K., Florens, L., Washburn, M. P., Correlation of relative abundance ratios derived from peptide ion chromatograms and spectrum counting for quantitative proteomic analysis using stable isotope labeling. *Anal Chem* 2005, *77*, 6218-6224.
[129] Dong, M. Q., Venable, J. D., Au, N., Xu, T.*, et al.*, Quantitative mass spectrometry identifies insulin signaling targets in C. elegans. *Science* 2007, *317*, 660-663.
[130] Florens, L., Carozza, M. J., Swanson, S. K., Fournier, M.*, et al.*, Analyzing chromatin remodeling complexes using shotgun proteomics and normalized spectral abundance factors. *Methods* 2006, *40*, 303-311.
[131] Zybailov, B., Mosley, A. L., Sardiu, M. E., Coleman, M. K.*, et al.*, Statistical analysis of membrane proteome expression changes in Saccharomyces cerevisiae. *J Proteome Res* 2006, *5*, 2339-2347.
[132] Lundgren, D. H., Hwang, S. I., Wu, L., Han, D. K., Role of spectral counting in quantitative proteomics. *Expert Rev Proteomics*, *7*, 39-53.
[133] Cheng, Y., Prusoff, W. H., Relationship between the inhibition constant (K1) and the concentration of inhibitor which causes 50 per cent inhibition (I50) of an enzymatic reaction. *Biochem Pharmacol* 1973, *22*, 3099-3108.
[134] Dolai, S., Xu, Q., Liu, F., Molloy, M. P., Quantitative chemical proteomics in small-scale culture of phorbol ester stimulated basal breast cancer cells. *Proteomics* 2011, *11*, 2683-2692.
[135] Shiyama, T., Furuya, M., Yamazaki, A., Terada, T., Tanaka, A., Design and synthesis of novel hydrophilic spacers for the reduction of nonspecific binding proteins on affinity resins. *Bioorg Med Chem* 2004, *12*, 2831-2841.
[136] Knockaert, M., Lenormand, P., Gray, N., Schultz, P.*, et al.*, p42/p44 MAPKs are intracellular targets of the CDK inhibitor purvalanol. *Oncogene* 2002, *21*, 6413-6424.
[137] Wilkinson, S. E., Parker, P. J., Nixon, J. S., Isoenzyme specificity of bisindolylmaleimides, selective inhibitors of protein kinase C. *Biochem J* 1993, *294 (Pt 2)*, 335-337.

[138] Bylund, D. B., Toews, M. L., Radioligand binding methods: practical guide and tips. *Am J Physiol* 1993, *265*, L421-429.
[139] Markiewski, M. M., DeAngelis, R. A., Lambris, J. D., Liver inflammation and regeneration: two distinct biological phenomena or parallel pathophysiologic processes? *Mol Immunol* 2006, *43*, 45-56.
[140] Ramadori, G., Armbrust, T., Cytokines in the liver. *Eur J Gastroenterol Hepatol* 2001, *13*, 777-784.
[141] Moshage, H., Cytokines and the hepatic acute phase response. *J Pathol* 1997, *181*, 257-266.
[142] Ramadori, G., Christ, B., Cytokines and the hepatic acute-phase response. *Semin Liver Dis* 1999, *19*, 141-155.
[143] Charles, K. A., Rivory, L. P., Brown, S. L., Liddle, C.*, et al.*, Transcriptional repression of hepatic cytochrome P450 3A4 gene in the presence of cancer. *Clin Cancer Res* 2006, *12*, 7492-7497.
[144] Corbett, T. H., Griswold, D. P., Jr., Roberts, B. J., Peckham, J. C., Schabel, F. M., Jr., Tumor induction relationships in development of transplantable cancers of the colon in mice for chemotherapy assays, with a note on carcinogen structure. *Cancer Res* 1975, *35*, 2434-2439.
[145] Tanaka, Y., Eda, H., Tanaka, T., Udagawa, T.*, et al.*, Experimental cancer cachexia induced by transplantable colon 26 adenocarcinoma in mice. *Cancer Res* 1990, *50*, 2290-2295.
[146] Tisdale, M. J., Biology of cachexia. *J Natl Cancer Inst* 1997, *89*, 1763-1773.
[147] Ghezzi, P., Saccardo, B., Bianchi, M., Recombinant tumor necrosis factor depresses cytochrome P450-dependent microsomal drug metabolism in mice. *Biochem Biophys Res Commun* 1986, *136*, 316-321.
[148] Ghezzi, P., Saccardo, B., Villa, P., Rossi, V.*, et al.*, Role of interleukin-1 in the depression of liver drug metabolism by endotoxin. *Infect Immun* 1986, *54*, 837-840.
[149] Tisdale, M. J., Mechanisms of cancer cachexia. *Physiol Rev* 2009, *89*, 381-410.
[150] Tisdale, M. J., Cancer cachexia. *Curr Opin Gastroenterol* 2010, *26*, 146-151.
[151] Houten, L., Reilley, A. A., An investigation of the cause of death from cancer. *J Surg Oncol* 1980, *13*, 111-116.
[152] Kotler, D. P., Tierney, A. R., Culpepper-Morgan, J. A., Wang, J., Pierson, R. N., Jr., Effect of home total parenteral nutrition on body composition in patients with acquired immunodeficiency syndrome. *JPEN J Parenter Enteral Nutr* 1990, *14*, 454-458.
[153] Bongaerts, G. P., van Halteren, H. K., Verhagen, C. A., Wagener, D. J., Cancer cachexia demonstrates the energetic impact of gluconeogenesis in human metabolism. *Med Hypotheses* 2006, *67*, 1213-1222.
[154] Khal, J., Wyke, S. M., Russell, S. T., Hine, A. V., Tisdale, M. J., Expression of the ubiquitin-proteasome pathway and muscle loss in experimental cancer cachexia. *Br J Cancer* 2005, *93*, 774-780.
[155] Schersten, T., Lundholm, K., Lysosomal enzyme activity in muscle tissue from patients with malignant tumor. *Cancer* 1972, *30*, 1246-1251.
[156] Barber, M. D., Fearon, K. C., McMillan, D. C., Slater, C.*, et al.*, Liver export protein synthetic rates are increased by oral meal feeding in weight-losing cancer patients. *Am J Physiol Endocrinol Metab* 2000, *279*, E707-714.
[157] Esper, D. H., Harb, W. A., The cancer cachexia syndrome: a review of metabolic and clinical manifestations. *Nutr Clin Pract* 2005, *20*, 369-376.
[158] Tijerina, A. J., The biochemical basis of metabolism in cancer cachexia. *Dimens Crit Care Nurs* 2004, *23*, 237-243.
[159] Tisdale, M. J., Molecular pathways leading to cancer cachexia. *Physiology (Bethesda)* 2005, *20*, 340-348.
[160] Matthys, P., Billiau, A., Cytokines and cachexia. *Nutrition* 1997, *13*, 763-770.

[161] Strassmann, G., Fong, M., Kenney, J. S., Jacob, C. O., Evidence for the involvement of interleukin 6 in experimental cancer cachexia. *J Clin Invest* 1992, *89*, 1681-1684.
[162] Carson, J. A., Baltgalvis, K. A., Interleukin 6 as a key regulator of muscle mass during cachexia. *Exerc Sport Sci Rev*, *38*, 168-176.
[163] Franckhauser, S., Elias, I., Rotter Sopasakis, V., Ferre, T.*, et al.*, Overexpression of Il6 leads to hyperinsulinaemia, liver inflammation and reduced body weight in mice. *Diabetologia* 2008, *51*, 1306-1316.
[164] Yanagawa, H., Sone, S., Takahashi, Y., Haku, T.*, et al.*, Serum levels of interleukin 6 in patients with lung cancer. *Br J Cancer* 1995, *71*, 1095-1098.
[165] Yeh, S. S., Schuster, M. W., Geriatric cachexia: the role of cytokines. *Am J Clin Nutr* 1999, *70*, 183-197.
[166] Soda, K., Kawakami, M., Kashii, A., Miyata, M., Manifestations of cancer cachexia induced by colon 26 adenocarcinoma are not fully ascribable to interleukin-6. *Int J Cancer* 1995, *62*, 332-336.
[167] Zybailov, B. L., Florens, L., Washburn, M. P., Quantitative shotgun proteomics using a protease with broad specificity and normalized spectral abundance factors. *Mol Biosyst* 2007, *3*, 354-360.
[168] Argiles, J. M., Alvarez, B., Lopez-Soriano, F. J., The metabolic basis of cancer cachexia. *Med Res Rev* 1997, *17*, 477-498.
[169] Bollen, M., Keppens, S., Stalmans, W., Specific features of glycogen metabolism in the liver. *Biochem J* 1998, *336 (Pt 1)*, 19-31.
[170] Hirai, K., Ishiko, O., Tisdale, M., Mechanism of depletion of liver glycogen in cancer cachexia. *Biochem Biophys Res Commun* 1997, *241*, 49-52.
[171] Schulze, B., Buchelt, L., Dittmann, H. W., Mensch, K. W., [Biochemical investigations of cancer cachexia. II. Depletion of glycogenolysis and stimulation of gluconeogenesis in Walker carcinoma 256 bearing rats (author's transl)]. *Z Krebsforsch Klin Onkol Cancer Res Clin Oncol* 1976, *85*, 29-38.
[172] Castell, J. V., Gomez-Lechon, M. J., David, M., Andus, T.*, et al.*, Interleukin-6 is the major regulator of acute phase protein synthesis in adult human hepatocytes. *FEBS Lett* 1989, *242*, 237-239.
[173] Ramadori, G., Van Damme, J., Rieder, H., Meyer zum Buschenfelde, K. H., Interleukin 6, the third mediator of acute-phase reaction, modulates hepatic protein synthesis in human and mouse. Comparison with interleukin 1 beta and tumor necrosis factor-alpha. *Eur J Immunol* 1988, *18*, 1259-1264.
[174] Fearon, K. C., Barber, M. D., Falconer, J. S., McMillan, D. C.*, et al.*, Pancreatic cancer as a model: inflammatory mediators, acute-phase response, and cancer cachexia. *World J Surg* 1999, *23*, 584-588.
[175] Harris, R. A., Popov, K. M., Zhao, Y., Shimomura, Y., Regulation of branched-chain amino acid catabolism. *J Nutr* 1994, *124*, 1499S-1502S.
[176] Doering, C. B., Coursey, C., Spangler, W., Danner, D. J., Murine branched chain alpha-ketoacid dehydrogenase kinase; cDNA cloning, tissue distribution, and temporal expression during embryonic development. *Gene* 1998, *212*, 213-219.
[177] Yeaman, S. J., The 2-oxo acid dehydrogenase complexes: recent advances. *Biochem J* 1989, *257*, 625-632.
[178] Shimomura, Y., Nanaumi, N., Suzuki, M., Popov, K. M., Harris, R. A., Purification and partial characterization of branched-chain alpha-ketoacid dehydrogenase kinase from rat liver and rat heart. *Arch Biochem Biophys* 1990, *283*, 293-299.
[179] Damuni, Z., Merryfield, M. L., Humphreys, J. S., Reed, L. J., Purification and properties of branched-chain alpha-keto acid dehydrogenase phosphatase from bovine kidney. *Proc Natl Acad Sci U S A* 1984, *81*, 4335-4338.

[180] Harris, R. A., Zhang, B., Goodwin, G. W., Kuntz, M. J., *et al.*, Regulation of the branched-chain alpha-ketoacid dehydrogenase and elucidation of a molecular basis for maple syrup urine disease. *Adv Enzyme Regul* 1990, *30*, 245-263.
[181] Hutson, S. M., Subcellular distribution of branched-chain aminotransferase activity in rat tissues. *J Nutr* 1988, *118*, 1475-1481.
[182] Hutson, S. M., Harper, A. E., Blood and tissue branched-chain amino and alpha-keto acid concentrations: effect of diet, starvation, and disease. *Am J Clin Nutr* 1981, *34*, 173-183.
[183] Lea, W., Abbas, A. S., Sprecher, H., Vockley, J., Schulz, H., Long-chain acyl-CoA dehydrogenase is a key enzyme in the mitochondrial beta-oxidation of unsaturated fatty acids. *Biochim Biophys Acta* 2000, *1485*, 121-128.
[184] Tisdale, M. J., Leung, Y. C., Changes in host liver fatty acid synthase in tumour-bearing mice. *Cancer Lett* 1988, *42*, 231-235.
[185] Schlichting, I., Berendzen, J., Chu, K., Stock, A. M., *et al.*, The catalytic pathway of cytochrome p450cam at atomic resolution. *Science* 2000, *287*, 1615-1622.
[186] Rivory, L. P., Slaviero, K. A., Clarke, S. J., Hepatic cytochrome P450 3A drug metabolism is reduced in cancer patients who have an acute-phase response. *Br J Cancer* 2002, *87*, 277-280.
[187] Slaviero, K. A., Clarke, S. J., Rivory, L. P., Inflammatory response: an unrecognised source of variability in the pharmacokinetics and pharmacodynamics of cancer chemotherapy. *Lancet Oncol* 2003, *4*, 224-232.
[188] Fang, C., Yoon, S., Tindberg, N., Jarvelainen, H. A., *et al.*, Hepatic expression of multiple acute phase proteins and down-regulation of nuclear receptors after acute endotoxin exposure. *Biochem Pharmacol* 2004, *67*, 1389-1397.
[189] Morgan, E. T., Regulation of cytochromes P450 during inflammation and infection. *Drug Metab Rev* 1997, *29*, 1129-1188.
[190] Down, M. J., Arkle, S., Mills, J. J., Regulation and induction of CYP3A11, CYP3A13 and CYP3A25 in C57BL/6J mouse liver. *Arch Biochem Biophys* 2007, *457*, 105-110.
[191] Ma, Q., Induction of CYP1A1. The AhR/DRE paradigm: transcription, receptor regulation, and expanding biological roles. *Curr Drug Metab* 2001, *2*, 149-164.
[192] Ratanavaraporn, J., Kanokpanont, S., Tabata, Y., Damrongsakkul, S., Growth and osteogenic differentiation of adipose-derived and bone marrow-derived stem cells on chitosan and chitooligosaccharide films. *Carbohydrate Polymers* 2009, *78*, 873-878.
[193] Conrad, C., Huss, R., Adult stem cell lines in regenerative medicine and reconstructive surgery. *Journal of Surgical Research* 2005, *124*, 201-208.
[194] Mackay, A. M., Beck, S. C., Murphy, J. M., Barry, F. P., *et al.*, Chondrogenic differentiation of cultured human mesenchymal stem cells from marrow. *Tissue Eng* 1998, *4*, 415 - 428.
[195] Vallée, M., Côté, J. F., Fradette, J., Adipose-tissue engineering: Taking advantage of the properties of human adipose-derived stem/stromal cells. *Pathologie Biologie* 2009, *57*, 309-317.
[196] Woodbury, D., Schwarz, E. J., Prockop, D. J., Black, I. B., Adult rat and human bone marrow stromal cells differentiate into neurons. . *J Neurosci Res* 2000 *61*
364–370

[197] Fujimura, J., Ogawa, R., Mizuno, H., Fukunaga, Y., Suzuki, H., Neural differentiation of adipose-derived stem cells isolated from GFP transgenic mice. *Biochemical and Biophysical Research Communications* 2005, *333*, 116-121.
[198] Zuk, P. A., Zhu, M., Ashjian, P., De Ugarte, D. A., *et al.*, Human Adipose Tissue Is a Source of Multipotent Stem Cells. *Mol. Biol. Cell* 2002, *13*, 4279-4295.

[199] Sanchez-Ramos, J., Song, S., Cardozo-Pelaez, F., Hazzi, C*., et al.*, Adult bone marrow stromal cells differentiate into neural cells in vitro. *Exp Neurol* 2000, *164*, 247-256.
[200] Barnabé, G. F., Schwindt, T. T., Calcagnotto, M. E., Motta, F. L*., et al.*, Chemically-Induced RAT Mesenchymal Stem Cells Adopt Molecular Properties of Neuronal-Like Cells but Do Not Have Basic Neuronal Functional Properties. *PLoS ONE* 2009, *4*, e5222.
[201] Radtke, C., Schmitz, B., Spies, M., Kocsis, J. D., Vogt, P. M., Peripheral glial cell differentiation from neurospheres derived from adipose mesenchymal stem cells. *International Journal of Developmental Neuroscience* 2009, *27*, 817-823.
[202] Medrano, S., Burns-Cusato, M., Atienza, M. B., Rahimi, D., Scrable, H., Regenerative capacity of neural precursors in the adult mammalian brain is under the control of p53. *Neurobiology of Aging* 2009, *30*, 483-497.
[203] Li, Q.-m., Fu, Y.-m., Shan, Z.-y., Shen, J.-l*., et al.*, MSCs guide neurite directional extension and promote oligodendrogenesis in NSCs. *Biochemical and Biophysical Research Communications* 2009, *384*, 372-377.
[204] Kimura, I., Konishi, M., Asaki, T., Furukawa, N*., et al.*, Neudesin, an extracellular heme-binding protein, suppresses adipogenesis in 3T3-L1 cells via the MAPK cascade. *Biochemical and Biophysical Research Communications* 2009, *381*, 75-80.
[205] Franco Lambert, A. P., Fraga Zandonai, A., Bonatto, D., Cantarelli Machado, D., Pêgas Henriques, J. A., Differentiation of human adipose-derived adult stem cells into neuronal tissue: Does it work? *Differentiation* 2009, *77*, 221-228.
[206] Xu, Y., Liu, L., Li, Y., Zhou, C*., et al.*, Myelin-forming ability of Schwann cell-like cells induced from rat adipose-derived stem cells in vitro. *Brain Research* 2008, *1239*, 49-55.
[207] Mattingly, M., Chakrabarti, D., Ghosh, S. K., Promotion of murine B cell differentiation by 2-mercaptoethanol in contrast to glutathione. *FASEB J* 1992, *6*, 3002-3007.
[208] Grill, R. J., Jr., Pixley, S. K., 2-Mercaptoethanol is a survival factor for olfactory, cortical and hippocampal neurons in short-term dissociated cell culture. *Brain Res* 1993, *613*, 168-172.
[209] Oblinger, M. M., Foe, L. G., Kwiatkowska, D., Kemp, R. G., Phosphofructokinase in the rat nervous system: regional differences in activity and characteristics of axonal transport. *J Neurosci Res* 1988, *21*, 25-34.
[210] Facchinetti, P., Rose, C., Rostaing, P., Triller, A., Schwartz, J. C., Immunolocalization of tripeptidyl peptidase II, a cholecystokinin-inactivating enzyme, in rat brain. *Neuroscience* 1999, *88*, 1225-1240.
[211] Buono, P., D'Armiento, F. P., Terzi, G., Alfieri, A., Salvatore, F., Differential distribution of aldolase A and C in the human central nervous system. *J Neurocytol* 2001, *30*, 957-965.
[212] Larcher, J. C., Gasmi, L., Viranaicken, W., Edde, B*., et al.*, Ilf3 and NF90 associate with the axonal targeting element of Tau mRNA. *FASEB J* 2004, *18*, 1761-1763.
[213] Abdelhaleem, M., RNA helicases: regulators of differentiation. *Clin Biochem* 2005, *38*, 499-503.
[214] Shannon, P., Markiel, A., Ozier, O., Baliga, N. S*., et al.*, Cytoscape: a software environment for integrated models of biomolecular interaction networks. *Genome Res* 2003, *13*, 2498-2504.
[215] Kamada, T., Kawai, S., Advanced graphics for visualization of shielding relations *Computer Vision, Graph, Image Process* 1988, *43*, 294-312.
[216] Eades, P., Congressus Numerantium 1984, *42*, 149-160.
[217] Wissing, J., Jansch, L., Nimtz, M., Dieterich, G*., et al.*, Proteomics Analysis of Protein Kinases by Target Class-selective Prefractionation and Tandem Mass Spectrometry. *Mol Cell Proteomics* 2007, *6*, 537-547.

[218] Cho, J., Rameshwar, P., Sadoshima, J., Distinct roles of glycogen synthase kinase (GSK)-3alpha and GSK-3beta in mediating cardiomyocyte differentiation in murine bone marrow-derived mesenchymal stem cells. *J Biol Chem* 2009, *284*, 36647-36658.
[219] Daub, H., Olsen, J. V., Bairlein, M., Gnad, F.*, et al.*, Kinase-Selective Enrichment Enables Quantitative Phosphoproteomics of the Kinome across the Cell Cycle. *Molecular cell* 2008, *31*, 438-448.
[220] Lie, D.-C., Colamarino, S. A., Song, H.-J., Desire, L.*, et al.*, Wnt signalling regulates adult hippocampal neurogenesis. *Nature* 2005, *437*, 1370-1375.
[221] Maurer, M. H., Bromme, J. O., Feldmann, R. E., Jr., Jarve, A.*, et al.*, Glycogen synthase kinase 3beta (GSK3beta) regulates differentiation and proliferation in neural stem cells from the rat subventricular zone. *J Proteome Res* 2007, *6*, 1198-1208.
[222] Sparatore, B., Patrone, M., Passalacqua, M., Pedrazzi, M.*, et al.*, Neuronal differentiation of PC12 cells involves changes in protein kinase C-theta distribution and molecular properties. *Biochem Biophys Res Commun* 2000, *275*, 149-153.
[223] Tsutsumi, H., Tani, K., Fujii, H., Miwa, S., Expression of L- and M-type pyruvate kinase in human tissues. *Genomics* 1988, *2*, 86-89.
[224] Todd, A. G., Morse, R., Shaw, D. J., McGinley, S.*, et al.*, SMN, Gemin2 and Gemin3 Associate with [beta]-Actin mRNA in the Cytoplasm of Neuronal Cells In Vitro. *Journal of Molecular Biology* 2010, *401*, 681-689.
[225] Zhu, M., Yang, T., Wei, S., DeWan, A. T.*, et al.*, Mutations in the Gamma-Actin Gene (ACTG1) Are Associated with Dominant Progressive Deafness (DFNA20/26). *American journal of human genetics* 2003, *73*, 1082-1091.
[226] Kakita, A., Hayashi, S., Moro, F., Guerrini, R.*, et al.*, Bilateral periventricular nodular heterotopia due to<SMALL> filamin 1</SMALL> gene mutation: widespread glomeruloid microvascular anomaly and dysplastic cytoarchitecture in the cerebral cortex. *Acta Neuropathologica* 2002, *104*, 649-657.
[227] Schultz, A., Jonsson, J. I., Larsson, C., The regulatory domain of protein kinase Ctheta localises to the Golgi complex and induces apoptosis in neuroblastoma and Jurkat cells. *Cell Death Differ* 2003, *10*, 662-675.
[228] Barnabe, G. F., Schwindt, T. T., Calcagnotto, M. E., Motta, F. L.*, et al.*, Chemically-induced RAT mesenchymal stem cells adopt molecular properties of neuronal-like cells but do not have basic neuronal functional properties. *PLoS One* 2009, *4*, e5222.
[229] Briggs, M. W., Sacks, D. B., IQGAP proteins are integral components of cytoskeletal regulation. *EMBO Rep* 2003, *4*, 571-574.
[230] Swart-Mataraza, J. M., Li, Z., Sacks, D. B., IQGAP1 is a component of Cdc42 signaling to the cytoskeleton. *J Biol Chem* 2002, *277*, 24753-24763.
[231] Li, Z., McNulty, D. E., Marler, K. J., Lim, L.*, et al.*, IQGAP1 promotes neurite outgrowth in a phosphorylation-dependent manner. *J Biol Chem* 2005, *280*, 13871-13878.
[232] da Silva, J. S., Dotti, C. G., Breaking the neuronal sphere: regulation of the actin cytoskeleton in neuritogenesis. *Nat Rev Neurosci* 2002, *3*, 694-704.
[233] Helfand, B. T., Mendez, M. G., Pugh, J., Delsert, C., Goldman, R. D., A role for intermediate filaments in determining and maintaining the shape of nerve cells. *Mol Biol Cell* 2003, *14*, 5069-5081.
[234] Bashour, A. M., Fullerton, A. T., Hart, M. J., Bloom, G. S., IQGAP1, a Rac- and Cdc42-binding protein, directly binds and cross-links microfilaments. *J Cell Biol* 1997, *137*, 1555-1566.
[235] Erickson, J. W., Cerione, R. A., Hart, M. J., Identification of an actin cytoskeletal complex that includes IQGAP and the Cdc42 GTPase. *J Biol Chem* 1997, *272*, 24443-24447.
[236] Zhao, F., Wu, T., Lau, A., Jiang, T.*, et al.*, Nrf2 promotes neuronal cell differentiation. *Free Radic Biol Med* 2009, *47*, 867-879.

[237] Lu, P., Blesch, A., Tuszynski, M. H., Induction of bone marrow stromal cells to neurons: differentiation, transdifferentiation, or artifact? *J Neurosci Res* 2004, *77*, 174-191.
[238] Yamasaki, M., Yamada, K., Furuya, S., Mitoma, J.*, et al.*, 3-Phosphoglycerate dehydrogenase, a key enzyme for l-serine biosynthesis, is preferentially expressed in the radial glia/astrocyte lineage and olfactory ensheathing glia in the mouse brain. *J Neurosci* 2001, *21*, 7691-7704.
[239] Hall, A., Sankaran, B., Poole, L. B., Karplus, P. A., Structural changes common to catalysis in the Tpx peroxiredoxin subfamily. *J Mol Biol* 2009, *393*, 867-881.
[240] Jang, H. H., Lee, K. O., Chi, Y. H., Jung, B. G.*, et al.*, Two enzymes in one; two yeast peroxiredoxins display oxidative stress-dependent switching from a peroxidase to a molecular chaperone function. *Cell* 2004, *117*, 625-635.
[241] Yan, Y., Sabharwal, P., Rao, M., Sockanathan, S., The antioxidant enzyme Prdx1 controls neuronal differentiation by thiol-redox-dependent activation of GDE2. *Cell* 2009, *138*, 1209-1221.
[242] Berger, A. B., Vitorino, P. M., Bogyo, M., Activity-based protein profiling: applications to biomarker discovery, in vivo imaging and drug discovery. *Am J Pharmacogenomics* 2004, *4*, 371-381.
[243] Cravatt, B. F., Wright, A. T., Kozarich, J. W., Activity-based protein profiling: from enzyme chemistry to proteomic chemistry. *Annu Rev Biochem* 2008, *77*, 383-414.
[244] Jessani, N., Cravatt, B. F., The development and application of methods for activity-based protein profiling. *Curr Opin Chem Biol* 2004, *8*, 54-59.
[245] Okerberg, E. S., Wu, J., Zhang, B., Samii, B.*, et al.*, High-resolution functional proteomics by active-site peptide profiling. *Proc Natl Acad Sci U S A* 2005, *102*, 4996-5001.
[246] Qiu, H., Wang, Y., Probing adenosine nucleotide-binding proteins with an affinity-labeled nucleotide probe and mass spectrometry. *Anal Chem* 2007, *79*, 5547-5556.
[247] Wong, J. W., McRedmond, J. P., Cagney, G., Activity profiling of platelets by chemical proteomics. *Proteomics* 2009, *9*, 40-50.
[248] Khandekar, S. S., Feng, B., Yi, T., Chen, S.*, et al.*, A liquid chromatography/mass spectrometry-based method for the selection of ATP competitive kinase inhibitors. *J Biomol Screen* 2005, *10*, 447-455.
[249] Hanoulle, X., Van Damme, J., Staes, A., Martens, L.*, et al.*, A new functional, chemical proteomics technology to identify purine nucleotide binding sites in complex proteomes. *J Proteome Res* 2006, *5*, 3438-3445.
[250] Ly, L., Wasinger, V. C., Protein and peptide fractionation, enrichment and depletion: tools for the complex proteome. *Proteomics* 2011, *11*, 513-534.
[251] Matsumura, H., Matsuda, K., Nakamura, N., Ohtaki, A.*, et al.*, Monooxygenation by a thermophilic cytochrome P450 via direct electron donation from NADH. *Metallomics* 2011, *3*, 389-395.
[252] Lee, H. K., Lee, B. H., Park, S. A., Kim, C. W., The proteomic analysis of an adipocyte differentiated from human mesenchymal stem cells using two-dimensional gel electrophoresis. *Proteomics* 2006, *6*, 1223-1229.
[253] Roche, S., Delorme, B., Oostendorp, R. A., Barbet, R.*, et al.*, Comparative proteomic analysis of human mesenchymal and embryonic stem cells: towards the definition of a mesenchymal stem cell proteomic signature. *Proteomics* 2009, *9*, 223-232.
[254] Roche, S., Provansal, M., Tiers, L., Jorgensen, C., Lehmann, S., Proteomics of primary mesenchymal stem cells. *Regen Med* 2006, *1*, 511-517.
[255] Kalas, W., Matuszyk, J., Ziolo, E., Strzadala, L., FK506 restores sensitivity of thymic lymphomas to calcium-mediated apoptosis and the inducible expression of Fas ligand. *Anticancer Res* 2003, *23*, 1613-1617.
[256] Speers, A. E., Cravatt, B. F., A tandem orthogonal proteolysis strategy for high-content chemical proteomics. *J Am Chem Soc* 2005, *127*, 10018-10019.

[257] van der Veken, P., Dirksen, E. H., Ruijter, E., Elgersma, R. C.*, et al.*, Development of a novel chemical probe for the selective enrichment of phosphorylated serine- and threonine-containing peptides. *Chembiochem* 2005, *6*, 2271-2280.
[258] Fauq, A. H., Kache, R., Khan, M. A., Vega, I. E., Synthesis of acid-cleavable light isotope-coded affinity tags (ICAT-L) for potential use in proteomic expression profiling analysis. *Bioconjug Chem* 2006, *17*, 248-254.
[259] Shimkus, M., Levy, J., Herman, T., A chemically cleavable biotinylated nucleotide: usefulness in the recovery of protein-DNA complexes from avidin affinity columns. *Proc Natl Acad Sci U S A* 1985, *82*, 2593-2597.
[260] Verhelst, S. H., Fonovic, M., Bogyo, M., A mild chemically cleavable linker system for functional proteomic applications. *Angew Chem Int Ed Engl* 2007, *46*, 1284-1286.
[261] Fonovic, M., Verhelst, S. H., Sorum, M. T., Bogyo, M., Proteomics evaluation of chemically cleavable activity-based probes. *Mol Cell Proteomics* 2007, *6*, 1761-1770.
[262] Fischer, J. J., Graebner Baessler, O. Y., Dalhoff, C., Michaelis, S.*, et al.*, Comprehensive identification of staurosporine-binding kinases in the hepatocyte cell line HepG2 using Capture Compound Mass Spectrometry (CCMS). *J Proteome Res* 2010, *9*, 806-817.
[263] Ghoreschi, K., Laurence, A., O'Shea, J. J., Selectivity and therapeutic inhibition of kinases: to be or not to be? *Nat Immunol* 2009, *10*, 356-360.
[264] Piggott, A. M., Karuso, P., Quality, not quantity: the role of natural products and chemical proteomics in modern drug discovery. *Comb Chem High Throughput Screen* 2004, *7*, 607-630.
[265] Brehme, M., Hantschel, O., Colinge, J., Kaupe, I.*, et al.*, Charting the molecular network of the drug target Bcr-Abl. *Proc Natl Acad Sci U S A* 2009, *106*, 7414-7419.
[266] Burckstummer, T., Bennett, K. L., Preradovic, A., Schutze, G.*, et al.*, An efficient tandem affinity purification procedure for interaction proteomics in mammalian cells. *Nat Methods* 2006, *3*, 1013-1019.
[267] Rigaut, G., Shevchenko, A., Rutz, B., Wilm, M.*, et al.*, A generic protein purification method for protein complex characterization and proteome exploration. *Nat Biotechnol* 1999, *17*, 1030-1032.
[268] Fonovic, M., Bogyo, M., Activity based probes for proteases: applications to biomarker discovery, molecular imaging and drug screening. *Curr Pharm Des* 2007, *13*, 253-261.

Appendix A

Figure 1A: Representative spectra for SRPK1 peptide.

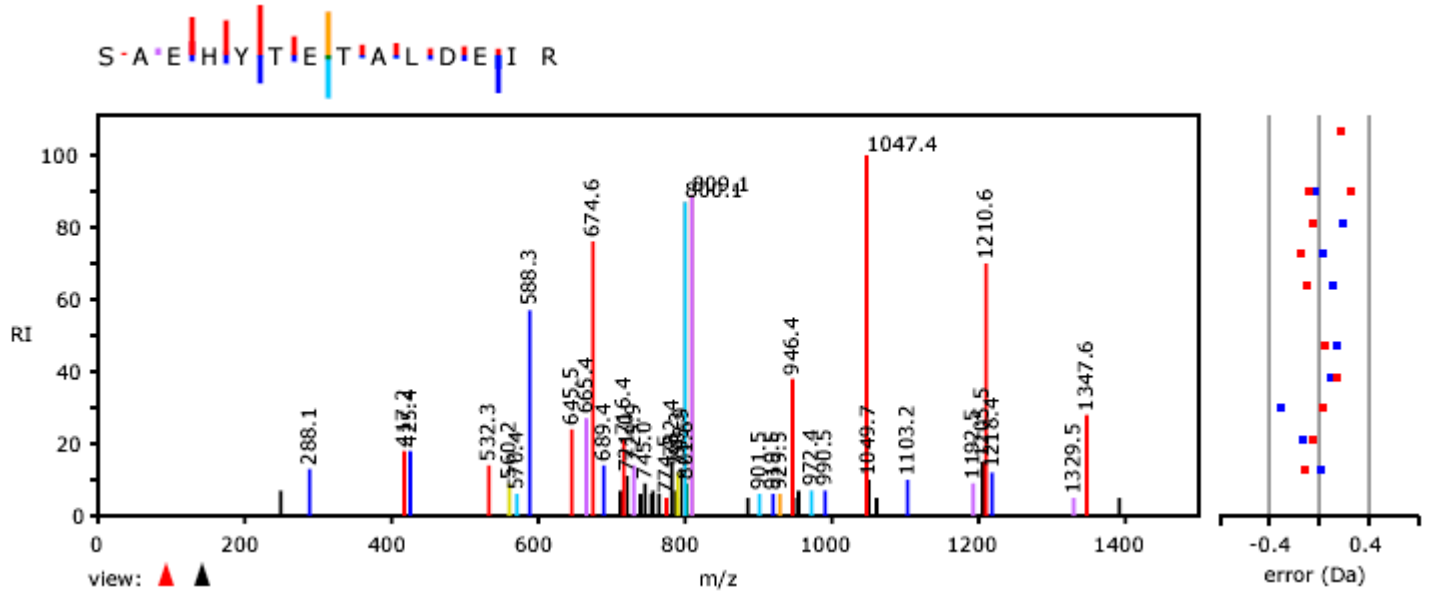

bond	^{+1}y	$^{+1}y^{-17}$	$^{+1}y^{-18}$	^{+1}b	$^{+1}b^{-17}$	$^{+1}b^{-18}$
S_1	$^{+2}$1547.734	1530.707	1529.723	88.039	71.013	70.029
A_2	1476.696	1459.670	1458.686	159.076	142.050	141.066
E_3	$^{+1,2}$1347.654	1330.627	1329.643	288.119	271.092	270.108
H_4	1210.595	1193.568	1192.584	425.178	408.151	407.167
Y_5	1047.532	1030.505	1029.521	588.241	571.215	570.231
T_6	946.484	929.457	928.473	689.289	672.262	671.278
E_7	817.441	800.415	799.431	818.332	801.305	800.321
T_8	716.394	699.367	698.383	919.379	902.353	901.369
A_9	645.357	628.330	627.346	990.416	973.390	972.406
L_{10}	532.273	515.246	514.262	1103.500	1086.474	1085.490
D_{11}	417.246	400.219	399.235	1218.527	1201.501	1200.517
E_{12}	288.203	271.176	270.192	$^{+1,2}$1347.570	1330.543	1329.559
I_{13}	175.119	158.092	157.108	1460.654	1443.627	1442.643

Figure 1 B: Representative spectra for PKR peptide.

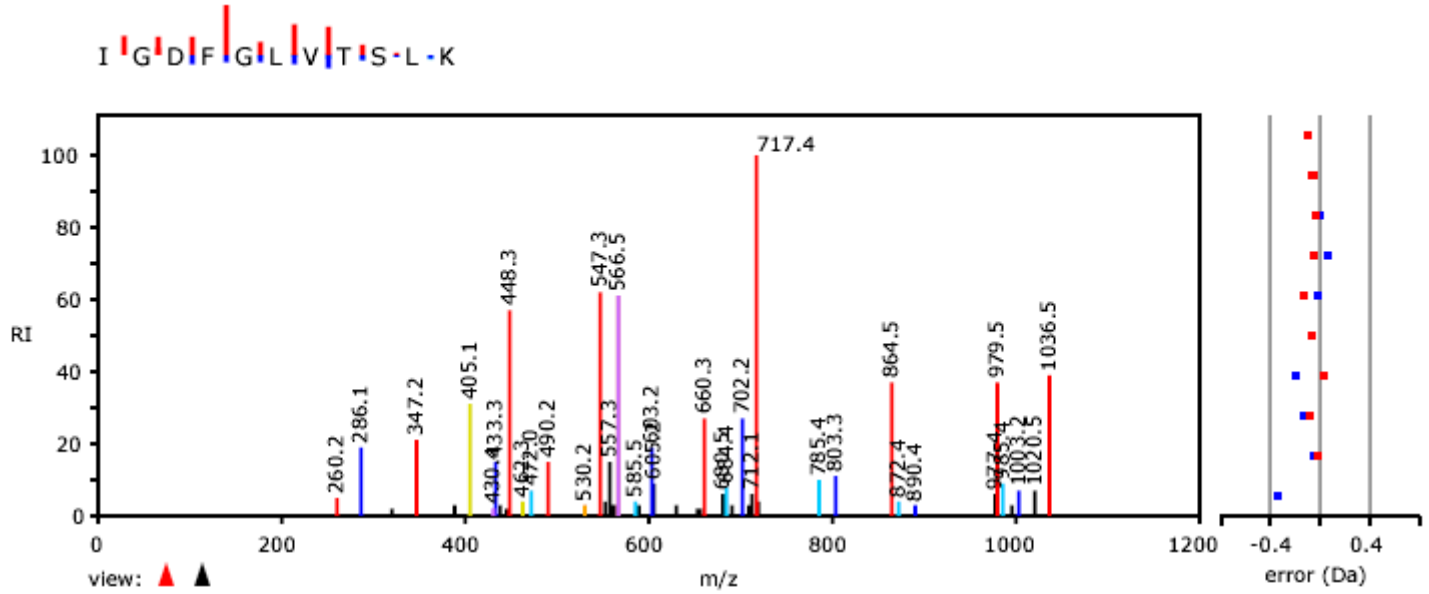

bond	^{+1}y	$^{+1}y^{-17}$	$^{+1}y^{-18}$	^{+1}b	$^{+1}b^{-17}$	$^{+1}b^{-18}$
I_1	1036.567	1019.541	1018.557	114.091	97.065	96.081
G_2	$^{+1,2}$979.546	962.519	961.535	171.113	154.086	153.102
D_3	864.519	847.492	846.508	286.140	269.113	268.129
F_4	717.451	700.424	699.440	433.208	416.182	415.198
G_5	660.429	643.402	642.418	490.230	473.203	472.219
L_6	547.345	530.318	529.334	603.314	586.287	585.303
V_7	448.277	431.250	430.266	702.382	685.356	684.372
T_8	347.229	330.202	329.218	803.430	786.403	785.419
S_9	260.197	243.170	242.186	890.462	873.435	872.451
L_{10}	147.113	130.086	129.102	1003.546	986.519	985.535

Table 1A: Proteins targets captured by the Bis-probe in PMA stimulated MDA-MB-231.

Identifier	#peptides	log(e)	Description	Accession no
ENSP00000262414	24	-201	116 kDa U5 small nuclear ribonucleoprotein component	Q15029
ENSP00000324173	11	-71.1	78 kDa glucose-regulated protein precursor	P11021
ENSP00000348068	4	-16.7	Alpha-1-antitrypsin Precursor	P01009
ENSP00000252699	4	-20.7	Alpha-actinin-4	O43707
ENSP00000265109	17	-89.3	Ankycorbin	Q9P0K7
ENSP00000348640	4	-15.2	Annexin A2	P07355
ENSP00000314414	6	-18.7	AP-2 complex subunit beta-1	P63010
ENSP00000231572	46	-283	Arginyl-tRNA synthetase, cytoplasmic	P54136
ENSP00000368767	4	-19.8	Aspartyl/asparaginyl beta-hydroxylase	Q12797
ENSP00000282050	5	-31.1	ATP synthase subunit alpha, mitochondrial precursor	P25705
ENSP00000368031	6	-22.4	ATPase family AAA domain-containing protein 3A	Q9NVI7
ENSP00000296577	10	-40.9	ATP-binding cassette sub-family E member 1	P61221
ENSP00000372929	18	-104	ATP-binding cassette sub-family F member 1	Q8NE71
ENSP00000222388	3	-18.1	ATP-binding cassette sub-family F member 2	Q9UG63
ENSP00000352257	10	-57.5	ATP-dependent DNA helicase 2 subunit 1	P12956
ENSP00000329528	9	-73.1	ATP-dependent DNA helicase 2 subunit 2	P13010
ENSP00000356520	18	-112	ATP-dependent RNA helicase A	Q08211
ENSP00000370745	5	-36.4	ATP-dependent RNA helicase DDX1	Q92499
ENSP00000367478	22	-156	ATP-dependent RNA helicase DDX3X	O00571
ENSP00000362687	6	-26.6	ATP-dependent RNA helicase DDX50	Q9BQ39
ENSP00000304072	3	-16	ATP-dependent RNA helicase DDX54	Q8TDD1
ENSP00000238146	2	-9.4	ATP-dependent RNA helicase DDX55	Q8NHQ9
ENSP00000355890	6	-30.3	Bifunctional aminoacyl-tRNA synthetase	P07814
ENSP00000279247	4	-24.9	Calpain-1 catalytic subunit	P07384
ENSP00000340329	12	-65.2	Caprin-1	Q14444
ENSP00000233072	5	-21	Carbamoyl-phosphate synthase [ammonia], mitochondrial precursor	P31327
ENSP00000269305	7	-39.4	Cellular tumor antigen p53	P04637
ENSP00000266679	3	-22.1	Cleavage and polyadenylation specificity factor subunit 6	Q16630
ENSP00000357048	3	-9.6	Coatomer subunit alpha	P53621
ENSP00000342408	4	-18.4	Cold shock domain-containing protein E1	O75534
ENSP00000321706	5	-24.7	Component of gems 4	P57678
ENSP00000277165	13	-80.3	Constitutive coactivator of PPAR-gamma-like protein 1	Q9NZB2
ENSP00000326804	3	-11.4	Cullin-1	Q13616
ENSP00000293371	4	-16.8	Dermcidin precursor	P81605
ENSP00000354522	20	-137	DNA topoisomerase 1	P11387
ENSP00000228251	13	-61.1	DNA-binding protein A	P16989
ENSP00000344030	4	-24.4	Double-stranded RNA-binding protein Staufen homolog 2.	Q9NUL3
ENSP00000217182	6	-19.9	Elongation factor 1-alpha 2	Q05639
ENSP00000350896	2	-9	Ephrin type-B receptor 4 precursor	P54760
ENSP00000332874	13	-70.7	Eukaryotic translation elongation factor 1 alpha-like 3.	Q5VTE0

ENSP00000253861	3	-26.2	Exocyst complex component 4	Q96A65
ENSP00000366135	4	-30.9	Exosome component 10	Q01780
ENSP00000251527	2	-11.6	Extended synaptotagmin-2	A0FGR8
ENSP00000278412	3	-13.4	FACT complex subunit SSRP1	Q08945
ENSP00000341469	3	-11.7	Fibrinogen gamma chain Precursor	P02679
ENSP00000350170	16	-108	Fragile X mental retardation syndrome-related protein 1	P51114
ENSP00000250113	23	-125	Fragile X mental retardation syndrome-related protein 2.	P51116
ENSP00000352740	15	-90.2	Gamma-interferon-inducible protein Ifi-16	Q16666
ENSP00000361219	3	-17.1	General transcription factor 3C polypeptide 4	Q9UKN8
ENSP00000349860	5	-25.1	Glucosamine--fructose-6-phosphate aminotransferase [isomerizing] 1	Q06210
ENSP00000253778	5	-22.9	Glucosamine--fructose-6-phosphate aminotransferase [isomerizing] 2	O94808
ENSP00000277865	8	-39.7	Glutamate dehydrogenase 1, mitochondrial Precursor	P00367
ENSP00000360326	8	-35.3	Glutamate dehydrogenase 2, mitochondrial precursor	P49448
ENSP00000253237	2	-12.9	Glutamate-rich WD repeat-containing protein 1	Q9BQ67
ENSP00000307567	37	-217	Glutaminyl-tRNA synthetase	P47897
ENSP00000229239	23	-20.7	Glyceraldehyde-3-phosphate dehydrogenase	P04406
ENSP00000222330	16	-102.1	Glycogen synthase kinase-3 alpha	P49840
ENSP00000264235	14	-23.3	Glycogen synthase kinase-3 beta	P49841
ENSP00000358563	2	-13.9	H/ACA ribonucleoprotein complex subunit 4	O60832
ENSP00000228929	9	-30.6	H2A histone family, member J	Q9BTM1
ENSP00000364802	11	-67.3	Heat shock 70 kDa protein 1	P08107
ENSP00000227378	43	-231	Heat shock cognate 71 kDa protein	P11142
ENSP00000365458	14	-76.4	Heterogeneous nuclear ribonucleoprotein K	P61978
ENSP00000221419	11	-79.9	Heterogeneous nuclear ribonucleoprotein L	P14866
ENSP00000325376	51	-204	Heterogeneous nuclear ribonucleoprotein M	P52272
ENSP00000257768	6	-39.5	Heterogeneous nuclear ribonucleoprotein Q	O60506
ENSP00000363745	3	-19.6	Heterogeneous nuclear ribonucleoprotein R	O43390
ENSP00000340857	4	-16.4	Heterogeneous nuclear ribonucleoprotein U-like protein 1	Q9BUJ2
ENSP00000357621	3	-13.5	Histone deacetylase 2	Q92769
ENSP00000259791	6	-16.9	Histone H2A type 1-E	P28001
ENSP00000354403	14	-26.2	Histone H2B type F-S	P57053
ENSP00000371634	4	-10.6	Insulin-like growth factor 2 mRNA-binding protein 2	Q9Y6M1
ENSP00000371410	2	-11.2	Insulin-like growth factor 2 mRNA-binding protein 3	O00425
ENSP00000368453	9	-57.3	Interferon-induced, double-stranded RNA-activated protein kinase	P19525
ENSP00000369957	22	-122	Interleukin enhancer-binding factor 3	Q12906
ENSP00000364811	18	-112	Isoleucyl-tRNA synthetase, cytoplasmic	P41252
ENSP00000364317	21	-142	Kinesin heavy chain	P33176
ENSP00000304978	10	-54.6	Kinesin-like protein KIF23	Q02241
ENSP00000370493	8	-33.9	Kinesin-like protein KIF2A	O00139

ENSP00000361298	7	-36.1	Kinesin-like protein KIF2C	Q99661
ENSP00000364864	4	-21.5	Kinesin-like protein KIF3B	O15066
ENSP00000372678	7	-35.4	Kinesin-like protein KIFC1	Q9BW19
ENSP00000266732	11	-82.7	Lamina-associated polypeptide 2, isoforms beta/gamma	P42167
ENSP00000363752	2	-16.5	Leucine zipper protein 1.	Q86V48
ENSP00000350012	4	-13.7	Long-chain-fatty-acid--CoA ligase 3	O95573
ENSP00000279068	2	-9.9	LS14B_HUMAN Isoform 2 of Q9BX40	Q9BX40-2
ENSP00000303043	18	-96.9	Lysyl-tRNA synthetase	Q15046
ENSP00000349977	5	-33.7	Major vault protein	Q14764
ENSP00000354346	9	-52.7	Matrin-3.	P43243
ENSP00000278823	7	-27.5	Metastasis-associated protein MTA2	O94776
ENSP00000262027	43	-294	Methionyl-tRNA synthetase, cytoplasmic	P56192
ENSP00000342379	17	-93.5	Myosin phosphatase Rho-interacting protein	Q6WCQ1
ENSP00000257829	9	-46.9	N-acetyltransferase 10	Q9H0A0
ENSP00000276079	51	-206	Non-POU domain-containing octamer-binding protein	Q15233
ENSP00000225388	7	-30.6	Nuclear fragile X mental retardation-interacting protein 2	Q7Z417
ENSP00000361626	14	-58.3	Nuclease-sensitive element-binding protein 1	P67809
ENSP00000370798	2	-8.8	Nucleolar GTP-binding protein 1	Q9BZE4
ENSP00000370589	3	-15.4	Nucleolar protein 5A	O00567
ENSP00000346120	10	-66.6	Nucleolar RNA helicase 2	Q9NR30
ENSP00000345297	8	-10.1	Nucleolar transcription factor 1	P17480
ENSP00000338582	3	-30.1	Paraspeckle component 1	Q8WXF1
ENSP00000360034	3	-17.4	Plasminogen activator inhibitor 1 RNA-binding protein	Q8NC51
ENSP00000355759	44	-276	Poly synthetase 1.	P09874
ENSP00000313007	42	-176	Polyadenylate-binding protein 1	P11940
ENSP00000371283	16	-86.4	Polyadenylate-binding protein 3	Q9H361
ENSP00000361953	31	-123	Polyadenylate-binding protein 4	Q13310
ENSP00000349541	32	-114	Polymerase I and transcript release factor.	Q6NZI2
ENSP00000014112	12	-92.3	Polypyrimidine tract-binding protein 1	P26599
ENSP00000227524	11	-62.8	Pre-mRNA-processing factor 19	Q9UMS4
ENSP00000266079	23	-112	Pre-mRNA-processing factor 6	O94906
ENSP00000301364	6	-34.5	Pre-rRNA-processing protein TSR1 homolog.	Q2NL82
ENSP00000216019	17	-81.8	Probable ATP-dependent RNA helicase DDX17	Q92841
ENSP00000358716	6	-43.3	Probable ATP-dependent RNA helicase DDX20	Q9UHI6
ENSP00000310723	6	-27.8	Probable ATP-dependent RNA helicase DDX23	Q9BUQ8
ENSP00000359588	3	-15.9	Probable phospholipid-transporting ATPase IG	Q8NB49
ENSP00000261973	3	-20.6	Probable RNA-binding protein 25	P49756
ENSP00000238823	3	-26.5	Protein FAM98A.	Q8NCA5
ENSP00000356548	2	-15.8	Protein LTV1 homolog.	Q96GA3
ENSP00000338235	7	-44.4	Protein LYRIC	Q86UE4
ENSP00000354068	6	-37.9	Protein phosphatase 1 regulatory subunit 12A	O14974
ENSP00000263433	7	-40.7	Protein phosphatase 1 regulatory subunit 12C	Q9BZL4

ENSP00000357727	12	-45.9	Protein S100-A9	P06702
ENSP00000355330	7	-21.8	Protein-glutamine gamma-glutamyltransferase 2	P21980
ENSP00000343442	5	-35.8	Putative ATP-dependent RNA helicase DHX30	Q7L2E3
ENSP00000358662	6	-35.7	Putative helicase MOV-10	Q9HCE1
ENSP00000336741	24	-136	Putative pre-mRNA-splicing factor ATP-dependent RNA helicase DHX15	O43143
ENSP00000347900	4	-25.5	Pyruvate carboxylase, mitochondrial precursor	P11498
ENSP00000334983	11	-81.1	Pyruvate kinase isozymes M1/M2	P14618
ENSP00000309871	3	-17	Rac GTPase-activating protein 1	Q9H0H5
ENSP00000348578	18	-85.8	Ras GTPase-activating protein-binding protein 1	Q13283
ENSP00000352738	14	-78.6	Ras GTPase-activating protein-binding protein 2	Q9UN86
ENSP00000262803	9	-67.1	Regulator of nonsense transcripts 1	Q92900
ENSP00000267163	2	-11	Retinoblastoma-associated protein	P06400
ENSP00000354837	12	-94.5	Rho/Rac guanine nucleotide exchange factor 2	Q92974
ENSP00000369822	6	-35.3	Ribosyldihydronicotinamide dehydrogenase [quinone]	P16083
ENSP00000366829	2	-10.1	RNA-binding protein 10	P98175
ENSP00000354437	5	-38.5	RNA-binding protein 39	Q14498
ENSP00000330516	2	-9.7	RNA-binding protein EWS	Q01844
ENSP00000254108	22	-81.9	RNA-binding protein FUS	P35637
ENSP00000221413	2	-12.1	RuvB-like 2	Q9Y230
ENSP00000366913	2	-8.8	Sarcoplasmic/endoplasmic reticulum calcium ATPase 2	P16615
ENSP00000294247	7	-37.3	Serine/threonine-protein kinase MARK2	Q7KZI7
ENSP00000354674	6	-24.3	Serine/threonine-protein kinase SRPK1	Q96SB4
ENSP00000305675	6	-47.7	Serum deprivation-response protein	O95810
ENSP00000312066	20	-94.4	Signal recognition particle 68 kDa protein	Q9UHB9
ENSP00000342181	8	-22.6	Signal recognition particle 72 kDa protein	O76094
ENSP00000351503	23	-92.7	SPATS2-like protein	Q9NUQ6
ENSP00000274008	2	-12.5	Spermatogenesis-associated protein 5	Q8NB90
ENSP00000305494	2	-11.8	Spermatogenesis-associated protein 5-like protein 1.	Q9BVQ7
ENSP00000299297	2	-10.4	Sphingosine-1-phosphate lyase 1	O95470
ENSP00000335321	6	-27.4	Splicing factor 3B subunit 1	O75533
ENSP00000318861	11	-31.9	Splicing factor 3B subunit 2	Q13435
ENSP00000305790	20	-112	Splicing factor 3B subunit 3	Q15393
ENSP00000271628	2	-13.8	Splicing factor 3B subunit 4	Q15427
ENSP00000369218	3	-17.2	Splicing factor 45	Q96I25
ENSP00000365482	4	-29.2	Splicing factor U2AF 65 kDa subunit	P26368
ENSP00000244020	2	-11.1	Splicing factor, arginine/serine-rich 6	Q13247
ENSP00000349748	42	-247	Splicing factor, proline- and glutamine-rich	P23246
ENSP00000346762	21	-120	Staphylococcal nuclease domain-containing protein 1	Q7KZF4
ENSP00000297185	5	-22.3	Stress-70 protein, mitochondrial precursor	P38646
ENSP00000317334	2	-8.7	T-complex protein 1 subunit alpha	P17987
ENSP00000357244	3	-17.3	T-complex protein 1 subunit gamma	P49368
ENSP00000350787	2	-10.4	THO complex subunit 5 homolog	Q13769
ENSP00000253024	3	-13.3	Transcription intermediary factor 1-beta	Q13263
ENSP00000327881	10	-41.2	TRIO and F-actin-binding protein	Q9H2D6
ENSP00000323889	32	-128	Tripartite motif-containing protein 25	Q14258

ENSP00000356476	4	-16.3	TRM1-like protein.	Q7Z2T5
ENSP00000315379	2	-9.6	U4/U6 small nuclear ribonucleoprotein Prp3	O43395
ENSP00000363313	2	-13.4	U4/U6 small nuclear ribonucleoprotein Prp4	O43172
ENSP00000310448	20	-94.9	U4/U6.U5 tri-snRNP-associated protein 1	O43290
ENSP00000216038	9	-64.7	UPF0027 protein C22orf28.	Q9Y3I0
ENSP00000211402	2	-9	Valyl-tRNA synthetase	P26640
ENSP00000308179	2	-10.6	WD repeat-containing protein 3.	Q9UNX4
ENSP00000349539	6	-29.1	Zinc finger CCCH type antiviral protein 1	Q7Z2W4

Table 1B: Proteins targets captured by the Bis-probe in resting MDA-MB-231.

Identifier	# peptide	log(e)	**Description**	Accession no
ENSP00000264326	4	-19.6	1,4-alpha-glucan-branching enzyme	Q04446
ENSP00000262414	16	-123	116 kDa U5 small nuclear ribonucleoprotein component	Q15029
ENSP00000310129	36	-155	26S proteasome non-ATPase regulatory subunit 2	Q13200
ENSP00000261772	17	-111	Alanyl-tRNA synthetase, cytoplasmic	P49588
ENSP00000346550	6	-38.1	Annexin A6	P08133
ENSP00000299980	2	-12.1	AP-1 complex subunit gamma-1	O43747
ENSP00000327694	3	-18.8	AP-2 complex subunit alpha-2	Q9UFK5
ENSP00000231572	12	-56.2	Arginyl-tRNA synthetase, cytoplasmic	P54136
ENSP00000352257	34	-179	ATP-dependent DNA helicase 2 subunit 1	P12956
ENSP00000329528	26	-156	ATP-dependent DNA helicase 2 subunit 2	P13010
ENSP00000263239	3	-12.6	ATP-dependent RNA helicase DDX18	Q9NVP1
ENSP00000355890	65	-341	Bifunctional aminoacyl-tRNA synthetase	P07814
ENSP00000247461	4	-20.5	Calnexin Precursor	P27824
ENSP00000279247	3	-19	Calpain-1 catalytic subunit	P07384
ENSP00000312419	11	-53	Chromodomain-helicase-DNA-binding protein 4	Q05CG6
ENSP00000269122	151	-720	Clathrin heavy chain 1	Q00610
ENSP00000249923	16	-88.6	Coatomer subunit beta	P53618
ENSP00000342408	10	-59.5	Cold shock domain-containing protein E1	Q8WU01
ENSP00000325017	18	-113	Condensin complex subunit 1	Q15021
ENSP00000361704	16	-63	CTP synthase 1	P17812
ENSP00000299218	14	-65.4	Cullin-associated NEDD8-dissociated protein 1	Q86VP6
ENSP00000369897	2	-11.6	Cysteinyl-tRNA synthetase, cytoplasmic	Q5HYE4
ENSP00000369255	5	-20	Cytoplasmic aconitate hydratase	P21399
ENSP00000324549	17	-68.5	Cytoplasmic FMR1-interacting protein 1	Q7L576
ENSP00000360182	4	-33.4	Dedicator of cytokinesis protein 7	Q96N67
ENSP00000360268	13	-79.6	Delta-1-pyrroline-5-carboxylate synthetase	P54886
ENSP00000352516	7	-36.8	DNA (cytosine-5)-methyltransferase 1	P26358
ENSP00000229854	6	-31.7	DNA replication licensing factor MCM3	P25205
ENSP00000262105	5	-41.6	DNA replication licensing factor MCM4	P33991
ENSP00000216122	4	-32	DNA replication licensing factor MCM5	P33992
ENSP00000264156	3	-20.9	DNA replication licensing factor MCM6	Q14566
ENSP00000354522	21	-84.3	DNA topoisomerase 1	P11387
ENSP00000296255	18	-99.5	Dolichyl-diphosphooligosaccharide--protein glycosyltransferase subunit 1 Precursor	P04843

ENSP00000354791	9	-62.7	Dynactin subunit 1	Q14203
ENSP00000266481	6	-37.5	Dynamin-1-like protein	O00429
ENSP00000340648	3	-18.2	E3 ubiquitin-protein ligase HUWE1	Q7Z6Z7
ENSP00000299767	25	-118	Endoplasmin Precursor	P14625
ENSP00000367011	7	-46.4	Exosome complex exonuclease RRP44	Q49AG4
ENSP00000262982	54	-248	Exportin-2	P55060
ENSP00000267113	7	-40.5	Extended-synaptotagmin-1	Q9BSJ8
ENSP00000349860	23	-125	Glucosamine--fructose-6-phosphate aminotransferase	Q06210
ENSP00000307567	10	-62.2	Glutaminyl-tRNA synthetase	P47897
ENSP00000229239	19	-71.4	Glyceraldehyde-3-phosphate dehydrogenase	P04406
ENSP00000216962	31	-152	Glycogen phosphorylase, brain form	P11216
ENSP00000331201	3	-9.8	Hepatocyte growth factor-regulated tyrosine kinase substrate	O14964
ENSP00000352398	28	-109	Hexokinase-1	P19367
ENSP00000290573	2	-12.4	Hexokinase-2	P52789
ENSP00000278752	5	-31.2	Hypoxia up-regulated protein 1 Precursor	Q9Y4L1
ENSP00000332455	12	-61.8	Importin subunit alpha-2	P52292
ENSP00000350219	60	-259	Importin-5	O00410
ENSP00000369042	36	-138	Importin-7	O95373
ENSP00000354742	16	-78.4	Importin-9	Q96P70
ENSP00000364811	16	-59.6	Isoleucyl-tRNA synthetase, cytoplasmic	P41252
ENSP00000355889	5	-16.2	Isoleucyl-tRNA synthetase, mitochondrial Precursor	A8K5W7
ENSP00000364317	76	-402	Kinesin heavy chain	P33176
ENSP00000227157	14	-52.6	L-lactate dehydrogenase A chain	D3YTI4
ENSP00000350012	4	-23.9	Long-chain-fatty-acid--CoA ligase 3	O95573
ENSP00000349977	9	-68.8	Major vault protein	Q14764
ENSP00000354346	25	-138	Matrin-3	P43243
ENSP00000245615	5	-21.6	Membrane-bound O-acyltransferase domain-containing protein 7	Q96N66
ENSP00000262027	9	-47.1	Methionyl-tRNA synthetase, cytoplasmic	P56192
ENSP00000370974	15	-93.3	Myb-binding protein 1A.	Q9BQG0
ENSP00000352208	38	-254	Myoferlin	Q9NZM1
ENSP00000367263	3	-19.4	Neuroblast differentiation-associated protein AHNAK	Q09666
ENSP00000362411	5	-28.5	Niban-like protein 1	Q96TA1
ENSP00000296543	3	-15	NMDA receptor-regulated protein 1	Q9BXJ9
ENSP00000310668	5	-20	Nuclear pore complex protein Nup93	Q8N1F7
ENSP00000352054	4	-11.1	Plasma membrane calcium-transporting ATPase 1	Q59H63
ENSP00000313007	10	-59.3	Polyadenylate-binding protein 1	P11940
ENSP00000361953	5	-26.9	Polyadenylate-binding protein 4	B1ANR0
ENSP00000301364	6	-22.6	Pre-rRNA-processing protein TSR1 homolog IPR012948 AARP2CNIPR007034 DUF663	Q2NL82
ENSP00000367558	5	-36.2	Probable ubiquitin carboxyl-terminal hydrolase FAF-X	Q93008
ENSP00000196061	7	-27.9	Procollagen-lysine,2-oxoglutarate 5-dioxygenase 1 Precursor	Q02809
ENSP00000307387	13	-67.3	Programmed cell death 6-interacting protein	Q8WUM4
ENSP00000296388	5	-40.3	Prolyl 3-hydroxylase 1 Precursor	Q32P28
ENSP00000300289	24	-134	Protein disulfide-isomerase A3 Precursor	P30101
ENSP00000324573	7	-38.7	Protein flightless-1 homolog	Q13045

ENSP00000306881	8	-67.7	Protein transport protein Sec23A	Q15436
ENSP00000207549	11	-86.7	Protein unc-13 homolog D	Q70J99
ENSP00000355330	43	-199	Protein-glutamine gamma-glutamyltransferase 2	P21980
ENSP00000320324	2	-13.9	Puromycin-sensitive aminopeptidase	P55786
ENSP00000351832	4	-17.4	Rab3 GTPase-activating protein non-catalytic subunit	Q9H2M9
ENSP00000267163	8	-15.3	Retinoblastoma-associated protein	P06400
ENSP00000367044	19	-146	Ribosome-binding protein 1	Q9P2E9
ENSP00000366913	36	-124	Sarcoplasmic/endoplasmic reticulum calcium ATPase 2	P16615
ENSP00000342181	6	-56.6	Signal recognition particle 72 kDa protein	O76094
ENSP00000354394	5	-19.3	Signal transducer and activator of transcription 1-alpha/beta	P42224
ENSP00000295598	3	-16.8	Sodium/potassium-transporting ATPase subunit alpha-1 Precursor	P05023
ENSP00000335321	25	-132	Splicing factor 3B subunit 1	O75533
ENSP00000349748	26	-141	Splicing factor, proline- and glutamine-rich	P23246
ENSP00000323421	10	-67.7	Structural maintenance of chromosomes protein 1A	Q14683
ENSP00000286398	18	-122	Structural maintenance of chromosomes protein 2	O95347
ENSP00000354720	11	-72.7	Structural maintenance of chromosomes protein 3	Q9UQE7
ENSP00000349961	20	-123	Structural maintenance of chromosomes protein 4	Q9NTJ3
ENSP00000317334	33	-173	T-complex protein 1 subunit alpha	P17987
ENSP00000299300	30	-137	T-complex protein 1 subunit beta	P78371
ENSP00000258091	21	-98.5	T-complex protein 1 subunit eta	Q99832
ENSP00000357244	41	-173	T-complex protein 1 subunit gamma	P49368
ENSP00000275603	24	-108	T-complex protein 1 subunit zeta	P40227
ENSP00000366453	5	-28.5	Tight junction protein ZO-2	Q9UDY2
ENSP00000253024	14	-59.1	Transcription intermediary factor 1-beta	Q13263
ENSP00000370023	7	-63.3	Trifunctional enzyme subunit alpha, mitochondrial Precursor	P40939
ENSP00000371261	12	-59.4	Trifunctional purine biosynthetic protein adenosine-3	P22102
ENSP00000323889	14	-79.8	Tripartite motif-containing protein 25	Q14258
ENSP00000366568	15	-133	Ubiquitin-like modifier-activating enzyme 1	P22314
ENSP00000356515	7	-44.4	Utrophin	P46939
ENSP00000314556	3	-18.9	Uveal autoantigen with coiled-coil domains and ankyrin repeats	Q9BZF9
ENSP00000299138	7	-40.3	Vacuolar protein sorting-associated protein 35	Q96QK1
ENSP00000211402	13	-96.6	Valyl-tRNA synthetase	P26640
ENSP00000312042	15	-98.8	Vigilin	Q00341
ENSP00000371890	10	-73.5	WD repeat-containing protein 1	O75083

Table 2: Proteins targets captured by the PEO-biotin control probe**.**

Identifier	#peptides	log(e)	Description	Accession no
ENSP00000311430	23	-61.8	60S ribosomal protein L4	P36578
ENSP00000370517	20	-58.9	6-phosphofructokinase type C	Q01813
ENSP00000224784	109	-114.1	Actin, aortic smooth muscle	P62736
ENSP00000349960	170	-282.4	Actin, cytoplasmic 1	P60709
ENSP00000331514	168	-241.8	Actin, cytoplasmic 2	P63261
ENSP00000331514	166	-283.6	Actin, cytoplasmic 2	P63261
ENSP00000234590	18	-62	Alpha-enolase	P06733
ENSP00000264161	6	-28.9	Aspartyl-tRNA synthetase, cytoplasmic	P14868
ENSP00000282050	10	-40	ATP synthase subunit alpha, mitochondrial Precursor	P25705
ENSP00000262030	4	-29.7	ATP synthase subunit beta, mitochondrial Precursor	P06576
ENSP00000253792	7	-28.4	ATP-citrate synthase	P53396
ENSP00000216605	12	-51.5	C-1-tetrahydrofolate synthase, cytoplasmic	P11586
ENSP00000258512	12	-47.9	Cytoskeleton-associated protein 4	Q07065
ENSP00000257192	2	-8.4	Desmoglein-1 Precursor	Q02413
ENSP00000313420	48	-192	DNA-dependent protein kinase catalytic subunit	P78527
ENSP00000339063	43	-69.1	Elongation factor 1-alpha 1	P68104
ENSP00000331901	11	-22.2	Elongation factor 1-gamma	P26641
ENSP00000322439	8	-24.5	Elongation factor Tu, mitochondrial Precursor	P49411
ENSP00000369881	27	-82.9	Eukaryotic initiation factor 4A-I	P60842
ENSP00000216297	5	-25.8	FACT complex subunit SPT16	Q9Y5B9
ENSP00000353467	42	-207.2	Filamin-A	P21333
ENSP00000335153	58	-138.2	Heat shock protein HSP 90-alpha	P07900
ENSP00000325875	84	-200.9	Heat shock protein HSP 90-beta	P08238
ENSP00000283179	9	-41.6	Heterogeneous nuclear ribonucleoprotein U	Q00839
ENSP00000321584	6	-30.4	Inosine-5--monophosphate dehydrogenase 2	P12268
ENSP00000357284	12	-50.4	Lamin-A/C	P02545
ENSP00000274562	8	-24.5	Leucyl-tRNA synthetase, cytoplasmic	Q9P2J5
ENSP00000369315	156	-392.9	Myosin-10	P35580
ENSP00000345136	79	-188.4	Myosin-11	P35749
ENSP00000216181	1150	-1698.1	Myosin-9	P35579
ENSP00000318195	7	-10.7	Nucleolin	P19338
ENSP00000296930	4	-20	Nucleophosmin	P06748
ENSP00000349868	10	-58.4	Plectin-1	Q15149
ENSP00000268182	13	-56.4	Ras GTPase-activating-like protein	P46940
ENSP00000336799	80	-179.5	Tubulin alpha-1B chain	P68363
ENSP00000341289	180	-235.5	Tubulin beta-2C chain	P68371
ENSP00000264071	149	-187.3	Tubulin beta-4 chain	P04350

Table 3: Enzymes groups captured by the Bis probe with their binding characteristics.

identifier	#peptides	log(e)	Description	Accession no.	Binding
			HYDROLASES		
ENSP00000346762	21	-120	Staphylococcal nuclease domain-containing protein 1	Q7KZF4	nucleic acid
ENSP00000361626	14	-58.3	Nuclease-sensitive element-binding protein 1	P67809	DNA/RNA
ENSP00000296577	10	-40.9	ATP-binding cassette sub-family E member 1	P61221	ATP/Nucleotide
ENSP00000367478	22	-156	ATP-dependent RNA helicase DDX3X	O00571	ATP/Nucleotide DNA/RNA
ENSP00000336741	24	-136	Putative pre-mRNA-splicing factor ATP-dependent RNA helicase DHX15	O43143	ATP/Nucleotide
ENSP00000356520	18	-112	ATP-dependent RNA helicase A	Q08211	ATP/Nucleotide DNA/RNA
ENSP00000348578	18	-85.8	Ras GTPase-activating protein-binding protein 1	Q13283	ATP/Nucleotide DNA/RNA
ENSP00000216019	17	-81.8	Probable ATP-dependent RNA helicase DDX17	Q92841	ATP/Nucleotide /RNA
ENSP00000329528	9	-73.1	ATP-dependent DNA helicase 2 subunit 2	P13010	ATP/Nucleotide /DNA
ENSP00000262803	9	-67.1	Regulator of nonsense transcripts 1	Q92900	ATP/Nucleotide
ENSP00000346120	10	-66.6	Nucleolar RNA helicase 2	Q9NR30	ATP/Nucleotide /RNA
ENSP00000352257	10	-57.5	ATP-dependent DNA helicase 2 subunit 1	P12956	DNA
ENSP00000358716	6	-43.3	Probable ATP-dependent RNA helicase DDX20	Q9UHI6	ATP/Nucleotide /DNA

ENSP00000370745	5	-36.4	ATP-dependent RNA helicase DDX1	Q92499	ATP/Nucleotide /RNA
ENSP00000343442	5	-35.8	Putative ATP-dependent RNA helicase DHX30	Q7L2E3	ATP/Nucleotide /RNA
ENSP00000358662	6	-35.7	Putative helicase MOV-10	Q9HCE1	ATP/Nucleotide /RNA
ENSP00000310723	6	-27.8	Probable ATP-dependent RNA helicase DDX23	Q9BUQ8	ATP/Nucleotide
ENSP00000362687	6	-26.6	ATP-dependent RNA helicase DDX50	Q9BQ39	ATP/Nucleotide /RNA
ENSP00000304072	3	-16	ATP-dependent RNA helicase DDX54	Q8TDD1	ATP/Nucleotide /RNA
ENSP00000238146	2	-9.4	ATP-dependent RNA helicase DDX55	Q8NHQ9	ATP/Nucleotide /RNA
ENSP00000342379	17	-93.5	Myosin phosphatase Rho-interacting protein	Q6WCQ1	actin
ENSP00000263433	7	-40.7	Protein phosphatase 1 regulatory subunit 12C	Q9BZL4	-
ENSP00000354068	6	-37.9	Protein phosphatase 1 regulatory subunit 12A	O14974	protein
ENSP00000309871	3	-17	Rac GTPase-activating protein 1	Q9H0H5	tubulin
ENSP00000352738	14	-78.6	Ras GTPase-activating protein-binding protein 2	Q9UN86	RNA
ENSP00000368031	6	-22.4	ATPase family AAA domain-containing protein 3A	Q9NVI7	ATP/Nucleotide
ENSP00000359588	3	-15.9	Probable phospholipid-transporting ATPase IG	Q8NB49	ATP/Nucleotide
ENSP00000274008	2	-12.5	Spermatogenesis-associated protein 5	Q8NB90	ATP/Nucleotide
ENSP00000366913	2	-8.8	Sarcoplasmic/endoplasmic reticulum calcium ATPase 2	P16615	ATP/Nucleotide
			TRANSFERASES		

ENSP00000257829	9	-46.9	N-acetyltransferase 10	Q9H0A0	ATP/Nucleotide
ENSP00000349860	5	-25.1	Glucosamine--fructose-6-phosphate aminotransferase [isomerizing] 1	Q06210	other
ENSP00000253778	5	-22.9	Glucosamine--fructose-6-phosphate aminotransferase [isomerizing] 2	O94808	other
ENSP00000355330	7	-21.8	Protein-glutamine gamma-glutamyltransferase 2	P21980	protein
ENSP00000222330	16	-102	Glycogen synthase kinase-3 alpha	P49840	ATP/Nucleotide
ENSP00000334983	11	-81.1	Pyruvate kinase isozymes M1/M2	P14618	ATP/Nucleotide
ENSP00000368453	9	-57.3	Interferon-induced, double-stranded RNA-activated protein kinase	P19525	ATP/Nucleotide /RNA
ENSP00000294247	7	-37.3	Serine/threonine-protein kinase MARK2	Q7KZI7	ATP/Nucleotide
ENSP00000354674	6	-24.3	Serine/threonine-protein kinase SRPK1	Q96SB4	ATP/Nucleotide
ENSP00000264235	4	-23.3	Glycogen synthase kinase-3 beta	P49841	ATP/Nucleotide
ENSP00000309438	3	-11	6-phosphofructokinase, liver type	P17858	ATP/Nucleotide
ENSP00000345771	3	-10.1	6-phosphofructokinase, muscle type	P08237	ATP/Nucleotide
ENSP00000350896	2	-9	Ephrin type-B receptor 4 precursor	P54760	ATP/Nucleotide
ENSP00000349541	32	-114	Polymerase I and transcript release factor.	Q6NZI2	RNA
ENSP00000351503	23	-92.7	SPATS2-like protein	Q9NUQ6	other
			LIGASES AND SYNTHETASES		
ENSP00000262027	43	-294	Methionyl-tRNA synthetase, cytoplasmic	P56192	ATP/Nucleotide /RNA

ENSP00000231572	46	-283	Arginyl-tRNA synthetase, cytoplasmic	P54136	ATP/Nucleotide
ENSP00000355759	44	-276	Poly synthetase 1).	P09874	DNA
ENSP00000307567	37	-217	Glutaminyl-tRNA synthetase	P47897	ATP/Nucleotide
ENSP00000364811	18	-112	Isoleucyl-tRNA synthetase, cytoplasmic	P41252	ATP/Nucleotide
ENSP00000303043	18	-96.9	Lysyl-tRNA synthetase	Q15046	ATP/Nucleotide
ENSP00000355890	6	-30.3	Bifunctional aminoacyl-tRNA synthetase	P07814	ATP/Nucleotide /RNA
ENSP00000364783	4	-24.2	Isoleucyl-tRNA synthetase, cytoplasmic	P41252	ATP/Nucleotide
ENSP00000233072	5	-21	Carbamoyl-phosphate synthase [ammonia], mitochondrial precursor	P31327	ATP/Nucleotide
ENSP00000350012	4	-13.7	Long-chain-fatty-acid--CoA ligase 3	O95573	ATP/Nucleotide
ENSP00000211402	2	-9	Valyl-tRNA synthetase	P26640	ATP/Nucleotide
ENSP00000347900	4	-25.5	Pyruvate carboxylase, mitochondrial precursor	P11498	ATP/Nucleotide
			OTHERS		
ENSP00000277865	8	-39.7	Glutamate dehydrogenase 1, mitochondrial Precursor	P00367	ATP/GTP/ Nucleotide
ENSP00000360326	8	-35.3	Glutamate dehydrogenase 2, mitochondrial precursor	P49448	other
ENSP00000369822	6	-35.3	Ribosyldihydronicotinamide dehydrogenase [quinone]	P16083	other
ENSP00000229239	3	-20.7	Glyceraldehyde-3-phosphate dehydrogenase	P04406	other
ENSP00000299297	2	-10.4	Sphingosine-1-phosphate lyase 1	O95470	other

ENSP00000278823	7	-27.5	Metastasis-associated protein MTA2	O94776	DNA
ENSP00000357621	3	-13.5	Histone deacetylase 2	Q92769	other
ENSP00000354522	20	-137	DNA topoisomerase 1	P11387	ATP/Nucleotide /DNA